Universidad Autónoma de Madrid
Departamento de Bioquímica

Role of the protease MT4-MMP in the arterial vasculature

Mara Martín Alonso

Madrid, 2016

Departamento de Bioquímica
Facultad de Medicina
Universidad Autónoma de Madrid

Role of the protease MT4-MMP in the arterial vasculature

Memoria presentada por Mara Martín Alonso licenciada en Ciencias Biológicas para optar al grado de Doctor.

Directora: Dra. Alicia García Arroyo

Centro Nacional de Investigaciones Cardiovasculares (CNIC)

Madrid, 2016

SUMMARY

Vascular smooth muscle cells (SMCs) within the media layer of the arterial vasculature define vessel wall mechano-elastic properties by the generation of a specific extracellular matrix (ECM) and contraction. This ECM is mainly composed by elastin and collagen fibres that confer the optimal elasticity and recoil necessary for the wall to support the energy load with every heart contraction as in big conductance vessels. These vessels conduct the blood flow to resistance vasculature that mediates distribution to the different organs/tissues of the body through vessel diameter regulation. Alterations in the mechano-elastic properties of the vessel wall result in pathological processes as vessel dilations and aneurysms. Mt4-mmp (membrane-type 4 matrix metalloproteinase, also called Mmp17) is expressed in mouse vascular SMCs with undescribed functions or substrates so far. Analysis of Mt4-mmp-deficient mice revealed impeded vascular SMC maturation with altered cell orientation and ECM connections, impacting in vessel wall structure and leading to hemodynamic vascular changes as hypotension. *Mt4-mmp*$^{-/-}$ aortas were unable to bear increased blood pressure presenting higher susceptibility to thoracic aortic aneurysms (TAA) development in response to angiotensin II. Also, null immature vascular SMCs produced larger neointima in a model of vessel injury. Normal phenotype of the arterial vessel wall was restored after expression of catalytic-active Mt4-mmp by lentivirus injection in null neonates, indicating the dependence of the vascular phenotype of *Mt4-mmp*$^{-/-}$ on its catalytic activity. Consistently, we demonstrated that Mt4-mmp cleaves the matricellular protein osteopontin (Opn) during aortic wall development leading to c-Jun N-terminal kinase (JNK) signalling. Lentiviral-driven restoration of the N-terminal Opn fragment generated by Mt4-mmp cleavage in the null mice rescued the aortic phenotype and JNK phosphorylation in *Mt4-mmp*$^{-/-}$ neonates. Reinforcing the importance of Mt4-mmp in arterial performance, we found a mutation in a patient suffering thoracic aortic aneurysms and dissections (TAAD) that impeded metalloproteinase expression (MT4-MMP-R373H), strengthening the implication of MT4-MMP in arterial vessel wall function and pathology.

RESUMEN

Las células de musculatura lisa vascular (del inglés smooth muscle cells, SMCs) de la pared arterial son las responsables de conferir las propiedades mecano-elásticas a las arterias mediante la síntesis y organización de una matriz extracelular específica (del inglés extracellular matrix, ECM) y la contracción. Esta ECM está compuesta principalmente por fibras de colágeno y de elastina que aportan la elasticidad y retroceso necesario para que la pared soporte la carga de energía derivada de cada contracción cardiaca en las grandes arterias de conductancia que transfieren el flujo sanguíneo a las arterias de resistencia, encargadas de regular el aporte de sangre a los órganos y tejidos mediante el control de su diámetro. Las alteraciones en estas propiedades mecánico-elásticas de la pared vascular están ligadas a la generación de patologías vasculares como la formación de aneurismas. Mt4-mmp (del inglés membrane-type 4 matrix metalloproteinase, también conocida como Mmp17) se expresa en SMCs vasculares, donde aún no se conoce la función o posible(s) sustrato(s). El análisis de la vasculatura del ratón deficiente en Mt4-mmp (*Mt4-mmp*$^{-/-}$) reveló que la ausencia de Mt4-mmp impide la correcta maduración de las SMCs en la aorta, que presentan una distribución y una conexión con la ECM alterada, lo que afecta a la estructura de la pared y genera cambios hemodinámicos. Como resultado, el ratón deficiente es hipotenso y tiene mayor susceptibilidad a daño. En particular, desarrolla más frecuentemente aneurismas torácicos aórticos en respuesta a angiotensina II y una mayor íntima en respuesta a daño. El fenotipo de la pared vascular pudo ser restaurado en el ratón *Mt4-mmp*$^{-/-}$ tras la inyección de lentivirus que codificaban para la proteína Mt4-mmp catalíticamente activa. En concordancia con lo anterior, hemos descubierto que la actividad catalítica de Mt4-mmp es necesaria durante el desarrollo de la aorta, procesando una proteína denominada osteopontin (Opn) que induce la señalización por la quinasa c-Jun N-terminal (JNK). De hecho, la expresión mediada por lentivirus del fragmento N-terminal de Opn resultante del corte de Mt4-mmp, rescata el fenotipo y la fosforilación de JNK en la aorta de ratones *Mt4-mmp*$^{-/-}$ neonatos. El análisis de mutaciones de MT4-MMP en pacientes con aneurisma torácico aórtico, determinó la presencia de una mutación que impide su expresión (MT4-MMP-R373H) reforzando el hecho de que Mt4-mmp es necesaria para el correcto funcionamiento de la pared vascular arterial.

INDEX

NON-STANDARD ABBREVIATIONS AND ACRONYMS

ADAMTS4	A Disintegrin and Metalloproteinase (with Thrombospondin Motifs)
βGal	β-Galactosidase
BSA	Bovine serum albumin
CNRQ	Calibrated Normalized Relative Quantity
Cys	Cysteine
DSS	Dextran sulfate sodium
EC(s)	Endothelial cell(s)
ECM	Extracellular matrix
EDTA	Ethylenediaminetetraacetic acid
EEL	External Elastic Layer
ER	Endoplasmic reticulum
EVS	European Variant Service
FBS	Fetal Bovine Serum
FDR	False Discovery Rate
FBN	Fibrillin
GO	Gene Ontology
HEK293	Human Embryonic kidney 293 cell line
H/L	Heavy/Light
H&E	Hematoxylin and eosin
IEL	Internal elastic layer
LC-MS	Liquid Chromatography – Mass Spectrometry
LV	Lentivirus
MFI	Mean Fluorescence Intensity
MFS	Marfan Syndrome
MMP(s)	Matrix metalloproteinase(s)
MRTF	Myocardin-related transcription factor
MS	Mass spectrometry
MT4-MMP	Membrane type-4 matrix metalloproteinase
OPN	Osteopontin
PBS	Phosphate Buffer Saline
pH3	Phospho-histone H3
PFA	Paraformaldehyde
SHG	Second Harmonic Generation
SILAC	Stable Isotope Labeling by Amino Acids in Cell Culture
SMA	Smooth Muscle Actin
SMC	Smooth muscle cells
SM-MHC	Smooth Muscle-Myosin Heavy Chain
SRF	Serum response factor
TAAD	Thoracic Aortic Aneurysms and Dissections
TEM	Transmission Electron Microscopy
TF	Transcription factor
TGF-β	Transforming Growth Factor-β
WGA	Wheat Germ Agglutinin
WT	Wild-type

Introduction

INTRODUCTION

-Matrix metalloproteinases-

Matrix metalloproteinases are a large family of calcium-dependent zinc-containing endopeptidases which have been traditionally associated with the degradation and turnover of the extracellular matrix (ECM) components (Page-McCaw et al. 2007). Today, MMPs are known to play fundamental roles in pathophysiological processes through proteolytic processing of a large variety of molecules acting as direct and indirect regulators of cell behavior and microenvironment (Rodriguez et al. 2010).

The founding member of the MMP family was discovered in 1962, by Gross and Lapiere, who reported a collagenolytic activity in tadpole tails during metamorphosis. The amphibian tail contained an interstitial collagenase that could degrade fibrillar collagen, named as collagenase-1 or MMP-1(Gross and Lapiere 1962). Further research led to the discovery of a family of structurally related proteinases in mammals, now referred as MMP family (Brinckerhoff and Matrisian 2002).

Matrix metalloproteinases (MMPs)

MMP structure and domains: MMPs share a conserved domain structure (Figure 1). Minimal domain structure consists of a catalytic domain with an active zinc site and an autoinhibitory pro-domain. The pro-domain contains a conserved motif (PRCGXPD) in which a cysteine (Cys) residue coordinates the active-site zinc of the catalytic domain; this pro-domain needs to be destabilized or removed to allow MMP catalytic activation (Page-McCaw et al. 2007). In this way, MMPs are expressed as latent forms or zymogens that need to be catalytically activated; such activation can occur outside of the cell, where the pro-domain can be cleaved by other MMPs, serin proteases or plasmin (among others) (Treadwell et al. 1986) (Sato et al. 1994), or intracellularly, usually by the pro-hormone convertase enzyme furin (Pei and Weiss 1995).The catalytic domain consists of five-stranded β-sheets and three α-helices that form a spherical pocket, a structure highly conserved among MMP members. In fact, the zinc-binding motif HEXGHXXGXXH, together with the Cys motif at the pro-domain are used to assign proteinases to the MMP family (Visse and Nagase 2003). Most MMPs also present a hinge region and a hemopexin-like domain (Page-McCaw et al. 2007). The hemopexin-like domain, a four blade-shaped β sheet, is attached to the MMP catalytic domain by a flexible hinge (or linker) that is up to 75 residues with no established secondary structure. This hemopexin-like domain mediates protein-protein interactions participating in substrate recognition and

binding of MMPs inhibitors known as TIMPs (tissue inhibitors of metalloproteinases) (Page-McCaw et al. 2007). Through these interactions, it regulates activation, localization, internalization and degradation of the MMPs (Brinckerhoff and Matrisian 2002).

In addition to these domains, all MMPs are synthetized with a signal peptide that drives the MMP to the endoplasmic reticulum where this peptide is cleaved during transport through the secretory pathway (Page-McCaw et al. 2007).

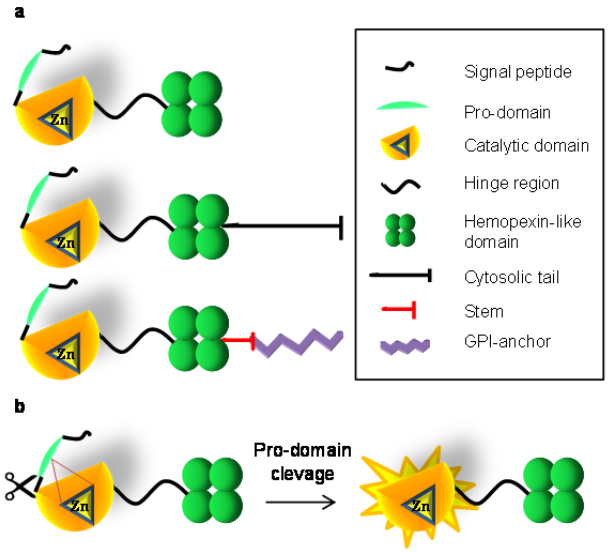

Figure 1. MMP family domains structure. (**a**) The figure depicts the conserved domains of the MMP family members. MMPs can be soluble or membrane-anchored by a cytosolic tail or a GPI-anchor. (**b**) Canonical pathway of MMP activation. The catalytic activity of the MMPs is inhibited by the presence of a pro-domain that can be cleaved extracellularly or intracellularly.

Most MMP members are secreted proteins, except for seven family members that present a hydrophobic domain that binds the metalloproteinase to the plasma membrane (membrane-type MMPs (MT-MMPs)) (Visse and Nagase 2003). This membrane anchorage could be through a transmembrane domain type I with a short cytosolic tail of 20-22 amino acids (this is the case of MT1-MMP (MMP14), MT2-MMP (MMP15), MT3-MMP (MMP16) and MT5-MMP (MMP24)), a type II transmembrane domain (MMP23) or a glycosylphosphatidylinositol (GPI) linkage (Page-McCaw et al. 2007). Only two members of the MMPs family are GPI-anchored to the plasma membrane; MT4-MMP (MMP17) and MT6-MMP (MMP25) (Sohail et al. 2008).

Membrane attachment confers diverse properties; first it facilitates MT-MMPs to reach and cleave membrane and peripheral proteins as well as closely associated ECM components to the membrane, impacting in the pericellular space; second, it localizes MT-MMPs at specific membrane domains, together with other transmembrane proteins as specific cellular receptors; and third, membrane insertion will confer the regulatory mechanisms that serve to control the pool of active protease at the cell surface including endocytosis, recycling, autocatalytic processing and ectodomain shedding (Sohail et al. 2008).

Another characteristic of MT-MMPs is that whereas soluble MMPs needs to be activated extracellularly (except MMP11 and MMP28) (Visse and Nagase 2003), MT-MMPs present a RXR/KF motif at the end of the pro-domain that furin recognizes and cleaves intracellularly, allowing protease activation before membrane tethering (Sohail et al. 2008). Once at the membrane, regulation of MT-MMP activity would be mediated by internalization, membrane distribution and catalytic inhibition by TIMPs (Page-McCaw et al. 2007).

MMP substrates and functions: Traditionally, MMPs has been classified on the basis of their specificity of ECM substrates in collagenases, gelatinases, stromelysins and matrilysins (Verma and Hansch 2007). However, MMPs are able to cleave all ECM proteins. Consequently, MMP functions are not only limited to degradation of structural components, but to regulation of cell microenvironment, impacting in cell behavior and signaling pathways (Rodriguez et al. 2010) depending on the specific substrate cleavage.
In this sense, MMP substrates include peptide growth factors, cell adhesion molecules, tyrosine kinase receptors, chemokines and cytokines, as well as other MMPs and unrelated proteases. In fact, a key role of MMPs is to mobilize growth factors through cleavage and release of cytokine masking carrier proteins that block growth factor function and activity. This is the case of transforming growth factor-β (TGF-β) and platelet-derived growth factor (PDGF) (Page-McCaw et al. 2007).
Increasing interest in MMPs is due to its upregulation in human pathologies as cancer, cardiovascular diseases and inflammatory pathologies as rheumatoid arthritis (Brinckerhoff and Matrisian 2002) (Chabottaux and Noel 2007); and different therapies were developed to target MMP activity. These therapies however failed, due to the uncomplete knowledge about MMP substrates and functions and the lack of a MMP-type specific inhibitor (Chabottaux and Noel 2007) (Rodriguez et al. 2010).
The complexity of MMP physiological and pathological functions derives from its multidomain structure, diverse substrate repertoire, differential tissue expression, interacting proteins and co-factors and their inhibitory profile, among other processes (Rodriguez et al. 2010). Generation of knockout mouse models for the different MMPs have been a valuable resort to study the possible function and substrates of the different MMPs. Surprisingly, most of the modified mice showed mild phenotypic alterations with little matrix remodeling defects. In fact, all MMP-knockout lines survived till birth. Only MMP14 (MT1-MMP) deficiency results in postnatal lethality through a non-well defined

mechanism. Those deficient mice have multiple abnormalities and are grossly defective in the remodeling of the connective tissue since MT1-MMP is the major collagenase (Holmbeck et al. 1999) (Zhou et al. 2000).

The possible explanation for the mild effect of MMP knockout mice models would be founded in mechanisms of MMP redundancy, compensation, or adaptive development or simply means that MMPs are not essential until embryonic development is completed, although further analysis of MMPs role during this process is required (Page-McCaw et al. 2007).

Membrane Type 4-matrix metalloproteinase (MT4-MMP)

MT4-MMP (also known as MMP17) was originally cloned from a human breast carcinoma cDNA library (Puente et al. 1996). Apart from the expression in different breast tumors, MT4-MMP expression was also detected in brain, colon, ovary, testis and leukocytes (eosinophils, lymphocytes and monocytes but not neutrophils) (Puente et al. 1996). Although discovered 20 years ago, the body of work on MT4-MMP today is still surprisingly limited when compared to others MT-MMPs (Sohail et al. 2008).

Structure of MT4-MMP: MT4-MMP structure is depicted in Figure 2 whose main particularity is the membrane anchorage through a GPI (Sohail et al. 2008). As in other MT-MMPs, the pro-peptide domain is recognized intracellularly by furin and removed, so the metalloproteinase would be active at the cell surface (Puente et al. 1996). The catalytic center of MT4-MMP is distantly related to other MMPs in terms of residue homology. Primary alignment of the catalytic domain of MT4-MMP and MT6-MMP (most similar MMP member) shows 56% of identity (77% of homology); when compared to MT1-MMP catalytic domain, MT4-MMP possesses only 37% identity (50% similarity) (Sohail et al. 2008). Having into account that sequence identity on the catalytic domain among other MMP members is more than 65%, this makes MT4-MMP a distant member of the MMP family (Itoh et al. 1999). MT4-MMP, as well as the other GPI-anchored MT6-MMP,

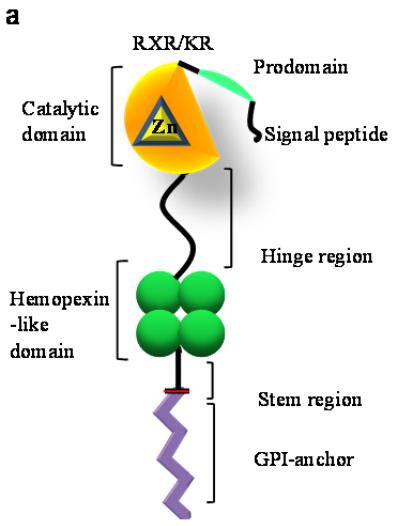

Figure 2. MT4-MMP structure. MT4-MMP domain structure is depicted showing the presence of the distinct protein domains and the GPI-anchor.

presents a stem region of ≈ 35-45 amino acids that is a linker between the hemopexin domain and the GPI-anchorage. This stem region is particularly enriched in hydrophobic residues as cysteine (Cys) (Sohail et al. 2008). Recently the MT4-MMP stem region has been implicated in the homodimerization of the metalloproteinase by disulfide bond formation between Cys^{564} residues of contiguous molecules during protein maturation. This dimerization stabilizes the metalloproteinase at the cellular membrane and is presumably necessary for MT4-MMP function (Sohail et al.).

The GPI anchorage of MT4-MMP to the plasma membrane was first demonstrated in 1999 by Dr. Seiki's laboratory (Itoh et al. 1999). The GPI is a lipidic-carbohydrate structure composed by 2-3 fatty acids inserted at the plasma membrane that connect to mannose residues through a phosphatidylinositol. The distal residue of a mannose is attached to the C-terminal protein through an ethanolamide phosphate bridge (Ferguson et al. 2009). Itoh et al demonstrated this binding for MT4-MMP through the incorporation of $[H^3]$ethanolamine required during the binding of the GPI to the C-terminal amino acid of the protease, and the sensitivity of MT4-MMP to the phosphatidylinositol-specific phospholipase C (PI-PLC) in transfected cells (Itoh et al. 1999).

It is described that MT4-MMP synthesis (Figure 3) likely follows the biosynthetic pathway of GPI-anchored proteins (Sohail et al. 2008). MT4-MMP would be synthetized as a transmembrane precursor; then the presence of 15 to 20 amino acids stretch highly

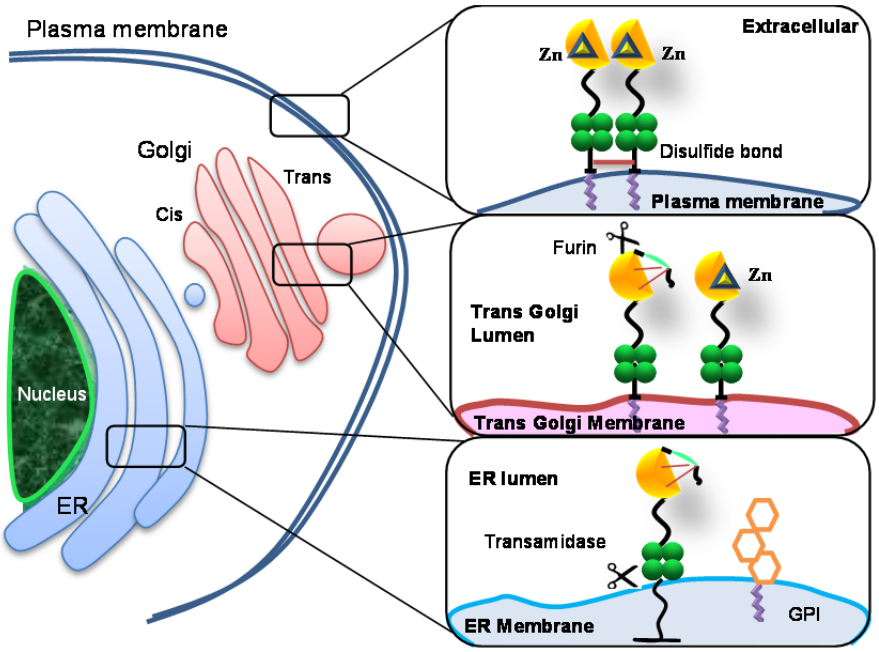

Figure 3. Biosynthetic pathway of MT4-MMP. MT4-MMP synthesis begins at the endoplasmic reticulum (ER) where a cytosolic tail is synthetized and the protein is attached to the ER membrane. At this location, a transamidase recognizes the protein, cleaves after the hemopexin domain and transfers the chain to the GPI-anchorage also present at the ER membrane. The modification of the carbohydrates of the GPI allows the bond. The pro-domain is removed during protein maturation at the trans Golgi network, by a furin that recognizes the RXR/KR domain. In this location also a disulfide bond is established between Cys^{564} of contiguous MT4-MMP molecules.

hydrophobic at the C-terminal tail (corresponding to a GPI signal) would be recognized by a transamidase at the endoplasmic reticulum. The transamidase cleaves the C-terminal (presumably at the Ala^{573} residue) and transfer MT4-MMP precursor chain to the pre-existing GPI molecule that contains 2-3 fatty acids (Cross 1990). The remodeling of these 2-3 fatty acids from unsaturated to saturated fatty chains occurs, most likely, at the Trans Golgi network and is an essential step for the integration of the GPI-anchored protease into membrane microdomains enriched in colesterol, glycosphingolipids and proteins receptors known as lipid rafts (Cross 1990) (Lingwood and Simons 2010). Lipid raft location of MT4-MMP was demonstrated by a sucrose gradient fractionation (Sohail et al. , 2011).
The presence of this GPI-anchor confers important biological properties as (i) being in contact to other GPI-anchored proteins at the membrane (ii) apical sorting (iii) sensitivity to phospholipases and (iv) a role in signal transduction (Sohail et al. 2008). Moreover, MT4-MMP can be internalized by early endosomes (mediated by the clathrin independent carrier/GPI-enriched early endosomal compartment pathway), leading to degradation or recycling of the protease, regulating in this way the amount of membrane active MT4-MMP (Truong et al. 2015).

MT4-MMP substrates: Unlike other MMP members, the lack of a specific MT4-MMP substrate(s) makes difficult to investigate its functionality (Sohail et al. , 2011). Early studies that attempted to find MT4-MMP substrates were achieved around 1999 using the metalloproteinase human recombinant catalytic domain produced in *E.Coli* (Kolkenbrock et al. 1999) (Wang Y. et al. 1999) (English et al. 2000). This kind of assay does not address the influence of the membrane insertion and other domains on catalytic activity, or the specific location of the protease and its substrates at the cellular sites (Sohail et al. 2008). In these experiments, MT4-MMP catalytic domain exerted minimal or no activity against many ECM components compared to other MMPs (Kolkenbrock et al. 1999) (Wang Y. et al. 1999). Later studies performed with the mouse recombinant catalytic domain of Mt4-mmp showed proteolytic activity only against gelatin, fibrin and fibrinogen (Wang Y. et al. 1999) (English et al. 2000) and sensitivity to TIMP 1, 2 and 3 (English et al. 2000), in contrast to the rest of the MT-MMPs which are insensitive to TIMP 1 (except for MT6-MMP) (Sohail et al. 2008).
Non-ECM substrates were also described for MT4-MMP; α_2-macroglobulin (English et al. 2000) and LRP (low density lipoprotein receptor-related protein) (Rozanov et al. 2004) were cleaved by MT4-MMP catalytic domain *in vitro*. Also, Mt4-mmp showed TNF-α

(Tumor necrosis factor-α) convertase activity *in vitro* (English et al. 2000), however, later assays using wild-type and Mt4-mmp-null macrophages showed no TNF-α shedding, indicating that Mt4-mmp does not appear to be a major TNF-α sheddase (Rikimaru et al. 2007).

Activation of the zymogen of ADAMTS-4 (a disintegrin and metalloproteinase with thrombospondin motifs-4) by MT4-MMP has been also described during inflammatory cartilage degradation (Clements et al. , 2011).

The way in which MMP substrates have been analyzed along time has evolved from primary digestion assays to cutting-edge proteomics (Rodriguez et al. 2010) that allow the identification of processed proteins on a specific cell type/tissue (proteome). This technique could be helpful in the identification of possible MT4-MMP substrates as previously demonstrated for other MMPs (Koziol et al. 2012).

MT4-MMP expression in tissues and cellular populations: The urge to study Mt4-mmp function *in vivo* lead Dr. Seiki's laboratory to the generation of an Mt4-mmp-deficient mouse line (referred here as *Mt4-mmp*$^{-/-}$). They established a constitutive mutant mouse strain in which *Mt4-mmp* genomic sequence was partially replaced by a LacZ cassette (Figure 4) (Rikimaru et al. 2007). In particular, *Mt4-mmp* first exon and part of the first intron were targeted by a vector carrying the LacZ cassette with a nuclear localization sequence (NLS), resulting in *Mt4-mmp* expression loss. This strategy also allowed the tracking of *Mt4-mmp* promoter activation following β-galactosidase activity (Rikimaru et al. 2007). For the first time, *Mt4-mmp* promoter activation could be reported showing high levels of *Mt4-mmp* and *LacZ* mRNA in brain, lung and uterus; intermediate levels in stomach, intestine, spleen, testis and ovary; and low levels in cerebellum, heart, liver, kidney, ovary and skeletal muscle in adult mice (Rikimaru et al. 2007). An interesting correlation was established between *Mt4-mmp* and *smooth muscle actin* (SMA) transcript, suggesting that *Mt4-mmp* was expressed in smooth muscle cells (SMCs) throughout the mouse body (as in lung, aorta, stomach, intestine, testis, ovary and uterus). *Mt4-mmp* promoter activation was also confirmed in neurons (in brain locations as cortex, hippocampus, caudate putamen) and in isolated peritoneal macrophages (Rikimaru et al. 2007).

Despite the high distribution of cells positive to LacZ in the *Mt4-mmp*$^{-/-}$ mice, no histological differences were detected between wild-type and *Mt4-mmp*$^{-/-}$ mice in any of

the analyzed tissues. In fact, *Mt4-mmp*-null mice showed no apparent pathologies; had normal appearance, behavior, life span and fertility (Rikimaru et al. 2007).

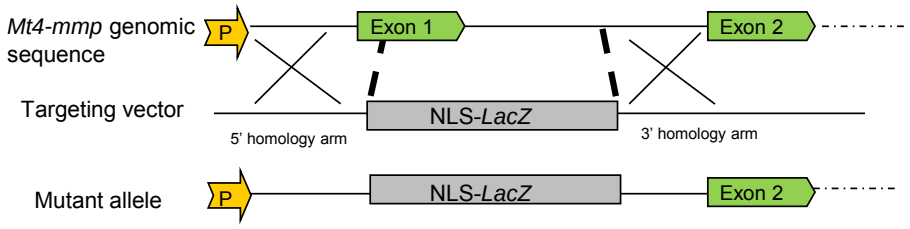

Figure 4. **Targeting strategy of the *Mt4-mmp* knockout/knockin mouse model**. *Mt4-mmp* genomic sequence was disrupted by homologous recombination with a *LacZ* cassette codifying for the bacterial reporter gene β-galactosidase. In this system, β-galactosidase protein is expressed as a fusion protein with a with a nuclear localization signal (NLS) that allows localization at the cellular nucleus. The resulting mutant allele expresses the β-galactosidase transcript under *Mt4-mmp* promoter control allowing the tracking of the metalloproteinase expression. (Adapted from Rikimaru, et al. 2007).

MT4-MMP physiological functions: In contrast to other MMPs that become upregulated in pathological situations, MT4-MMP is highly expressed in physiological conditions in some tissues as brain and smooth muscle however few functions are described so far. In brain, it has been described that Mt4-mmp plays a role controlling drinking behavior since *Mt4-mmp*$^{-/-}$ mice exhibit abnormally diminished thirst (50% decreased water intake compared to wild-type). This defect is presumably due to disrupted thirst regulation by the anterior hypothalamic area, with no alterations in kidney functionality or hormone secretion (Srichai et al. 2011). No vascular role for Mt4-mmp has been addressed so far, however a possible function during angiogenesis has been proposed since expression of this metalloproteinase have been described in human endometrial endothelial cells (ECs) in which MT4-MMP levels correlated to the angiogenic episodes of the menstrual cycle (Plaisier et al. 2006, Plaisier et al. 2004).

Recently it has been analyzed the expression and function of GPI-anchored MMPs during development in Zebrafish and Drosophila. In the first, inactivation of mmp17b (the MT4-MMP ortholog in zebrafish) results in neural crest aberrant migration affecting the dorsal root ganglia formation that will become neurons and glia of the sympathetic ganglia and adrenal chromaffin cells (Leigh et al. 2013). In the second, Mmp2 (a GPI-bound MMP in drosophila) cleaves a glypican (Division abnormally delayed (Dally)-like protein (Dlp)) that mediates Wnt signaling impacting on stem cell proliferation (Wang X. and Page-McCaw 2014).

MT4-MMP function in pathology: Contrary to the physiological functions, MT4-MMP role in pathology has been more extensively addressed (Sohail et al. 2008) (Sounni et al. 2011). MT4-MMP has been implicated in inflammatory processes as cartilage ECM degradation in osteoarthritis. In this pathology, MT4-MMP expression is induced by the cytokine interleukin 1β (IL1 β) that is up-regulated in osteoarthritic cartilage. MT4-MMP acts cleaving and activating ADAMTS-4 that is the responsible for aggrecan matrix degradation. Deletion of Mt4-mmp in fact protects mice against loss of articular aggrecan in response to IL1 β (Gao G. et al. 2004) (Patwari et al. 2005) (Clements et al. , 2011).

Also increased levels of MT4-MMP were found in cancer, as in breast carcinomas (Chabottaux et al. 2006) and head and neck cancer (Huang C. H. et al. 2009). Interestingly, in the characterization of the MT4-MMP role in head and neck cancers, a regulation of the MT4-MMP promoter by SLUG was discovered. SLUG transcription factor was in turn induced by hypoxia-inducible factor-1α (HIF-1α) in hypoxia, suggesting an inducible expression of MT4-MMP in cancer cells during hypoxic condition (Huang C. H. et al. 2009).

MT4-MMP overexpression in MDA-MB-231 breast cancer cells was shown to promote tumor growth and lung metastasis once subcutaneously injected in immunodeficient mice (Chabottaux et al. 2006) (Chabottaux et al. 2009). In the same way, expression of MT4-MMP in squamous cell carcinoma cell line also increased lung colonization after tail vein inoculation (Huang C. H. et al. 2009). These results demonstrate that MT4-MMP expression promotes experimental metastasis. However, the mechanism(s) by which MT4-MMP enhances metastasis remains unclear since conflicting results were obtained regarding the ability of MT4-MMP to promote *in vitro* cell migration and invasion (Chabottaux et al. 2006) (Huang C. H. et al. 2009). However, MT4-MMP acts as an important driver of cancer cell proliferation through induction of epidermal growth factor receptor (EGFR) activation and signaling in a non-proteolytic manner; this leads to retinoblastoma protein inactivation (Rb) conferring a proliferative advantage to MT4-MMP expressing tumor cells (Paye et al. 2014).

Further analysis of MDA-MB-231 tumor xenograft overexpressing MT4-MMP implanted in immunodeficient mice revealed alterations in the tumor vascular architecture; tumors presented dilated and leakier vessels compared to non-overexpressing MT4-MMP tumors (Chabottaux et al. 2009). MT4-MMP expression by tumor cells in this case affected host EC-SMC interaction, impeding pericyte coverage and vessel stabilization and this was proposed as the mechanism by which MT4-MMP increases tumor cell metastasis

(Chabottaux et al. 2009). During this process, MT4-MMP catalytic activity is responsible of the metastatic effect since mutations in the Glu248 residue on its catalytic domain significantly decreased tumor lung metastasis. Also, tumor-derived MT4-MMP contributes to angiogenesis in a permissive microenvironment (Host et al. , 2012). So, these data together with the endometrial expression of MT4-MMP suggest a role of this metalloproteinase in angiogenesis and vessel stabilization (Sounni et al. 2011), even though the *Mt4-mmp*$^{-/-}$ does not present any described vascular phenotype (Rikimaru et al. 2007).

-Smooth Muscle Cells-

Smooth muscle tissue is an involuntary non-striated muscle consisting of smooth muscle cells (SMCs), also called fibers. The smooth muscle is classified into multi-unit smooth muscle and unitary smooth muscle. In the former, each smooth muscle operates independently and is innervated by a single nerve ending; therefore, each SMC can contract independently from others under the nervous control. This is the case of the ciliary muscle of the eye, the iris, and the piloerector muscle at the skin. In the latter, SMCs contract together as a syncytium, in which membrane connections allow action potential and ion transmission. Unitary smooth muscle is found within the walls of the blood vessels (vascular SMCs) forming the media of arteries, arterioles and veins and in the lymphatic vessels. Also conform the thick muscular walls of organs (visceral SMCs) of gastrointestinal tract, reproductive female and male tracts and uterus, urinary tract and the bladder, and the respiratory tract (Guyton 1986).

Arterial vasculature and the vascular smooth muscle cells

The arterial vessel wall consists of three layers; (i) a monolayer of endothelial cells (EC) known as endothelium, longitudinally arranged along the vessel axis, (ii) the media, consisting of one or more concentric rings of vascular SMCs and elastin, and (iii) the adventitia, an outer layer made of fibroblasts embedded in a collagen matrix (Figure 5) (Wagenseil and Mecham 2009). Vascular SMCs are elongated contractile cells that synthetize, organize and maintain an ECM that defines the mechanic properties of the arterial wall (Wagenseil and Mecham 2009).

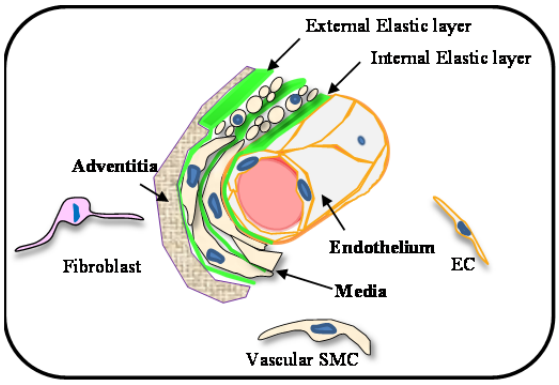

Figure 5. Structure of the arterial vessel wall. The arterial vessel wall consists of 3 layers: endothelium, media and adventitia. The endothelium is a monolayer of ECs in direct contact to blood flow on one side and to the internal elastic lamellae on the other. The media is composed of vascular SMCs embedded in an organized ECM network. Vascular SMCs encircle arterial vessels together with parallel elastic fibers. The external part of the arterial vessels is covered by adventitial tissue formed mainly by fibroblast/myofibroblast in a collagen network.

The arterial vasculature bears the tremendous surge of pressure ejected from the heart during systole and conduct the blood flow through it to the resistance vessels that will distribute the blood to the different tissues and organs. To achieve this, conductance (or conduit) arteries contain a thick elastic media able to store a portion of the stroke volume with each systole and discharge that volume with diastole, maintaining a continuous flow through the circulatory system (Wagenseil and Mecham 2009). They are able to accommodate the large cyclic circumferential stretch generated with the heart pump by the extreme compliance and elastic recoil of its wall, without changing the contraction of the vascular SMCs (Humphrey et al. 2014).

The number of vascular SMC-elastic fibers of this media wall is linearly related to tensional forces within the wall with the greatest number of vascular SMCs-elastic layers occurring in the larger, more proximal vessels to the heart, that experience the highest wall tension, as aorta (Wagenseil and Mecham 2009).

Resistance vasculature however maintains a variable contractile tone generated by the vascular SMCs within the wall and is responsible both for the regulation of the blood pressure and for the redistribution of blood flow after systole through changes in arterial diameter (Heberlein et al. 2009) (Lacolley et al. 2012). In both types of vessels, vascular SMCs act as sensors of mechanical environment and preserve mechanical homeostasis by modifications in the synthesis/composition and/or arrangement of the ECM or in its own contractility (Owens et al. 2004) (Humphrey et al. 2015) (Lacolley et al. 2012).

Arterial vessel wall development: vascular SMC differentiation and maturation

The development of the arterial vasculature occurs in three phases; first the formation of an endothelial tube, second the recruitment of vascular SMCs progenitors that third differentiate into vascular SMCs. The interaction established among ECs and progenitor

vascular SMCs will drive the differentiation, maturation and stabilization of the new vasculature (Simons and Eichmann 2015).

Nascent endothelial tubes are generated in the absence of blood flow (before embryonic day (E) 8 in mice) from vascular progenitor cells that migrate and proliferate through the developing embryo (Adams and Alitalo 2007). Although this processes of vasculogenesis and angiogenesis is well described (Adams and Alitalo 2007) (Carmeliet 2005), little is known about the subsequent events that create and pattern the arterial wall (Greif et al. 2012) (Hungerford and Little 1999).

Recently, Greif *et al*. described that the arterial wall is constructed radially from the inside out, by the study of pulmonary artery (PA) development in mice (Greif et al. 2012). This radial construction is based on a PDGF gradient produced by ECs (Gaengel et al. 2009) (Greif et al. 2012). From E11.5 to E13.5, vascular SMCs progenitors from lung mesenchyme start to express PDGFRβ, migrate closer and elongate longitudinally to ECs. These progenitors contribute to the formation of the first vascular SMCs layer through longitudinal proliferation and recruitment. Progressively, this first layer of cells acquire expression of SM markers as SMA (smooth muscle actin), SM-MHC (smooth muscle myosin heavy chain), Sm22α (Smooth muscle 22 alpha) and NG2 (neural/glial antigen 2) and downregulate the expression of PDGFRβ. Around E13.5, a second layer of vascular SMCs is generated by an equivalent process of progenitor recruitment together with cells originated from first layer progenitors division that change its division plane from longitudinal to radial oriented. PDGFβ availability (concentration) gets proportionally decreased in the developing PA towards the future adventitia, and at ≈E14.5, a third layer of mesenchymal progenitors do not complete the vascular SMCs differentiation program and become adventitial cells (Greif et al. 2012). It has been proposed that this process of recruitment and differentiation is common to all arteries with more than 2 SMC-elastin layers as the aorta (Greif et al. 2012).

This process of progenitor recruitment also needs other molecules as VEGF, sphingosine-1-phosphate (S1P) and Angiopoietin (Ang)-Tie axis since deficient mouse models in those factors present vessels with almost no vascular SMC coverage (Simons and Eichmann 2015) (Owens et al. 2004). Still other(s) factor(s) need to be identified that would explain the changes in mesenchymal progenitors migration and division (Greif et al. 2012).

At this point of development (E14.5), the definitive pattern of the circulatory system is established, so during further vessel wall maturation, the numbers of smooth muscle-elastic

fiber layers will not change; the arteries will alter geometry (length, diameter and wall thickness) without further changes in patterning (Wagenseil and Mecham 2009).

The following steps of maturation are mainly driven by TGFβ. TGFβ isoforms (from 1 to 3) are secreted as latent forms that binds to the large latent TGFβ-binding protein attached to ECM components such fibrillin-1. In this way, TGFβ remains inactive and needs to be proteolitically activated (Owens et al. 2004). When is released from the ECM, TGFβ signaling results in phosphorylation, dimerization and translocation to the nucleus of SMAD subunits, transcriptions factors (TFs) that regulate the expression of early differentiation markers in progenitor vascular SMCs (Owens et al. 2004). At later stages, myocardin or MRTFs (myocardin-related transcription factors), *via* serum response factor (SRF), SMADs and other TFs, enforce and accelerate SMC differentiation and maturation by the regulation of the expression of differentiation proteins as calponin, caldesmon and SM-MHC (ten Dijke and Arthur 2007).

Besides the acquisition of contractile proteins, during differentiation and maturation, vascular SMCs also synthetize and organize the ECM components, essential for the latter vessel wall performance. A mayor increase in ECM protein synthesis occurs at E14.5 with high rates of expression of genes related to elastin, collagen, proteoglycans, cadherins and integrins (Owens et al. 2004) (Kelleher et al. 2004) and is downregulated once the correct pressure in the circulatory system is obtained (≈ postnatal day (P) 35 in mice) (Wagenseil and Mecham 2009).

Unlike other adult tissues, vascular SMCs in the adult vasculature preserve plasticity and are able to experience phenotypical switch from a very specialized contractile cell to a more synthetically and proliferative active cell called synthetic (Owens et al. 2004). Between these two extremes, vascular SMCs exert a spectrum of intermediate phenotypes, a plasticity that allows them to reprogramme its expression pattern and adapt to changes in the environment (Lacolley et al. 2012); by remodeling and new synthesis of the ECM, proliferation and changes in contractility. When this vascular SMC adaptation is misbalanced, arterial pathologies as aneurysms and hypertension occurs (Owens et al. 2004). The phenotypical switch is controlled by many transcriptional regulatory pathways that are common to vessel development and maturation as the ones that implicate PDGF, SRF and myocardin (Owens et al. 2004). Recently it has been reported that microRNAs (miRs) also regulate vascular SMCs differentiation and phenotype by targeting different signaling pathways; this is the case for example of miR-143-145 that promotes the maintenance of the contractile phenotype (Boettger et al. 2009) (Cordes et al. 2009).

Vascular SMC functions

Vascular SMCs in the arterial vasculature are embedded in a very specialized ECM mesh that confers the mechanical properties to the vessel wall and allows cellular mechanosensing (Schwartz 2010).

ECM synthesis and organization. The synthesis and organization of a unique ECM by vascular SMCs is considered its defining "differentiated" phenotype (Wagenseil and Mecham 2009). The ECM is a dynamic structure that vascular SMCs synthetize and organize during development, and is continuously suffering adaptive changes. The constitutive proteins of the arterial vessels are classified in structural and non-structural ECM components (Kelleher et al. 2004).

Structural ECM proteins: Large structural proteins form the scaffold of the arterial vasculature; this is the case of several members of the collagen family, different types of proteoglycans and elastin. This scaffold is subjected to high pressure and mechanical forces, and this matrix is designed to bear them and to protect the cells within the wall from the excessive stress (Wagenseil and Mecham 2009). Mechanical properties of the arterial wall mainly rely on fibrillar collagen and elastin fibers that account for the approximately 60% of dry weigh in aorta (Humphrey et al. 2015). Elastin is arranged at the media in fenestrated sheets called fibers or lamellae. Each fiber encircles the vessel in parallel with other elastin fibers. The elastic fiber is a multicomponent structure whose main protein in elastin (90%) that forms the core of the fiber, surrounded by microfibrils. Elastin is synthetized by SMCs during vessel development (around E14.5 in mice) from monomers of tropoelastin (Wagenseil and Mecham 2009) that contain hydrophobic sequences alternating with lysine-containing cross-linking motifs. In the extracellular space, tropoelastin monomers self-assembly in a process denominate coacervation. Then, lysil oxidase enzymes cross-link between and within tropoelastin monomers (Arribas et al. 2006) and needs to associate with parallel microfibrils that provide a scaffold for this cross-linking (Wagenseil and Mecham 2009). Microfibrils are constituted by fibrillin family proteins (fibrillin (Fbn) 1 and 2) and fibulins (fibulin 1, 4 and 5) (Kielty et al. 2002). The resulting elastin polymer is the functional form of the protein and is maintained along life (elastin half-life once cross-linked is around 50 years in humans) (Arribas et al. 2006).

In addition to the essential mechanical role, elastin also contributes to a contractile and quiescent vascular SMCs phenotype (Karnik et al. 2003). During aortic wall development, a proper elastin fibers organization that connects to the cells inhibits vascular SMC

proliferation as demonstrated in elastin (Eln) knockout mice that die by overproliferation of vascular SMCs that finally occlude the aortic lumen (Wagenseil and Mecham 2009). Elastic fibers also control growth factor availability since some microfibril components as fibrillin-1 sequester latent TGF-β (Hynes 2009).

Located between elastic fibers are collagen fibers that confer strength and stiffness to the arterial vessel wall. The two primary types of collagen in the arterial wall are fibrillar collagen I and III, the former is found mainly in the adventitia and the latter in the media (Humphrey et al. 2015). These collagen bundles show no definitive overall arrangement at low pressure but became circumferentially aligned as pressure increases to support wall tension and restrict aortic distension (Wagenseil and Mecham 2009). In fact, adventitial collagen acts as a protective sheath, bearing wall stress during acute increases in pressure, thus shielding medial SMCs from excessive stress (Humphrey et al. 2015). Opposite to elastin, collagen fibers in the aorta have a short half-life (perhaps months), and continuous collagen turnover is necessary for vessel homeostasis and needs to adapt in response to mechanical changes or responses to injuries (Humphrey et al. 2015).

Of the remaining percentage of arterial vessel wall composition, approximately 35% of the wall consists of vascular SMCs and between 3 to 5% is constituted by glycosaminoglycans that contribute to the compressive stiffness (Humphrey et al. 2015) and regulate SMC proliferation and differentiation and collagen fibrillogenesis (Kelleher et al. 2004).

Non-structural ECM proteins: In addition to the structural proteins, vascular cells must produce matrix macromolecules that are important for cell movement, polarization, and anchorage. These molecules, which include adhesive glycoproteins such as fibronectin, basement membrane components (laminin, nidogen), and the matricellular proteins that modulate cell–matrix interactions, provide important informational signals to cells that can influence gene expression and cellular function (Kelleher et al. 2004).

Matricellular proteins are a group of extracellular proteins, mediators in ECM-cell communication, that act as bridge between matrix proteins and the cells by binding to cell surface receptors as integrins (Humphrey et al. 2015). Among these are thrombospondins, tenascin protein family, SPARC/osteonectin and osteopontin (Kelleher et al. 2004).

Osteopontin: Osteopontin (OPN, also known as spp1, secreted phosphoprotein 1) is a multifunctional protein that belongs to the small integrin-binding N-linked glycoprotein (SIBLING) family. OPN is predominantly a secreted phosphorylated protein although an intracellular form has also been described (Zohar et al. 1997). As a bridge protein, OPN presents several domains (Figure 6) implicated in cellular and ECM binding:

(1) an arginine-glycine-aspartate (RGD)-containing domain that interacts with cell surface integrins ($\alpha_v\beta_1$, $\alpha_v\beta_3$, , $\alpha_v\beta_5$, $\alpha_v\beta_5$, $\alpha_8\beta_1$) (2) SVVYGLR cryptic domain that mediates the binding to $\alpha_9\beta_1$, $\alpha_4\beta_1$, and $\alpha_4\beta_7$ and is exposed after cleavage, and (3) the ELVTDFPTDLPAT sequence, reported to bind to $\alpha_4\beta_1$ (Scatena et al. 2007). On the other hand, through heparin sulfate binding-domains OPN also interacts to ECM components as fibronectin and collagen although the sequences implicates in these interactions are not yet established (Liaw et al. 1998) (Scatena et al. 2007). The association to elastic fibers has also been proposed based on the positive OPN immunostaining observed in elastin fibers by immunogold (Baccarani-Contri et al. 1995, Pasquali-Ronchetti and Baccarani-Contri 1997).

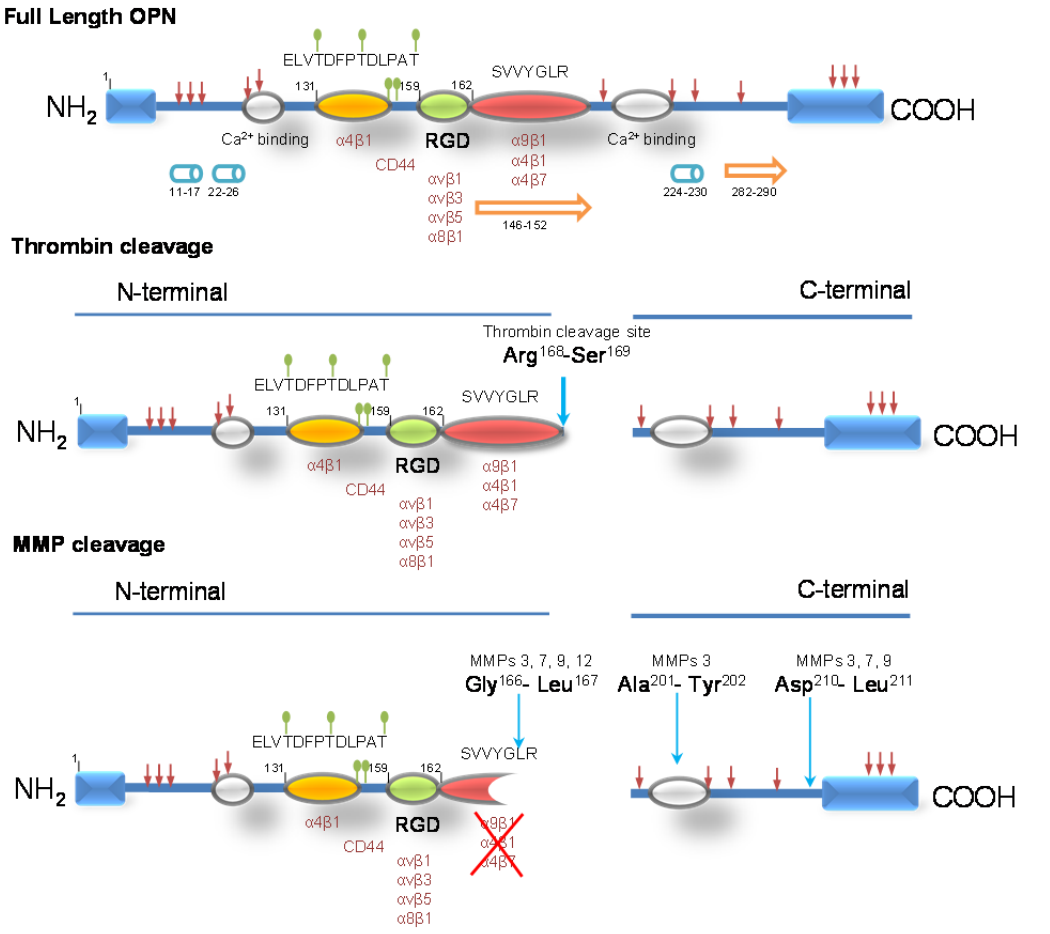

Figure 6. Osteopontin domains and modifications. Human Osteopontin (OPN) is depicted. Integrin binding domains are highlighted in colors and specific integrin interaction are indicated under the domains. Thrombin and MMP cleavage sites on OPN are highlighted also showing the generation of OPN N- and C-terminal fragments with different biological activity.

OPN function is to promote cell adhesion and to facilitate cell migration or survival through integrin/CD44 binding (Cho et al. 2009) (Okamoto 2007). Particularly, OPN is essential for SMC migration and adhesion mainly through $\alpha_v\beta_3$ interaction (Kazanecki et al. 2007a). These adhesive properties that determine the function, activity and signaling of OPN are regulated by cleavage, phosphorylation and glycosylation (Kazanecki et al. 2007a). OPN can be cleaved by thrombin, plasmin and cathepsin D and also is a substrate for MMP2, 3, 7, 9 and 12 producing two fragments with different activity (Scatena et al. 2007) (Agnihotri et al. 2001) (Christensen et al. 2010). Usually, the N-terminal OPN fragment generated after cleavage exerts increasing cellular binding either by the exposition of the cryptic site or by the increased in RGD accessibility. For example, N-terminal fragment generated by thrombin (Arg^{168}-Ser^{169}) exposes the SVVYGLR cryptic site in human (SLAYGLR in mouse), making the OPN N-terminal fragment more active in integrin binding than the full length OPN (Scatena et al. 2007). However, MMPs cleave at 3 different residues of the full length OPN including Gly^{166}-Leu^{167} of the SVVYGLR human sequence, compromising α_4/α_9 integrin binding of the resultant N-terminal OPN (Agnihotri et al. 2001) (Wolak 2014). On the other hand, the OPN C-terminal fragment is able to inhibit N-terminal OPN binding to αvβ3 integrin (Christensen et al. 2012). Proteases as thrombin fully degrades the C-terminal OPN impeding this C-terminal activity (Christensen et al. 2012).

In the arterial vessel wall OPN is expressed by ECs and vascular SMCs. In proinflammatory conditions it is also expressed by different inflammatory cells as macrophages (Okamoto 2007). In this regard, OPN levels are low in adult vessels (Bruemmer et al. 2003) (Isoda et al. 2002), and became upregulated in pathologies (Okamoto 2007) (Scatena et al. 2007) including hypertension, atherosclerosis, myocardial remodeling after infarct, vascular calcification and aneurysms (Okamoto 2007) (Scatena et al. 2007) (Bruemmer et al. 2003). As a matter of fact, OPN plasma levels are significantly associated with the presence and the extent of cardiovascular diseases (Golledge et al. 2007). In such cases, OPN expression can be induced by growth factors as TGFβ, PDGF and angiotensin II (Cho et al. 2009).

The generation of genetic modified mouse models of OPN shows the impact of OPN in the physiology of the vessel wall. *Opn*-null mice present decreased blood pressure values and more dilated vasculature in response to pressure, partially due a loosely organized collagen network when compared to wild-types (Myers et al. 2003). In a model of OPN transgenic mice, however, elastic fibers were destroyed in the adult aorta, and showed an increased

wall thickness (Isoda et al. 2002). Both examples show the physiologic role of OPN regulating ECM organization and cell behavior directly impacting in vessel wall homeostasis.

Vascular SMC mechanosensing and vessel wall adaptations: The arterial vessel wall is exposed to cyclic mechanical force, the ECM in which vascular SMCs are embedded bears most of the stress protecting the cells but also allows them to sense and respond to this forces (Schwartz 2010) (Humphrey et al. 2014). Vascular SMCs organized the ECM in a way that mechanical forces will be transmitted through the ECM scaffold to membrane integrins and the cellular cytoskeleton. In this way, SMCs sense the mechanical state of this matrix and transduce this information to intracellular signaling pathways directed to provide suitable compliance and yet sufficient strength to the vessel wall (Figure 7) (Wagenseil and Mecham 2009) (Humphrey et al. 2015).

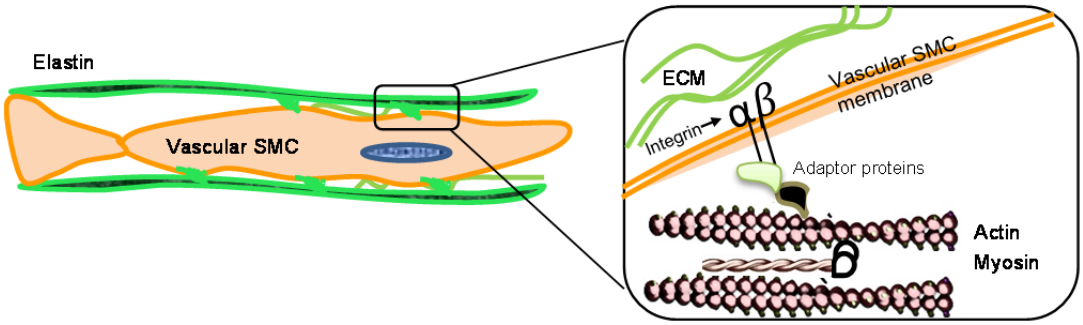

Figure 7. The mechanotransduction system in the arterial vessel wall. Contractile and cytoskeletal filaments containing actin and myosin contact the cytosolic tail of integrin at the membrane through adaptor proteinas (as talin, vinculin and filamin A). Integrins are membrane receptors that interact with different ECM components (as fibrillin present at the elastic fibers) triggering different signaling pathways implicated in the mechanosensing of the cells in the vessel wall.

Integrins are heterodimeric transmembrane complexes clustered at vascular SMC membrane in dense plaques/focal adhesions (Ross et al. 2013). In particular, vascular SMCs express $\alpha_1\beta_1$, $\alpha_2\beta_1$, $\alpha_3\beta_1$, $\alpha_5\beta_1$, $\alpha_7\beta_1$ and $\alpha_v\beta_3$ integrins. Some of them, as $\alpha_5\beta_1$ and $\alpha_v\beta_3$ integrins allow direct connection to elastic fibers through fibrillin-1 binding. These microfibrils tend to align coaxially to actomyosin fibers within the cells (Davis 1993). Therefore, depending on integrin expression and binding to different ECM components, cellular behavior can be altered, i.e. some integrins promote contractile phenotype through binding to laminin ($\alpha_7\beta_1$) and others synthetic phenotype through fibronectin binding ($\alpha_5\beta_1$, $\alpha_v\beta_3$, and $\alpha_v\beta_5$) (Humphrey et al. 2015). Apart from integrins, mechanosensing is also

mediated by membrane receptors as tyrosine kinase (eg, receptors epidermal growth-factor (EGF) and PDGF), serine-threonine (eg, TGF-β receptors type I and II) and G-coupled receptors (angiotensin II type I receptor) and stretch-activated cationic channels (Humphrey et al. 2015).

In physiological situation, the strain on the ECM stretches the vascular SMCs and generates a response of collagen synthesis. High-flow also increases endothelial cell shear inducing nitric oxide (NO) production. NO triggers vascular SMC relaxation, MMP synthesis, inhibits SMC proliferation and ultimately, induces apoptosis. Low-flow however induces mitogenic and fibrogenic growth factors production, such as PDGFβ, increasing vascular SMC proliferation, collagen synthesis/crosslinking and MMP production (Ward et al. 2000) This vessel remodeling is a homeostatic response to changes in the flow and circumferential stretch to restore normal shear stress and wall tension, respectively (Wagenseil and Mecham 2009).

Vascular SMC alterations in vascular pathologies

Vascular SMCs phenotypical adaptations in response to local environment signals consist on changes in their proliferation, migration, ECM synthesis, inflammatory signals production and/or cell calcification aimed at vessel wall homeostasis recovery (Owens et al. 2004).

Acute stimuli (i.e. increased blood pressure) produce a temporal adaptation of its phenotype, whereas chronic stimuli (i.e. sustained high blood pressure levels; hypertension) induce long term variations on vascular SMC gene expression and cell behavior. Pathological processes as hypertension, atherosclerosis (AT) and aneurysms rely on continuous changes in vessel wall homeostasis that have a direct impact in vascular SMC phenotype, together with other cell types alterations as ECs and macrophages (Lacolley et al. 2012). In this sense, during hypertension, for example, resistance vasculature contracts to encircle increased pressure and avoid dilation. If sustained, this stimulus led vascular SMCs to contract and synthetize an ECM composed mainly by collagen fibers that result in increased vessel wall stiffness. As a result, peripheral resistance is increased. Vessel remodeling in this case results in maladaptation that finally produces higher blood pressure levels and, if sustained, cardiac hypertrophy (Briones et al. 2010) (Renna et al. 2013) (Intengan and Schiffrin 2001).

During aneurysm generation however, vascular SMCs are unable to adapt vessel wall hemodynamics and these pathological distensions are generated by the overcome of the arterial wall strength. Aortic aneurysms accounts for 1-2% of deaths in industrialized countries. Most common forms, abdominal aortic aneurysms (AAA), are typically associated with age and metabolic problems, on the contrary, thoracic aortic aneurysms (TAA) afflict young people too and arise primarily from noninflammatory mechanisms that often are associated to hereditary influences (Lindsay and Dietz 2011) (Humphrey et al. 2014). In TAA, the progressive dilatation of the aorta can cause acute dissection and rupture (TAAD), causing life-threatening bleeding. This aortic wall weakening relies on dysfunctional mechanosensing and improper ECM remodeling by the vascular SMCs (Humphrey et al. 2015). In fact, the genetic mutations that predispose patients to TAADs affect as much structural components as cellular force generation and transmembrane structures that transduce mechanical stimuli (Humphrey et al. 2014). In this way, it has been described mutations in collagen type III (*COL3A1*), fibrillin-1 (Marfan Syndrome, MFS), SMA, SM-MHC, and TGF-β signaling pathways among other molecules (Humphrey et al. 2015). Although there is not a good defined mechanism of TAA generation, one possibility that explains how different mutations gets to the same phenotype is that a misinterpretation of high stress suffered by the vessel wall, due to alteration in the mechanosensing apparatus, would lead to the formation of defective structures and activate the degradative pathways observed in TAADs (Humphrey et al. 2015).

OBJECTIVES

Matrix metalloproteinases (MMPs) regulate extracellular matrix organization and are implicated in several pathologies. Mt4-mmp promoter is active in vascular SMCs with undescribed functions or substrates so far. We decided to study the possible role of this metalloproteinase in the pathophysiology of the arterial vessel wall using the Mt4-mmp-null mouse model.

We proposed the following specific aims:

1.- Define the role of Mt4-mmp in the arterial vessel wall by the study of the Mt4-mmp null mouse arterial vasculature;

2.- Identify and validate the possible Mt4-mmp substrates in the arterial vessel wall;

3.- Investigate the possible impact of MT4-MMP in human aortic pathology.

Materials and methods

MATERIALS AND METHODS

Animal model. *Mt4-mmp*$^{-/-}$ mice in the C57BL/6 background have been described previously (Rikimaru et al. 2007). Mice were handled under pathogen-free conditions in accordance with CNIC institutional guidelines. Experiments were performed in accordance with Spanish legislation on animal protection and were approved by the local governmental animal care committee. All mice were genotyped by PCR of tail samples using the following primers: *Mt4-mmp* SK1 5'-TCAGACACAGCCAGATCAGG-3' SK2 5'-AGCAACACGGCATCCACTAC-3' and SK3 5'-AATATGCGAAGTGGACCTGG-3'. Experiments were conducted on mice in three age groups: embryos (E10.5 to E18.5), neonates (P0 to P30), or male adults (8- to 26-weeks old).

Patient population. The study protocol was approved by the Committee for the Protection of Human Subjects at the University of Texas Health Science Center at Houston, and the study participants gave informed consent. Genomic DNA was extracted from peripheral blood lymphocytes using standard protocols.

EXPERIMENTAL PROCEDURES

Histological, LacZ and immunohistochemical studies. Aortas were excised after perfusion under constant pressure with 4% PFA, 2% sucrose in PBS (pressure-fixed aortas) or perfusion with PBS alone (non-pressure-fixed aortas). Aortas were then either embedded directly in OCT or further fixed for 12 hours and embedded in paraffin. Paraffin-embedded aorta cross-sections (7 µm) were stained with H&E, picrosirius red, alcian blue or Verhoeff-van Gieson stain. Aortic medial thickness, density of nucleus, lumen area, and elastin lamellae number were measured and quantified using MetaMorph software (Molecular Devices LLC. Sunnyvale, California). Aortic medial thickness was independently analyzed by two researchers blinded to sample identity. For LacZ analysis, OCT frozen sections (5 µm) of vessels and embryos were fixed in 0.125% glutaraldehyde in PBS for 5 minutes, rinsed in PBS and incubated at 37°C overnight in X-gal buffer (5 mM potassium ferrocyanide, 5 mM potassium ferricyanate, 2 mM $MgCl_2$ and 0.1% X-gal in PBS). Immunohistochemical staining for Mt4-mmp (PAB4785, Abnova, Taipei, Taiwan) was performed on OCT sections fixed in 4% PFA, 2% sucrose for 7 minutes; for SM-MHC (BT-562, Biomedical Technologies Inc., Alfa Aesar, Ward Hill, USA), calponin

(E798Y clone, ab46794, Abcam, Cambridge, UK), and anti- pH3 (06-570, Millipore, Billerica, USA), OCT sections were first permeabilized with 0.1% Triton X-100 for 5 minutes. Sections were then processed for incubation with specific secondary antibody and Hoechst stain. pH3-positive medial aortic cells were quantified by counting the number of positive vascular SMCs per transverse section. One to five sections were analyzed per mouse. For GFP analysis, overnight fixed (4% PFA) aortas were embedded in OCT and sections were stained with anti-GFP antibody (ab13970, Abcam). For analysis of aortas in embryos, E14.5 embryos were perfused and fixed overnight in 4% PFA, 2% sucrose solution followed by 30% sucrose solution for 3 hours. OCT sections were stained for Opn (AF808 polyclonal antibody, R&D, Minneapolis, USA), βGal (ab4761, Abcam), phospho-JNK (9255, Cell signaling, Danvers, USA) and CD31 (MAB1398Z, Millipore) followed by the specific secondary antibody (Alexa Fluor, Invitrogen). Images were acquired with Zeiss LSM 700 confocal microscope at 21-23ºC using 25X (LD LCI Plan Apo 25X/0.8) and 63X (Plan Apo 63X/1.4 oil DICII) objectives. Images were analyzed using Zen 2011 software (Zeiss, Jena, Germany) and maximal projections are shown (25X magnification). Quantification of phospho-JNK was performed using MetaMorph software.

RNA purification and quantitative reverse transcriptase PCR (Q-RT-PCR). Total RNA was isolated from E14.5 embryonic aortas, neonate or adult aortas, or cultured cells with the RNeasy® Mini Kit (Qiagen, Venlo, Netherlands). Aortas were first placed in lysis buffer and disrupted with sterile ceramic beads using a MagNA Lyser (Roche), with two rounds of 6500 rpm for 30 seconds each, with care taken to maintain the sample cold. RNA was quantified by spectrophotometry (ND1000 Spectrophotometer, NanoDrop, (Thermo Scientific, Wilmington, USA)) and RNA integrity was monitored by ethidium bromide staining after agarose gel electrophoresis. cDNA was synthetized from 1 µg of total RNA using the Qiagen Omniscript RT Kit (Qiagen). For determination of *Mt4-mmp* and *LacZ* expression in aortas the following primers were used in RT-PCR: *mMt4-mmp*: FW 5'-GAGTGGCTAAGCAGGTTTGG-3', RV 5'-TCCTCTTGCTCCATTTGGTT-3' and *lacZ*: FW 5'-ATCGTGCGGTGGTTGAACTG-3', RV 5'-TGCTGACGGTTAACGCCTCG-3'.
Q-RT-PCR was performed using TaqMan probes for mouse (m) *Mt4-mmp* (Mm00449292), human (h) *MT4-MMP* (Hs00211734), *mMt1-mmp* (Mm01318966), *mMt6-mmp* (Mm0139189), *mCnn1* (Calponin) (Mm00487032) and *mTgfβ2* (Mm00436955) in an ABI PRISM® 7900HT FAST Q-RT-PCR System. All samples were analyzed in triplicate, and RNA levels (CNRQ; calibrated normalized relative quantity) were obtained with

Biogazelle qBase PLUS software. For mouse analysis, *mGapdh* (99999915), *mTbp* (00446973) and *mHprt* (00446968) probes were used for normalization (Taqman). For human analysis, *hTFRC* (00951083_m1), *hHMBS* (00609297) and *hTBP* (00427621) housekeeping genes were used. SYBR green (Applied Biosystems, Carlsbad, USA) was used in the evaluation of contractile markers, *Opn* and in the study of MMPs and TIMPs expression. SYBR probes for the mouse genes were as follow:

Gene name	Forward primer (5'-3')	Reverse primer (5'-3')
Acta2 (SMA)	GCTATTCAGGCTGTGCTGTC	GGTAGTCGGTGAGATCTCGG
Myh11 (SM-MHC)	CCCCAACCATGAGAAGAGGT	TCGCTGCCAGGATCTCATAG
Spp1 (Opn)	AGCAAGAAACTCTTCCAAGCAA	GTGAGATTCGTCAGATTCATCCG
Mt1-mmp	CAGTATGGCTACCTACCTCCAG	GCCTTGCCTGTCACTTGTAAA
Mt6-mmp	CTCCTGCCCGTCTCTACTACC	GACCTTCGCATCGGGATTCTG
Mmp2	CAAGTTCCCCGCCGATGTC	TTCTGGTCAAGGTCACCTGTC
Mmp3	GGCCTGGAACAGTCTTGGC	TGTCCATCGTTCATCATCGTCA
Mmp7	CTTACCTCGGATCGTAGTGGA	CCCCAACTAACCCTCTTGAAGT
Mmp19	CTGTGGCTGGCATTCTTACTT	GGGCAGTCCAGATGCTTCC
Timp1	GCAACTCGGACCTGGTCATAA	CGGCCCGTGATGAGAAACT
Timp2	TCAGAGCCAAAGCAGTGAGC	GCCGTGTAGATAAACTCGATCTC
Timp3	CTTCTGCAACTCCGACATCGT	GGGGCATCTTACTGAAGCCTC
Timp4	TGTGGCTGCCAAATCACCA	TCATGCAGACATAGTGCTGGG
Gapdh (House keeping)	AATGCATCCTGCACCACCAA	GTGGCAGTGATGGCATGGA
Tbp (House keeping)	GCTCTGGAATTGTACCGCAG	CTGGCTCATAGCTCTTGGCTC

Protein extraction and western-blot analysis. Protein extracts were obtained from cell cultures as described (Sohail et al.). Briefly, cell monolayers were covered with cold lysis buffer (25 mM Tris-HCl [pH 8.0], 100 mM NaCl, 1% IGEPAL CA-630 and 60 mM Octyl glucoside) supplemented with 20 mM N-ethylmaleimide (NEM, Sigma-Aldrich) and protease inhibitors (Complete, Mini, EDTA-free, Roche). Descending aortas were disrupted with MagNA Lyser (Roche) in cold regular RIPA buffer or the specific Tris-based lysis buffer described above. Proteins (50 to 150 µg) were resolved by 7-12% SDS-PAGE in reducing or non-reducing conditions and transferred onto nitrocellulose

membranes (0.45 µm, Bio-Rad, Hercules, California). Antibodies against MT4-MMP (EP1270Y clone, ab51075, Abcam,), calponin (E798Y clone, ab46794, Abcam), SMA (ab5694, Abcam), tubulin (ab6160, Abcam,) and β-actin (A5441, Sigma-Aldrich,) were used at 1:1000 dilution. For Opn analysis in E14.5 embryos a pool of 8-to-10 aortas or a piece of cartilage were disrupted as before and resolved on 4-20% gradient gels (Bio-Rad). Antibody to Opn (18621, IBL, Fujioka, Japan) and was used at a 1:1000 dilution at 4ºC overnight. Immunoreactive proteins were visualized with corresponding fluorochrome-conjugated secondary antibodies (680 or 800 ODYSSEY IRDye®) and recorded by Licor Odyssey technology. Quantification of western-blot bands was performed using ODYSSEY software (LI-COR Biosciences, Lincoln, USA).

Myography experiments. Contractility of mouse aorta and first-order branches of the mesenteric artery was studied in a wire myograph as previously described (Martinez-Revelles et al. 2013). After a 30-min equilibration period in oxygenated KHS, arterial segments were stretched to their optimal lumen diameter for active tension development. Contractility of segments was then tested by exposure to a high-K^+ solution (K^+-KHS, 120). The presence of endothelium was determined by the ability of 10 M acetylcholine (ACh) to relax arteries pre-contracted with phenylephrine at 50% K^+-KHS contraction. Afterward, concentration–response curves to Ach were done. Vasodilator responses were expressed as a percentage of the previous tone generated by phenylephrine. The structural and mechanical properties of mesenteric resistance arteries were studied with a pressure myograph (Danish Myo Tech, Model P100, J.P. Trading I/S, Aarhus, Denmark). Briefly, the vessel was placed on two glass microcannulae and secured with a nylon surgical suture. After tying off any small branches, vessel length was adjusted so that the vessel walls were parallel without stretch. Intraluminal pressure was then raised to 120 mmHg and the artery was unbuckled by adjusting the cannula. The segment was then set to a pressure of 70 mmHg and allowed to equilibrate for 30 minutes at 37ºC in calcium-free KHS ($0Ca^{2+}$-KHS, prepared by omitting calcium and adding 10 mM EGTA). Intraluminal pressure was reduced to 3 mmHg. A pressure-diameter curve was obtained by increasing intraluminal pressure in 20 mmHg steps between 3 and 120 mmHg. Internal and external diameters were continuously measured under passive conditions (D_{i0Ca}, D_{e0Ca}) for 3 minutes at each intraluminal pressure. The final value used was the mean of the measurements taken during the last 30 seconds, when the measurements reached a steady state. Finally, the artery was set to 70 mmHg in $0Ca^{2+}$-KHS, pressure-fixed with 4% PFA in 0.2 mM phosphate buffer

[pH 7.2-7.4] at 37ºC for 60 minutes, and kept in 4% PFA at 4ºC for confocal microscopy studies. Passive structural and mechanical parameters were calculated from internal and external diameter measurements in passive conditions as follows: wall thickness, WT $=(D_{e0Ca}-D_{i0Ca})/2$ and circumferential wall stress ($(\sigma= (P \times D_{i0Ca})/(2WT)$, where P is the intraluminal pressure (1 mmHg = 1.334×10^3 dynes/cm^2) and WT is wall thickness at each intraluminal pressure in $0Ca^{2+}$-KHS. The content and organization of elastin and the number of vascular SMCs in mesenteric arteries were studied in pressure-fixed (70 mmHg), maximally relaxed intact segments using a confocal microscope (Briones et al. 2009). Briefly, stacks of images from the adventitia to the lumen (z step= 0.5 µm) were captured using the 488-nm line of the confocal microscope. A minimum of 2 image stacks from different regions was captured in each arterial segment. All the images were taken under identical conditions of laser intensity, brightness and contrast. Quantitative analysis was performed with MetaMorph image analysis software (Briones et al. 2009). Internal elastic lamina (IEL) thickness was measured from each stack of serial images. Thereafter, individual projections of the IEL were reconstructed and total fenestrae area was measured.

Magnetic resonance imaging. Magnetic resonance images were obtained in anesthetized adult mice (12 weeks old) using a Bruker Biospec 47/40 instrument (60 mm gradient, 35 mm internal diameter quadrature coil). Images were taken every millimeter in the descending thoracic and abdominal aorta and the lumen area was measured using Image J (NIH, http://imagej.nih.gov/ij/), (Schneider et al. 2012) and OsiriX software (Geneva, Switzerland).

Hemodynamic measurements. Tail cuff measurements of blood pressure were taken in groups of 10 mice per genotype and condition, using BP2000 (Visitech Systems, Apex, USA). Ten recordings of each conscious mouse were obtained after one week of training over 5 consecutive days at the same hour of the day. Average values were calculated for each mouse from the measurements recorded over the 5 days.

Transmission electron microscopy. Mice were anesthetized and trans-cardially perfused with Sörensen solution [pH 7.3] at 100 mmHg pressure (50 ml) followed by fixation solution (50 ml PBS containing 4% PFA and 1% glutaraldehyde) using a peristaltic pump (Dynamax, Rainin RP1, Mettler Toledo, Greifensee, Switzerland). Dissected arteries were additionally fixed in the same solution for 16 hours. Arteries were then embedded in resin

(Durcupan ACM Fluka, Sigma-Aldrich) for transverse or longitudinal sectioning, and ultrathin sections were cut and counterstained by the Electron Microscopy core (SIdI service) at the Universidad Autónoma de Madrid (Madrid). Sections were imaged using a transmission electron microscope (Jeol Jem 1010, 80Kv, Jeol Ltd. Tokyo, Japan) and recorded with a Gatan camera (Orius, SC200, Pleasenton, California) at the indicated magnifications. Vascular SMC phenotype was determined according to reported criteria (Boettger et al. 2009). Thoracic descending aortas and mesenteric arteries of adults or neonatal mice of each genotype and condition were visualized and used for morphological and ultrastructural analysis and for quantification of medial thickness in the case of the mesenteric arteries, with MetaMorph software.

Vascular SMC isolation and culture. Six to eight aortas from 8-week-old male mice were pooled to obtain a cell suspension (Fogelstrand et al. 2009). Briefly, after fat removal under a microscope, aortas were incubated in collagenase solution (collagenase type I, 3.33 mg/ml, Worthington, Lakewood, USA) for 5 minutes at 37ºC, allowing the removal of the adventitia with forceps. The aortas were then cut into small pieces (1-2 mm) and a cell suspension was obtained by incubation for 45 minutes at 37ºC in 6 mg/ml type I collagenase and 2.5 mg/ml elastase (Worthington) diluted in DMEM. Vascular SMCs were counted and cultured or used for flow cytometry. To check vascular SMCs size and complexity by flow cytometry, a cellular suspension was immunolabeled with CD31 (Millipore MAB1398) to allow exclusion of endothelial cells and analyzed in a flow cytometer (Fascanto II, BDBiosciences) equipped with FACs DiVa software to determine size and complexity. Cultured vascular SMC were plated on 0.02% gelatin-coated plates in DMEM supplemented with 20% fetal bovine serum (FBS) (Gibco, Invitrogen), 2 mM L-glutamine (Lonza, BioWhittaker, Basel, Switzerland), 0.1 mM nonessential amino acids (Sigma-Aldrich) and penicillin (50 UI/ml), streptomycin (50 µg/ml) (P/S) (Lonza, BioWhittaker). To perform monocultures to test *Mt4-mmp* expression, endothelial cells (mouse aortic endothelial cells, MAEC) were positively selected from the SMC culture with an antibody to intercellular adhesion molecule 2 (anti-ICAM-2; 553325 BD Biosciences, Franklin Lakes, USA) coupled to magnetic beads, and were cultured as indicated (Koziol et al. 2012). Macrophages were differentiated from bone marrow cells by treatment for 5 days with MCS-F (PeproTech) (10 ng/ml) in IMDM medium (Lonza) supplemented with 10% FBS. Vascular SMC morphology was analyzed at passage 0 by fixing cultures in 4% PFA, 2% sucrose for 10 minutes and staining with Texas Red®-X-

phalloidin (1:200; Invitrogen). Total cell area and shape factor or roundness (4πArea/Perimeter^2) were calculated by masking with MetaMorph software. Lentiviruses encoding GFP (Mock), N-term Opn or full-length Opn (see below) were incubated for 5 hours at 1-10 MOI (multiplicity of infection) with cultured vascular SMC (passage 0). After virus removal, GFP signal was analyzed at 24 h and 48 h (maximum of protein generation) after infection. Cells were fixed 48 h after virus infection in 4% PFA for 10 min and washed with PBS. Vascular SMC area and shape factor were evaluated in GFP-positive cells by analysis of confocal maximal projections (Zeiss LSM 700 confocal microscope) with Image J (NIH, http://imagej.nih.gov/ij/) (Schneider et al. 2012). Shape factor (or roundness) values close to 1 indicate a circular form, whereas values closer to 0 indicate an elongated object.

Second harmonic generation multi-photon microscopy. Autofluorescence of organized collagen (425-465 nm filter) and elastin auto-fluorescence (478-573 nm filter) was visualized in fresh aortic sections from wild-type or *Mt4-mmp*$^{-/-}$ adult mice with a Zeiss LSM 780 microscope (Spectra-Physics Mai Tai DS [pulse<70 ps] Laser). 3D rendering reconstruction of aorta thickness (Z stack between 35 and 54 µm) was performed using Imaris software (Bitplane, Switzerland).

Angiotensin II infusion by miniosmotic pump. 16-week-old mice were administered with angiotensin II by subcutaneous osmotic minipump infusion (Alzet DURECT Corporation, Cupertino, USA) as described previously (Esteban et al. 2011). Angiotensin II (Sigma-Aldrich) was administrated at 1 µg/kg/min during 28 days and blood pressure was monitored once a week by tail cuff. Aortic lumen diameter of ascending thoracic aorta and abdominal aorta was analyzed by high-frequency ultrasound with the VEVO770 system (VisualSonics, Toronto, Canada) For lumen diameter in thoracic ascending aorta, measurements after the valsalva sinus were performed. TAA was defined as $\geq$ 25% increase in aortic arch intraluminal diameter together with the presence of the following histological features: breakage and loss of elastin fibers, inflammatory infiltrate in the adventitia and/or media, vascular SMC loss, and thickening of the media on one side and thinning on the opposite site of the aortic section (Kanematsu et al. 2010). The abdominal aortic lumen diameter was measured approximately 1 cm before renal bifurcation. AAA was defined by intraluminal diameter of the abdominal aorta (suprarenal area) $\geq$ 1.3 mm together with the presence of pronounced ECM remodeling and thrombus (Daugherty et

al. 2001). After perfusion with 4% PFA and 2% sucrose in PBS, aortas were embedded in paraffin for histological analysis.

Carotid artery ligation. The left carotid artery was ligated as described previously (Kumar and Lindner 1997). Twenty-eight days later, mice were anesthetized and perfused with PBS (5 ml) and left and right carotid arteries were excised, embedded in OCT and frozen (for LacZ staining) or further fixed overnight in 4% PFA (5 ml, for 3 minutes), and embedded in paraffin. Ligated vessels were sectioned from the aortic arch to the beginning of the ligature, and morphometric analysis was performed along the whole vessel length (approximately 9 mm). H&E-stained paraffin-embedded sections were quantified for neointima or external area (external elastic layer area) using MetaMorph software. OCT sections were stained for Ki67 (ab16667, Abcam) proliferation marker at 1:100 dilution, followed by a fluorescent anti-Rabbit secondary antibody.

Proteomic analysis based on isobaric tags for relative and absolute quantitation (iTRAQ). Samples (200 µg) were trypsin-digested separately using the whole proteome in-gel digestion protocol (Bonzon-Kulichenko et al.). Peptide iTRAQ labeling was performed essentially according to the manufacturer's instructions. After labeling, the samples were vacuum-dried and redissolved in 1% trifluoroacetic acid for both desalting and removal of excess labeling reagent in reversed-phase C-18 extraction cartridges (Oasis, Waters Corporation, Milford, MA, USA). High-resolution analysis of iTRAQ-labeled peptides was carried out on an Easy nLC 1000 nano-HPLC apparatus (Thermo Scientific, San Jose, CA, USA) coupled to a linear ion trap Orbitrap mass spectrometer (Orbitrap Elite, Thermo Scientific). Peptides were suspended in 0.1% formic acid and then loaded onto a home-made C-18 reversed-phase nano-column (100 µm I.D., 45 cm) and separated in a continuous gradient consisting of 8-31% B for 180 min and 31-90% B for 2 min (B = 90% acetonitrile, 0.1% formic acid) at 300 nL/min. Peptides were ionized using a Picotip emitter nanospray needle (New Objective, Woburn, MA, USA). Each mass spectrometry (MS) run consisted of enhanced FT-resolution spectra (120,000 resolution) in the 390–1,200 m/z range followed by data-dependent MS/MS spectra of the 20 most intense parent ions acquired during the chromatographic run. The AGC target value in the Orbitrap for the survey scan was set to 1,000,000. Fragmentation in the linear ion trap was performed at 32% normalized collision energy with a target value of 10,000 ions. The full target was set to 30,000, with 1 microscan and a 100 miliseconds injection time, and the dynamic

exclusion was set to 0.5 min. For peptide identification the MS/MS spectra were searched with the Sequest algorithm implemented in Proteome Discoverer 1.3 (Thermo Scientific). The results were analyzed using the probability ratio method (Martinez-Bartolome et al. 2008), and a false discovery rate (FDR) for peptide identification was calculated based on the search results against a decoy database using the refined method (Navarro and Vazquez 2009). The iTRAQ reporter ion intensities were retrieved from MS/MS scans by QuiXoT software (Lopez-Ferrer et al. 2006, Ramos-Fernandez et al. 2007), and used as inputs to the weighted spectrum, peptide and protein statistical (WSPP) model (Navarro and Vazquez 2009), to obtain peptide and protein abundance changes. In a further step, proteins were classified into ontological categories according to the GO database, and abundance changes at the protein function level were analyzed as described (Navarro and Vazquez 2009). Protein or functional abundance changes were considered statistically significant when they had an FDR below 5%.

Proteomic analysis based on stable isotope labeling by amino acids in cell culture (SILAC). SILAC assay was performed as previously described (Koziol et al. 2012) in highly proliferative cells. Briefly, macrophages were differentiated from bone marrow cells from wild-type or *Mt4-mmp*$^{-/-}$ mice by treatment for 7 days with interleukin-3 (IL-3, PeproTech, Rocky Hill, USA), granulocyte macrophage colony-stimulating factor (GM-CSF, PeproTech) and stem cell factor (SCF, PeproTech) (20 ng/ml) in IMDM medium (Lonza) supplemented with 10% FBS, followed by incubation for 5 days with M-CSF (PeproTech) (10 ng/ml) in the same medium. Bone-marrow-derived macrophages were cultured in p100 plates (10 plates per genotype; pool of 3 mice per genotype) by seeding $6.5x10^6$ cells per plate in SILAC medium (Invitrogen) supplemented with penicillin/streptomycin, L-glutamine, Hepes and 10% bovine fetal serum, and isotopic amino acids (heavy Lysine and Arginine in wild-type, and light in *Mt4-mmp*$^{-/-}$). Supernatants (SN) were collected and processed as per the manufacturer's instructions. In brief, the SN of both genotypes were mixed 1:1 and enriched for glycosylated proteins by incubation with lectin WGA beads. Proteins were then reduced and alkylated, resolved by SDS-PAGE, and stained with colloidal Coomassie, and 20 bands were cut. Bands were processed at the Vall d'Hebron Research Institute (Barcelona, Spain), where proteins were digested with trypsin and the obtained peptides analyzed by mass spectrometry. The data obtained were analyzed with Protein Scape 2.1 and WARP-LC 1.2 software platform (Bruker, Billerica, USA).

In vitro digestion assay and N-terminal sequencing. Human recombinant OPN (500 to 2 µg; hrOPN, R&D, 1433-OP/CF) and the catalytic domain of human recombinant MT4-MMP (500 ng) (hrMT4-MMP, 475940, Calbiochem, Billerica, USA) were incubated in digestion buffer (50 mM Tris-HCl, 10 mM $CaCl_2$, 80 mM NaCl, [pH7.4]) for 2 hours at 37ºC. Samples were separated by 12% SDS-PAGE and transferred to nitrocellulose membranes (Bio-Rad 0.45 µm). Full-length OPN and fragments were detected with anti-C-terminal OPN antibody recognizing aminoacids 234 to 240 of the human OPN sequence (1H3F7) (Kazanecki et al. 2007b). An anti-mouse secondary antibody was used. N-terminal sequencing was performed according to Alphalyse guidelines (www.alphalyse.com/nterm_preparation_guideline.html, Palo Alto, USA). Briefly, 6 µg of hrOPN and 3 µg of hrMT4-MMP catalytic domain were incubated as described and the digestion mixture separated on a 4-16% Tricine gel (Mini-Protean® Tris-Tricine precast gel; Bio-Rad). Proteins were transferred to a PVDF membrane (Immobilon-PSQ, Millipore), and the obtained OPN C-terminal cleavage-derived band in the membrane was visualized by Coomassie staining and used for N-terminal sequencing.

Lentiviral vector generation and infection. Lentiviral vectors were generated using the mouse full-length *Mt4-mmp* vector (ID 5716458, Invitrogen) or the E248A mutant, using the QuikChange Site-Directed mutagenesis Kit (Agilent Technologies, Santa Clara, USA) with the following primers: Fw 5'-GTGGCCGTCCATGCGTTTGGTCATGCC-3' and RV 5'- GGCATGACCAAACGCATGGACGGCCAC-3'. Vectors were cloned into the SFFV-IRES-GFP lentiviral backbone and sequenced to check proper sequence mutation. Lentiviruses expressing Mock-GFP, Mt4-mmp-GFP or Mt4-mmp E248A-GFP were prepared and titered as previously described (Garaulet et al. 2013). Mouse full length *Opn* was obtained from Sino Biological Inc. (MG50116-M), and subcloned into the same lentivirus backbone. N-terminal *Opn* were obtained with the following primers: FW 5' GGATCCGCATGAGATTGGCAGTGA 3', RV 5' CTAAAGCTGGGGAACAG 3'. Analysis of lentivirus-driven protein production was first analyzed by infection in HEK293 cells. Lentiviruses were injected intravenously at approximately 1×10^8 pfu/ml. P1-stage mice were injected with ~10 µl of virus solution into the jugular vein after ice anesthesia, using a Hamilton syringe inserted through the neck skin. Mice were sacrificed 1 week (P8) or 8 weeks after injection. For injection into adult mice (8 weeks-old), 100 µl of virus solution (1×10^8 pfu/ml) was injected into the jugular vein after skin excision, and mice were sacrificed 8 weeks later. Aortas were collected and processed for protein extraction,

RNA extraction, microscopy or electron microscopy analysis according to the protocols described above.

Exome and Sanger sequencing. Five µg samples of DNA from probands were used for construction of the shotgun sequencing library using adaptors for paired-end sequencing (Regalado et al. 2011). Exome sequences were captured with SeqCap EZ. Exome probes version 1.0 (Roche, Basilea, Switzerland) and recovered according to manufacturer's directions. Enriched libraries were then sequenced on an Illumina (San Diego, USA) GAIIx. Reads were mapped to the reference human genome (UCSC hg19, Santa Cruz, USA) with BWA (Burrows-Wheeler Aligner) (Li H. and Durbin 2010), and variants called with SAMtools. Insertion-deletion (indel) variants affecting the coding sequence were identified after a Smith-Waterman realignment of the BWA calls. Single nucleotide variants (SNVs) and indels were filtered to >8X and quality >30. Variants were annotated using the SeattleSeq server (http://gvs.gs.washington.edu/SeattleSeqAnnotation/). The identified variants were then filtered against the NHLBI Exome Sequencing Project to exclude variants with minor allele frequencies (MAF) above 0.005 for indel and SNV calls to identify novel non-synonymous and splice-acceptor and donor-site variant that was present as heterozygous genotype. Bidirectional DNA sequencing of *MT4-MMP* variants were done using primers designed 60-120 base pairs from the variant. Polymerase chain reaction (PCR) amplifications were carried out using HotStar TaqTM DNA polymerase (Qiagen Inc.Valencia, CA). PCR products were treated with EXOSAP-IT (Affymetrix, Inc. OH) to digest the primers and followed with sequencing PCR using the BigDye™ sequencing reaction mix (Applied Biosystems, CA). The sequencing PCR products were purified using the BigDye XTerminator kit (Applied Biosystems, CA) and then loaded on an ABI3730xl sequencing instrument using the Rapid36 run module. DNA sequencing results were analyzed using the Mutation Surveyor software (SoftGenetics, PA).

MT4-MMP *in silico* modeling. A theoretical model of the MT4-MMP protein was calculated using the *de novo* prediction method with the structural homologs comparison approach. The Fasta sequence (603 aminoacids (aa)) of the MT4-MMP protein precursor (UniProtKB: Q9ULZ9.4) was processed to eliminate the signal peptide and pro-peptide sequences and yield a new sequence for the mature wild-type protein (440 aa: positions 126 to 565 of the precursor protein). A similar process was used with a point mutation (R373H) in the precursor protein sequence. Both MT4-MMP sequences were submitted to

the iTASSER server (http://zhanglab.ccmb.med.umich.edu/I-TASSER/) (Roy et al. 2010). We selected the PDB (Protein Data Bank) model with highest probability and minimal energy compatible with biochemical properties (di-S intrachain, accessible and exposed glycosylation sites and accessible active region [active site and neighboring zinc binding sites] C-score= -0.43 for wild-type (WT) and C-score= -0.18 for R373H-mutant). Both models were aligned, visualized and decorated using PyMol v1.6.0.0. *In silico* models of wild-type and R373H-mut MT4-MMP homodimers were calculated by submitting PDB models of monomeric MT4-MMP or monomeric MT4-MMP-R373H to Hex server v 6.9 (http://hexserver.loria.fr/) (Ghoorah et al. , 2013). Docking in dimer mode was predicted with shape and electrostatic restrictions to select the best (minimal energy) model of each dimer type compatible with biochemical properties (di-S interchain) (Sohail et al.). Docking predictions for the MT4-MMP dimer (WT) as receptor and OPN as ligand were submitted to the ClusPro server (http://cluspro.bu.edu) (Comeau et al. 2004), and the best model compatible with the biological topology of the MT4-MMP binding site was selected. The model was then refined by closer pre-alignment of the MT4-MMP dimer to the binding site using PyMol v 1.6.0.0, and this refined preliminary model was submitted to the docking application of the ROSIE server (http://rosie.rosettacommons.org) with default values. From the ten models with the lowest energy, we selected the model with best topology (and smallest binding distance, score = -770.875).

MT4-MMP R373H generation and HEK293 transfection. The human *MT4-MMP*-PSG5 vector was mutated with the QuikChange Site-Directed Mutagenesis Kit (Agilent Technologies, Santa Clara, USA) to yield the hMT4-MMP R373H mutant. The following primers were used: Fw 5'-GGCACAGATGCACCACTTCTGGCGGG-3' and Rv 5'-CCCGCCAGAAGTGGTGCATCTGTGCC-3'. HEK293 cells (80% confluence) were transfected over 3 hours with wild-type or R373H-mutated MT4-MMP vectors using Lipofectamine 2000 (Invitrogen, Waltham, USA), and expression was analyzed during the subsequent 24 hours. The transfected cells were treated with 100 µg/ml bortezomib (Sigma-Aldrich, St. Louis, USA) for 24 hours. Protein and RNA were extracted as described before. For immunofluorescence assay, HEK293 cells were fixed for 10 minutes in 4% PFA in PBS and permeabilized with 0.1% Triton X-100 for 5 minutes. The anti-human MT4-MMP antibody (M3684, Sigma-Aldrich) was used at 1:100 dilution followed by secondary anti-rabbit antibody and cells were visualized under a Zeiss LSM 700 microscope. Figure panels show maximal projections of confocal images.

Statistical analysis. The statistical analysis performed in each case is explained in detail in the corresponding figure legend. Data were analyzed by two-tailed Student's *t*-test or by one- or two-way ANOVA followed by the indicated comparison test for data with Gaussian normal distribution. Non-normal distributions were analyzed by Wilcoxon test, Mann-Whitney test, or by one sample t-test for fold-induction comparisons. The one-tailed Fisher's exact test was used to analyze the incidence of aneurysm. For comparison of different groups or conditions, one- or two-way ANOVA was used, followed by the indicated comparison test in each case (Bonferroni or Tukey multiple comparison tests). Statistical tests were conducted with Prism 5 software (GraphPad Software, Inc., La Jolla, USA). Data are presented as mean ± s.e.m. and differences were considered statistically significant at $p < 0.05$: *p value < 0.05, ** p value < 0.01, and *** p value < 0.001.

Results

RESULTS

-MT4-MMP IS EXPRESSED BY VASCULAR SMOOTH MUSCLE CELLS DURING AORTIC WALL DEVELOPMENT -

The generation of the *Mt4-mmp*$^{LacZ/LacZ}$ mice (referred here as *Mt4-mmp*$^{-/-}$) (Rikimaru et al. 2007) allowed us to study *Mt4-mmp* expression *in vivo*, specifically in the arterial vasculature. *LacZ* expression (representative of *Mt4-mmp* promoter activation) was evaluated first by RT-PCR showing the presence of *LacZ* and the absence of *Mt4-mmp* transcripts in total aortic lysates (Figure 8 a). Quantitative RT-PCR (Q-RT-PCR) and western blot confirmed the lack of *Mt4-mmp* mRNA transcript and protein, respectively, in *Mt4-mmp*-null mice aortas (Figure 8 b and c).

Mt4-mmp expression in the arterial vasculature was then analyzed during aortic vessel wall development by LacZ staining of embryonic aortas. LacZ positive staining was observed since early developmental stages (E10.5 and E12.5) in scattered endothelial cells, that presumably form the primordial tube and some vascular SMC progenitors that are recruited to the developing aorta (Figure 8 d). At E14.5, the aortic media layer was already visible formed by 3-4 vascular SMCs layers with *Mt4-mmp* promoter activation in most of the cells of the wall. At E16.5 and E18.5, LacZ staining was reduced to some scattered vascular SMCs.

As a complementary approach, *Mt4-mmp* expression was confirmed using an anti-βGal antibody (Figure 8 e). mRNA was then isolated from aortas at the different stages of aortic development and maturation from E14.5 to 2 months of age. As showed in Figure 8 f, *Mt4-mmp* relative expression follows a pattern from relatively medium levels at E14.5, decreased at P0 and progressively increased levels till adulthood.

In adult aortas, we further confirmed Mt4-mmp protein expression by specific immunostaining, showing positive signal located at the media layer of the vessel (Figure 9 a). To confirm the cellular type expressing Mt4-mmp in the vessel wall, we next performed cultures of ECs, vascular SMCs and macrophages. Using *Mt4-mmp* specific primers, we showed by Q-RT-PCR that vascular SMCs were the cellular type expressing highest *Mt4-mmp* levels (Figure 9 b).

By LacZ staining we also showed *Mt4-mmp* promoter activation in vascular SMCs of other vascular beds analyzed as mesenteric arteries and coronary arterioles (Figure 9 c).

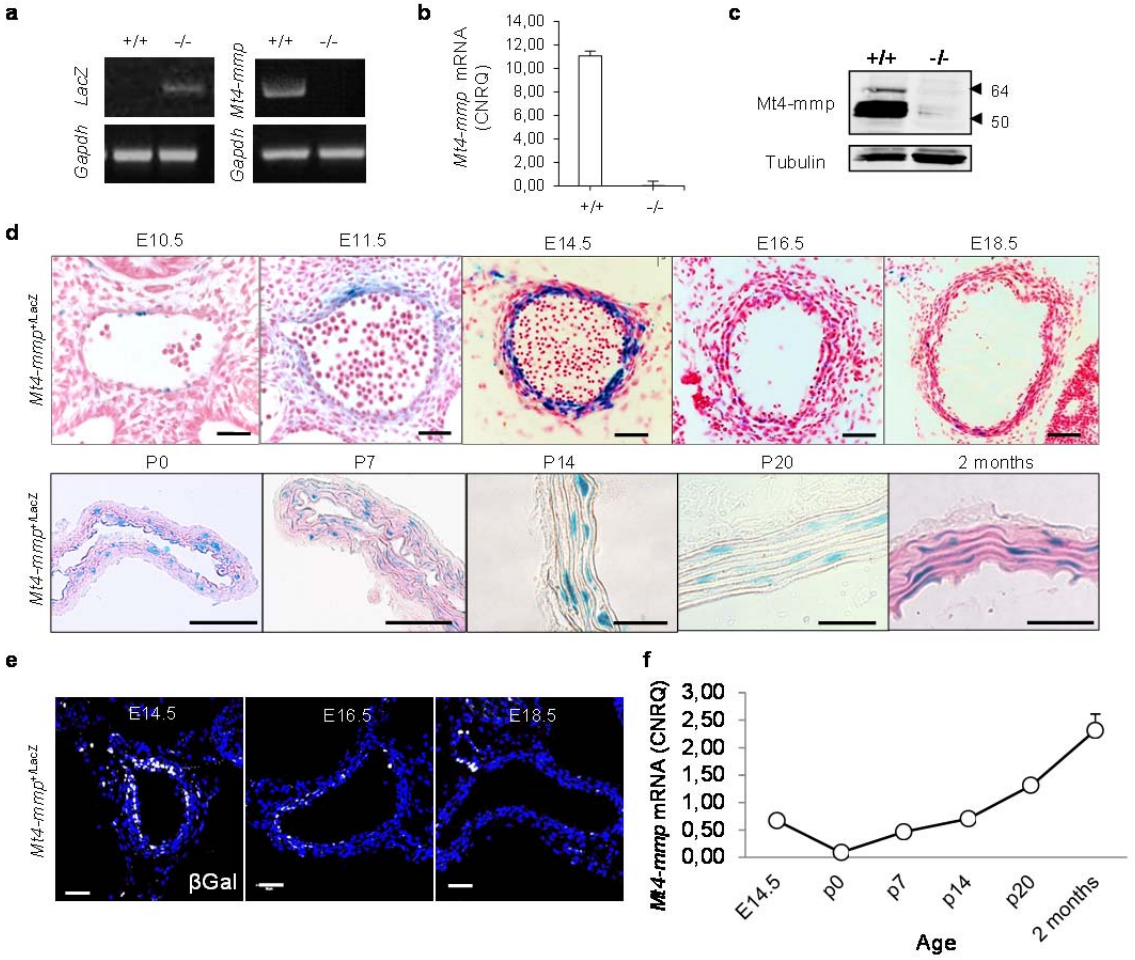

Figure 8. Mt4-mmp is expressed in the aorta during development. (**a**) RT-PCR of aortic lysates shows presence of *Mt4-mmp* transcript only in wild-type aortas and *LacZ* only in *Mt4-mmp*$^{-/-}$ mice. n = 6 mice per genotype analyzed in 2 independent experiments. (**b**) Q-RT-PCR of wild-type and *Mt4*-mmp$^{-/-}$ aortas showing relative expression of *Mt4-mmp* transcript presented as calibrated normalized relative quantity (CNRQ) obtained in qBase analysis. n = 9 mice per genotype analyzed in 3 independent experiments. (**c**) Representative western-blot showing absence of Mt4-mmp protein in null mice aorta lysates. n = 16 mice per genotype analyzed in 5 independent experiments. **(d)** Representative images of LacZ staining in aortas from *Mt4-mmp*$^{+/LacZ}$ embryos, neonates and 2 month old mice. n = 2 mice per time point. Scale bar 20 µm in embryo and P14, 50 µm in P0 and P7 images, and 25 µm in 2 months-old picture. (**e**) Representative confocal microscopy images of E14.5, E16.5 and E18.5 *Mt4*-mmp$^{+/LacZ}$ embryo aortas showing anti-βGal nuclear immunostaining (white) and nuclei Hoechst (blue). n = 2-3 mice per time point. Scale bar 50 µm. (**f**) *Mt4-mmp* mRNA levels in aortas from E14.5 to 2 months old mice. n = 2 to 8 aortas per time point. Grapics in **b** and **f** represents means ± s.e.m of CNRQ.

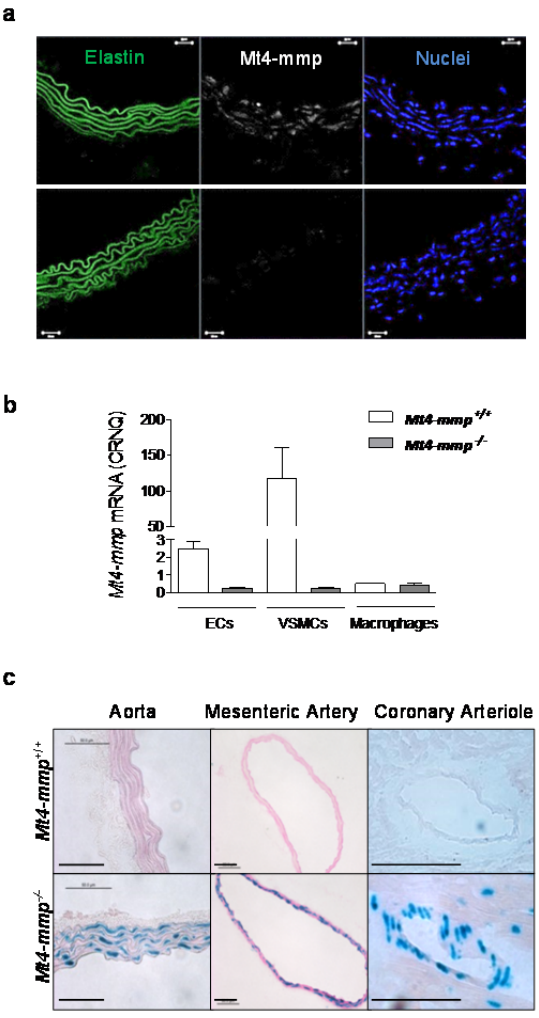

Figure 9. **Mt4-mmp is expressed by vascular SMCs in the arterial media layer**. (**a**) Representative confocal images showing Mt4-mmp immunostaining in transversal cuts of thoracic descending aortas. Scale bar 20 µm. n = 5 mice per genotype analyzed in 2 independent experiments. (**b**) Graphs show Q-RT-PCR of cultured endothelial cells, vascular SMCs and macrophages. One representative experiment is shown from 3 independent experiments with similar results. n = 8 mice per genotype and experiment. Bars are means of ± s.e.m of CNRQ. (**c**) Representative images of LacZ staining in transversal cuts of arterial vessels showing positive nuclear β-Gal activity. Scale bar 50 µm. n = 5-10 mice per genotype tested in 3 independent experiments.

- MT4-MMP ABSENCE INDUCES VASCULAR SMC MORPHOLOGICAL DEFFECTS AND ECM ALTERATIONS IN THE CONDUCTANCE ARTERIAL VASCULATURE-

To determine the impact of Mt4-mmp loss in the vessel wall, we first analyzed the histological features of conductance vasculature, performing transverse cuts of adult aortas fixed or not under pressure. No differences in vessel wall thickness were observed by H&E staining in pressure-fixed aortas (Figure 10 a), however, same analysis in non-fixed aortas showed increased vessel wall thickness suggestive of alterations in structural organization of the wall (Figure 10 b). To address this point, a more detailed analysis of aortic ultrastructural features was performed using transmission electron microscopy (TEM) that revealed mayor changes in vascular SMCs morphology and orientation and ECM organization within the wall (Figure 10 c). Vascular SMC alterations found in *Mt4-mmp*-

null aortas included round, instead of elongated, morphology, thinner ECM connections, multilayered number of vascular SMCs between elastic fibers and helically/radially oriented cells in contrast to the circumferential orientation in wild-type aortas. Also the presence of intracellular vacuoles was more commonly observed in *Mt4-mmp*$^{-/-}$ aortas (Figure 10 c). Similar ultrastructural features were observed when one of the Mt4-mmp alleles was knockout in the heterozygous mice (Supplemental information).

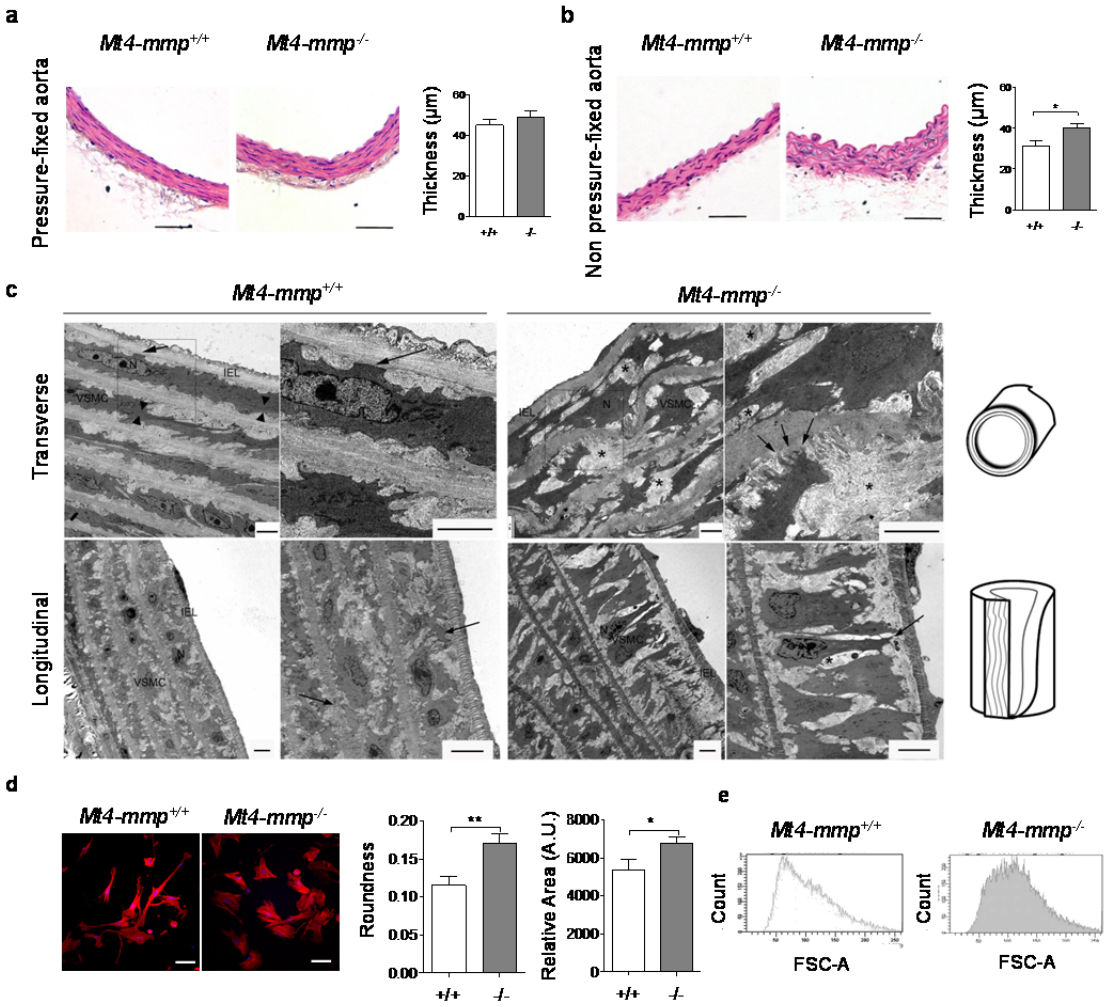

Figure 10. ***Mt4-mmp*$^{-/-}$ aortas contain morphologically aberrant and mis-oriented vascular SMCs.** (**a** and **b**) Representative images of transverse sections of thoracic aorta from wild-type and *Mt4-mmp*$^{-/-}$ mice stained for H&E fixed under pressure (left) or not. Media layer thickness and its quantification is represented; n = 4-5 mice analyzed per genotype in **a** and 15 mice per genotype analyzed in 3 independent experiments in **b**. Scale bar 50 µm. (**c**) Representative TEM images of ultrathin transverse (top) and longitudinal (bottom) sections of thoracic aorta. Note the differences in vascular SMC morphology, cell-ECM connections (arrows), and cell-cell connections (arrowheads) between wild-type and *Mt4-mmp*$^{-/-}$ aortas. *Mt4-mmp*$^{-/-}$ mice also showed ECM (asterisks) and frayed elastin layers (inset, right panel). Scale bar 4 µm. n = 10 mice per genotype in transversal and 2 in longitudinal. IEL, internal elastic lamina; N, nuclei. (**d**) Representative epifluorescence microscopy images from cultured vascular SMCs stained for F-actin (phalloidin, red). Scale bar 10 µm. Cellular area and roundness quantified in cultured vascular SMCs isolated from wild-type or null aortas (A.U. arbitrary units). n = 5 independent experiments performed, 100 cells quantified per genotype. (**e**) Flow cytometry histograms show cellular size distribution (FSC-A) of vascular SMC freshly isolated from wild-type or *Mt4-mmp*$^{-/-}$ aortas. n = 8 mice per genotype. Numerical data in **a**, **b** and **d** are means ± s.e.m., and were tested by unpaired Student's *t*-test (* $p<0.05$, ** $p<0.01$).

The rounder morphology of null vascular SMCs was confirmed in early passage cultured vascular SMCs isolated from *Mt4-mmp*$^{-/-}$ aortas (Figure 10 d) where larger cellular size was also observed (Figure 10 e). In the same sense, flow cytometry analysis showed a larger average cell size (Forward scatter channel, FSC) in the case of vascular SMCs isolated from null aortas (Figure 10 f).

Since vascular SMC round morphology might be indicative of a synthetic phenotype (Boettger et al. 2009), we further analyzed the expression of contractile markers in wild-type versus null mouse aortas. No differences were observed by western blot in protein levels of SMA, calponin between genotypes (Figure 11 a and b) however, the distribution of contractile protein calponin and SM-MHC in wild-type aortas presented a continuous staining pattern along the vessel compared to discontinuous pattern observed in the null mice (Figure 11 c) indicative of a different cellular distribution/organization.

Related to the multilayered vascular SMCs between elastic fibers, the number of vascular SMCs was quantified showing higher density of cellular nuclei in *Mt4-mmp*-null aortic media (Figure 11 d). In accordance with this result, significantly higher number of vascular SMCs was isolated from null mice aortas compared to wild-types (Figure 11 e). No differences in proliferation by phospho-histone-H3 (pH3), Ki67 staining or BrdU assay were observed, or in apoptosis by TUNEL assay in adult aortas (data not shown).

As shown in Figure 10 c, Mt4-mmp loss also altered vascular SMC-ECM interaction showing smaller and line-like connections between vascular SMCs and elastin layers. ECM was also affected in null aortas, presenting increased fibrillar matrix deposition, cellular debris and frayed elastin layers more observed commonly in *Mt4-mmp*-null aortas. Study of ECM main components by specific staining however revealed no differences in elastic fiber number in ascending and descending thoracic aortas, as well as no differences in proteoglycan amount (Figure 12 a to c). On the contrary, fibrillar collagen was increased in the adventitial area as shown by second harmonic generation (SHG) (Figure 12 d and e).

Taking these data together indicates that the overall disposition of vascular SMCs and the ECM organization is affected in the null aortas. We then decided to determine the functional impact of these defects in vascular performance.

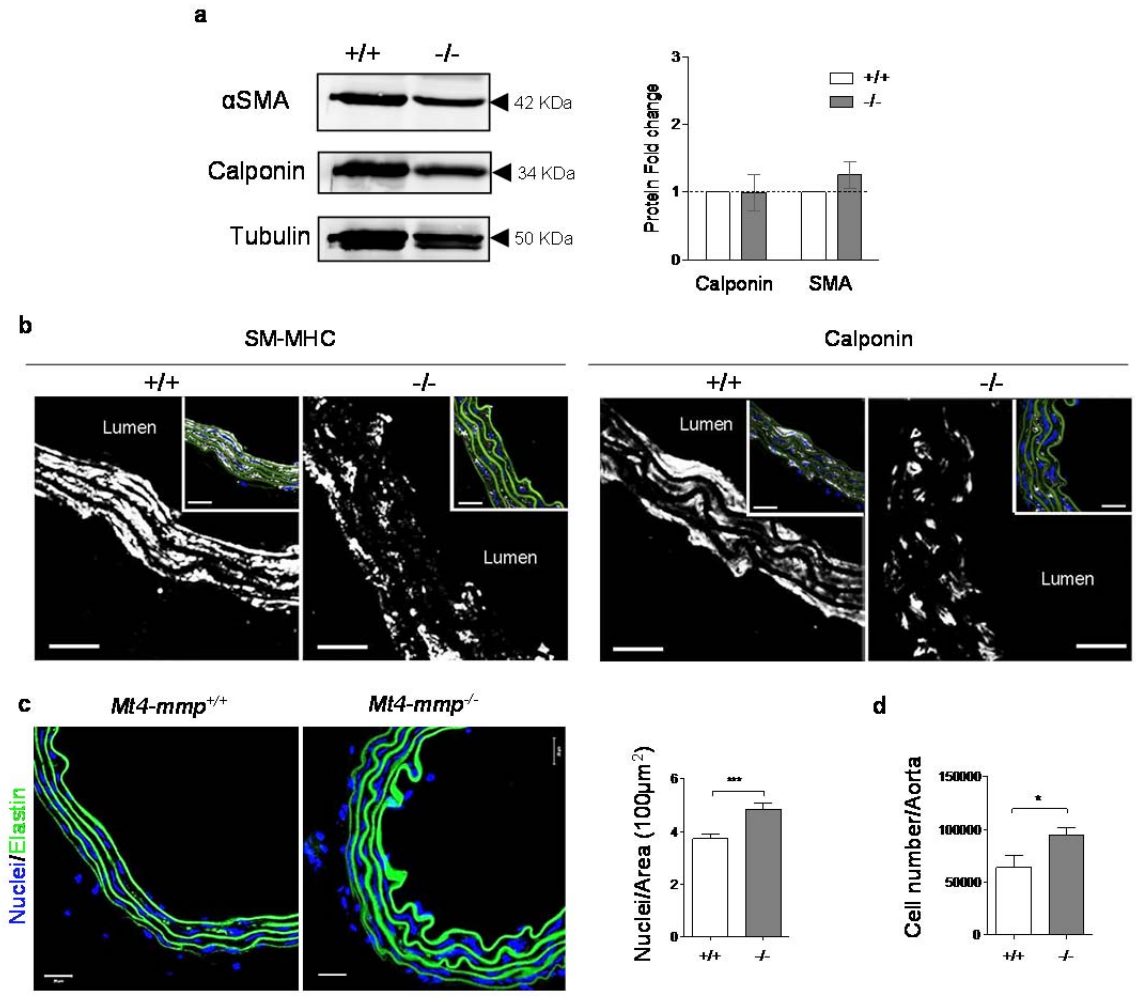

Figure 11. Mt4-mmp loss affects vascular SMC contractile protein distribution. (**a**) Representative western-blot of αSMA, calponin and tubulin as control (left) from adult aortas lysate. Bars represent western-blot quantification of aorta total lysates. n = 2-3 pooled aortas in 2 independent experiments. (**b**) Representative confocal microscopy images of SM-MHC and calponin staining (white), elastin auto-fluorescence (green) and nuclear Hoechst staining (blue) in transverse aortic sections from wild-type or *Mt4-mmp*$^{-/-}$ mice. Scale bar 20 µm. n = 7 mice per genotype. (**c**) Representative confocal pictures of thoracic aortas showing nuclei (blue) and elastin (autofluorescence, green) (left). Quantification of nuclei density showed higher number of vascular SMCs in null mice aortas (right). n = 30 mice per genotype. (**d**) Bars represent quantification of number of vascular SMCs isolated from wild-type and *Mt4-mmp*$^{-/-}$ aortas. n = 8 aortas pooled per experiment and genotype analyzed in 7 independent experiments. Numerical data are means ± s.e.m., and were tested by one sample *t*-test in **a** and unpaired Student's *t*-test in **c** and **d** (* $p<0.05$, *** $p<0.001$).

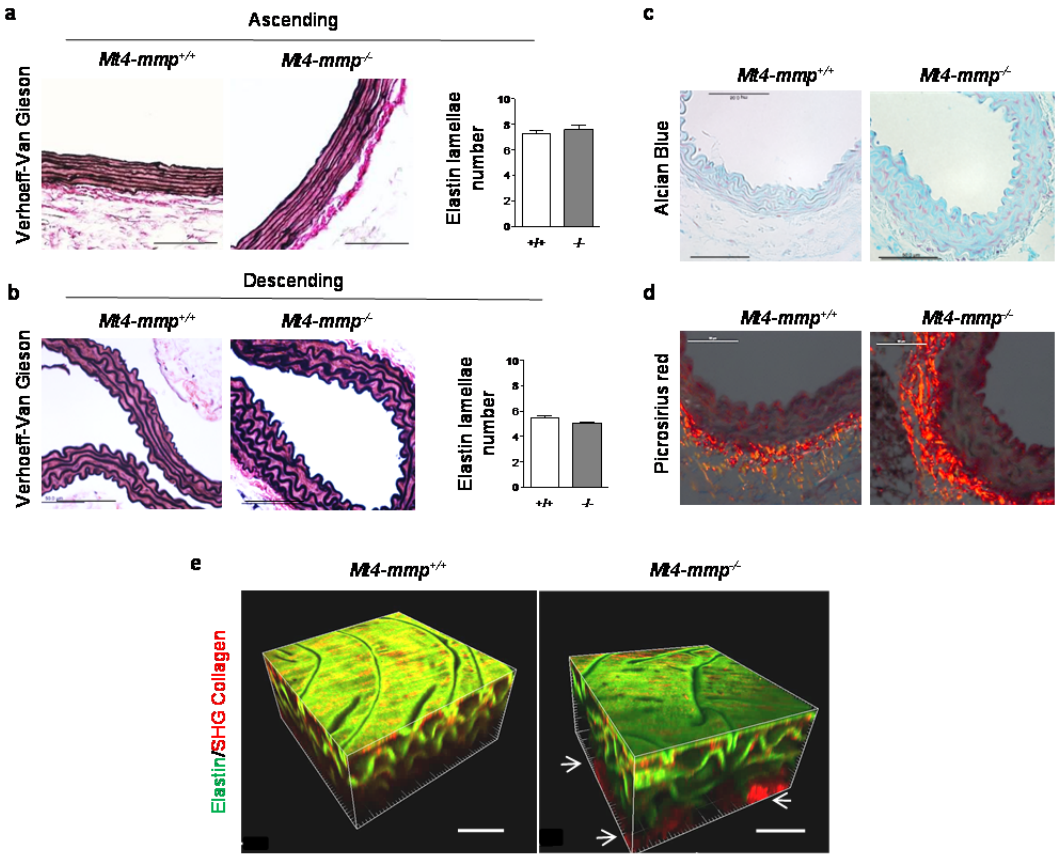

Figure 12. Increased fibrillar collagen deposition in *Mt4-mmp*$^{-/-}$ aortas with no changes in other structural ECM proteins. (**a** and **b**) Representative images of Verhoeff-van Gieson stain in thoracic ascending (**a**) and descending (**b**) aortas revealed no differences in the number of elastin layers. n = 5 (pressure-fixed) to 15 (non-pressure fixed) mice, respectively, analyzed in 3 independent experiments. Scale bar 50 µm. (**c** and **d**) Representative images of transverse sections of thoracic aortas from wild-type and *Mt4-mmp*$^{-/-}$ mice stained for proteoglycans (Alcian blue) or collagen (picrosirius red) in polarized light. Scale bar 50 µm. n = 4 to 8 mice per genotype. Scale bar 50 µm. (**e**) 3D-rendering reconstruction of second harmonic generation multi-photon microscopy images from wild-type and *Mt4-mmp*$^{-/-}$ aortas (SHG fibrillar collagen in red, and auto-fluorescent elastin in green). Arrows point to collagen deposits in the adventitia of null mice (n = 4 mice per genotype analyzed in 3 independent experiments). Scale bar 30 µm. Numerical data are means ± s.e.m., and were tested by unpaired Student's *t*-test.

-MT4-MMP LOSS IN THE CONDUCTANCE ARTERIAL VASCULATURE LEADS TO DILATED VESSELS-

Since ECM organization/vascular SMC phenotype define vessel wall hemodynamics and behavior, we next evaluated aortic performance. First, aortic contractility was investigated using an *ex vivo* wire-myograph assay. In response to total depolarization by potassium, null aortas showed a trend towards less contractile strength (wild-type 2.96 ± 0.47 *vs* 2.51 ±

0.32 mN in *Mt4-mmp*$^{-/-}$, a reduction of 15.21%) (Figure 13 a). Endothelial-induced relaxation was preserved in *Mt4-mmp*-null aortas, as shown by acetylcholine (Ach) response (Figure 13 a).

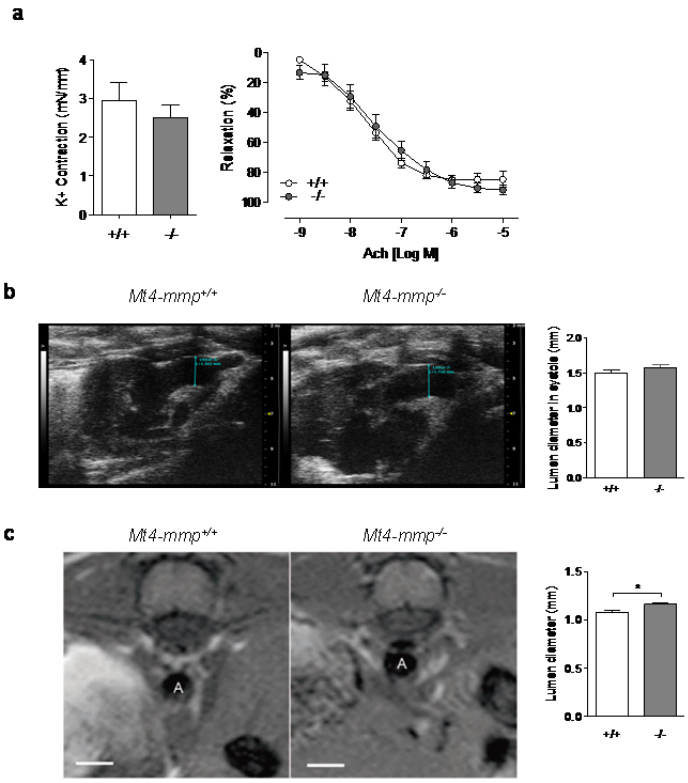

Figure 13. *Mt4-mmp*$^{-/-}$ mice aortas have increased lumen diameter (**a**) Aortic contraction in response to total depolarization by potassium (K^+). Endothelial integrity was assessed by relaxation in response to Acetylcholine (Ach) (right). n = 4-5 mice per genotype. (**b**) Representative images of echocardiography in adult aortic arch (ascending thoracic aorta). Bars represent lumen area (right). n = 8 mice per genotype. (**c**) Representative magnetic resonance images of thoracic descending aorta (left) and lumen diameter quantification (right) in wild-type or *Mt4-mmp*$^{-/-}$ adult mice (12 weeks old; n = 8 mice per genotype). A, aorta lumen; scale bar 1 mm. Numerical data are means of ± s.e.m. and were tested by unpaired Student's *t*-test (**a** (left), **b** and **c**) and two-way ANOVA followed by Bonferroni post-test in **a** (right).

For *in vivo* analysis, we used complementary approaches; ascending thoracic aortas were monitored by echocardiography, showing a trend to increased lumen diameters (Figure 13 b). Due to the limitation of the echocardiography technique for thoracic descending aorta recording (the ribcage hampers aortic display), we used instead magnetic resonance imaging (MRI) (Figure 13 c). Null mouse thoracic descending aortas showed a statistically significant increase in lumen area compared to wild-type (1.076 ± 0.026 mm^2 in wild-type

vs 1.159 ± 0.018 mm^2 in *Mt4-mmp*$^{-/-}$) (Figure 13 c). Also arterial performance was affected as shown in the supplemental videos (video 1 for wild-type and video 2 for *Mt4-mmp*$^{-/-}$).

- MT4-MMP LOSS IN THE RESISTANCE ARTERIAL VASCULATURE RESULTS IN STRUCTURAL ALTERATIONS AND VESSEL DILATION-

The fact that Mt4-mmp is also expressed in the resistance vasculature (Figure 9 c), prompted us to analyze the possible impact of Mt4-mmp absence in this type of vasculature. TEM images of mesenteric arteries showed similar features to thus found in aorta. We observed rounder and bigger vascular SMCs with fibrillar ECM deposits (Figure 14 a). Wall thickness and vascular SMCs density was increased in null mesenteric arteries (Figure 14 b). Mesenteric artery contractility was then evaluated by wire myograph to measure vessel wall strength. In response to potassium depolarization mesenteric arteries also exert a trend towards lower contractile strength (wild-type 1.61 ± 0.05 *vs* 1.33 ± 0.16 mN in *Mt4-mmp*$^{-/-}$ mice, a 21% reduction) (Figure 14 c). In response to acetylcholine, the vessel wall relaxed as wild-type, indicating that endothelium function was preserved in *Mt4-mmp*-null mesenteric arteries (Figure 14 d). To analyze the structural features of this resistance vasculature, we used an *ex vivo* pressure assay. This assay could be only performed in mesenteric arteries and not in aorta due to technical limitations. *Mt4-mmp*$^{-/-}$ mesenteric arteries showed significantly increased internal and external diameters in response to increasing levels of pressure (Figure 14 e), indicative of different structural organization. In fact, null mesenteric arteries exhibited higher vessel wall stress in response to pressure (Figure 14 f) and below-normal fenestrae area in the internal elastic layer (IEL) (Figure 14 g), both features related to structural changes affecting the ECM.

-MT4-MMP-NULL MICE ARE HYPOTENSIVE-

The structural characteristics of the vasculature are key factors in the regulation of blood pressure levels. Therefore, in order to know the hemodynamic impact of the structural and cellular changes observed in *Mt4-mmp*-null arterial vessels, blood pressure levels were evaluated in a group of wild-type and *Mt4-mmp*-null mice by tail cuff. Adult deficient-mice displayed significantly decreased systolic pressure (124.8 ± 2.28 mmHg in wild-type *vs*. 116.1 ± 1.6 mmHg in *Mt4-mmp*$^{-/-}$) and diastolic pressure (76.58 ± 2.18 mmHg in wild-type

vs. 65.48 ± 1.85 mmHg in *Mt4-mmp*) (Figure 15) with no changes in pulse. These data indicate a defect of the null arterial vasculature controlling blood pressure levels.

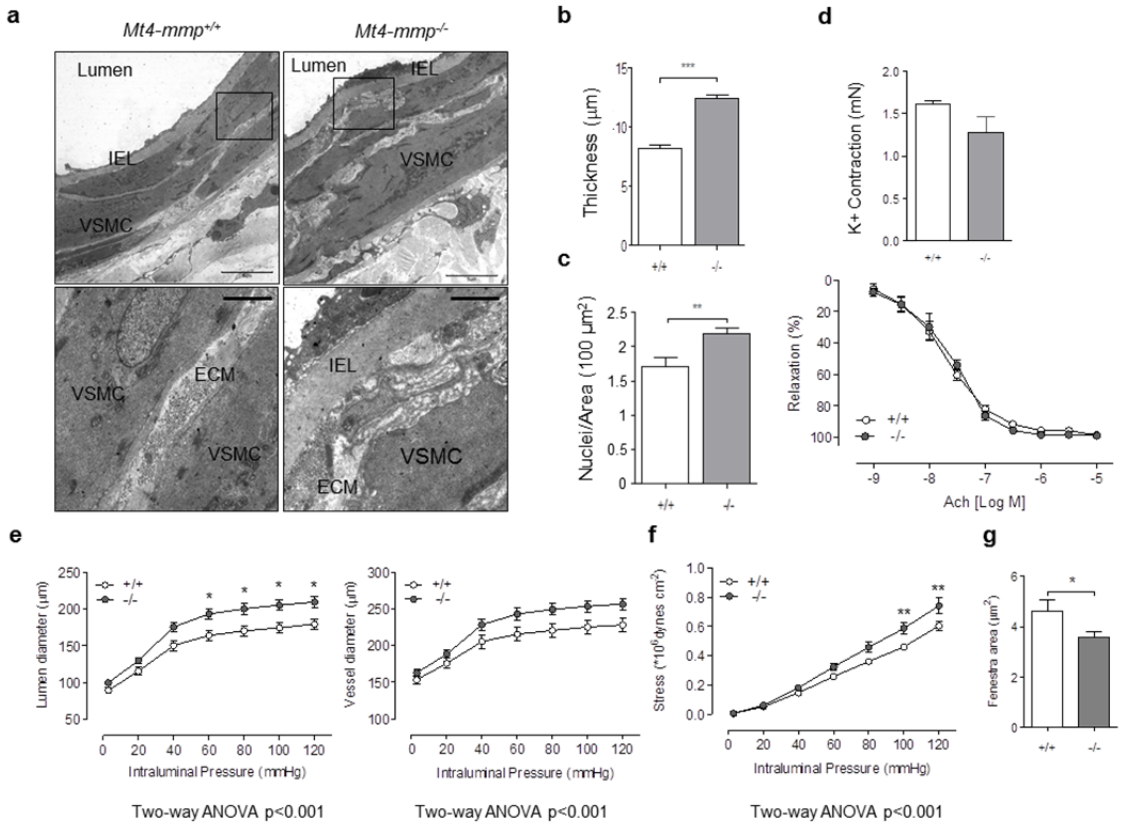

Figure 14. *Mt4-mmp*$^{-/-}$ resistance vasculature presents structural alterations. (**a**) Representative TEM images of mesenteric artery transverse sections from wild-type and *Mt4-mmp*-null mice. IEL, internal elastic lamina. n = 5 mice per genotype. Scale bar 5 µm and 0.5 µm in inset (bottom). (**b** and **c**) Vessel wall thickness and vascular SMC nuclear density in mesenteric arteries from wild-type or *Mt4-mmp*-null mice. n = 3 mice per genotype (thickness) and 9 mice per genotype analyzed in 4 independent experiments (vascular SMC nuclear density). (**d**) Mesenteric artery contraction in response to total depolarization by potassium (K^+). Endothelial integrity was assessed by relaxation in response to Acetylcholine (Ach) (right). n = 4-5 mice per genotype. (**e**) Lumen and external diameter of mesenteric artery in wild-type and *Mt4-mmp*$^{-/-}$ mice in response to intraluminal pressures applied *ex vivo* between 0 and 120 mmHg (n = 9 mice per genotype). (**f**) Vessel wall stress in response to intraluminal pressure in mesenteric arteries from wild-type and *Mt4-mmp*-null mice and (**g**), fenestra area in the internal elastic lamina (n = 9 mice per genotype analyzed in 3 independent experiments). Numerical data are means of ± s.e.m. and were tested by unpaired Student's *t*-test (**b**, **c, d** (up) and **g**) and two-way ANOVA followed by Bonferroni post-test in **d** (down), **e** and **f** (* p<0.05, ** p<0.01, *** p<0.001).

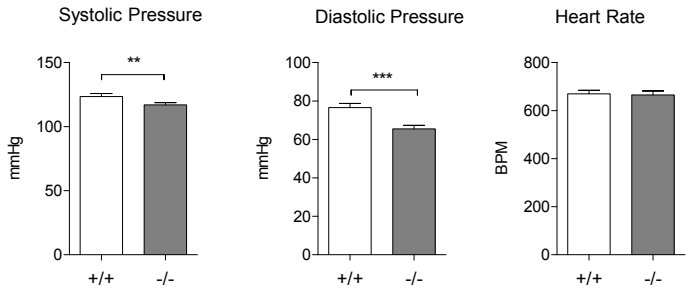

Figure 15. *Mt4-mmp*$^{-/-}$ mice are hypotensive. Blood pressure values in 8 weeks-old mice measured by tail-cuff. One representative experiment of 4 with similar result is shown. n = 10 mice in this experiment. Data are means ± s.e.m. and were tested by unpaired Student *t*-test (** $p<0.01$, *** $p<0.001$).

-MT4-MMP-NULL MICE ARE MORE SUSCEPTIBLE TO THORACIC AORTIC ANEURYSMS IN RESPONSE TO ANGIOTENSIN II-

Aortic wall mechanics directly depends on structural organization and vascular SMC differentiated phenotype. When any of these features is altered, as when structural components are mutated (i.e. collagen (Collagen 3a), microfibril component (Fibrillin-1)) or vascular SMC differentiation or contractility is affected (i.e. mutations in TGFB or contractile machinery) aortic wall weakens and can dilate abnormally (aneurysms), rupture and/or dissect. Since *Mt4-mmp*-null aortas present important defects in vascular SMCs and ECM, and hypothension can mask this pathology, we next challenge *Mt4-mmp*-null vasculature by angiotensin II infusion. Angiotensin II caused equally increases in blood pressure values either in wild-type or in *Mt4-mmp*$^{-/-}$ mice (Figure 16 a). In response to angiotensin II 3 out of 14 null mice died by aortic rupture or dissection (21.43%), whereas no deaths were registered in the wild-type group. Consistent with this finding, *Mt4-mmp*-null mice developed TAA at a higher incidence than wild-types (42.86% in *Mt4-mmp*-null mice vs 7.14% in wild-type; p=0.0384 by one-tailed Fisher's exact test); thoracic aortas in *Mt4-mmp*-deficient mice were also significantly more dilated after 4 weeks-exposition to angiotensin II (Figures 16 b, c, and d). Although *Mt4-mmp*-deficient mice showed no overall increased incidence of abdominal aortic aneurysm (AAA) in response to angiotensin II (33.33% in Mt4-mmp-null mice vs 28.54% in wild-type; p=0.5629 by one-tailed Fisher's exact test), abdominal aortic diameter was significantly larger than in wild-

types (Figures 16 e, f and g). These data suggest that *Mt4-mmp*-null aortas fail to respond to increases mechanical forces leading to more frequent TAA in response to angiotensin II.

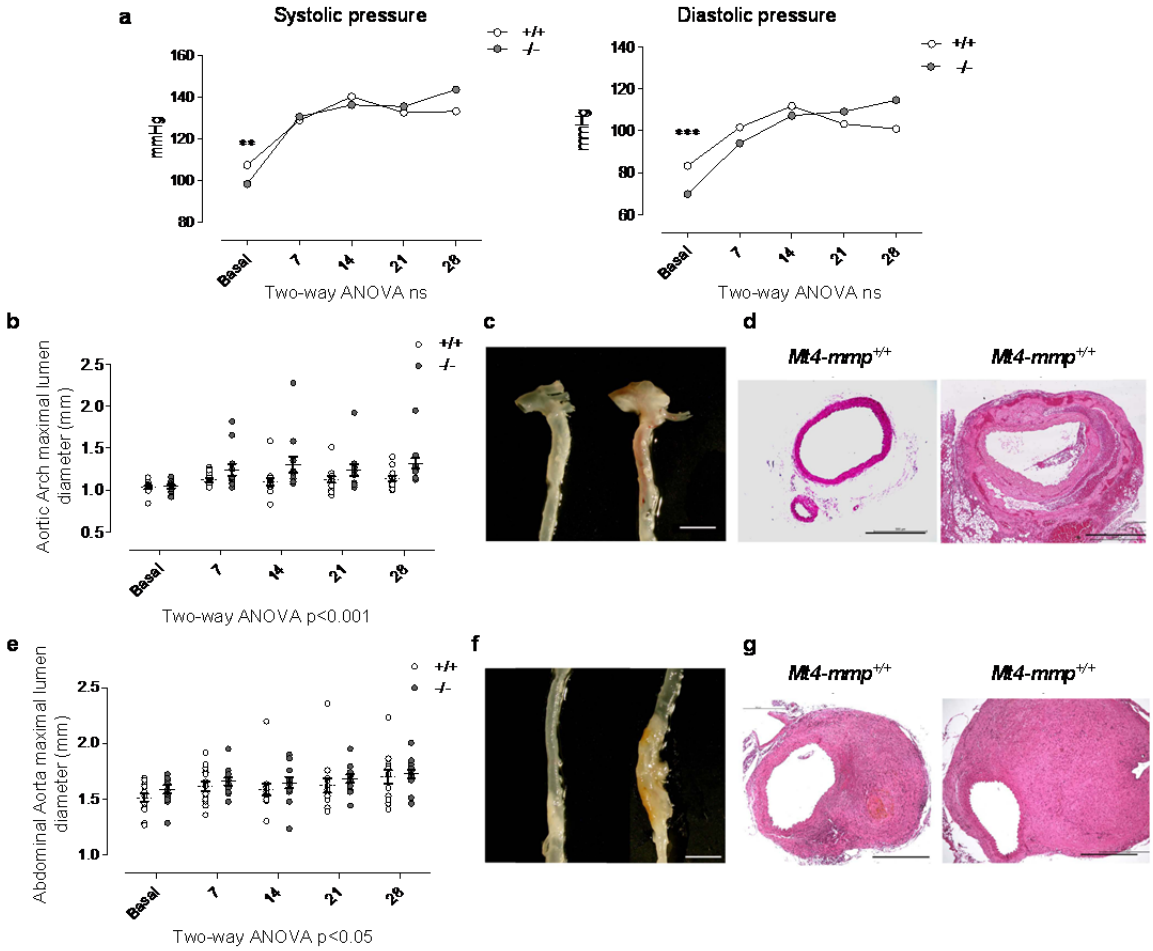

Figure 16. *Mt4-mmp*$^{-/-}$ mice are more susceptible to develop thoracic aortic aneurysm in response to angiotensin II. (**a**) Systolic and diastolic pressure evolution during angiotensin II administration in wild-type and *Mt4-mmp*$^{-/-}$ mice (**b**) Ultrasound-measured lumen diameter of thoracic ascending aorta (aortic arch after the valsalva sinus) (n=14 mice per genotype tested in two independent experiments). (**c**) Representative pictures of thoracic aortas from wild-type and *Mt4-mmp*$^{-/-}$ mice treated with angiotensin II for 28 days (left, wild-type; right, *Mt4-mmp*$^{-/-}$). Scale bar 2000 µm. (**d**) Histological transverse cuts of ascending thoracic aortas (aortic arch) from angiotensin II-treated wild-type (left) and *Mt4-mmp*$^{-/-}$ mice (right). Scale bar 500 µm. (**e**) Ultrasound-measured lumen diameter of abdominal aorta (n=14 mice per genotype tested in two independent experiments). (**f**) Representative pictures of abdominal aortas from wild-type and *Mt4-mmp*$^{-/-}$ mice treated with angiotensin II for 28 days (left, wild-type; right, *Mt4-mmp*$^{-/-}$). Scale bar 2000 µm. (**g**) Histological transverse cuts of abdominal aortas from angiotensin II-treated wild-type (left) and *Mt4-mmp*$^{-/-}$ mice (right). Scale bar 500 µm. Numerical data are means ± s.e.m. Data in **a**, **b** and **e** were compared by two-way ANOVA followed by Bonferroni post-test.

- EXACERBATED INJURY RESPONSE IN THE *MT4-MMP*$^{-/-}$ ARTERIAL VASCULATURE-

To further dissect the role of vascular SMCs in vascular insult response, we next analyzed the response of the *Mt4-mmp*-null vasculature to another model of vascular injury. Ligation of the carotid artery is a well-established model that induces neointima formation due to de-differentiation, proliferation and migration of vascular SMC within the vessel wall. First, LacZ staining in uninjured carotid arteries confirmed *Mt4-mmp* expression in medial vascular SMC and in medial and neointima cells after injury (Figure 17 a). In wild-type mice, ligation of the left carotid artery promoted the generation of neointima that increased its area progressively, together with an inward remodeling derived from the normal constrictive response of the vessel (Figure 17 b to d). However, in *Mt4-mmp*$^{-/-}$ left ligated carotid arteries, neointima development was significantly increased in area and longitude, extending along the whole vessel with outward remodeling (increased external vessel area) (Figure 17 b to d). Consistently, greater proliferation was observed in null injured carotid arteries as assessed by Ki67 (Figure 17 e).

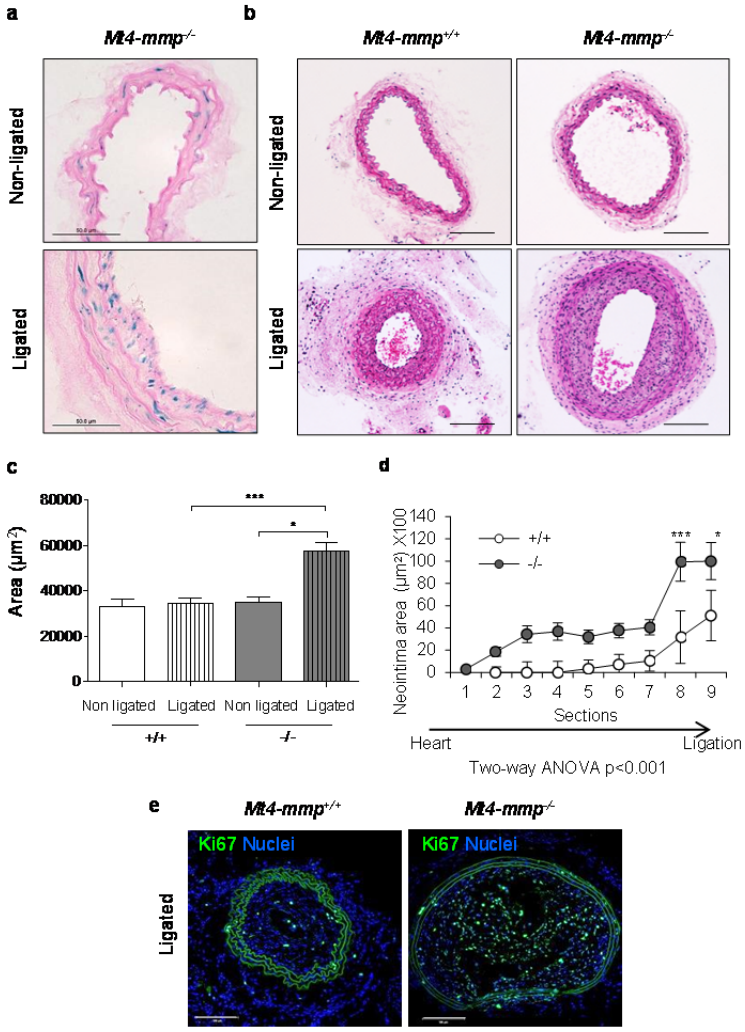

Figure 17. Carotid ligation induces outward remodeling and formation of a larger neointima in *Mt4-mmp*$^{-/-}$ mice. (**a**) Representative images of LacZ staining in carotid arteries of null mice. Scale bar 50 µm. n = 3 mice. (**b**) Representative images of sections stained with H&E from right non-ligated (upper panel) and left ligated carotid arteries (lower panel) 28 days after ligation. Scale bar 100 µm. (**c**) External elastic lamina (EEL) area in wild-type and *Mt4-mmp*$^{-/-}$ carotid arteries and (**d**) neointima area quantified along the carotid artery from the aortic arch to the ligation site. One representative experiment is shown of representative of 2 independent experiments. n = 10 mice per genotype. (**e**) Representative confocal images of carotid arteries 28 days after ligation immunostained with anti-Ki67 (green). Elastin (auto-fluorescence, green) and nuclei (Hoechst, blue) are also shown. n = 3 mice per genotype. Scale bar 100 µm. Numerical data in **c** and **d** are presented as means ± s.e.m. and were tested by one-way ANOVA (*** $p<0.001$) followed by Tukey's multiple comparison, (* $p<0.05$, *** $p<0.001$) in **c** and two-way ANOVA (*** $p<0.001$) followed by Bonferroni post-test in **d**.

-AORTIC PHENOTYPE IN NEONATAL MICE LACKING MT4-MMP-

Since *Mt4-mmp*-null vascular SMCs present characteristics of de-differentiated cells, we next analyzed the features of neonatal aortas, when maturation of vascular SMCs occurs. At postnatal day 0 (P0) we observed by TEM rounder vascular SMCs in transverse and longitudinal sections of aorta (Figure 18 a). *Mt4-mmp*$^{-/-}$ vascular SMCs contained fewer contractile filaments, more rough endoplasmic reticulum and abundant cellular debris compared to stage-matched wild-type aortas. Elastic fibers in null aortas were wrapped and frayed with big gaps and abundant microfibrils bundles that fail to connect to the vascular SMC dense plaques. Vascular SMC were also elliptically oriented in null aortas (Figure 18 a). All of these features are indicative of immature vascular SMCs.

Further analysis of *Mt4-mmp*-null aortas showed active proliferation of vascular SMC from P0 to P7 (pH3 staining) (Figure 18 b and c). Since TGFβ is a regulator of vascular SMC differentiation during development, we next analyzed *Tgfβ1 and 2* transcript levels. *Tgfβ2* mRNA levels were significantly decreased in *Mt4-mmp*$^{-/-}$ aortas (Figure 18 d) that further suggest a defect in vascular SMC maturation.

-PROTEOMIC STUDY OF NEONATAL AND ADULT AORTAS SHOWED ALTERATIONS IN BIOLOGICAL PROCESSES RELATED TO VASCULAR SMC MATURATION AND ECM/VASCULAR SMC MECHANO-COUPLING-

To understand the molecular mechanisms altered in Mt4-mmp absence, we performed a quantitative proteomics analysis of protein extracts from neonatal (P7) and adult (8-week-old) aortas obtained from wild-type and *Mt4-mmp*$^{-/-}$ mice. We determined the relative abundance of 2096 proteins in neonates and 2767 proteins in adults. Significant abundance differences ($Zq<0.05$) between the two genotypes were found for 219 proteins in neonates and 207 proteins in adults. Functional category analysis based in gene ontology (GO) was performed (proteins in the GO categories are specified in Table I). We identified differences in abundance of proteins that indicated impaired SMC maturation (increased ribonucleoprotein complex/protein synthesis and decreased muscle contraction and intermediate filaments in null aortas) as the early event in neonatal *Mt4-mmp*-null aortas (Figure 19 a); whereas adult deficient aortas were characterized by an overrepresentation of categories related to ECM (in particular collagen) and very importantly, to cellular shape

and adhesion (Figure 19 b). Notably, neonatal and adult *Mt4-mmp*$^{-/-}$ aortas both had a below normal representation of the mitochondrion category.

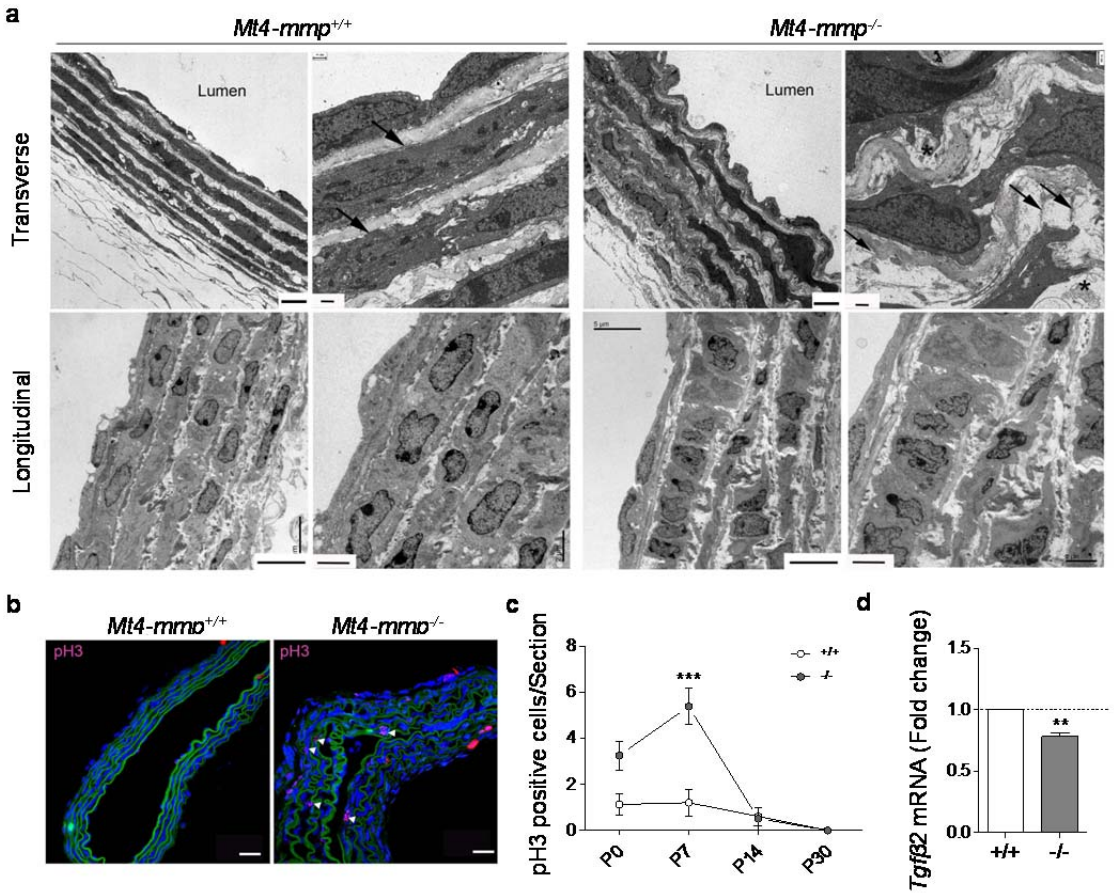

Figure 18. Perinatal onset of the arterial phenotype of *Mt4-mmp*$^{-/-}$ mice. (**a**) Representative TEM images of ultrathin transverse (top) and longitudinal (bottom) aortic sections from neonate (P0) wild-type and *Mt4-mmp*$^{-/-}$ mice. Note the cell-ECM connections (arrows) in wild-type tissue, contrasting with the abundance of microfibril bundles (arrows) and cellular debris (asterisks) in *Mt4-mmp*$^{-/-}$ aortas. Scale bars, 5 and 0.5 µm for transverse and 5 and 2 µm for longitudinal sections (n = 3 mice per genotype). (**b**) Representative confocal microscope images of aortas from 7-day-old (P7) wild-type and *Mt4-mmp*$^{-/-}$ mice, showing anti-pH3 immunostaining (red), elastin auto-fluorescence (green) and Hoechst nuclear staining (blue). Scale bar 20 µm. White arrowheads highlight pH3 positive nuclei. (**c**) Numbers of pH3-positive nuclei in the media layer of aortas from P0 to P30; n = 15-17 mice per genotype and time point analyzed in 3 independent experiments. (**d**) Q-RT-PCR analysis of *Tgfβ2* mRNA levels in P7 total aorta extracts, presented as fold change from CNRQ obtained in qBase analysis; n = 21 mice per genotype analyzed in 3 independent experiments. Numerical data are means ± s.e.m., and were tested by one-way ANOVA in **c** (*** $p<0.001$) and one-sample t-test in **d** (** $p<0.01$).

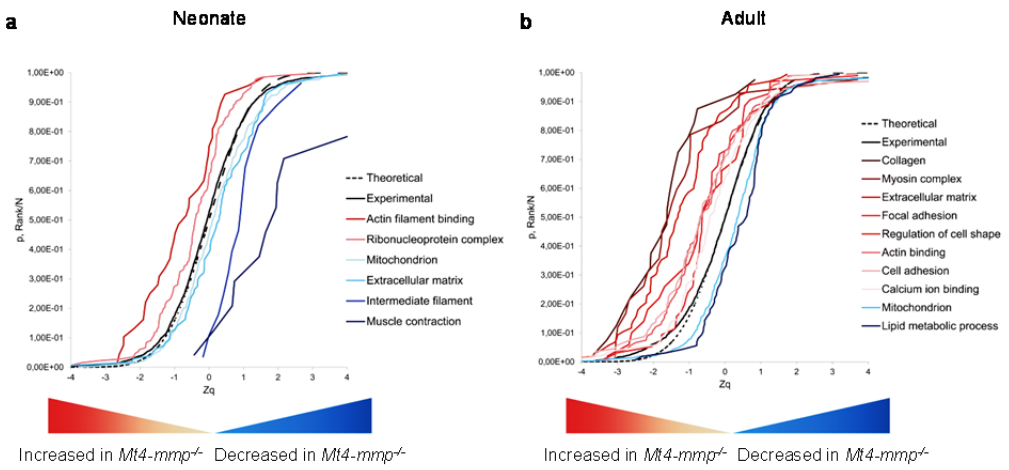

Figure 19. Quantitative proteomics comparison of the proteomes of aortas from wild-type and *Mt4-mmp*$^{-/-}$ neonatal (a) and adult (b) mice. Proteins were extracted from 7 pooled aortas per genotype at P7 and from 3 pooled aortas per genotype in adults. Protein pools were digested, and the resulting peptides were subjected to relative quantification by mass spectrometry in multiplexed mode using isobaric tag for relative and absolute quantification (iTRAQ) labeling. The quantitative protein data were grouped into gene ontology (GO) functional categories and the data were analyzed to determine significant category changes. Cumulative frequency distributions of standardized log2 ratios of proteins (Zq) were plotted to show the coordinated alterations (up or down) in proteins belonging to the changing categories. These functional categories showed an abundance decrease (Zq > 0, right shift of sigmoidal curves, blue) or an abundance increase (Zq < 0, left shift of curves, red) in *Mt4-mmp*-null mice relative to the wild-type mice. The dashed lines represent the null-hypothesis distribution, and the black lines show the distribution of all proteins quantified in each experiment.

-LENTIVIRUS EXPRESSING CATALYTIC ACTIVE MT4-MMP RESCUES THE ARTERIAL PHENOTYPE OF MT4-MMP-NULL MICE –

To elucidate whether the catalytic activity of Mt4-mmp was required for its role in the arterial vasculature, we design lentivirus encoding the wild-type or catalytic-dead mutant protease. *Mt4-mmp*-codifing lentivirus (Figure 20 a) were injected into null mice at postnatal day 1 (P1). We used catalytic active Mt4-mmp (referred as wild-type (WT)) and catalytic inactive Mt4-mmp-codifing virus by mutation of glutamic acid in the catalytic center (referred as E248A), this catalytic-dead mutant has been previously described (Itoh et al. 1999). As soon as day 7 after lentiviral injection, we detected Mt4-mmp protein and mRNA in aortas by inmunostaining and Q-RT-PCR, respectively (Figure 20 b and c). We

analyzed then early (P8) and late (8 weeks) phenotypic features in aorta (Figure 21 a). Expression of catalytically active Mt4-mmp from P1 restored vascular SMC proliferation to normal levels at P8 (Figure 21 b) and prevented aortic wall alterations in adult *Mt4-mmp*$^{-/-}$ mice, including diastolic pressure, density of vascular SMC nuclei, wall thickness in non-pressure-fixed aortas, vascular SMC morphology and orientation and ECM organization, and distribution of the contractility marker calponin (Figures 21 c to g). Injection of lentivirus encoding E248A catalytic inactive mutant however did not rescue any of the phenotypic features observed in null aortas (Figure 21), thus demonstrating that Mt4-mmp catalytic activity is necessary for its function in the vessel wall.

To test the impact of the restoration of Mt4-mmp expression in adult aortas, we inject same wild-type (WT) or E248A lentivirus in 8 weeks-old mice. Eight weeks later we observed that reexpression of catalytically active Mt4-mmp in adult *Mt4-mmp*$^{-/-}$ mice rescued some of the aortic features, in particular density of nuclei, while the inactive E248A Mt4-mmp had no effect (Figure 22).

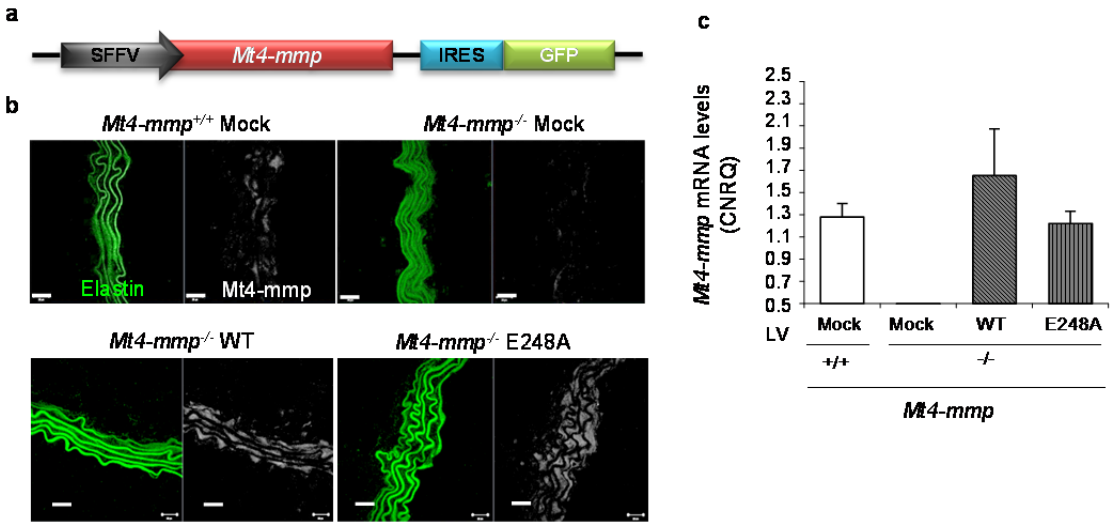

Figure 20. Lentiviral injection strategy targets vascular SMC. (**a**), Design of the lentiviral (LV) vector. The vector directs SFFV (spleen focus-forming virus)-driven *Mt4-mmp* expression and IRES (internal ribosome entry site)-driven expression of GFP. (**b**) Representative immunofluorescence images of aortic sections stained for Mt4-mmp (white) 8 weeks after lentiviral injection of mock vector (SFFV-driven, IRES-GFP), Mt4-mmp-WT or Mt4-mmp-E248A vector at P1. n = 19 to 21 mice in 3 independent experiments. Scale bar 20 µm. Auto-fluorescent elastin, green. (**c**) *Mt4-mmp* mRNA levels 8 weeks after injection at P1 of the different lentivirus encoding for Mt4-mmp (n = 12 mice per genotype analyzed in 3 independent experiments). Numerical data are means ± s.e.m. of mRNA levels obtained in qBase analysis.

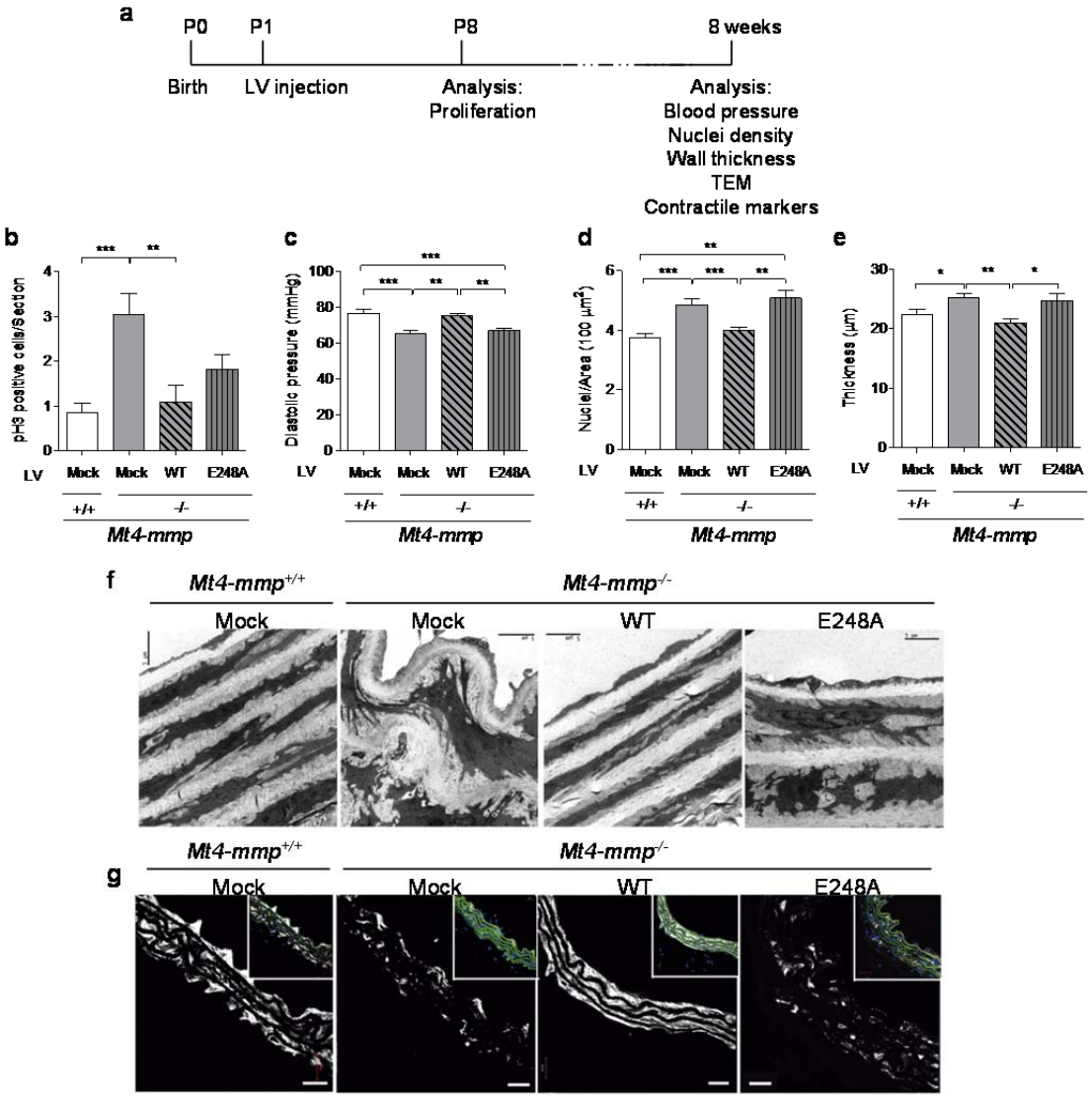

Figure 21. Expression of catalytically active Mt4-mmp in *Mt4-mmp*$^{-/-}$ mice prevents aortic phenotype. (**a**) Lentiviral rescue strategy. LV was injected one day after birth (P1) and mice were sacrificed for analysis 7 days or 8 weeks later. (**b**) Numbers of pH3-positive vascular SMCs 7 days after LV injection of mock (empty vector encoding GFP), wild-type Mt4-mmp (WT) or E248A mutant Mt4-mmp (E248A) into wild-type or null mice (n = 10-19 mice per condition analyzed in 3 independent experiments). (**c-e**) Diastolic blood pressure, density of cell nuclei, and media thickness in non-pressure fixed aortas 8 weeks after injection with the different LV (n = 12-20 mice per condition analyzed in 4 independent experiments). (**f**) Representative TEM images of thoracic aortic sections 8 weeks after injection with the different LV encoding for Mt4-mmp (n = 4 mice per condition analyzed in 3 independent experiments). Scale bar 5 µm. (**g**) Representative confocal microscopy images of calponin immunostaining (white), elastin auto-fluorescence (green), and Hoechst nuclear staining (blue) in thoracic aortic sections 8 weeks after injection with the LV forms (n = 10 mice per condition analyzed in 3 independent experiments). Scale bar 20 µm. Data in **b-e** are presented as means ± s.e.m., and were tested by one-way ANOVA followed by Tukey's multiple comparison test (* $p<0.05$, ** $p<0.01$, *** $p<0.001$).

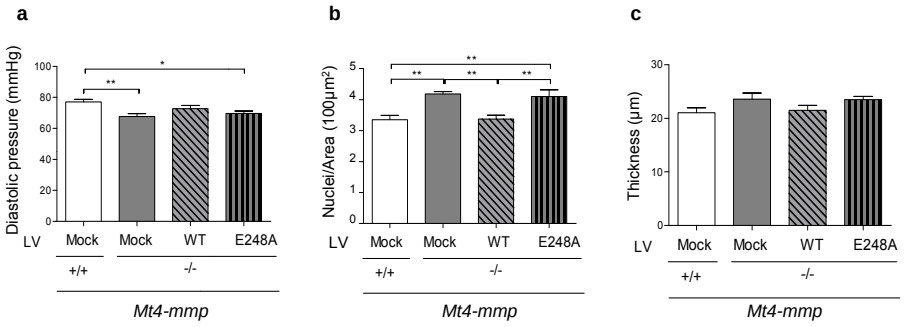

Figure 22. Expression of catalytically active Mt4-mmp in Mt4-mmp-null vascular SMCs of adult mice ameliorates the vascular phenotype. (**a-c**) Diastolic pressure, vascular SMC nuclei density and media thickness, 8 weeks after LV injection of mock vector (SFFV-driven, IRES-GFP), Mt4-mmp-WT or Mt4-mmp-E248A vector in adults (8-week-old). n = 9 to 11 mice per condition in 3 independent experiments. Numerical data are means ± s.e.m. and were tested by one-way ANOVA followed by Tukey's multiple comparison test (* $p<0.05$, ** $p<0.01$).

-IDENTIFICATION OF A NOVEL MT4-MMP SUBSTRATE: OSTEOPONTIN (OPN)-

The dependence of the vascular action of Mt4-mmp on its catalytic activity and the absence of known vascular substrates for this metalloproteinase, prompted us to search for new Mt4-mmp substrates in the vessel wall. By SILAC proteomic assay, we identify candidates for the Mt4-mmp cleavage. In this assay, bone marrow derived-macrophages were used since SILAC approach needs sequential rounds of cellular proliferation to incorporate the tagged aminoacids that, in the case of vascular SMC, would lead to de-differentiation. Comparison of supernatants of cultured wild-type and null cells showed several proteins with decreased peptides release in *Mt4-mmp*-deficient cell supernatants. From a list of putative substrates, we selected those expressed in the vessel wall, including osteopontin (Opn), and cartilage oligomeric matrix protein (Comp-1, also known as thrombospondin-5), and tested the possible cleavage by Mt4-mmp. Whereas human recombinant (hr) MT4-MMP catalytic domain showed no cleavage of hrCOMP, hrOPN cleavage was observed by *in vitro* digestion (Figure 23 a). We next determined the cleavage site in human OPN between the residues Asp^{210} and Leu^{211} by N-terminal sequencing of the fragment generated by MT4-MMP cleavage (Figure 23 b). Apposition of OPN to dimeric MT4-MMP was modelled by *in silico* docking, obtaining a stable model of human OPN in the catalytic center of the MT4-MMP dimer (Figure 23 c) that further supported the cleavage of OPN by MT4-MMP.

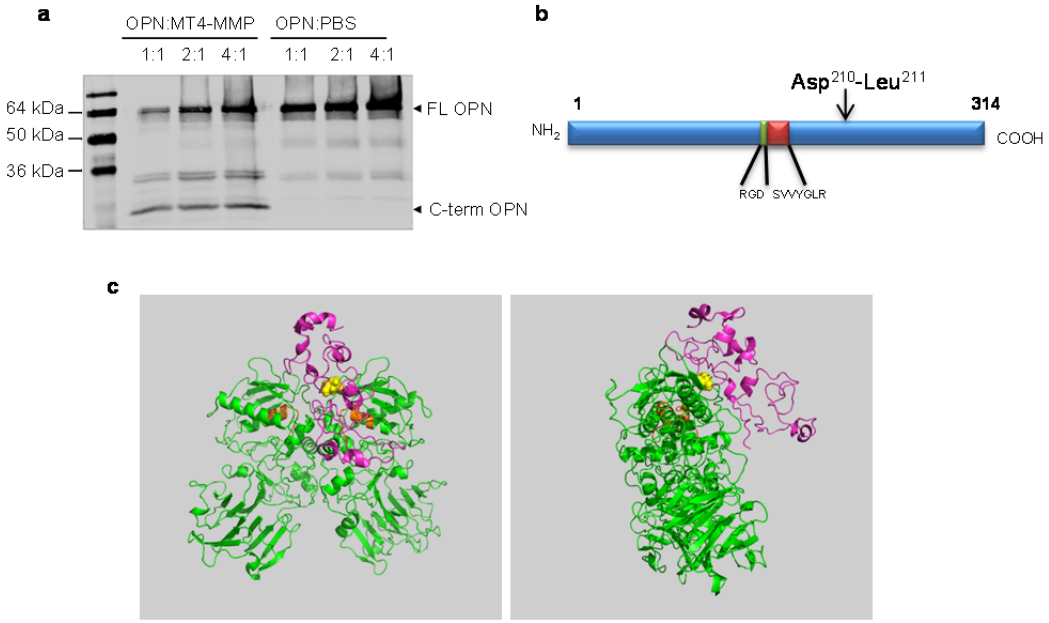

Figure 23. MT4-MMP cleaves the matricellular protein Osteopontin (OPN). (**a**) Representative western-blot of human recombinant OPN after *in vitro* digestion by human recombinant MT4-MMP. Full length OPN and its C-terminal fragment are detected with the OPN antibody anti-C-terminal (1H3F7). n = 3 independent experiments. (**b**) Scheme of human OPN protein. The cleavage site for human MT4-MMP is localized between 210 and 211 residues (arrow). (**c**) *In silico* model of OPN (purple) bound to human MT4-MMP homodimer (green); front view (left) and lateral view (right) are represented. Note the location of the OPN cleavage site (yellow) close to the MT4-MMP catalytic center (orange).

-OPN CLEAVAGE BY MT4-MMP IS NECESSARY DURING AORTIC DEVELOPMENT-

We next analyzed Opn expression and cleavage in *Mt4-mmp*-null mouse aorta. Whereas in neonates or adult aortas, Opn expression was not detected by immunostaining, positive Opn staining was observed in embryonic aortas (E14.5) (Figure 24 a), correlating with the reported *Mt4-mmp* expression by lacZ and anti-βGal staining (Figure 8 d and e). At E14.5, western-blot showed accumulation of full length (FL) Opn in aortic extracts from *Mt4-mmp*-null embryos with no changes in *Opn* mRNA levels (Figure 24 b and c). Opn accumulation was also observed in E14.5 null mice cartilage extracts, a tissue in which Mt4-mmp is also expressed (Figure 24 b). Moreover, the N-terminal (N-term) Opn fragment was significantly less abundant in *Mt4-mmp*-null E14.5 aortas (Figure 24 b) indicating less Opn cleavage in Mt4-mmp absence.

We next investigated the possible dysregulation among the signaling pathways triggered by this N-term Opn fragment. We found decreased phospho-JNK staining in vascular SMC of E14.5 null aortas (Figure 24 d). These data suggest that the cleavage of OPN needs to be timely regulated and is required for proper JNK signaling in the developing vessel wall.

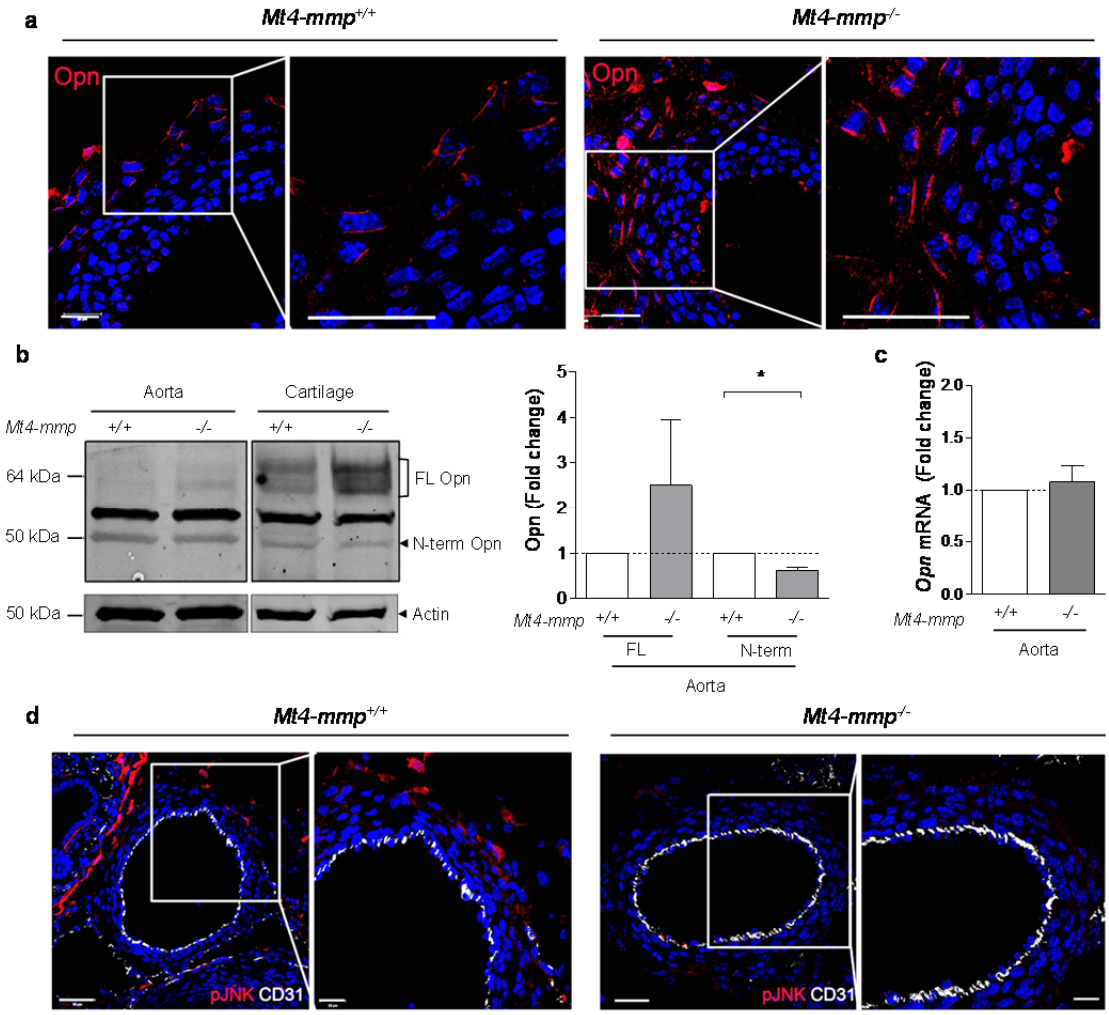

Figure 24. Osteopontin (Opn) cleavage by Mt4-mmp is required for JNK activation in vascular SMC during aorta development. (**a**) Representative confocal microscopy images of E14.5 *Mt4-mmp*-null aortas stained for Opn (red), with nuclear Hoechst staining in blue. Scale bar 20 µm. n = 5-7 embryos per genotype. (**b**) Representative western-blot of Opn in aortic extracts from E14.5 wild-type (+/+) and *Mt4-mmp*$^{-/-}$ (-/-) embryos (pool of 8-10 embryonic aortas or sternal cartilage pieces per genotype). The chart shows average fold-change of the quantification of the bands in aorta corresponding to full length (FL) and the N-terminal Opn fragment (N-term) as indicated in the western-blot; n = 3 independent experiments. (**c**) Graph shows quantification (fold change) of *Opn* mRNA levels by Q-RT-PCR in aortic extracts from E14.5 wild-type (+/+) and *Mt4-mmp*$^{-/-}$ (-/-) embryos (pool of 4-10 embryonic aortas; n = 4 independent experiments). (**d**) Representative confocal microscopy images of E14.5 wild-type and *Mt4-mmp*-null aortas stained for phospho-JNK (red) and CD31 (white), with nuclear Hoechst staining in blue (n = 5-7 embryos per genotype). Scale bar 50 µm (left) and 20 µm (right). Numerical data in **b** and **c** are means ± s.e.m. and were tested by one-sample *t*-test.

The expression of other MMPs that are described to cleave Opn (Scatena et al. 2007) and the expression of TIMPs were evaluated by Q-RT-PCR in E14.5, P0 and P7 mice aortas (Figure 25 a to c). No significant changes in MMPs or TIMPs levels were observed between wild-type and *Mt4-mmp*-null aortas indicating no compensation by other MMPs for Opn cleavage.

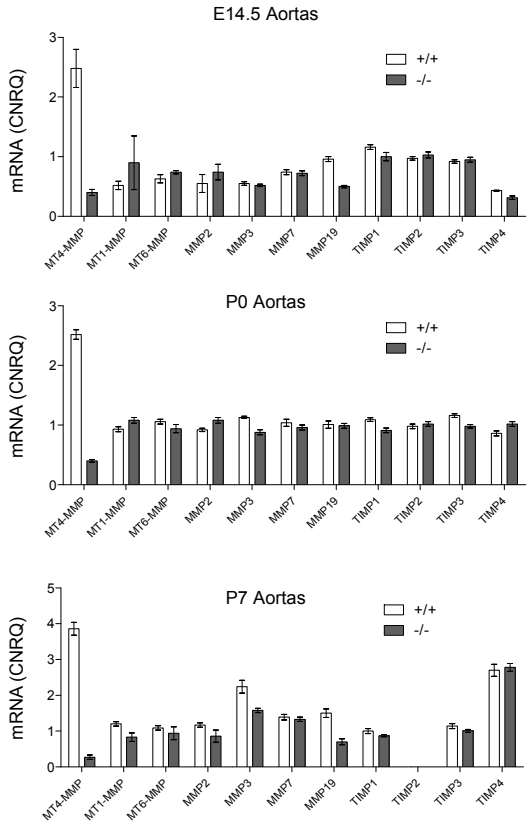

Figure 25. No changes in other MMPs or TIMPs were observed in *Mt4-mmp*$^{-/-}$ embryonic and neonatal aortas. Q-RT-PCR of mRNA levels of MMPs closely related to Mt4-mmp either by structure (Mt1-mmp, Mt6-mmp) or by their ability to cleave Opn (Mmp2, Mmp3, Mmp7) or with different abundance found in proteomics analysis (Mmp2 and Mmp19) and of tissue inhibitors of MMPs (TIMPs) in embryo (E14.5) and neonate (P0 and P7) aorta extracts. n = 8 to 10 pooled aortas. Bars represent relative mRNA quantity obtained by qBase (CNRQ).

-LENTIVIRAL-BASED EXPRESSION OF N-TERMINAL OPN RESCUES VASCULAR SMC PHENOTYPE IN MT4-MMP NULL MICE AORTAS-

To investigate the possible link between the reduction of Opn cleavage and the vascular phenotype observed in *Mt4-mmp*-null mice, we next generated lentiviruses encoding mouse full length (FL) Opn or the predicted cleaved N-terminal (N-term) Opn fragment (Figure 26 a). To confirm lentivirus products, we infected HEK293 cells with Opn viruses and western-blot analysis of culture supernatants showed FL and N-term Opn fragment production (Figure 26 b). We next injected FL or N-term Opn virus in the jugular vein of

P1 mice. On day 7 after lentivirus injection, GFP signal was already detected in the aorta (Figure 26 c).

At this time point, we show that expression of the N-term Opn fragment, but not full length Opn, restored normal proliferation levels of vascular SMCs (pH3-positive cells) (Figure 27 a). Immunostaining of aortas from neonate null mice injected with the N-term Opn fragment lentivirus also showed significantly increased phospho-JNK in the arterial media (Figure 27 b), indicating that the N-term Opn fragment is required for proper activation of JNK signaling in the vessel wall. Also, restoration of vascular SMC morphological features and ECM contacts was observed after N-terminal Opn expression (Figure 27 c). Not adult phenotype was analyzed since continued Opn overexpression is known to affect vessel wall mechanics and features in a similar way to Mt4-mmp deficiency (Isoda et al. 2002). We then investigate the rescue of other features as cellular area and roundness in cultured vascular SMC isolated from aortas (Figure 28). Overexpression of the N-term Opn fragment rescued the area and roundness in cultured *Mt4-mmp*-null vascular SMC but not the full length Opn, reinforcing the role of N-term Opn-mediated signaling in determining a normal vascular SMC phenotype (Figure 28 a to c).

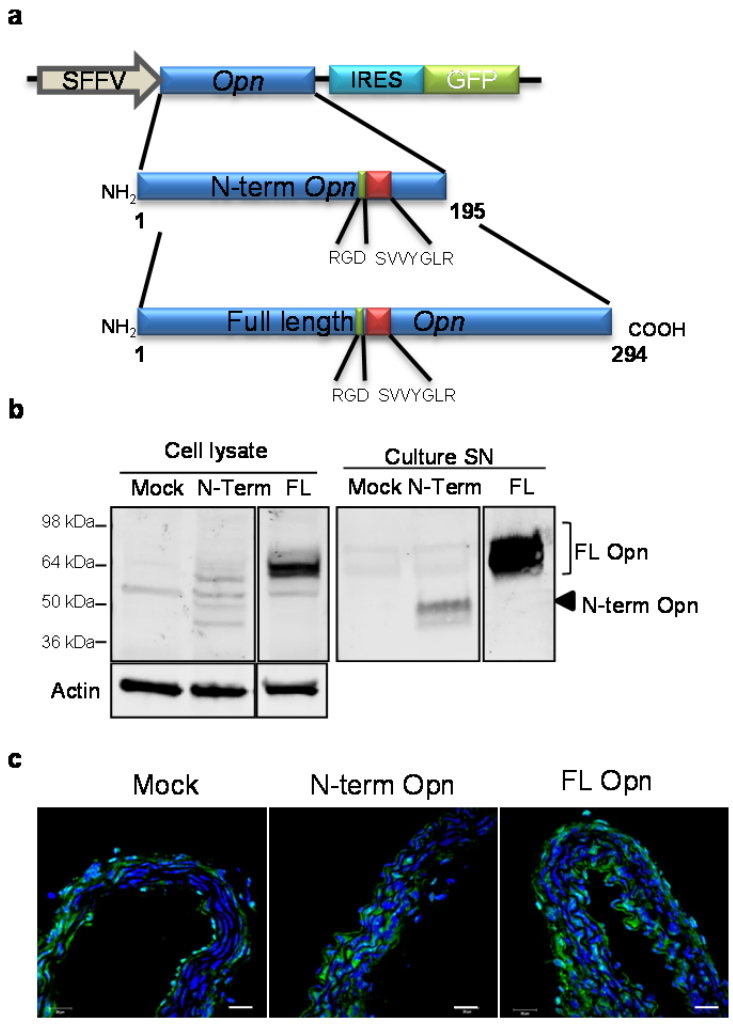

Figure 26. Lentivirus codifying for full length and N-terminal Opn. (**a**) Design of the lentiviral (LV) vector. The vector directs SFFV (spleen focus-forming virus)-driven mouse Opn full length or N-terminal expression followed by IRES (internal ribosome entry site)-driven expression of GFP in both cases. (**b**) Western-blot of cell lysates and supernatants (SN) of HEK293 cells infected with mock, N-term or full-length (FL) Opn LV. n= 2 independent experiments (**c**) Confocal images of anti-GFP immunostaining (green) of transverse aortic sections from P8 neonates 1 week after injection with the Opn LV. Scale bar 20 µm. n= 3-5 aortas visualized per condition.

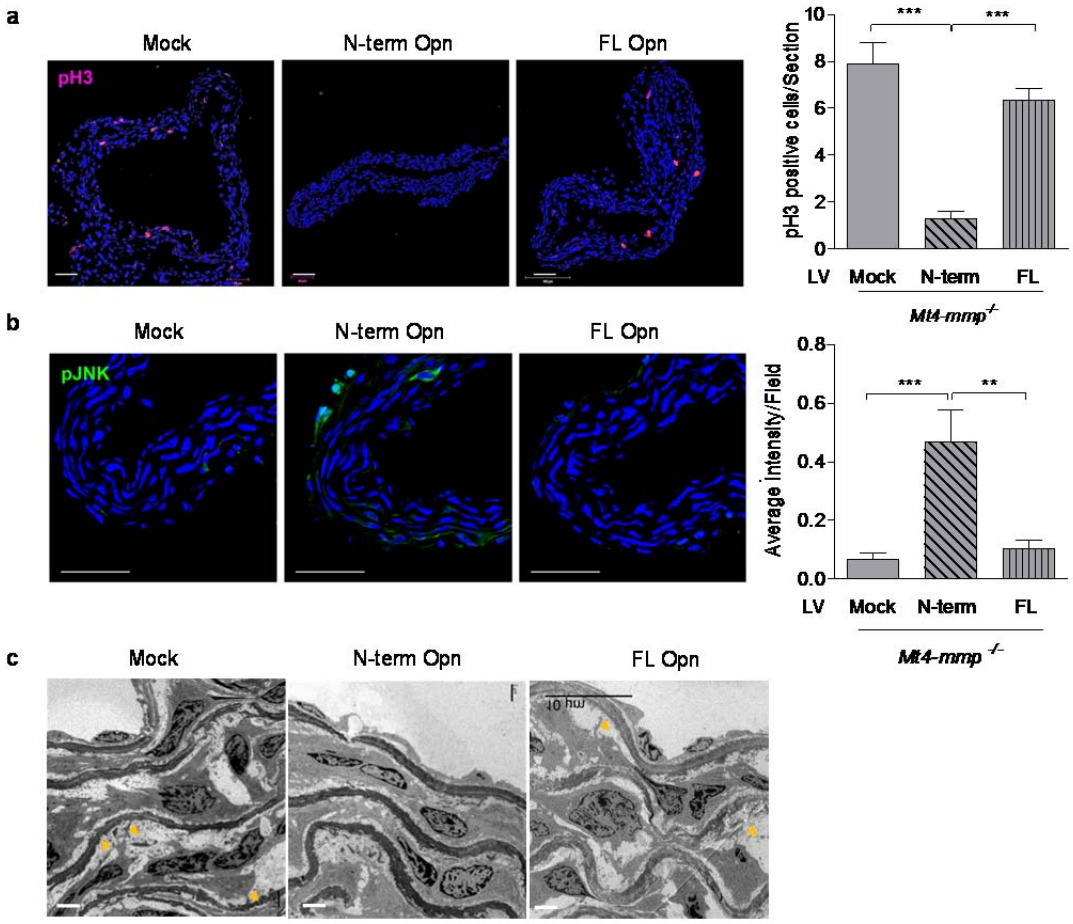

Figure 27. Lentiviral injection of N-terminal Opn fragment rescues vascular SMC proliferation and JNK signaling in *Mt4-mmp*$^{-/-}$ neonatal aortas. (**a**) Representative confocal images of pH3 staining (red) in P8 aortas from *Mt4-mmp*-null mice injected at P1 with N-term, FL Opn or control (mock) LV (left) and quantification of pH3-positive cells (right). Scale bar 50 µm. n = 16 to 20 mice per condition, analyzed in two independent experiments. (**b**) Representative confocal images of P8 aortas from null mice injected with LV as in **a**, stained for phospho-JNK (green) (left) and quantification of average fluorescence intensity in the arterial media (right); nuclear Hoechst staining in blue. Scale bar 50 µm. n = 16 to 20 mice were analyzed per condition in two independent experiments. (**c**) Representative TEM images of transversal P7 aortas after Opn LV injection. Arrowheads points to vascular SMCs extensions that connect to ECM. Notice the elongated form of vascular SMCs in N-terminal Opn LV-injected aorta. Scale bar 2 µm (n = 2 mice per condition). Numerical data in **a** and **b** are means ± s.e.m. and were tested by one-way ANOVA followed by Tukey's multiple comparison test (** $p<0.01$, *** $p<0.001$).

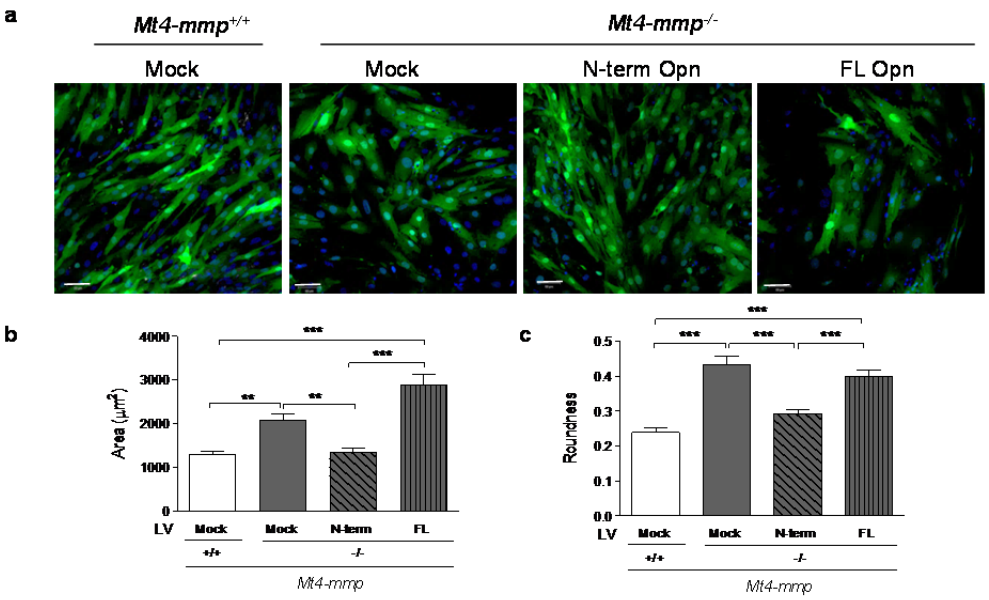

Figure 28. Expression of N-terminal Opn fragment in *Mt4mmp*-null vascular SMCs rescues vascular SMC morphological alterations. (**a**) Representative pictures of wild-type and null vascular SMC infected with mock, N-term or FL Opn LV showing GFP-positive-infected cells. Scale bar 50 µm. Quantification of cellular area and roundness are depicted (**b** and **c**). n= 2 independent experiments. One representative experiment is shown with 35 to 50 cells quantified per condition. Data in **b** and **c** are means ± s.e.m. and were analyzed by one-way ANOVA (*** $p<0.001$) followed by Bonferroni post-test (** $p<0.01$, *** $p<0.001$).

-GENETIC ANALYSIS OF PATIENTS AFFECTED BY TAAD IDENTIFIED AN MT4-MMP MISSENSE MUTATION-

To know whether the increased incidence of TAA in *Mt4-mmp*$^{-/-}$ mice might have any clinical implication, we next investigate genetic mutations in *MT4-MMP* in individuals with a familiar history of TAAD. We performed Illumina exome beadchip assay to study rare *MT4-MMP* variants in 800 European cases of sporadic thoracic aortic dissection (STAAD). Comparison of the allele frequencies of *MT4-MMP* variants in this cohort with the allele frequencies of variants in the European American cohort (exome variant service, EVS) revealed association of the rare variant rs4964883 (p.Ala129Gly) with sporadic dissection ($p = 0.0044$), of which 61.6% were type A (ascending thoracic) and 38.5% were type B (non-ascending aorta) dissections. Since a significance of $p<0.0025$ is necessary to conclude a genome wide association to a rare variant, we then performed whole exome sequencing (WES) in samples from 58 probands from families with an inherited

predisposition to TAAD. This analysis identified the missense mutation R373H (p.Arg373His) in the *MT4-MMP* gene (Figure 29 a) of a 43 years old European American male. This patient had a type A aortic dissection with an aortic root diameter of 5.5 cm and also suffered a stable chronic type B dissection. Unfortunately no DNA samples were available from the proband's family to determine segregation of the R373H variant with disease. However, the father's proband presented a type A dissection and two out of three of the proband's siblings developed ascending thoracic aortic aneurysm.

Polyphen analysis determined that the R373H mutation in MT4-MMP was likely to be deleterious, so we forward modelled *in silico* the predicted conformation. This mutation, would cause a conformational change in the C-terminal region (Figure 29 b) that presumably impede GPI-tail binding by transamidases during synthesis of the MT4-MMP variant on the endoplasmic reticulum. Since MT4-MMP binds to the plasma membrane through this GPI-tail, this conformational change would affect its expression at the plasma membrane. To confirm this data, we next modeled the MT4-MMP homodimer conformation *in silico*, finding that the R373H mutation might also affect the arrangement of the catalytic center of the homodimer (Figure 29 b). *In silico* modeling of a heterodimer formed by wild-type MT4-MMP and R373H mutant monomers yielded no energetically stable conformation, suggesting that the mutation in heterozygosity might behave as a functional homozygous loss.

To test whether R373H mutation affects MT4-MMP expression, we transfected then HEK 293 cells with wild-type or R373H mutant MT4-MMP and tested its expression. Although the levels of *MT4-MMP* mRNA were similar in wild-type- and R373H-transfected HEK293 cells (Figure 29 c), the mutant MT4-MMP protein was undetectable by western-blot or immunostaining (Figure 29 d and e). However, treatment with the proteasome inhibitor bortezomib revealed mutant protein accumulation in intracellular vesicles of R373H-MT4-MMP-transfected HEK293 cells (Figure 29 e), suggesting that the mutant MT4-MMP gets degraded during its synthesis in the endoplasmic reticulum.

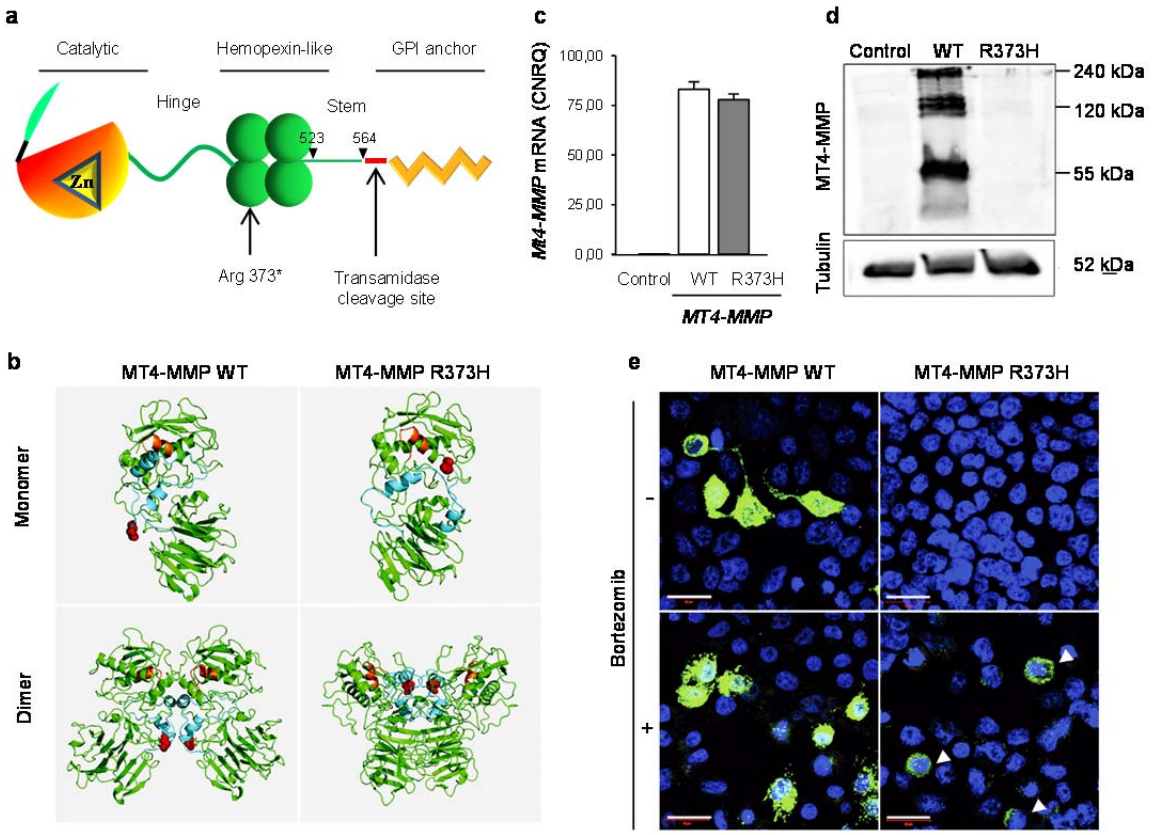

Figure 29. R373H mutation in MT4-MMP found in human TAAD impairs protein expression. (**a**) Protein domain structure of human MT4-MMP. The arrow marks the mutation found in a TAAD patient at Arg373. (**b**) 3D tertiary protein structures of the lowest energy models for human wild-type MT4-MMP (left panels) and the R373H mutant (right). Monomers (upper panels) and homodimers (lower panels) are shown. The same colors used for the domain structure (**a**) are used in the 3D models (orange, catalytic center; red, C-terminal residue). Domains with a different orientation in the wild-type and mutant versions are shown in blue. (**c**) Q-RT-PCR analysis of *MT4-MMP* mRNA levels in HEK293 cells non-transfected (control) or transfected with wild-type or R373H mutated human MT4-MMP. n = 4 independent experiments. (**d**) Representative western-blot of MT4-MMP protein expression in HEK293 cells transfected with wild-type or R373H mutated human MT4-MMP. (**e**) Representative confocal microscope images of transfected HEK293 cells with or without treatment with bortezomib. Cells were stained with anti-human MT4-MMP antibody (green) and Hoechst (blue). Scale bar 20 µm. n = 5 independent experiments.

Discussion

DISCUSSION

Understanding the mechanisms implicated in arterial vasculature homeostasis and pathology is relevant in cardiovascular diseases, where mouse models have proved to be a valuable tool to discover the role of specific proteins in the arterial vasculature (Wagenseil and Mecham 2009) (Dietz et al. 1991) (Yanagisawa et al. 2002) (Habashi et al. 2006) (Elia et al. 2009) (Moltzer et al. 2011).

In this regard, the generation of the constitutive *Mt4-mmp* knockout/knockin mouse meant an important advance in the identification of the cellular types and the organ distribution of *Mt4-mmp* expression (Rikimaru et al. 2007), however little progress in the characterization of the Mt4-mmp role in physiology had been provided since then (Sohail et al. 2008). Our work further reveals the biological function of this metalloproteinase *in vivo* during arterial vasculature development, homeostasis and in life-threatening diseases as TAA(D).

We demonstrated that Mt4-mmp catalytic activity is required during the development of large arteries as aorta, where the metalloproteinase cleaves a small matricellular protein, Opn. The release of the N-terminal Opn fragment is necessary to induce JNK phosphorylation in the cells forming the developing aortic wall, resulting in vascular SMC maturation. In this sense, Mt4-mmp absence produces a transitory increased vascular SMC proliferation, and structural changes in arterial vasculature with morphologically aberrant vascular SMC and altered cell/ECM mechano-coupling. The resultant Mt4-mmp null vasculature is dysfunctional and presents an increased predisposition to thoracic aortic aneurysms and neointima development after injury (Figure 30).

Vascular SMC is a highly specialized and plastic cell type in the arterial vessel wall that mediates vessel wall adaptations to mechanical changes. These cells are able to sense its environment (mechanosensing) and respond by inducing changes in ECM synthesis/organization, cell contraction, proliferation, migration or even cell death (Owens 1995) (Wagenseil and Mecham 2009). Mechanosensing apparatus is form by oblique extensions of elastic fibers (enriched in microfibrils) that are structurally

linked to the vascular SMC surface by membrane receptor binding. Those ECM structures are aligned to the intracellular cytoskeleton (Milewicz et al. 2008). The primary mechanosensors are integrins that allow direct interaction with the ECM and are clustered in dense plaques or focal adhesions. Integrins act as mechanotransductors transmitting the ECM information to intracellular protein adaptors as vinculin and talin that mediates actin/myosin binding (Schwartz 2010). This cellular complex, termed the mechanotrasduction complex, provides the interface between the contractile machinery on the interior of the cell and the ECM on the exterior, to which force is transmitted, triggering the different cellular response to changes in the mechanical environment that aims to restore vessel homeostasis (Milewicz et al. 2008) (Humphrey et al. 2015).

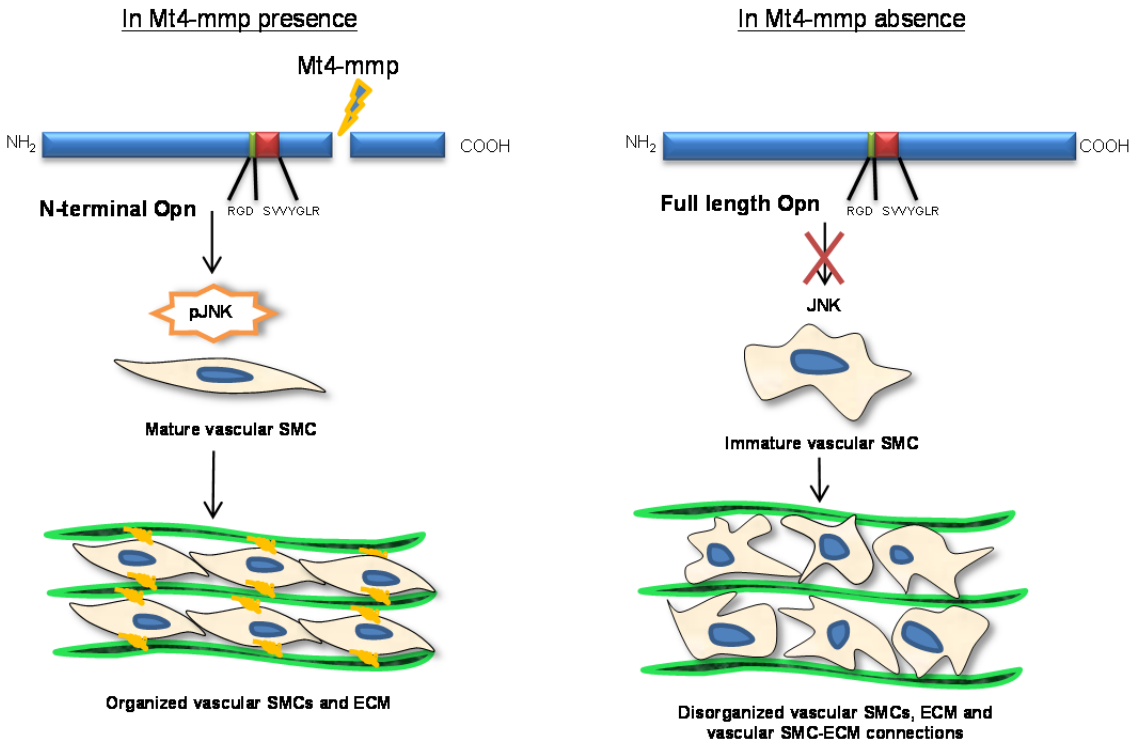

Figure 30. Arterial vessel wall alterations in Mt4-mmp absence. Osteopontin (Opn) is a new substrate for Mt4-mmp that needs to be cleaved during aortic development. The generation of the N-terminal Opn fragment is necessary to induce JNK phosporylation that facilitates vascular SMC maturation. Mature vascular SMC organized among elastin fibers and establish contacts among them and with the ECM. Loss of Mt4-mmp impairs Opn cleavage during aortic development impairing pJNK signaling, and resulting in immature vascular SMC. Null vascular SMCs fail to establish ECM connections and organize along the vessel wall.

When any of the components implicated in vascular SMC mechanosensing and force production is altered, the adaptation of the vessel wall to changes in the mechanical environment is compromised (Wagenseil and Mecham 2009) (Humphrey et al. 2015). In vascular pathologies as aneurysms, the vessel wall weakens because is no longer able to bear the hemodynamic forces (Humphrey et al. 2014). In this regard, since the first mutation predisposing to TAAD was found affecting *Fibrillin1* (*FBN1*) gene in individuals with MFS (Dietz et al. 1991), many other genes implicated in mechanosensing and mechanoregulation in the arterial wall have been reported in inheritable cases of aneurysms as the underlying cause of TAAD development in human (Humphrey et al. 2015) (Milewicz et al. 2008) (Lindsay and Dietz 2011) (Boileau et al. 2012) (Inamoto et al. 2010) (Regalado et al. 2011) (Kuang et al. 2012).

Also several mouse models have been developed based on these mutations mimicking human pathology and allowing to recapitulate some key molecular pathways disrupted. For example, MFS mouse models of Fibrillin1$^{-/-}$ (*Fbn1*$^{-/-}$) mice or Fibulins 4 and 5 knockout mice in which loss of elastic fiber integrity and vascular SMC de-differentiated phenotype contribute to aneurysms generation (Bunton et al. 2001) (Pereira et al. 1997) (Huang J. et al. 2010) (Spencer et al. 2005).

Some ultrastructural alterations observed by TEM in *Mt4-mmp*$^{-/-}$ aortas resembled those in *Fbn1*$^{-/-}$ mice (Pereira et al. 1997) as the vascular SMC aberrant morphology, the abundant cytoplasmic extensions that fail to connect to elastic fibers, and the presence of intracellular vacuoles (Bunton et al. 2001). These data highlight common processes occurring in both models as could be the altered vascular SMC/ECM mechanical coupling. However, other features of *Mt4-mmp*$^{-/-}$ arterial vessels, as the defect in vascular SMC orientation within the wall, was only reported in *Mt4-mmp*-null vasculature, suggesting the specific implication of this metalloproteinase in the orientation and distribution of vascular SMCs during arterial vessel wall development.

In MFS mouse models that spontaneously develop aneurysms, vascular SMCs present a de-differentiated or synthetic-like phenotype that has been traditionally characterized by a decrease in the expression of contractile markers (Owens et al.

2004). However on some mouse models of MFS, no significant changes on the levels of some of those contractile markers are found (Bunton et al. 2001) in spite of the striking alterations revealed by TEM. Our data demonstrate that vascular SMCs in the *Mt4-mmp*-null mouse aorta can express normal levels of contractile markers and yet be dysfunctional because of their misorientation within the arterial vessel wall.

In this sense, *Mt4-mmp*-null vasculature presents a defective hemodynamic control with significant increases in aortic and mesenteric artery diameters and the inability to maintain normal blood pressure levels.

Blood pressure levels are determined by different factors including peripheral vessel resistance, cardiac output and the blood volume. Previous studies in the *Mt4-mmp*-null mice revealed defects in water intake that at first could be indicative of a lower blood volume in the null mice. However, even though water intake of *Mt4-mmp*$^{-/-}$ mice was 50% lower than in wild-types, those mice presented same blood osmolality since they were induced higher urine concentration. Primary defect observed in the *Mt4-mmp*$^{-/-}$ mice in this study pointed to an alteration affecting the anterior hypothalamus that contains the thirst centers (Srichai et al. 2011). So presumably the null mice hypodipsia is not the cause of the low blood pressure levels observed in the absence of *Mt4-mmp* since blood osmolality is preserved in the *Mt4-mmp*$^{-/-}$ mice.

Mt4-mmp-null vessels had also a defective response to challenging stimuli. Although no spontaneous aneurysms or dissections were observed in Mt4-mmp absence, probably by the decreased blood pressure, angiotensin II infusion produced higher incidence of TAA but not AAA.

The mechanisms of generation of one or the other type of aneurysms is different; TAA usually affects young people and arise primarily from noninflammatory mechanisms that often involve underlying genetic mutations, whereas AAA is more related to degradative processes in the vessel wall related to age, smoke, hypertension, hyperlipidemia and atherosclerosis, that triggers the degradation of the ECM usually driven by MMPs (Isselbacher 2005).

Therefore, MMPs have been usually linked to the pathology of the aneurysms; contribution of MMP2, MMP9 and MMP12 in elastin degradation during TAA and AAA has been proved (Longo et al. 2005) (Huusko et al. 2013) and also it has been

reported increased levels of MT1-MMP and MMP19 in aneurysms (Jackson et al. 2012). Even deletion of MMP2 in a mouse model of MFS improved aneurysm phenotype and survival (Xiong et al. 2012). Although MT4-MMP mRNA levels have been analyzed in tissue samples and vascular SMC from patients with thoracic and abdominal aortic aneurysms and other arterial pathologies, these previous studies yielded inconclusive results about a pathogenic effect of altered Mt4-mmp in these disorders (Inamoto et al. 2010) (Jackson et al. 2012) (Carrell et al. 2002) (Lenk et al. 2007). However, our results suggest that Mt4-mmp role in the vessel wall is the opposite to the others MMPs; likely being necessary for the maintenance of the vessel homeostasis. This difference could be related to the substrate specificity of Mt4-mmp since this metalloproteinase presents no catalytic activity against ECM major structural proteins (Sohail et al. 2008).

Using a proteomic assay, allowed us to reveal the biological processes altered in *Mt4-mmp*-null neonate and adult aortas.

The defects observed in neonate mice likely derived from deficient vascular SMC maturation during development as indicated by the proteomic assay performed in P7 aortas in which we observed decreases in the levels of proteins implicated in the biological processes of SMC maturation and muscle contraction and increases in the synthetic activity of the null cells. The presence of increased number of proliferative vascular SMCs in P0 and P7 aortas and the decreased levels on *Tgfβ* expression in null neonatal aortas point in the same direction since is described that those are features ligated to immature vascular SMCs (Owens 1995). Vascular SMC proliferation can be regulated by elastin, since deficient elastic fibers or impaired vascular SMC/elastin interaction induce proliferation (Li D. Y. et al. 1998). The major regulator of vascular SMC maturation is TGFβ, whose expression was reduced in the null mice. Importantly, TGFβ signaling has to be carefully regulated since decreases or increases in this pathway are described in vascular pathologies, especially aneurysms. An impaired TGFβ signaling has been reported in patients of MFS, other familiar TAAD, and in the corresponding mice models, where TGFβ levels are usually misbalanced (ten Dijke and Arthur 2007) (Milewicz et al. 2008) (Li W. et al. 2014) (Humphrey et al. 2015). In the case of the *Mt4-mmp*$^{-/-}$ mice,

although *Tgfβ2* mRNA levels are significantly decreased, it would be necessary to confirm the possible defect in the *Tgfβ* signaling, since the regulation and availability of this molecule depends on the activation and binding to ECM proteins (ten Dijke and Arthur 2007).

In adult aortas, however, proteomic analysis confirmed the alteration in vascular SMC shape, cell adhesion and contractile complex further supporting the aberrant SMC/ECM mehano-coupling and reflected that the long-term absence of this metalloproteinase impacts on the ECM (particularly collagen levels) that has been described before aneurysms (Gillis et al. 2013). This effect on the ECM in adult could be a consequence of the incapability of these immature cells to produce an adequate ECM and also a compensatory effect for the hemodynamic changes happening in the null vasculature (Gillis et al. 2013). In fact, in the case of the *Mt4-mmp*-null mice, adult vessels support higher stress and present collagen adventitial remodeling; two hallmarks of vessel structural alterations directly related to impair vessel hemodynamics (Briones et al. 2010).

Besides TGFβ, other signaling pathways drive vascular SMC maturation as PDGF and micro RNAs, however still some of them are still undefined (Owens et al. 2004). We found high *Mt4-mmp* expression at E14.5, when the expression of the majority of vascular ECM proteins, including fibrillar collagens, elastin and fibrillin-1 is upregulated (Kelleher et al. 2004). During this embryonic development, first interactions of the maturating vascular SMCs are established to the surrounding matrix, generating the mechanosensitive structure (Davis 1993) and interestingly, integrin expression during aortic embryonic development differs from adults (McLean et al 2005).

The absence of defined substrate(s) for Mt4-mmp in the arterial vasculature adds complexity to the study of the mechanisms of action of this metalloproteinase. Currently, MMPs substrate identification protocols are moving towards proteomic technics that allow the study of the differences in the peptide profile generated by wild-type versus null mice cells (Rodriguez et al. 2010) (Koziol et al. 2012). SILAC proteomic assay in our case enabled the identification of the matricellular protein

Opn with decreased abundance of peptides in the supernatant of cultured *Mt4-mmp*-null cells.

So, we have described Opn as a novel substrate for Mt4-mmp in the vascular context that by specific space and time-regulated cleavage impacts on vascular SMCs maturation during the aortic vessel wall development. Moreover, the *in silico* modeling of the MT4-MMP dimer shows the catalytic center arrangement and the Opn interaction for the first time that can further help to the substrate identification.

The presence and role of Opn in the arterial vessel wall has been previously analyzed but mainly focused in pathological vascular circumstances (Scatena et al. 2007) (Okamoto 2007) where Opn acts as chemoattractant/activator of inflammatory cells and as a chemoattractant/adhesive molecule for vascular SMCs and ECs (Liaw et al. 1994) (Cho et al. 2009). Opn promotes cellular survival, adhesion and migration of vascular SMCs and inhibits calcification and is even able to control contractile marker expression (Scatena et al. 2007) (Kazanecki et al. 2007a) (Speer et al. 2005) (Jalvy et al. 2007) (Gao H. et al. 2012). However a role of Opn during vessel wall development has not been addressed and the function of OPN in vessel wall physiology remains unclear.

Interestingly, *Opn*-deficient and *Opn*-overexpressing transgenic mouse models showed arterial phenotypes similar to those of *Mt4-mmp*$^{-/-}$ mice. First *Opn*-null mice presented increased diameter of vessels under pressure and hypotension, suggesting that the absence of Opn or its N-terminal fragment (as in the case of *Mt4-mmp*$^{-/-}$ mice) generates this vascular phenotype (Myers et al. 2003). On the other hand, *Opn*-transgenic mice showed thicker aortic media with higher number of vascular SMCs that proliferate in the adult aorta and elastic fiber destruction (Isoda et al. 2002) that could be related to the impaired Opn full-length cleavage. Both phenotypes in the mouse models of Opn further support the requirement of proper Opn levels and processing for correct vascular structure and performance.

In fact, Opn role in pathology could be related to the phenotype that we described in *Mt4-mmp*-null vessels. *Opn*-overexpressing transgenic mouse produces higher neointima in a model of femoral artery cuff-induced injury (Isoda et al. 2002), and on the other way around, smaller neointima in a model of CIL in *Opn*-null mice (Myers

et al. 2003), supporting a direct contribution of Opn to this pathology. In these studies is proposed that Opn interacts to vascular SMCs presumably via αvβ3 integrin increasing MMPs expression, particularly of MMP2 and MMP9, that leads to elastic fiber degradation (Isoda et al. 2002) (Han et al. 2007).

Even though the possible different role of the Opn fragments is not addressed in those studies, it is known that the cleavage of Opn by thrombin or MMPs generates two fragments with different biologic activity (Kazanecki et al. 2007a), and recently it has been demonstrated the different contribution of those fragments to pathology (Wolak et al. 2013). This is confirmed in the *Mt4-mmp*$^{-/-}$ mice model since restoration of N-terminal Opn generated after Mt4-mmp cleavage recovers the neonate phenotype, whereas Opn full-length Opn was unable to achieve this recovery.

It is described that the N-terminal OPN fragments generated by thrombin or MMPs cleavage presented higher integrin affinity, by exposition of the RGD domain and, in the case of thrombin cleavage, the SVVYGLR (SLAYGLR in mouse) cryptic site (Kazanecki et al. 2007a) (Cho et al. 2009). Although Opn has been shown to be a target for others MMPs, as MMP2, 3, 7, 9 and 12 (Lund et al. 2009) (Scatena et al. 2007) (Agnihotri et al. 2001), in the null mice any of those MMPs compensated the loss of Opn cleavage by Mt4-mmp. Interestingly, Mt4-mmp cleavage at the Ala^{210}-Leu^{211} of Opn preserves the SVVYGLR cryptic domain of Opn, whereas all other MMPs target and disable this integrin binding site. So, main difference of Mt4-mmp-Opn cleavage would be the exposition of this cryptic site that binds $\alpha_9\beta_1$, $\alpha_4\beta_1$, and $\alpha_4\beta_7$. Precisely α_4 and β_7 integrin chains are highly express during embryonic aortic development (McLean et al. 2005). Therefore, an interesting possibility is that during aortic development N-terminal Opn generated by Mt4-mmp cleavage could mediates signaling through $\alpha_4\beta_7$ integrin. Whether this signaling is be important for aortic development and vascular SMC maturation needs to be further investigated.

Altered integrin signaling is related to vascular SMC maturation and arterial organization. β_1 integrin chain specific deletion in vascular SMC (under the *Pdgfrβ* promoter) generates vessels with poor vascular SMC coverage and increased proliferation of these cells, showing that β_1 controls vascular SMC shape, adhesion

and proliferation (Abraham et al. 2008). β_3 integrin also controls vascular SMC proliferation in MFS pathology (Misra et al. 2016). Both chains, β_1 and β_3, signaling is mediated by integrin-linked kinase (ILK). Loss of ILK expression in vascular SMC produce arterial vessel aneurysms and ruptures in mouse embryo, showing that integrin signaling is necessary during vessel wall formation since ILK induces vascular SMC differentiation through myocardin-related transcription factor A (MRTFA) (Shen et al. 2011). Therefore we can speculate that Opn N-terminal fragment could be inducing integrin-mediated signaling necessary for the proper maturation of vascular SMC.

Even though OPN expression has not been analyzed during development, it is known that its expression in the vessel wall can be induced by mechanical stretch, growth factors as PDGF, TGFβ, angiotensin II and also by hypoxia (Kubota et al. 1989) (Giachelli et al. 1993) (deBlois et al. 1996) (Sodhi et al. 2001) (Seo et al. 2015). In response to these stimuli, OPN can induce vascular SMC migration mainly through activation of FAK/ERK, p38 MAPK, and JNK, and/or proliferation through activation of ERK1/2 signaling pathways (Li J. J. et al. 2007) (Han et al. 2007) (Jalvy et al. 2007) (Cho et al. 2009) (Yu et al. 2010). In particular, TGFβ induces OPN expression in a positive feedback loop that leads to JNK phosphorylation and vascular SMC migration (Yu et al. 2010).

In our study, we could no address whether Opn fragments could also rescue the phenotypic features in the adult, since Opn expression *per se* has demonstrated to have an impact in the physiology of the vasculature or in pathological processes. In this sense, Opn acts for example as driver of neointima lesion generation (Isoda et al. 2002) (Myers et al. 2003) and it is highly related to aneurysms pathology (Bruemmer et al. 2003).

Interestingly, TGFβ also induces JNK phosphorylation in a Marfan's mouse model (Smad-4-deficient mice). In those mice, increased activation of JNK correlated to aneurysms pathology and administration of a JNK antagonist ameliorated the aortic disease (Holm et al. 2011). This result, compared to the pJNK requirement in the Mt4-mmp null mice, highlight the importance of time-specific signaling in the vessel

wall and determination of whether MT4-MMP-OPN-pJNK signaling pathway is implicated in TAA is also of interest.

Since Mt4-mmp is also expressed after birth and Opn is induced by stretch, it would be of interest to determine the possible effect of both during the first days of life. The establishment of accurate vascular SMC/ECM connection would determine the posterior adaptations of the vasculature to the hemodynamic changes that occurs specially during the first weeks of life, when blood pressure increases from approximately 30 mmHg at birth to 80 mmHg. In this time period, the aorta undergoes rapid remodeling in response to the hemodynamic changes (Huang Y. et al. 2006).

Our study opens some questions regarding the Mt4-mmp/Opn/JNK axis that still need to be answered. First, further investigation of the cellular types expressing Opn in the developing aorta need to be accomplished since we detected Opn and pJNK staining mainly in cells at the periphery of the vessel (presumably vascular SMCs progenitors that are being recruited) in E14.5 aortas.

Second, it would be interesting to corroborate the possible existence of an OPN (N-terminal) gradient generated by Mt4-mmp that could be impacting in vascular SMCs orientation within the wall, since it is a coordinated process in which proliferation and orientation is carefully regulated and the specific molecular signals implicated are still not fully identified (Greif et al. 2012).

Third, how we are able to rescue the phenotype in neonates by inducing Mt4-mmp catalytic active or N-terminal Opn expression when the Mt4-mmp/N-terminal Opn/JNK signaling occurs earlier in developmental stages. We think that either Mt4-mmp cleaves Opn full length still available at P1 in the null mice aortic wall or N-terminal Opn directly restore proper signaling that leads to vascular SMC maturation and orientation in the wall.

And fourth, to determine if the phenotype observed in *Mt4-mmp*-null vasculature relies on the vascular SMC-specific expression or the phenotype is not cell autonomous. To solve this question, we are currently generating the vascular SMC specific knockout mutant for Mt4-mmp.

Even though we have focused our research in arterial big vessels as aorta, it was previously described the possible role of MT4-MMP impacting in pericytes coverage in tumor vasculature (Chabottaux et al. 2006) (Chabottaux et al. 2009) (Sounni et al. 2011). Overexpression of this metalloproteinase by breast cancer cells (as MDA-MB-231) produced bigger and leakier vessels when subcutaneously injected in RAG1 immunodeficient mice (Chabottaux et al. 2009). In this way, MT4-MMP expression at the surface of the cancer cells affected the host pericyte coverage of the tumor vessels, an *in-trans* effect. By TEM they showed that those pericytes were irregularly shaped, with extended cytoplasm and were poorly associated to endothelial cells (Chabottaux et al. 2009), further supporting an impact of MT4-MMP in the vascular SMC morphology and adhesion. This is the fundamental defect that increases metastatic cell intravasation leading to lung metastasis in breast tumor cells overexpressing MT4-MMP (Chabottaux et al. 2009) (Sounni et al. 2011).

Taking into account this in-trans effect of Mt4-mmp expression over the vasculature, Mt4-mmp is expressed in other cellular types with undescribed functions so far. In fact, Mt4-mmp is express in other SMC population, as the visceral SMCs forming the muscle walls of the intestinal tract (Rikimaru et al. 2007), and our laboratory is currently analyzing Mt4-mmp role in this cellular type.

Other interesting point is whether Mt4-mmp by cleaving Opn could be implicated in other pathologies. In rheumatoid arthritis, for instance, both, Mt4-mmp and Opn contribute to disease progression in inflammatory processes either cleaving ADAMTS4 and contributing to cartilage destruction (Gao G. et al. 2004) (Patwari et al. 2005) (Clements et al. 2011) or in the case of Opn that is directly associated with the destruction of the joint cartilage (Yumoto et al. 2002) (Ohshima et al. 2002). Since we have observed that Opn full length gets accumulated in *Mt4-mmp*$^{-/-}$ mice cartilage it will be interesting to explore the role of this Mt4-mmp-Opn mediated cleavage in rheumatoid arthritis also as a possible therapeutic target.

OPN has also been reported to be expressed in cardiac tissue after mechanical stress including pressure/volume loading and hypoxia, where it regulates fibrosis after myocardial infarction. In *Opn*$^{-/-}$ mice, collagen deposition after myocardial infarction is in fact impaired, heart ventricle is dilated and cardiac contractility is reduced

(Trueblood et al. 2001) (Okamoto 2007). Since Mt4-mmp is also expressed in the heart (in the vessel wall and in other cellular types currently under study) it could be interesting to address the response of the *Mt4-mmp*-null mice to myocardial infarction and to analyze if the pathology of the process depends also on Opn cleavage.

In human pathology, TAAD generation, contrary to AAA, have a strong genetic component. Although several genes whose mutations predispose to TAAD generation have been identified, (as mutations found in diseases as Marfan (Fibrillin-1), Loeys-Dietz (TGFBRI and II)) and Aneurysms-Osteoarthritis (SMAD3) syndroms) (Milewicz et al. 2008), still up to 20% of TAAD patients have a family history of aneurysms with non-identified genetic cause. Recent advances in the study of this familial cases of TAAD has been performed by whole exome sequencing (WES) that demonstrated to be an effective technique for the identification of new mutations causative of TAAD (Milewicz et al. 2014). WES analysis of patients with familial TAAD uncovered a mutation in *MT4-MMP* gene (R373H) that further proved to impair protein expression. Surprisingly, the loss of MT4-MMP in one allele rendered a homozygous loss, since heterodimers formed by wild-type and MT4-MMP-R373H mutant were presumably unstable. In fact, analysis of *Mt4-mmp*$^{+/-}$ mice ultrastructure showed similar alterations to knockout aortas. Still a deep study of other possible mutations in this patient is necessary and a larger patient sample analysis is required to determine the prevalence of this mutation in the TAAD population.

To date, pharmacological treatment of aneurysms is limited; treatment of patients with inhibitors of β-adrenergic blockers or angiotensin II inhibitors as Losartan has improve aortic phenotype, however still prophylactic surgery is necessary for most of these patients to avoid aortic dissection or rupture (Braverman 2013) (Isselbacher 2005). Therefore the identification of additional therapeutic targets that ameliorate aneurysms growth and prevent the disease is needed. Taking into account the limitations aforementioned, lentiviral experiments showed that restoration of Mt4-mmp expression or the delivery of the N-terminal Opn fragment in the vasculature

rescues phenotypical features providing a possible gene therapy approach for TAAD patients with *MT4-MMP* mutations.

Conclusions

1. The Mt4-mmp metalloproteinase is expressed by vascular SMCs in the vessel wall of conductance and resistance arterial vessels. In the aorta, particularly, Mt4-mmp is expressed since embryonic development until adulthood.
2. The absence of Mt4-mmp impacts on the aortic features, including vascular SMC morphology, organization/disposition, distribution of marker proteins and connections to ECM, increased collagen deposition and a transient increase in vascular SMC proliferation, affecting vascular SMC maturation.
3. The altered mechano-coupling in the *Mt4-mmp*-null arterial vasculature generates dilated vessels and hypotension.
4. The response of the Mt4-mmp deficient vasculature to injury is altered showing increased thoracic aortic aneurysms in response to angiotensin II and the development of larger neointimas after injury.
5. The *Mt4-mmp*$^{-/-}$ arterial phenotype relies on the metalloproteinase catalytic activity since the phenotypical alterations in the Mt4-mmp-null aortas could be rescued only by the re-expression of the catalytic active Mt4-mmp protein.
6. Mt4-mmp cleaves osteopontin during aortic development and decreases N-terminal osteopontin generation and JNK phosphorylation in the aortic vessel wall.
7. The axis Mt4-mmp-osteopontin-pJNK is necessary during aortic vessel wall development and disruption of this signaling impairs vascular SMC maturation.
8. An MT4-MMP missense mutation found in a patient suffering of thoracic aortic aneurysms impairs protein expression suggesting the implication of MT4-MMP in human thoracic aortic aneurysms.

Conclusiones

1. Las células musculares lisas de los vasos arteriales de conductancia y de resistencia expresan la metaloproteinasa Mt4-mmp. En la aorta, específicamente, Mt4-mmp se expresa desde el desarrollo embrionario de la pared aórtica hasta la vida adulta.
2. La ausencia de Mt4-mmp afecta a las características de la aorta, específicamente a la morfología de las células de la musculatura lisa, a su orientación/ disposición, a la disposición intracelular de los marcadores contráctiles y a su interacción con las proteínas de matriz celular, también presentan un aumento en la deposición de colágeno y un aumento transitorio de la proliferación celular, afectando a la maduración de las células de musculatura lisa de la pared vascular.
3. La alteración mecano-elástica de la vasculatura arterial del ratón deficiente en Mt4-mmp genera dilatación de las arterias e hipotensión.
4. La respuesta de la vasculatura arterial del ratón deficiente en Mt4-mmp a daño está alterada, presentando mayor incidencia de aneurismas aórticos torácicos en respuesta a angiotensina II, y mayores neointimas en respuesta a un estímulo de daño.
5. El fenotipo arterial del ratón deficiente en Mt4-mmp depende de la pérdida de la actividad catalítica de la metaloproteinasa ya que las alteraciones fenotípicas de las aortas deficientes en Mt4-mmp pueden ser rescatadas por la re-expresión mediada por lentivirus de Mt4-mmp.
6. Mt4-mmp procesa osteopontin y la ausencia de este corte durante el desarrollo embrionario de la aorta disminuye la generación del fragmento N-terminal de osteopontin y la fosforilación de JNK en la pared aórtica.
7. El eje formado por Mt4-mmp-osteopontin-pJNK es necesario durante el desarrollo de la pared aórtica y la alteración de este eje de señalización impide la correcta maduración de las células de musculatura lisa vascular.
8. La mutación puntual en MT4-MMP encontrada en un paciente con aneurisma torácico aórtico impide la expresión de la proteína, lo que sugiere una implicación de MT4-MMP en los aneurismas torácicos aórticos en humanos.

Bibliography

BIBLIOGRAPHY

- Abraham S, Kogata N, Fassler R, Adams RH. 2008. Integrin beta1 subunit controls mural cell adhesion, spreading, and blood vessel wall stability. Circ Res 102: 562-570.
- Adams RH, Alitalo K. 2007. Molecular regulation of angiogenesis and lymphangiogenesis. Nat Rev Mol Cell Biol 8: 464-478.
- Agnihotri R, Crawford HC, Haro H, Matrisian LM, Havrda MC, Liaw L. 2001. Osteopontin, a novel substrate for matrix metalloproteinase-3 (stromelysin-1) and matrix metalloproteinase-7 (matrilysin). J Biol Chem 276: 28261-28267.
- Arribas SM, Hinek A, Gonzalez MC. 2006. Elastic fibres and vascular structure in hypertension. Pharmacol Ther 111: 771-791.
- Baccarani-Contri M, Taparelli F, Pasquali-Ronchetti I. 1995. Osteopontin is a constitutive component of normal elastic fibers in human skin and aorta. Matrix Biol 14: 553-560.
- Boettger T, Beetz N, Kostin S, Schneider J, Kruger M, Hein L, Braun T. 2009. Acquisition of the contractile phenotype by murine arterial smooth muscle cells depends on the Mir143/145 gene cluster. J Clin Invest 119: 2634-2647.
- Boileau C, Guo DC, Hanna N, Regalado ES, Detaint D, Gong L, Varret M, Prakash SK, Li AH, d'Indy H, Braverman AC, Grandchamp B, Kwartler CS, Gouya L, Santos-Cortez RL, Abifadel M, Leal SM, Muti C, Shendure J, Gross MS, Rieder MJ, Vahanian A, Nickerson DA, Michel JB, National Heart L, Blood Institute Go Exome Sequencing P, Jondeau G, Milewicz DM. 2012. TGFB2 mutations cause familial thoracic aortic aneurysms and dissections associated with mild systemic features of Marfan syndrome. Nat Genet 44: 916-921.
- Bonzon-Kulichenko E, Perez-Hernandez D, Nunez E, Martinez-Acedo P, Navarro P, Trevisan-Herraz M, Ramos Mdel C, Sierra S, Martinez-Martinez S, Ruiz-Meana M, Miro-Casas E, Garcia-Dorado D, Redondo JM, Burgos JS, Vazquez J. A robust method for quantitative high-throughput analysis of proteomes by 18O labeling. Mol Cell Proteomics 10: M110 003335.
- Braverman AC. 2013. Medical management of thoracic aortic aneurysm disease. J Thorac Cardiovasc Surg 145: S2-6.
- Brinckerhoff CE, Matrisian LM. 2002. Matrix metalloproteinases: a tail of a frog that became a prince. Nat Rev Mol Cell Biol 3: 207-214.
- Briones AM, Arribas SM, Salaices M. 2010. Role of extracellular matrix in vascular remodeling of hypertension. Curr Opin Nephrol Hypertens 19: 187-194.
- Briones AM, Rodriguez-Criado N, Hernanz R, Garcia-Redondo AB, Rodrigues-Diez RR, Alonso MJ, Egido J, Ruiz-Ortega M, Salaices M. 2009. Atorvastatin prevents angiotensin II-induced vascular remodeling and oxidative stress. Hypertension 54: 142-149.
- Bruemmer D, Collins AR, Noh G, Wang W, Territo M, Arias-Magallona S, Fishbein MC, Blaschke F, Kintscher U, Graf K, Law RE, Hsueh WA. 2003. Angiotensin II-accelerated atherosclerosis and aneurysm formation is attenuated in osteopontin-deficient mice. J Clin Invest 112: 1318-1331.

- Bunton TE, Biery NJ, Myers L, Gayraud B, Ramirez F, Dietz HC. 2001. Phenotypic alteration of vascular smooth muscle cells precedes elastolysis in a mouse model of Marfan syndrome. Circ Res 88: 37-43.
- Carmeliet P. 2005. Angiogenesis in life, disease and medicine. Nature 438: 932-936.
- Carrell TW, Burnand KG, Wells GM, Clements JM, Smith A. 2002. Stromelysin-1 (matrix metalloproteinase-3) and tissue inhibitor of metalloproteinase-3 are overexpressed in the wall of abdominal aortic aneurysms. Circulation 105: 477-482.
- Clements KM, Flannelly JK, Tart J, Brockbank SM, Wardale J, Freeth J, Parker AE, Newham P. 2011. Matrix metalloproteinase 17 is necessary for cartilage aggrecan degradation in an inflammatory environment. Ann Rheum Dis 70: 683-689.
- Comeau SR, Gatchell DW, Vajda S, Camacho CJ. 2004. ClusPro: a fully automated algorithm for protein-protein docking. Nucleic Acids Res 32: W96-99.
- Cordes KR, Sheehy NT, White MP, Berry EC, Morton SU, Muth AN, Lee TH, Miano JM, Ivey KN, Srivastava D. 2009. miR-145 and miR-143 regulate smooth muscle cell fate and plasticity. Nature 460: 705-710.
- Cross GA. 1990. Glycolipid anchoring of plasma membrane proteins. Annu Rev Cell Biol 6: 1-39.
- Chabottaux V, Noel A. 2007. Breast cancer progression: insights into multifaceted matrix metalloproteinases. Clin Exp Metastasis 24: 647-656.
- Chabottaux V, Sounni NE, Pennington CJ, English WR, van den Brule F, Blacher S, Gilles C, Munaut C, Maquoi E, Lopez-Otin C, Murphy G, Edwards DR, Foidart JM, Noel A. 2006. Membrane-type 4 matrix metalloproteinase promotes breast cancer growth and metastases. Cancer Res 66: 5165-5172.
- Chabottaux V, Ricaud S, Host L, Blacher S, Paye A, Thiry M, Garofalakis A, Pestourie C, Gombert K, Bruyere F, Lewandowsky D, Tavitian B, Foidart JM, Duconge F, Noel A. 2009. Membrane-type 4 matrix metalloproteinase (MT4-MMP) induces lung metastasis by alteration of primary breast tumour vascular architecture. J Cell Mol Med 13: 4002-4013.
- Cho HJ, Cho HJ, Kim HS. 2009. Osteopontin: a multifunctional protein at the crossroads of inflammation, atherosclerosis, and vascular calcification. Curr Atheroscler Rep 11: 206-213.
- Christensen B, Schack L, Klaning E, Sorensen ES. 2010. Osteopontin is cleaved at multiple sites close to its integrin-binding motifs in milk and is a novel substrate for plasmin and cathepsin D. J Biol Chem 285: 7929-7937.
- Christensen B, Klaning E, Nielsen MS, Andersen MH, Sorensen ES. 2012. C-terminal modification of osteopontin inhibits interaction with the alphaVbeta3-integrin. J Biol Chem 287: 3788-3797.
- Daugherty A, Manning MW, Cassis LA. 2001. Antagonism of AT2 receptors augments angiotensin II-induced abdominal aortic aneurysms and atherosclerosis. Br J Pharmacol 134: 865-870.
- Davis EC. 1993. Smooth muscle cell to elastic lamina connections in developing mouse aorta. Role in aortic medial organization. Lab Invest 68: 89-99.
- deBlois D, Lombardi DM, Su EJ, Clowes AW, Schwartz SM, Giachelli CM. 1996. Angiotensin II induction of osteopontin expression and DNA replication in rat arteries. Hypertension 28: 1055-1063.

- Dietz HC, Cutting GR, Pyeritz RE, Maslen CL, Sakai LY, Corson GM, Puffenberger EG, Hamosh A, Nanthakumar EJ, Curristin SM, et al. 1991. Marfan syndrome caused by a recurrent de novo missense mutation in the fibrillin gene. Nature 352: 337-339.
- Elia L, Quintavalle M, Zhang J, Contu R, Cossu L, Latronico MV, Peterson KL, Indolfi C, Catalucci D, Chen J, Courtneidge SA, Condorelli G. 2009. The knockout of miR-143 and -145 alters smooth muscle cell maintenance and vascular homeostasis in mice: correlates with human disease. Cell Death Differ 16: 1590-1598.
- English WR, Puente XS, Freije JM, Knauper V, Amour A, Merryweather A, Lopez-Otin C, Murphy G. 2000. Membrane type 4 matrix metalloproteinase (MMP17) has tumor necrosis factor-alpha convertase activity but does not activate pro-MMP2. J Biol Chem 275: 14046-14055.
- Esteban V, Mendez-Barbero N, Jimenez-Borreguero LJ, Roque M, Novensa L, Garcia-Redondo AB, Salaices M, Vila L, Arbones ML, Campanero MR, Redondo JM. 2011. Regulator of calcineurin 1 mediates pathological vascular wall remodeling. J Exp Med 208: 2125-2139.
- Ferguson MAJ, Kinoshita T, Hart GW. 2009. Glycosylphosphatidylinositol Anchors in Varki A, Cummings RD, Esko JD, Freeze HH, Stanley P, Bertozzi CR, Hart GW, Etzler ME, eds. Essentials of Glycobiology. Cold Spring Harbor (NY).
- Fogelstrand P, Feral CC, Zargham R, Ginsberg MH. 2009. Dependence of proliferative vascular smooth muscle cells on CD98hc (4F2hc, SLC3A2). J Exp Med 206: 2397-2406.
- Gaengel K, Genove G, Armulik A, Betsholtz C. 2009. Endothelial-mural cell signaling in vascular development and angiogenesis. Arterioscler Thromb Vasc Biol 29: 630-638.
- Gao G, Plaas A, Thompson VP, Jin S, Zuo F, Sandy JD. 2004. ADAMTS4 (aggrecanase-1) activation on the cell surface involves C-terminal cleavage by glycosylphosphatidyl inositol-anchored membrane type 4-matrix metalloproteinase and binding of the activated proteinase to chondroitin sulfate and heparan sulfate on syndecan-1. J Biol Chem 279: 10042-10051.
- Gao H, Steffen MC, Ramos KS. 2012. Osteopontin regulates alpha-smooth muscle actin and calponin in vascular smooth muscle cells. Cell Biol Int 36: 155-161.
- Garaulet G, Alfranca A, Torrente M, Escolano A, Lopez-Fontal R, Hortelano S, Redondo JM, Rodriguez A. 2013. IL10 released by a new inflammation-regulated lentiviral system efficiently attenuates zymosan-induced arthritis. Mol Ther 21: 119-130.
- Ghoorah AW, Devignes MD, Smail-Tabbone M, Ritchie DW. 2013. Protein docking using case-based reasoning. Proteins.
- Giachelli CM, Bae N, Almeida M, Denhardt DT, Alpers CE, Schwartz SM. 1993. Osteopontin is elevated during neointima formation in rat arteries and is a novel component of human atherosclerotic plaques. J Clin Invest 92: 1686-1696.
- Gillis E, Van Laer L, Loeys BL. 2013. Genetics of thoracic aortic aneurysm: at the crossroad of transforming growth factor-beta signaling and vascular smooth muscle cell contractility. Circ Res 113: 327-340.
- Golledge J, Muller J, Shephard N, Clancy P, Smallwood L, Moran C, Dear AE, Palmer LJ, Norman PE. 2007. Association between osteopontin and human abdominal aortic aneurysm. Arterioscler Thromb Vasc Biol 27: 655-660.
- Greif DM, Kumar M, Lighthouse JK, Hum J, An A, Ding L, Red-Horse K, Espinoza FH, Olson L, Offermanns S, Krasnow MA. 2012. Radial construction of an arterial wall. Dev Cell 23: 482-493.

- Gross J, Lapiere CM. 1962. Collagenolytic activity in amphibian tissues: a tissue culture assay. Proc Natl Acad Sci U S A 48: 1014-1022.
- Guyton AC. 1986. Textbook of medical physiology. Philadelphia etc.: W. B. Saunders Company.
- Habashi JP, Judge DP, Holm TM, Cohn RD, Loeys BL, Cooper TK, Myers L, Klein EC, Liu G, Calvi C, Podowski M, Neptune ER, Halushka MK, Bedja D, Gabrielson K, Rifkin DB, Carta L, Ramirez F, Huso DL, Dietz HC. 2006. Losartan, an AT1 antagonist, prevents aortic aneurysm in a mouse model of Marfan syndrome. Science 312: 117-121.
- Han M, Wen JK, Zheng B, Liu Z, Chen Y. 2007. Blockade of integrin beta3-FAK signaling pathway activated by osteopontin inhibits neointimal formation after balloon injury. Cardiovasc Pathol 16: 283-290.
- Heberlein KR, Straub AC, Isakson BE. 2009. The myoendothelial junction: breaking through the matrix? Microcirculation 16: 307-322.
- Holm TM, Habashi JP, Doyle JJ, Bedja D, Chen Y, van Erp C, Lindsay ME, Kim D, Schoenhoff F, Cohn RD, Loeys BL, Thomas CJ, Patnaik S, Marugan JJ, Judge DP, Dietz HC. 2011. Noncanonical TGFbeta signaling contributes to aortic aneurysm progression in Marfan syndrome mice. Science 332: 358-361.
- Holmbeck K, Bianco P, Caterina J, Yamada S, Kromer M, Kuznetsov SA, Mankani M, Robey PG, Poole AR, Pidoux I, Ward JM, Birkedal-Hansen H. 1999. MT1-MMP-deficient mice develop dwarfism, osteopenia, arthritis, and connective tissue disease due to inadequate collagen turnover. Cell 99: 81-92.
- Host L, Paye A, Detry B, Blacher S, Munaut C, Foidart JM, Seiki M, Sounni NE, Noel A. 2012. The proteolytic activity of MT4-MMP is required for its pro-angiogenic and pro-metastatic promoting effects. Int J Cancer 131: 1537-1548.
- Huang CH, Yang WH, Chang SY, Tai SK, Tzeng CH, Kao JY, Wu KJ, Yang MH. 2009. Regulation of membrane-type 4 matrix metalloproteinase by SLUG contributes to hypoxia-mediated metastasis. Neoplasia 11: 1371-1382.
- Huang J, Davis EC, Chapman SL, Budatha M, Marmorstein LY, Word RA, Yanagisawa H. 2010. Fibulin-4 deficiency results in ascending aortic aneurysms: a potential link between abnormal smooth muscle cell phenotype and aneurysm progression. Circ Res 106: 583-592.
- Huang Y, Guo X, Kassab GS. 2006. Axial nonuniformity of geometric and mechanical properties of mouse aorta is increased during postnatal growth. Am J Physiol Heart Circ Physiol 290: H657-664.
- Humphrey JD, Milewicz DM, Tellides G, Schwartz MA. 2014. Cell biology. Dysfunctional mechanosensing in aneurysms. Science 344: 477-479.
- Humphrey JD, Schwartz MA, Tellides G, Milewicz DM. 2015. Role of mechanotransduction in vascular biology: focus on thoracic aortic aneurysms and dissections. Circ Res 116: 1448-1461.
- Hungerford JE, Little CD. 1999. Developmental biology of the vascular smooth muscle cell: building a multilayered vessel wall. J Vasc Res 36: 2-27.
- Huusko T, Salonurmi T, Taskinen P, Liinamaa J, Juvonen T, Paakko P, Savolainen M, Kakko S. 2013. Elevated messenger RNA expression and plasma protein levels of osteopontin and matrix metalloproteinase types 2 and 9 in patients with ascending aortic aneurysms. J Thorac Cardiovasc Surg 145: 1117-1123.
- Hynes RO. 2009. The extracellular matrix: not just pretty fibrils. Science 326: 1216-1219.

- Inamoto S, Kwartler CS, Lafont AL, Liang YY, Fadulu VT, Duraisamy S, Willing M, Estrera A, Safi H, Hannibal MC, Carey J, Wiktorowicz J, Tan FK, Feng XH, Pannu H, Milewicz DM. 2010. TGFBR2 mutations alter smooth muscle cell phenotype and predispose to thoracic aortic aneurysms and dissections. Cardiovasc Res 88: 520-529.
- Intengan HD, Schiffrin EL. 2001. Vascular remodeling in hypertension: roles of apoptosis, inflammation, and fibrosis. Hypertension 38: 581-587.
- Isoda K, Nishikawa K, Kamezawa Y, Yoshida M, Kusuhara M, Moroi M, Tada N, Ohsuzu F. 2002. Osteopontin plays an important role in the development of medial thickening and neointimal formation. Circ Res 91: 77-82.
- Isselbacher EM. 2005. Thoracic and abdominal aortic aneurysms. Circulation 111: 816-828.
- Itoh Y, Kajita M, Kinoh H, Mori H, Okada A, Seiki M. 1999. Membrane type 4 matrix metalloproteinase (MT4-MMP, MMP-17) is a glycosylphosphatidylinositol-anchored proteinase. J Biol Chem 274: 34260-34266.
- Jackson V, Olsson T, Kurtovic S, Folkersen L, Paloschi V, Wagsater D, Franco-Cereceda A, Eriksson P. 2012. Matrix metalloproteinase 14 and 19 expression is associated with thoracic aortic aneurysms. J Thorac Cardiovasc Surg 144: 459-466.
- Jalvy S, Renault MA, Leen LL, Belloc I, Bonnet J, Gadeau AP, Desgranges C. 2007. Autocrine expression of osteopontin contributes to PDGF-mediated arterial smooth muscle cell migration. Cardiovasc Res 75: 738-747.
- Kanematsu Y, Kanematsu M, Kurihara C, Tsou TL, Nuki Y, Liang EI, Makino H, Hashimoto T. 2010. Pharmacologically induced thoracic and abdominal aortic aneurysms in mice. Hypertension 55: 1267-1274.
- Karnik SK, Brooke BS, Bayes-Genis A, Sorensen L, Wythe JD, Schwartz RS, Keating MT, Li DY. 2003. A critical role for elastin signaling in vascular morphogenesis and disease. Development 130: 411-423.
- Kazanecki CC, Uzwiak DJ, Denhardt DT. 2007a. Control of osteopontin signaling and function by post-translational phosphorylation and protein folding. J Cell Biochem 102: 912-924.
- Kazanecki CC, Kowalski AJ, Ding T, Rittling SR, Denhardt DT. 2007b. Characterization of anti-osteopontin monoclonal antibodies: Binding sensitivity to post-translational modifications. J Cell Biochem 102: 925-935.
- Kelleher CM, McLean SE, Mecham RP. 2004. Vascular extracellular matrix and aortic development. Curr Top Dev Biol 62: 153-188.
- Kielty CM, Sherratt MJ, Shuttleworth CA. 2002. Elastic fibres. J Cell Sci 115: 2817-2828.
- Kolkenbrock H, Essers L, Ulbrich N, Will H. 1999. Biochemical characterization of the catalytic domain of membrane-type 4 matrix metalloproteinase. Biol Chem 380: 1103-1108.
- Koziol A, Gonzalo P, Mota A, Pollan A, Lorenzo C, Colome N, Montaner D, Dopazo J, Arribas J, Canals F, Arroyo AG. 2012. The protease MT1-MMP drives a combinatorial proteolytic program in activated endothelial cells. FASEB J 26: 4481-4494.
- Kuang SQ, Kwartler CS, Byanova KL, Pham J, Gong L, Prakash SK, Huang J, Kamm KE, Stull JT, Sweeney HL, Milewicz DM. 2012. Rare, nonsynonymous variant in the smooth muscle-specific isoform of myosin heavy chain, MYH11, R247C, alters force generation in the aorta and phenotype of smooth muscle cells. Circ Res 110: 1411-1422.
- Kubota T, Zhang Q, Wrana JL, Ber R, Aubin JE, Butler WT, Sodek J. 1989. Multiple forms of SppI (secreted phosphoprotein, osteopontin) synthesized by normal and

transformed rat bone cell populations: regulation by TGF-beta. Biochem Biophys Res Commun 162: 1453-1459.
- Kumar A, Lindner V. 1997. Remodeling with neointima formation in the mouse carotid artery after cessation of blood flow. Arterioscler Thromb Vasc Biol 17: 2238-2244.
- Lacolley P, Regnault V, Nicoletti A, Li Z, Michel JB. 2012. The vascular smooth muscle cell in arterial pathology: a cell that can take on multiple roles. Cardiovasc Res 95: 194-204.
- Leigh NR, Schupp MO, Li K, Padmanabhan V, Gastonguay A, Wang L, Chun CZ, Wilkinson GA, Ramchandran R. 2013. Mmp17b is essential for proper neural crest cell migration in vivo. PLoS One 8: e76484.
- Lenk GM, Tromp G, Weinsheimer S, Gatalica Z, Berguer R, Kuivaniemi H. 2007. Whole genome expression profiling reveals a significant role for immune function in human abdominal aortic aneurysms. BMC Genomics 8: 237.
- Li DY, Brooke B, Davis EC, Mecham RP, Sorensen LK, Boak BB, Eichwald E, Keating MT. 1998. Elastin is an essential determinant of arterial morphogenesis. Nature 393: 276-280.
- Li H, Durbin R. 2010. Fast and accurate long-read alignment with Burrows-Wheeler transform. Bioinformatics 26: 589-595.
- Li JJ, Han M, Wen JK, Li AY. 2007. Osteopontin stimulates vascular smooth muscle cell migration by inducing FAK phosphorylation and ILK dephosphorylation. Biochem Biophys Res Commun 356: 13-19.
- Li W, Li Q, Jiao Y, Qin L, Ali R, Zhou J, Ferruzzi J, Kim RW, Geirsson A, Dietz HC, Offermanns S, Humphrey JD, Tellides G. 2014. Tgfbr2 disruption in postnatal smooth muscle impairs aortic wall homeostasis. J Clin Invest 124: 755-767.
- Liaw L, Almeida M, Hart CE, Schwartz SM, Giachelli CM. 1994. Osteopontin promotes vascular cell adhesion and spreading and is chemotactic for smooth muscle cells in vitro. Circ Res 74: 214-224.
- Liaw L, Birk DE, Ballas CB, Whitsitt JS, Davidson JM, Hogan BL. 1998. Altered wound healing in mice lacking a functional osteopontin gene (spp1). J Clin Invest 101: 1468-1478.
- Lindsay ME, Dietz HC. 2011. Lessons on the pathogenesis of aneurysm from heritable conditions. Nature 473: 308-316.
- Lingwood D, Simons K. 2010. Lipid rafts as a membrane-organizing principle. Science 327: 46-50.
- Longo GM, Buda SJ, Fiotta N, Xiong W, Griener T, Shapiro S, Baxter BT. 2005. MMP-12 has a role in abdominal aortic aneurysms in mice. Surgery 137: 457-462.
- Lopez-Ferrer D, Ramos-Fernandez A, Martinez-Bartolome S, Garcia-Ruiz P, Vazquez J. 2006. Quantitative proteomics using 16O/18O labeling and linear ion trap mass spectrometry. Proteomics 6 Suppl 1: S4-11.
- Lund SA, Giachelli CM, Scatena M. 2009. The role of osteopontin in inflammatory processes. J Cell Commun Signal 3: 311-322.
- Martinez-Bartolome S, Navarro P, Martin-Maroto F, Lopez-Ferrer D, Ramos-Fernandez A, Villar M, Garcia-Ruiz JP, Vazquez J. 2008. Properties of average score distributions of SEQUEST: the probability ratio method. Mol Cell Proteomics 7: 1135-1145.
- Martinez-Revelles S, Avendano MS, Garcia-Redondo AB, Alvarez Y, Aguado A, Perez-Giron JV, Garcia-Redondo L, Esteban V, Redondo JM, Alonso MJ, Briones AM, Salaices

M. 2013. Reciprocal relationship between reactive oxygen species and cyclooxygenase-2 and vascular dysfunction in hypertension. Antioxid Redox Signal 18: 51-65.
- McLean SE, Mecham BH, Kelleher CM, Mariani TJ, Mecham RP. 2005. Extracellular matrix gene expression in the developing mouse aorta. In:Miner JH, ed. Extracellular Matrix in Development and Disease. San Diego, CA: Elsevier; 2005;15:81–128.
- Milewicz DM, Regalado ES, Shendure J, Nickerson DA, Guo DC. 2014. Successes and challenges of using whole exome sequencing to identify novel genes underlying an inherited predisposition for thoracic aortic aneurysms and acute aortic dissections. Trends Cardiovasc Med 24: 53-60.
- Milewicz DM, Guo DC, Tran-Fadulu V, Lafont AL, Papke CL, Inamoto S, Kwartler CS, Pannu H. 2008. Genetic basis of thoracic aortic aneurysms and dissections: focus on smooth muscle cell contractile dysfunction. Annu Rev Genomics Hum Genet 9: 283-302.
- Misra A, Sheikh AQ, Kumar A, Luo J, Zhang J, Hinton RB, Smoot L, Kaplan P, Urban Z, Qyang Y, Tellides G, Greif DM. 2016. Integrin beta3 inhibition is a therapeutic strategy for supravalvular aortic stenosis. J Exp Med.
- Moltzer E, te Riet L, Swagemakers SM, van Heijningen PM, Vermeij M, van Veghel R, Bouhuizen AM, van Esch JH, Lankhorst S, Ramnath NW, de Waard MC, Duncker DJ, van der Spek PJ, Rouwet EV, Danser AH, Essers J. 2011. Impaired vascular contractility and aortic wall degeneration in fibulin-4 deficient mice: effect of angiotensin II type 1 (AT1) receptor blockade. PLoS One 6: e23411.
- Myers DL, Harmon KJ, Lindner V, Liaw L. 2003. Alterations of arterial physiology in osteopontin-null mice. Arterioscler Thromb Vasc Biol 23: 1021-1028.
- Navarro P, Vazquez J. 2009. A refined method to calculate false discovery rates for peptide identification using decoy databases. J Proteome Res 8: 1792-1796.
- Ohshima S, Yamaguchi N, Nishioka K, Mima T, Ishii T, Umeshita-Sasai M, Kobayashi H, Shimizu M, Katada Y, Wakitani S, Murata N, Nomura S, Matsuno H, Katayama R, Kon S, Inobe M, Uede T, Kawase I, Saeki Y. 2002. Enhanced local production of osteopontin in rheumatoid joints. J Rheumatol 29: 2061-2067.
- Okamoto H. 2007. Osteopontin and cardiovascular system. Mol Cell Biochem 300: 1-7.
- Owens GK. 1995. Regulation of differentiation of vascular smooth muscle cells. Physiol Rev 75: 487-517.
- Owens GK, Kumar MS, Wamhoff BR. 2004. Molecular regulation of vascular smooth muscle cell differentiation in development and disease. Physiol Rev 84: 767-801.
- Page-McCaw A, Ewald AJ, Werb Z. 2007. Matrix metalloproteinases and the regulation of tissue remodelling. Nat Rev Mol Cell Biol 8: 221-233.
- Pasquali-Ronchetti I, Baccarani-Contri M. 1997. Elastic fiber during development and aging. Microsc Res Tech 38: 428-435.
- Patwari P, Gao G, Lee JH, Grodzinsky AJ, Sandy JD. 2005. Analysis of ADAMTS4 and MT4-MMP indicates that both are involved in aggrecanolysis in interleukin-1-treated bovine cartilage. Osteoarthritis Cartilage 13: 269-277.
- Paye A, Truong A, Yip C, Cimino J, Blacher S, Munaut C, Cataldo D, Foidart JM, Maquoi E, Collignon J, Delvenne P, Jerusalem G, Noel A, Sounni NE. 2014. EGFR activation and signaling in cancer cells are enhanced by the membrane-bound metalloprotease MT4-MMP. Cancer Res 74: 6758-6770.
- Pei D, Weiss SJ. 1995. Furin-dependent intracellular activation of the human stromelysin-3 zymogen. Nature 375: 244-247.

- Pereira L, Andrikopoulos K, Tian J, Lee SY, Keene DR, Ono R, Reinhardt DP, Sakai LY, Biery NJ, Bunton T, Dietz HC, Ramirez F. 1997. Targetting of the gene encoding fibrillin-1 recapitulates the vascular aspect of Marfan syndrome. Nat Genet 17: 218-222.
- Plaisier M, Koolwijk P, Hanemaaijer R, Verwey RA, van der Weiden RM, Risse EK, Jungerius C, Helmerhorst FM, van Hinsbergh VW. 2006. Membrane-type matrix metalloproteinases and vascularization in human endometrium during the menstrual cycle. Mol Hum Reprod 12: 11-18.
- Plaisier M, Kapiteijn K, Koolwijk P, Fijten C, Hanemaaijer R, Grimbergen JM, Mulder-Stapel A, Quax PH, Helmerhorst FM, van Hinsbergh VW. 2004. Involvement of membrane-type matrix metalloproteinases (MT-MMPs) in capillary tube formation by human endometrial microvascular endothelial cells: role of MT3-MMP. J Clin Endocrinol Metab 89: 5828-5836.
- Puente XS, Pendas AM, Llano E, Velasco G, Lopez-Otin C. 1996. Molecular cloning of a novel membrane-type matrix metalloproteinase from a human breast carcinoma. Cancer Res 56: 944-949.
- Ramos-Fernandez A, Lopez-Ferrer D, Vazquez J. 2007. Improved method for differential expression proteomics using trypsin-catalyzed 18O labeling with a correction for labeling efficiency. Mol Cell Proteomics 6: 1274-1286.
- Regalado ES, Guo DC, Villamizar C, Avidan N, Gilchrist D, McGillivray B, Clarke L, Bernier F, Santos-Cortez RL, Leal SM, Bertoli-Avella AM, Shendure J, Rieder MJ, Nickerson DA, Project NGES, Milewicz DM. 2011. Exome sequencing identifies SMAD3 mutations as a cause of familial thoracic aortic aneurysm and dissection with intracranial and other arterial aneurysms. Circ Res 109: 680-686.
- Renna NF, de Las Heras N, Miatello RM. 2013. Pathophysiology of vascular remodeling in hypertension. Int J Hypertens 2013: 808353.
- Rikimaru A, Komori K, Sakamoto T, Ichise H, Yoshida N, Yana I, Seiki M. 2007. Establishment of an MT4-MMP-deficient mouse strain representing an efficient tracking system for MT4-MMP/MMP-17 expression in vivo using beta-galactosidase. Genes Cells 12: 1091-1100.
- Rodriguez D, Morrison CJ, Overall CM. 2010. Matrix metalloproteinases: what do they not do? New substrates and biological roles identified by murine models and proteomics. Biochim Biophys Acta 1803: 39-54.
- Ross TD, Coon BG, Yun S, Baeyens N, Tanaka K, Ouyang M, Schwartz MA. 2013. Integrins in mechanotransduction. Curr Opin Cell Biol 25: 613-618.
- Roy A, Kucukural A, Zhang Y. 2010. I-TASSER: a unified platform for automated protein structure and function prediction. Nat Protoc 5: 725-738.
- Rozanov DV, Hahn-Dantona E, Strickland DK, Strongin AY. 2004. The low density lipoprotein receptor-related protein LRP is regulated by membrane type-1 matrix metalloproteinase (MT1-MMP) proteolysis in malignant cells. J Biol Chem 279: 4260-4268.
- Sato H, Takino T, Okada Y, Cao J, Shinagawa A, Yamamoto E, Seiki M. 1994. A matrix metalloproteinase expressed on the surface of invasive tumour cells. Nature 370: 61-65.
- Scatena M, Liaw L, Giachelli CM. 2007. Osteopontin: a multifunctional molecule regulating chronic inflammation and vascular disease. Arterioscler Thromb Vasc Biol 27: 2302-2309.

- Schneider CA, Rasband WS, Eliceiri KW. 2012. NIH Image to ImageJ: 25 years of image analysis. Nat Methods 9: 671-675.
- Schwartz MA. 2010. Integrins and extracellular matrix in mechanotransduction. Cold Spring Harb Perspect Biol 2: a005066.
- Seo KW, Lee SJ, Ye BH, Kim YW, Bae SS, Kim CD. 2015. Mechanical stretch enhances the expression and activity of osteopontin and MMP-2 via the Akt1/AP-1 pathways in VSMC. J Mol Cell Cardiol 85: 13-24.
- Shen D, Li J, Lepore JJ, Anderson TJ, Sinha S, Lin AY, Cheng L, Cohen ED, Roberts JD, Jr., Dedhar S, Parmacek MS, Gerszten RE. 2011. Aortic aneurysm generation in mice with targeted deletion of integrin-linked kinase in vascular smooth muscle cells. Circ Res 109: 616-628.
- Simons M, Eichmann A. 2015. Molecular controls of arterial morphogenesis. Circ Res 116: 1712-1724.
- Sodhi CP, Phadke SA, Batlle D, Sahai A. 2001. Hypoxia stimulates osteopontin expression and proliferation of cultured vascular smooth muscle cells: potentiation by high glucose. Diabetes 50: 1482-1490.
- Sohail A, Sun Q, Zhao H, Bernardo MM, Cho JA, Fridman R. 2008. MT4-(MMP17) and MT6-MMP (MMP25), A unique set of membrane-anchored matrix metalloproteinases: properties and expression in cancer. Cancer Metastasis Rev 27: 289-302.
- Sohail A, Marco M, Zhao H, Shi Q, Merriman S, Mobashery S, Fridman R. 2011. Characterization of the dimerization interface of membrane type 4 (MT4)-matrix metalloproteinase. J Biol Chem 286: 33178-33189.
- Sounni NE, Paye A, Host L, Noel A. 2011. MT-MMPS as Regulators of Vessel Stability Associated with Angiogenesis. Front Pharmacol 2: 111.
- Speer MY, Chien YC, Quan M, Yang HY, Vali H, McKee MD, Giachelli CM. 2005. Smooth muscle cells deficient in osteopontin have enhanced susceptibility to calcification in vitro. Cardiovasc Res 66: 324-333.
- Spencer JA, Hacker SL, Davis EC, Mecham RP, Knutsen RH, Li DY, Gerard RD, Richardson JA, Olson EN, Yanagisawa H. 2005. Altered vascular remodeling in fibulin-5-deficient mice reveals a role of fibulin-5 in smooth muscle cell proliferation and migration. Proc Natl Acad Sci U S A 102: 2946-2951.
- Srichai MB, Colleta H, Gewin L, Matrisian L, Abel TW, Koshikawa N, Seiki M, Pozzi A, Harris RC, Zent R. 2011. Membrane-type 4 matrix metalloproteinase (MT4-MMP) modulates water homeostasis in mice. PLoS One 6: e17099.
- ten Dijke P, Arthur HM. 2007. Extracellular control of TGFbeta signalling in vascular development and disease. Nat Rev Mol Cell Biol 8: 857-869.
- Treadwell BV, Neidel J, Pavia M, Towle CA, Trice ME, Mankin HJ. 1986. Purification and characterization of collagenase activator protein synthesized by articular cartilage. Arch Biochem Biophys 251: 715-723.
- Trueblood NA, Xie Z, Communal C, Sam F, Ngoy S, Liaw L, Jenkins AW, Wang J, Sawyer DB, Bing OH, Apstein CS, Colucci WS, Singh K. 2001. Exaggerated left ventricular dilation and reduced collagen deposition after myocardial infarction in mice lacking osteopontin. Circ Res 88: 1080-1087.
- Truong A, Yip C, Paye A, Blacher S, Munaut C, Deroanne C, Noel A, Sounni NE. 2015. Dynamics of internalization and recycling of the prometastatic membrane type 4 matrix metalloproteinase (MT4-MMP) in breast cancer cells. FEBS J.

- Verma RP, Hansch C. 2007. Matrix metalloproteinases (MMPs): chemical-biological functions and (Q)SARs. Bioorg Med Chem 15: 2223-2268.
- Visse R, Nagase H. 2003. Matrix metalloproteinases and tissue inhibitors of metalloproteinases: structure, function, and biochemistry. Circ Res 92: 827-839.
- Wagenseil JE, Mecham RP. 2009. Vascular extracellular matrix and arterial mechanics. Physiol Rev 89: 957-989.
- Wang X, Page-McCaw A. 2014. A matrix metalloproteinase mediates long-distance attenuation of stem cell proliferation. J Cell Biol 206: 923-936.
- Wang Y, Johnson AR, Ye QZ, Dyer RD. 1999. Catalytic activities and substrate specificity of the human membrane type 4 matrix metalloproteinase catalytic domain. J Biol Chem 274: 33043-33049.
- Ward MR, Pasterkamp G, Yeung AC, Borst C. 2000. Arterial remodeling. Mechanisms and clinical implications. Circulation 102: 1186-1191.
- Wolak T. 2014. Osteopontin - a multi-modal marker and mediator in atherosclerotic vascular disease. Atherosclerosis 236: 327-337.
- Wolak T, Sion-Vardi N, Novack V, Greenberg G, Szendro G, Tarnovscki T, Nov O, Shelef I, Paran E, Rudich A. 2013. N-terminal rather than full-length osteopontin or its C-terminal fragment is associated with carotid-plaque inflammation in hypertensive patients. Am J Hypertens 26: 326-333.
- Xiong W, Meisinger T, Knispel R, Worth JM, Baxter BT. 2012. MMP-2 regulates Erk1/2 phosphorylation and aortic dilatation in Marfan syndrome. Circ Res 110: e92-e101.
- Yanagisawa H, Davis EC, Starcher BC, Ouchi T, Yanagisawa M, Richardson JA, Olson EN. 2002. Fibulin-5 is an elastin-binding protein essential for elastic fibre development in vivo. Nature 415: 168-171.
- Yu HW, Liu QF, Liu GN. 2010. Positive regulation of the Egr-1/osteopontin positive feedback loop in rat vascular smooth muscle cells by TGF-beta, ERK, JNK, and p38 MAPK signaling. Biochem Biophys Res Commun 396: 451-456.
- Yumoto K, Ishijima M, Rittling SR, Tsuji K, Tsuchiya Y, Kon S, Nifuji A, Uede T, Denhardt DT, Noda M. 2002. Osteopontin deficiency protects joints against destruction in anti-type II collagen antibody-induced arthritis in mice. Proc Natl Acad Sci U S A 99: 4556-4561.
- Zhou Z, Apte SS, Soininen R, Cao R, Baaklini GY, Rauser RW, Wang J, Cao Y, Tryggvason K. 2000. Impaired endochondral ossification and angiogenesis in mice deficient in membrane-type matrix metalloproteinase I. Proc Natl Acad Sci U S A 97: 4052-4057.
- Zohar R, Lee W, Arora P, Cheifetz S, McCulloch C, Sodek J. 1997. Single cell analysis of intracellular osteopontin in osteogenic cultures of fetal rat calvarial cells. J Cell Physiol 170: 88-100.

Supplemental Material

Supplemental Figure I

Mt4-mmp$^{+/-}$

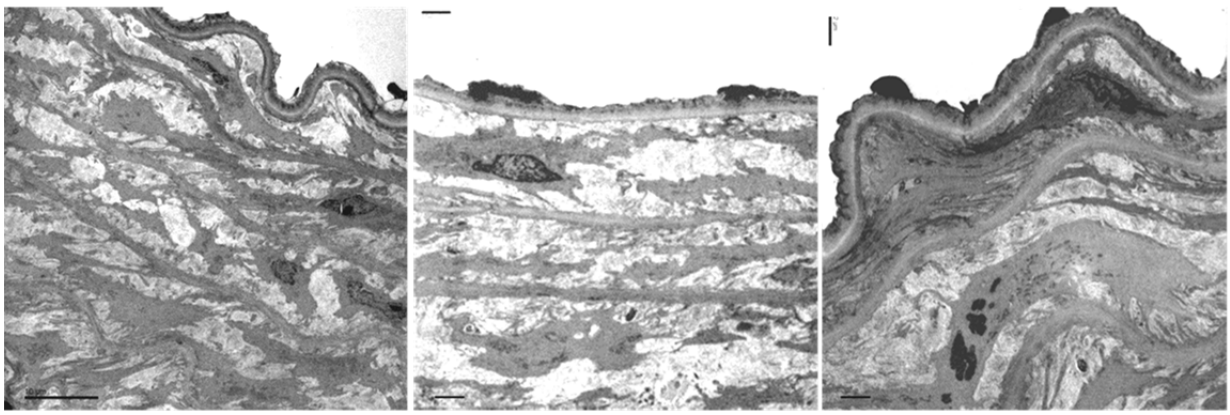

Supplemental Figure I. TEM analysis of transverse sections shows accumulation of extracellular matrix and altered vascular SMC phenotype and distribution (rounder cells and more than one vascular SMC per layer) in some areas of the aortic wall from *Mt4-mmp*-heterozygous mice. Scale bar 10 μm (left) and 2 μm (middle and right).

Supplemental material

Table I. Neonate (P7) and adult protein components of the GO categories found significantly altered in the iTRAQ proteomics experiment Proteins were classified into GO categories and statistically significant differences at the protein function level were determined as explained in Supplemental Methods. Proteins are sorted according to Zq, the standardized log2-ratio of protein abundance, which describes the variation of protein log2-ratio around the grand mean of the experiment in units of standard deviation, according to the formulation of the WSPP model.

Neonate (P7) iTRAQ proteins in categories

Actin filament binding GO:0051015

Protein identification	Zq	rank/N
>sp|Q61879|MYH10_MOUSE Myosin-10 OS=Mus musculus GN=Myh10 PE=1 SV=2	-2.659	0.015
>sp|O88990|ACTN3_MOUSE Alpha-actinin-3 OS=Mus musculus GN=Actn3 PE=2 SV=1	-2.598	0.044
>sp|Q8VDD5|MYH9_MOUSE Myosin-9 OS=Mus musculus GN=Myh9 PE=1 SV=4	-2.481	0.074
>sp|Q9JI91|ACTN2_MOUSE Alpha-actinin-2 OS=Mus musculus GN=Actn2 PE=1 SV=2	-2.471	0.103
>sp|O89053|COR1A_MOUSE Coronin-1A OS=Mus musculus GN=Coro1a PE=1 SV=5	-2.163	0.132
>sp|Q8BTM8|FLNA_MOUSE Filamin-A OS=Mus musculus GN=Flna PE=1 SV=5	-1.903	0.162
>tr|A1BN54|A1BN54_MOUSE Alpha actinin 1a OS=Mus musculus GN=Actn1 PE=2 SV=1	-1.873	0.191
>sp|Q01279|EGFR_MOUSE Epidermal growth factor receptor OS=Mus musculus GN=Egfr PE=1 SV	-1.839	0.221
>sp|P26040|EZRI_MOUSE Ezrin OS=Mus musculus GN=Ezr PE=1 SV=3	-1.714	0.250
>sp|Q7TMB8|CYFP1_MOUSE Cytoplasmic FMR1-interacting protein 1 OS=Mus musculus GN=Cyfi	-1.485	0.279
>sp|P57780|ACTN4_MOUSE Alpha-actinin-4 OS=Mus musculus GN=Actn4 PE=1 SV=1	-1.441	0.309
>sp|Q61233|PLSL_MOUSE Plastin-2 OS=Mus musculus GN=Lcp1 PE=1 SV=4	-1.265	0.338
>sp|P28650|PURA1_MOUSE Adenylosuccinate synthetase isozyme 1 OS=Mus musculus GN=Adssl1	-1.133	0.368
>sp|Q9WUM4|COR1C_MOUSE Coronin-1C OS=Mus musculus GN=Coro1c PE=1 SV=2	-1.090	0.397
>sp|P26231|CTNA1_MOUSE Catenin alpha-1 OS=Mus musculus GN=Ctnna1 PE=1 SV=1	-1.026	0.426
>sp|Q9QYC0|ADDA_MOUSE Alpha-adducin OS=Mus musculus GN=Add1 PE=1 SV=2	-0.981	0.456
>sp|Q6PB66|LPPRC_MOUSE Leucine-rich PPR motif-containing protein, mitochondrial OS=Mus mu	-0.883	0.485
>sp|Q7TPR4|ACTN1_MOUSE Alpha-actinin-1 OS=Mus musculus GN=Actn1 PE=1 SV=1	-0.667	0.515
>sp|A2ALU4|SHRM2_MOUSE Protein Shroom2 OS=Mus musculus GN=Shroom2 PE=1 SV=1	-0.588	0.544
>sp|Q9WUM3|COR1B_MOUSE Coronin-1B OS=Mus musculus GN=Coro1b PE=1 SV=1	-0.573	0.574
>sp|Q62418|DBNL_MOUSE Drebrin-like protein OS=Mus musculus GN=Dbnl PE=1 SV=2	-0.323	0.603
>sp|Q9QYB8|ADDB_MOUSE Beta-adducin OS=Mus musculus GN=Add2 PE=1 SV=4	-0.152	0.632
>sp|Q8K4L3|SVIL_MOUSE Supervillin OS=Mus musculus GN=Svil PE=1 SV=1	-0.101	0.662
>sp|Q6ZWR6|SYNE1_MOUSE Nesprin-1 OS=Mus musculus GN=Syne1 PE=1 SV=2	-0.067	0.691
>sp|Q61553|FSCN1_MOUSE Fascin OS=Mus musculus GN=Fscn1 PE=1 SV=4	-0.020	0.721
>sp|Q9ERG0|LIMA1_MOUSE LIM domain and actin-binding protein 1 OS=Mus musculus GN=Lima	0.000	0.750
>sp|P47757|CAPZB_MOUSE F-actin-capping protein subunit beta OS=Mus musculus GN=Capzb PE=	0.099	0.779
>sp|Q64331|MYO6_MOUSE Unconventional myosin-VI OS=Mus musculus GN=Myo6 PE=1 SV=1	0.103	0.809
>sp|Q7TPW1|NEXN_MOUSE Nexilin OS=Mus musculus GN=Nexn PE=1 SV=3	0.219	0.838
>sp|Q6URW6|MYH14_MOUSE Myosin-14 OS=Mus musculus GN=Myh14 PE=1 SV=1	0.273	0.868
>sp|P47753|CAZA1_MOUSE F-actin-capping protein subunit alpha-1 OS=Mus musculus GN=Capza1	0.345	0.897
>sp|Q91XC0|AJUBA_MOUSE LIM domain-containing protein ajuba OS=Mus musculus GN=Ajuba I	0.459	0.926
>tr|Q3TN34|Q3TN34_MOUSE JRAB OS=Mus musculus GN=Micall2 PE=2 SV=1	1.137	0.956
>sp|Q61792|LASP1_MOUSE LIM and SH3 domain protein 1 OS=Mus musculus GN=Lasp1 PE=1 SV	1.596	0.985

Ribonucleoprotein complex GO:0030529

Protein identification	Zq	rank/N
>tr|Q5FWB6|Q5FWB6_MOUSE MCG17387, isoform CRA_a OS=Mus musculus GN=Rplp0 PE=2 S	-4.122	0.003
>sp|P62702|RS4X_MOUSE 40S ribosomal protein S4, X isoform OS=Mus musculus GN=Rps4x PE=	-3.903	0.009
>sp|Q9JJI8|RL38_MOUSE 60S ribosomal protein L38 OS=Mus musculus GN=Rpl38 PE=2 SV=3	-3.675	0.016
>sp|Q6ZWV3|RL10_MOUSE 60S ribosomal protein L10 OS=Mus musculus GN=Rpl10 PE=2 SV=3	-3.197	0.022

Adult iTRAQ proteins in categories

Collagen GO:0005581

Protein identification	Zq	rank/N
>sp|P28481|CO2A1_MOUSE Collagen alpha-1(II) chain OS=Mus musculus GN=Col2a1 PE	-3.672	0.025
>sp|Q3U962|CO5A2_MOUSE Collagen alpha-2(V) chain OS=Mus musculus GN=Col5a2 P	-3.301	0.075
>tr|B1AVK5|B1AVK5_MOUSE Procollagen type IV alpha 6 OS=Mus musculus GN=Col4a	-3.035	0.125
>sp|P39061|COIA1_MOUSE Collagen alpha-1(XVIII) chain OS=Mus musculus GN=Col18a	-2.832	0.175
>sp|P28301|LYOX_MOUSE Protein-lysine 6-oxidase OS=Mus musculus GN=Lox PE=1 SV	-2.625	0.225
>sp|P11087|CO1A1_MOUSE Collagen alpha-1(I) chain OS=Mus musculus GN=Col1a1 PE=	-2.341	0.275
>sp|O88207|CO5A1_MOUSE Collagen alpha-1(V) chain OS=Mus musculus GN=Col5a1 PE	-2.086	0.325
>sp|Q01149|CO1A2_MOUSE Collagen alpha-2(I) chain OS=Mus musculus GN=Col1a2 PE=	-2.071	0.375
>sp|Q04857|CO6A1_MOUSE Collagen alpha-1(VI) chain OS=Mus musculus GN=Col6a1 P	-1.838	0.425
>sp|Q80X19|COEA1_MOUSE Collagen alpha-1(XIV) chain OS=Mus musculus GN=Col14a	-1.625	0.475
>sp|Q8C6K9|CO6A6_MOUSE Collagen alpha-6(VI) chain OS=Mus musculus GN=Col6a6 I	-1.617	0.525
>sp|A6H584|CO6A5_MOUSE Collagen alpha-5(VI) chain OS=Mus musculus GN=Col6a5 P	-1.559	0.575
>sp|O35206|COFA1_MOUSE Collagen alpha-1(XV) chain OS=Mus musculus GN=Col15a1	-1.486	0.625
>sp|P08122|CO4A2_MOUSE Collagen alpha-2(IV) chain OS=Mus musculus GN=Col4a2 PI	-1.401	0.675
>sp|Q99K41|EMIL1_MOUSE EMILIN-1 OS=Mus musculus GN=Emilin1 PE=1 SV=1	-1.307	0.725
>sp|P02463|CO4A1_MOUSE Collagen alpha-1(IV) chain OS=Mus musculus GN=Col4a1 PI	-1.034	0.775
>sp|Q02788|CO6A2_MOUSE Collagen alpha-2(VI) chain OS=Mus musculus GN=Col6a2 P	-0.863	0.825
>tr|B7ZNH7|B7ZNH7_MOUSE Collagen alpha-1(XIV) chain OS=Mus musculus GN=Col14	-0.770	0.875
>sp|Q60847|COCA1_MOUSE Collagen alpha-1(XII) chain OS=Mus musculus GN=Col12a1	0.294	0.925
>sp|Q60994|ADIPO_MOUSE Adiponectin OS=Mus musculus GN=Adipoq PE=1 SV=2	0.829	0.975

Myosin complex GO:0016459

Protein identification	Zq	rank/N
>sp|Q64331|MYO6_MOUSE Unconventional myosin-VI OS=Mus musculus GN=Myo6 PE=	-3.068	0.024
>tr|Q69ZX3|Q69ZX3_MOUSE MKIAA0866 protein (Fragment) OS=Mus musculus GN=M	-3.047	0.071
>sp|Q5SX40|MYH1_MOUSE Myosin-1 OS=Mus musculus GN=Myh1 PE=1 SV=1	-2.997	0.119
>sp|Q5SYD0|MYO1D_MOUSE Unconventional myosin-Id OS=Mus musculus GN=Myo1d	-2.771	0.167
>sp|Q6URW6|MYH14_MOUSE Myosin-14 OS=Mus musculus GN=Myh14 PE=1 SV=1	-2.680	0.214
>tr|Q3UFT0|Q3UFT0_MOUSE Putative uncharacterized protein (Fragment) OS=Mus muscu	-2.267	0.262
>sp|Q8VDD5|MYH9_MOUSE Myosin-9 OS=Mus musculus GN=Myh9 PE=1 SV=4	-2.160	0.310
>sp|Q3THE2|ML12B_MOUSE Myosin regulatory light chain 12B OS=Mus musculus GN=M	-1.838	0.357
>sp|Q5SX39|MYH4_MOUSE Myosin-4 OS=Mus musculus GN=Myh4 PE=1 SV=1	-1.783	0.405
>sp|Q60605|MYL6_MOUSE Myosin light polypeptide 6 OS=Mus musculus GN=Myl6 PE=	-1.760	0.452
>sp|Q9CQ19|MYL9_MOUSE Myosin regulatory light polypeptide 9 OS=Mus musculus GN	-1.587	0.500
>sp|Q8CI43|MYL6B_MOUSE Myosin light chain 6B OS=Mus musculus GN=Myl6b PE=2	-1.483	0.548
>sp|Q61879|MYH10_MOUSE Myosin-10 OS=Mus musculus GN=Myh10 PE=1 SV=2	-1.350	0.595
>sp|P46735|MYO1B_MOUSE Unconventional myosin-Ib OS=Mus musculus GN=Myo1b P	-1.122	0.643
>tr|Q8BWY8|Q8BWY8_MOUSE Putative uncharacterized protein (Fragment) OS=Mus mus	-0.997	0.690
>sp|Q9WTI7|MYO1C_MOUSE Unconventional myosin-Ic OS=Mus musculus GN=Myo1c I	-0.969	0.738
>sp|O08638|MYH11_MOUSE Myosin-11 OS=Mus musculus GN=Myh11 PE=1 SV=1	-0.965	0.786
>sp|Q6AW69|CGNL1_MOUSE Cingulin-like protein 1 OS=Mus musculus GN=Cgnl1 PE=1	-0.084	0.833

>sp|Q8BP67|RL24_MOUSE 60S ribosomal protein L24 OS=Mus musculus GN=Rpl24 PE=2 SV=2	-2.545	0.028	>sp|P59242|CING_MOUSE Cingulin OS=Mus musculus GN=Cgn PE=1 SV=1	0.379	0.881
>tr|Q3TPD2|Q3TPD2_MOUSE Putative uncharacterized protein (Fragment) OS=Mus musculus GN=I	-2.211	0.035	>sp|Q9D0M5|DYL2_MOUSE Dynein light chain 2, cytoplasmic OS=Mus musculus GN=Dy	0.403	0.929
>sp|P60122|RUVB1_MOUSE RuvB-like 1 OS=Mus musculus GN=Ruvbl1 PE=1 SV=1	-2.159	0.041	>sp|Q02566|MYH6_MOUSE Myosin-6 OS=Mus musculus GN=Myh6 PE=1 SV=2	3.701	0.976
>sp|P62862|RS30_MOUSE 40S ribosomal protein S30 OS=Mus musculus GN=Fau PE=3 SV=1	-2.137	0.047			
>sp|P62900|RL31_MOUSE 60S ribosomal protein L31 OS=Mus musculus GN=Rpl31 PE=2 SV=1	-2.042	0.053	**Extracellular matrix GO:0031012**		
>sp|Q8CGC7|SYEP_MOUSE Bifunctional glutamate/proline--tRNA ligase OS=Mus musculus GN=Ep	-2.025	0.060	Protein identification	Zq	rank/N
>sp|P62082|RS7_MOUSE 40S ribosomal protein S7 OS=Mus musculus GN=Rps7 PE=2 SV=1	-1.846	0.066	>sp|Q61282|PGCA_MOUSE Aggrecan core protein OS=Mus musculus GN=Acan PE=1 SV=	-4.710	0.006
>sp|O70133|DHX9_MOUSE ATP-dependent RNA helicase A OS=Mus musculus GN=Dhx9 PE=1 SV	-1.830	0.072	>sp|P28481|CO2A1_MOUSE Collagen alpha-1(II) chain OS=Mus musculus GN=Col2a1 PE	-3.672	0.019
>sp|P62849|RS24_MOUSE 40S ribosomal protein S24 OS=Mus musculus GN=Rps24 PE=1 SV=1	-1.829	0.079	>sp|Q9QZZ6|DERM_MOUSE Dermatopontin OS=Mus musculus GN=Dpt PE=2 SV=1	-3.617	0.031
>tr|Q80UW7|Q80UW7_MOUSE IQ motif containing GTPase activating protein 1 OS=Mus musculus	-1.810	0.085	>sp|Q8BPB5|FBLN3_MOUSE EGF-containing fibulin-like extracellular matrix protein 1 OS	-3.415	0.043
>sp|P62830|RL23_MOUSE 60S ribosomal protein L23 OS=Mus musculus GN=Rpl23 PE=1 SV=1	-1.682	0.091	>sp|Q06890|CLUS_MOUSE Clusterin OS=Mus musculus GN=Clu PE=1 SV=1	-3.265	0.056
>sp|Q9CQI7|RU2B_MOUSE U2 small nuclear ribonucleoprotein B" OS=Mus musculus GN=Snrpb2 P	-1.656	0.097	>sp|P29788|VTNC_MOUSE Vitronectin OS=Mus musculus GN=Vtn PE=1 SV=2	-3.072	0.068
>sp|Q6ZWY3|RS27L_MOUSE 40S ribosomal protein S27-like OS=Mus musculus GN=Rps27l PE=2	-1.622	0.104	>sp|Q91V88|NPNT_MOUSE Nephronectin OS=Mus musculus GN=Npnt PE=1 SV=1	-3.021	0.080
>sp|P97351|RS3A_MOUSE 40S ribosomal protein S3a OS=Mus musculus GN=Rps3a PE=1 SV=3	-1.590	0.110	>sp|Q3UTY6|THSD4_MOUSE Thrombospondin type-1 domain-containing protein 4 OS=M	-3.002	0.093
>sp|Q9Z204|HNRPC_MOUSE Heterogeneous nuclear ribonucleoproteins C1/C2 OS=Mus musculus C	-1.588	0.116	>sp|P39061|COIA1_MOUSE Collagen alpha-1(XVIII) chain OS=Mus musculus GN=Col18a	-2.832	0.105
>sp|P62267|RS23_MOUSE 40S ribosomal protein S23 OS=Mus musculus GN=Rps23 PE=2 SV=3	-1.512	0.123	>sp|P11276|FINC_MOUSE Fibronectin OS=Mus musculus GN=Fn1 PE=1 SV=4	-2.610	0.117
>sp|P62281|RS11_MOUSE 40S ribosomal protein S11 OS=Mus musculus GN=Rps11 PE=2 SV=3	-1.505	0.129	>sp|Q8C4U3|SFRP1_MOUSE Secreted frizzled-related protein 1 OS=Mus musculus GN=Sfr	-2.608	0.130
>tr|Q8CDT3|Q8CDT3_MOUSE Putative uncharacterized protein (Fragment) OS=Mus musculus GN=	-1.465	0.135	>sp|O09164|SODE_MOUSE Extracellular superoxide dismutase [Cu-Zn] OS=Mus musculus	-2.564	0.142
>sp|Q6P5F9|XPO1_MOUSE Exportin-1 OS=Mus musculus GN=Xpo1 PE=1 SV=1	-1.461	0.142	>sp|Q8K4G1|LTBP4_MOUSE Latent-transforming growth factor beta-binding protein 4 OS=	-2.490	0.154
>sp|Q3UEB3|PUF60_MOUSE Poly(U)-binding-splicing factor PUF60 OS=Mus musculus GN=Puf60	-1.457	0.148	>tr|Q3UHH3|Q3UHH3_MOUSE Putative uncharacterized protein OS=Mus musculus GN=H	-2.457	0.167
>sp|P62855|RS26_MOUSE 40S ribosomal protein S26 OS=Mus musculus GN=Rps26 PE=2 SV=3	-1.453	0.154	>sp|Q99JR5|TINAL_MOUSE Tubulointerstitial nephritis antigen-like OS=Mus musculus GN	-2.434	0.179
>sp|P57780|ACTN4_MOUSE Alpha-actinin-4 OS=Mus musculus GN=Actn4 PE=1 SV=1	-1.441	0.160	>sp|P11087|CO1A1_MOUSE Collagen alpha-1(I) chain OS=Mus musculus GN=Col1a1 PE=	-2.341	0.191
>sp|P27048|RSMB_MOUSE Small nuclear ribonucleoprotein-associated protein B OS=Mus musculus	-1.434	0.167	>sp|P97873|LOXL1_MOUSE Lysyl oxidase homolog 1 OS=Mus musculus GN=Loxl1 PE=2	-2.209	0.204
>sp|Q61656|DDX5_MOUSE Probable ATP-dependent RNA helicase DDX5 OS=Mus musculus GN=I	-1.424	0.173	>sp|Q9R118|HTRA1_MOUSE Serine protease HTRA1 OS=Mus musculus GN=Htra1 PE=1	-2.193	0.216
>sp|P57784|RU2A_MOUSE U2 small nuclear ribonucleoprotein A' OS=Mus musculus GN=Snrpa1 PE	-1.423	0.179	>sp|P21956|MFGM_MOUSE Lactadherin OS=Mus musculus GN=Mfge8 PE=1 SV=3	-2.184	0.228
>sp|Q6ZWV7|RL35_MOUSE 60S ribosomal protein L35 OS=Mus musculus GN=Rpl35 PE=2 SV=1	-1.361	0.186	>sp|O88207|CO5A1_MOUSE Collagen alpha-1(V) chain OS=Mus musculus GN=Col5a1 PE	-2.086	0.241
>sp|P62301|RS13_MOUSE 40S ribosomal protein S13 OS=Mus musculus GN=Rps13 PE=1 SV=2	-1.341	0.192	>sp|P50608|FMOD_MOUSE Fibromodulin OS=Mus musculus GN=Fmod PE=2 SV=1	-2.085	0.253
>sp|P32067|LA_MOUSE Lupus La protein homolog OS=Mus musculus GN=Ssb PE=2 SV=1	-1.326	0.198	>sp|Q05793|PGBM_MOUSE Basement membrane-specific heparan sulfate proteoglycan cor	-2.073	0.265
>sp|P62751|RL23A_MOUSE 60S ribosomal protein L23a OS=Mus musculus GN=Rpl23a PE=1 SV=	-1.272	0.204	>sp|Q01339|APOH_MOUSE Beta-2-glycoprotein 1 OS=Mus musculus GN=Apoh PE=1 SV=	-2.071	0.278
>sp|P09405|NUCL_MOUSE Nucleolin OS=Mus musculus GN=Ncl PE=1 SV=2	-1.270	0.211	>sp|Q01149|CO1A2_MOUSE Collagen alpha-2(I) chain OS=Mus musculus GN=Col1a2 PE=	-2.071	0.290
>sp|Q9CPR4|RL17_MOUSE 60S ribosomal protein L17 OS=Mus musculus GN=Rpl17 PE=2 SV=3	-1.257	0.217	>sp|Q61001|LAMA5_MOUSE Laminin subunit alpha-5 OS=Mus musculus GN=Lama5 PE=	-1.923	0.302
>sp|Q9D1R9|RL34_MOUSE 60S ribosomal protein L34 OS=Mus musculus GN=Rpl34 PE=3 SV=2	-1.220	0.223	>sp|P21844|CMA1_MOUSE Chymase OS=Mus musculus GN=Cma1 PE=1 SV=2	-1.887	0.315
>sp|P14115|RL27A_MOUSE 60S ribosomal protein L27a OS=Mus musculus GN=Rpl27a PE=2 SV=5	-1.139	0.230	>tr|B1B0C7|B1B0C7_MOUSE Basement membrane-specific heparan sulfate proteoglycan c	-1.887	0.327
>sp|P29341|PABP1_MOUSE Polyadenylate-binding protein 1 OS=Mus musculus GN=Pabpc1 PE=1 S	-1.106	0.236	>sp|Q04857|CO6A1_MOUSE Collagen alpha-1(VI) chain OS=Mus musculus GN=Col6a1 P	-1.838	0.340
>sp|Q61937|NPM_MOUSE Nucleophosmin OS=Mus musculus GN=Npm1 PE=1 SV=1	-1.084	0.242	>tr|Q3TAF9|Q3TAF9_MOUSE Putative uncharacterized protein OS=Mus musculus GN=Bg	-1.782	0.352
>sp|Q8VDM6|HNRL1_MOUSE Heterogeneous nuclear ribonucleoprotein U-like protein 1 OS=Mus m	-1.067	0.248	>sp|Q8C6K9|CO6A6_MOUSE Collagen alpha-6(VI) chain OS=Mus musculus GN=Col6a6 I	-1.617	0.364
>sp|Q921F4|HNRLL_MOUSE Heterogeneous nuclear ribonucleoprotein L-like OS=Mus musculus GN	-1.045	0.255	>sp|P28654|PGS2_MOUSE Decorin OS=Mus musculus GN=Dcn PE=2 SV=1	-1.615	0.377
>sp|P51410|RL9_MOUSE 60S ribosomal protein L9 OS=Mus musculus GN=Rpl9 PE=2 SV=2	-1.036	0.261	>sp|Q640N1|AEBP1_MOUSE Adipocyte enhancer-binding protein 1 OS=Mus musculus GN	-1.583	0.389
>sp|Q9CXW4|RL11_MOUSE 60S ribosomal protein L11 OS=Mus musculus GN=Rpl11 PE=1 SV=4	-1.029	0.267	>sp|Q9JK53|PRELP_MOUSE Prolargin OS=Mus musculus GN=Prelp PE=2 SV=2	-1.559	0.401
>sp|Q7TMK9|HNRPQ_MOUSE Heterogeneous nuclear ribonucleoprotein Q OS=Mus musculus GN=	-1.009	0.274	>sp|Q62000|MIME_MOUSE Mimecan OS=Mus musculus GN=Ogn PE=2 SV=1	-1.550	0.414
>sp|P19253|RL13A_MOUSE 60S ribosomal protein L13a OS=Mus musculus GN=Rpl13a PE=1 SV=4	-0.910	0.280	>tr|A2AQ53|A2AQ53_MOUSE Fibrillin 1 OS=Mus musculus GN=Fbn1 PE=4 SV=1	-1.539	0.426
>sp|P62717|RL18A_MOUSE 60S ribosomal protein L18a OS=Mus musculus GN=Rpl18a PE=1 SV=	-0.901	0.286	>sp|O35206|COFA1_MOUSE Collagen alpha-1(XV) chain OS=Mus musculus GN=Col15a1	-1.486	0.438
>sp|Q8CCS6|PABP2_MOUSE Polyadenylate-binding protein 2 OS=Mus musculus GN=Pabpn1 PE=2	-0.898	0.292	>sp|Q61508|ECM1_MOUSE Extracellular matrix protein 1 OS=Mus musculus GN=Ecm1 PI	-1.437	0.451
>sp|Q6PB66|LPPRC_MOUSE Leucine-rich PPR motif-containing protein, mitochondrial OS=Mus mu	-0.883	0.299	>sp|Q07235|GDN_MOUSE Glia-derived nexin OS=Mus musculus GN=Serpine2 PE=2 SV=	-1.422	0.463
>sp|P47964|RL36_MOUSE 60S ribosomal protein L36 OS=Mus musculus GN=Rpl36 PE=2 SV=2	-0.866	0.305	>sp|P08122|CO4A2_MOUSE Collagen alpha-2(IV) chain OS=Mus musculus GN=Col4a2 PI	-1.401	0.475
>sp|P12970|RL7A_MOUSE 60S ribosomal protein L7a OS=Mus musculus GN=Rpl7a PE=2 SV=2	-0.863	0.311	>sp|Q62009|POSTN_MOUSE Periostin OS=Mus musculus GN=Postn PE=1 SV=2	-1.372	0.488
>sp|Q91VR5|DDX1_MOUSE ATP-dependent RNA helicase DDX1 OS=Mus musculus GN=Ddx1 PE	-0.850	0.318	>tr|J3QQ16|J3QQ16_MOUSE Protein Col6a3 OS=Mus musculus GN=Col6a3 PE=4 SV=1	-1.313	0.500
>sp|P62245|RS15A_MOUSE 40S ribosomal protein S15a OS=Mus musculus GN=Rps15a PE=2 SV=2	-0.848	0.324	>sp|Q99K41|EMIL1_MOUSE EMILIN-1 OS=Mus musculus GN=Emilin1 PE=1 SV=1	-1.307	0.512
>sp|Q9D0E1|HNRPM_MOUSE Heterogeneous nuclear ribonucleoprotein M OS=Mus musculus GN=I	-0.755	0.330	>tr|Q8BP04|Q8BP04_MOUSE Putative uncharacterized protein OS=Mus musculus GN=Lox	-1.261	0.525
>sp|P63017|HSP7C_MOUSE Heat shock cognate 71 kDa protein OS=Mus musculus GN=Hspa8 PE=1	-0.723	0.336	>sp|O88322|NID2_MOUSE Nidogen-2 OS=Mus musculus GN=Nid2 PE=1 SV=2	-1.257	0.537
>sp|P62754|RS6_MOUSE 40S ribosomal protein S6 OS=Mus musculus GN=Rps6 PE=1 SV=1	-0.720	0.343	>sp|Q08879|FBLN1_MOUSE Fibulin-1 OS=Mus musculus GN=Fbln1 PE=1 SV=2	-1.197	0.549
>sp|P62313|LSM6_MOUSE U6 snRNA-associated Sm-like protein LSm6 OS=Mus musculus GN=Lsr	-0.637	0.349	>sp|Q9DCT8|CRIP2_MOUSE Cysteine-rich protein 2 OS=Mus musculus GN=Crip2 PE=1 S	-1.158	0.562
>tr|Q3TT41|Q3TT41_MOUSE Putative uncharacterized protein OS=Mus musculus GN=Ncl PE=2 SV	-0.632	0.355	>tr|D3YWD1|D3YWD1_MOUSE Protein Col6a3 (Fragment) OS=Mus musculus GN=Col6a	-1.103	0.574

>sp|P62320|SMD3_MOUSE Small nuclear ribonucleoprotein Sm D3 OS=Mus musculus GN=Snrpd3	-0.583	0.362
>sp|P47915|RL29_MOUSE 60S ribosomal protein L29 OS=Mus musculus GN=Rpl29 PE=2 SV=2	-0.579	0.368
>tr|Q91V55|Q91V55_MOUSE 40S ribosomal protein S5 OS=Mus musculus GN=Rps5 PE=2 SV=1	-0.559	0.374
>sp|P62274|RS29_MOUSE 40S ribosomal protein S29 OS=Mus musculus GN=Rps29 PE=2 SV=2	-0.557	0.381
>sp|Q6NVF9|CPSF6_MOUSE Cleavage and polyadenylation specificity factor subunit 6 OS=Mus mu	-0.555	0.387
>sp|P97461|RS5_MOUSE 40S ribosomal protein S5 OS=Mus musculus GN=Rps5 PE=2 SV=3	-0.546	0.393
>tr|Q3TF92|Q3TF92_MOUSE Putative uncharacterized protein (Fragment) OS=Mus musculus GN=D	-0.532	0.399
>sp|P47962|RL5_MOUSE 60S ribosomal protein L5 OS=Mus musculus GN=Rpl5 PE=1 SV=3	-0.527	0.406
>sp|P62317|SMD2_MOUSE Small nuclear ribonucleoprotein Sm D2 OS=Mus musculus GN=Snrpd2	-0.521	0.412
>sp|Q60668|HNRPD_MOUSE Heterogeneous nuclear ribonucleoprotein D0 OS=Mus musculus GN=H	-0.496	0.418
>sp|Q921S7|RM37_MOUSE 39S ribosomal protein L37, mitochondrial OS=Mus musculus GN=Mrpl3	-0.493	0.425
>sp|P53026|RL10A_MOUSE 60S ribosomal protein L10a OS=Mus musculus GN=Rpl10a PE=1 SV=3	-0.491	0.431
>sp|P62305|RUXE_MOUSE Small nuclear ribonucleoprotein E OS=Mus musculus GN=Snrpe PE=2 S	-0.488	0.437
>sp|Q9CXY6|ILF2_MOUSE Interleukin enhancer-binding factor 2 OS=Mus musculus GN=Ilf2 PE=1	-0.484	0.443
>sp|P14148|RL7_MOUSE 60S ribosomal protein L7 OS=Mus musculus GN=Rpl7 PE=2 SV=2	-0.476	0.450
>sp|P62264|RS14_MOUSE 40S ribosomal protein S14 OS=Mus musculus GN=Rps14 PE=2 SV=3	-0.465	0.456
>sp|P99027|RLA2_MOUSE 60S acidic ribosomal protein P2 OS=Mus musculus GN=Rplp2 PE=1 SV	-0.457	0.462
>sp|P58252|EF2_MOUSE Elongation factor 2 OS=Mus musculus GN=Eef2 PE=1 SV=2	-0.437	0.469
>sp|P62918|RL8_MOUSE 60S ribosomal protein L8 OS=Mus musculus GN=Rpl8 PE=2 SV=2	-0.436	0.475
>sp|Q8R081|HNRPL_MOUSE Heterogeneous nuclear ribonucleoprotein L OS=Mus musculus GN=H	-0.429	0.481
>sp|P62852|RS25_MOUSE 40S ribosomal protein S25 OS=Mus musculus GN=Rps25 PE=2 SV=1	-0.414	0.487
>sp|P62960|YBOX1_MOUSE Nuclease-sensitive element-binding protein 1 OS=Mus musculus GN=Y	-0.410	0.494
>sp|Q8VEK3|HNRPU_MOUSE Heterogeneous nuclear ribonucleoprotein U OS=Mus musculus GN=H	-0.404	0.500
>tr|A2AW41|A2AW41_MOUSE Heterogeneous nuclear ribonucleoprotein R (Fragment) OS=Mus mu	-0.387	0.506
>tr|Q6P4T2|Q6P4T2_MOUSE Activating signal cointegrator 1 complex subunit 3-like 1 OS=Mus mus	-0.375	0.513
>sp|Q61990|PCBP2_MOUSE Poly(rC)-binding protein 2 OS=Mus musculus GN=Pcbp2 PE=1 SV=1	-0.374	0.519
>sp|Q9EQK5|MVP_MOUSE Major vault protein OS=Mus musculus GN=Mvp PE=1 SV=4	-0.320	0.525
>sp|Q9WTM5|RUVB2_MOUSE RuvB-like 2 OS=Mus musculus GN=Ruvbl2 PE=2 SV=3	-0.307	0.531
>sp|P35980|RL18_MOUSE 60S ribosomal protein L18 OS=Mus musculus GN=Rpl18 PE=2 SV=3	-0.298	0.538
>sp|Q6ZWN5|RS9_MOUSE 40S ribosomal protein S9 OS=Mus musculus GN=Rps9 PE=2 SV=3	-0.295	0.544
>sp|Q99020|ROAA_MOUSE Heterogeneous nuclear ribonucleoprotein A/B OS=Mus musculus GN=H	-0.292	0.550
>sp|P63276|RS17_MOUSE 40S ribosomal protein S17 OS=Mus musculus GN=Rps17 PE=1 SV=2	-0.248	0.557
>sp|O09167|RL21_MOUSE 60S ribosomal protein L21 OS=Mus musculus GN=Rpl21 PE=2 SV=3	-0.228	0.563
>sp|Q62376|RU17_MOUSE U1 small nuclear ribonucleoprotein 70 kDa OS=Mus musculus GN=Snrn	-0.227	0.569
>tr|E9QNN1|E9QNN1_MOUSE ATP-dependent RNA helicase A OS=Mus musculus GN=Dhx9 PE=4	-0.224	0.575
>sp|P97499|TEP1_MOUSE Telomerase protein component 1 OS=Mus musculus GN=Tep1 PE=1 SV=	-0.175	0.582
>sp|Q9CR57|RL14_MOUSE 60S ribosomal protein L14 OS=Mus musculus GN=Rpl14 PE=2 SV=3	-0.151	0.588
>sp|P27659|RL3_MOUSE 60S ribosomal protein L3 OS=Mus musculus GN=Rpl3 PE=2 SV=3	-0.131	0.594
>sp|P62984|RL40_MOUSE Ubiquitin-60S ribosomal protein L40 OS=Mus musculus GN=Uba52 PE=	-0.067	0.601
>sp|Q99PV0|PRP8_MOUSE Pre-mRNA-processing-splicing factor 8 OS=Mus musculus GN=Prpf8 P	-0.046	0.607
>sp|P62270|RS18_MOUSE 40S ribosomal protein S18 OS=Mus musculus GN=Rps18 PE=1 SV=3	-0.041	0.613
>tr|E9Q3T0|E9Q3T0_MOUSE Uncharacterized protein OS=Mus musculus GN=Gm10073 PE=4 SV=	-0.029	0.619
>sp|P61358|RL27_MOUSE 60S ribosomal protein L27 OS=Mus musculus GN=Rpl27 PE=2 SV=2	-0.024	0.626
>sp|Q91VM5|RMXL1_MOUSE RNA binding motif protein, X-linked-like-1 OS=Mus musculus GN=	-0.022	0.632
>sp|O35737|HNRH1_MOUSE Heterogeneous nuclear ribonucleoprotein H OS=Mus musculus GN=H	-0.009	0.638
>sp|P62843|RS15_MOUSE 40S ribosomal protein S15 OS=Mus musculus GN=Rps15 PE=2 SV=2	-0.008	0.645
>sp|Q6ZWM4|NAA38_MOUSE N-alpha-acetyltransferase 38, NatC auxiliary subunit OS=Mus muscu	0.004	0.651
>sp|P86048|RL10L_MOUSE 60S ribosomal protein L10-like OS=Mus musculus GN=Rpl10l PE=2 SV	0.006	0.657
>sp|Q9D823|RL37_MOUSE 60S ribosomal protein L37 OS=Mus musculus GN=Rpl37 PE=2 SV=3	0.056	0.664
>tr|Q3U1C4|Q3U1C4_MOUSE MCG1271 OS=Mus musculus GN=Secisbp2 PE=2 SV=1	0.056	0.670
>sp|P14131|RS16_MOUSE 40S ribosomal protein S16 OS=Mus musculus GN=Rps16 PE=2 SV=4	0.066	0.676
>sp|Q9CZM2|RL15_MOUSE 60S ribosomal protein L15 OS=Mus musculus GN=Rpl15 PE=2 SV=4	0.072	0.682
>sp|P62309|RUXG_MOUSE Small nuclear ribonucleoprotein G OS=Mus musculus GN=Snrpg PE=1	0.074	0.689
>sp|Q8VEE1|LMCD1_MOUSE LIM and cysteine-rich domains protein 1 OS=Mus musculus	-1.019	0.586
>sp|Q61292|LAMB2_MOUSE Laminin subunit beta-2 OS=Mus musculus GN=Lamb2 PE=2	-0.875	0.599
>sp|Q02788|CO6A2_MOUSE Collagen alpha-2(VI) chain OS=Mus musculus GN=Col6a2 P	-0.863	0.611
>sp|Q80YX1|TENA_MOUSE Tenascin OS=Mus musculus GN=Tnc PE=1 SV=1	-0.836	0.623
>sp|Q8CG19|LTBP1_MOUSE Latent-transforming growth factor beta-binding protein 1 OS=	-0.808	0.636
>sp|Q9WVH9|FBLN5_MOUSE Fibulin-5 OS=Mus musculus GN=Fbln5 PE=2 SV=1	-0.800	0.648
>sp|P20352|TF_MOUSE Tissue factor OS=Mus musculus GN=F3 PE=1 SV=2	-0.784	0.660
>tr|B7ZNH7|B7ZNH7_MOUSE Collagen alpha-1(XIV) chain OS=Mus musculus GN=Col14	-0.770	0.673
>tr|Q59IW6|Q59IW6_MOUSE Protein Abi3bp OS=Mus musculus GN=Abi3bp PE=2 SV=1	-0.766	0.685
>tr|B9EHT6|B9EHT6_MOUSE Fn1 protein OS=Mus musculus GN=Fn1 PE=2 SV=1	-0.756	0.698
>tr|F8VQJ3|F8VQJ3_MOUSE Laminin subunit gamma-1 OS=Mus musculus GN=Lamc1 PE	-0.750	0.710
>sp|P51885|LUM_MOUSE Lumican OS=Mus musculus GN=Lum PE=1 SV=2	-0.735	0.722
>sp|Q62219|TGFI1_MOUSE Transforming growth factor beta-1-induced transcript 1 protein	-0.636	0.735
>sp|P28653|PGS1_MOUSE Biglycan OS=Mus musculus GN=Bgn PE=2 SV=1	-0.631	0.747
>sp|Q8CIZ8|VWF_MOUSE von Willebrand factor OS=Mus musculus GN=Vwf PE=1 SV=2	-0.628	0.759
>sp|P97298|PEDF_MOUSE Pigment epithelium-derived factor OS=Mus musculus GN=Serp	-0.588	0.772
>sp|O70503|DHB12_MOUSE Estradiol 17-beta-dehydrogenase 12 OS=Mus musculus GN=H	-0.501	0.784
>sp|Q61543|GSLG1_MOUSE Golgi apparatus protein 1 OS=Mus musculus GN=Glg1 PE=1	-0.482	0.796
>sp|Q9QUP5|HPLN1_MOUSE Hyaluronan and proteoglycan link protein 1 OS=Mus muscul	-0.434	0.809
>sp|P08228|SODC_MOUSE Superoxide dismutase [Cu-Zn] OS=Mus musculus GN=Sod1 P	-0.301	0.821
>sp|Q9D1H9|MFAP4_MOUSE Microfibril-associated glycoprotein 4 OS=Mus musculus GN	-0.237	0.833
>sp|P09242|PPBT_MOUSE Alkaline phosphatase, tissue-nonspecific isozyme OS=Mus mus	-0.209	0.846
>sp|Q61554|FBN1_MOUSE Fibrillin-1 OS=Mus musculus GN=Fbn1 PE=1 SV=1	-0.142	0.858
>sp|P16045|LEG1_MOUSE Galectin-1 OS=Mus musculus GN=Lgals1 PE=1 SV=3	0.035	0.870
>sp|P82198|BGH3_MOUSE Transforming growth factor-beta-induced protein ig-h3 OS=Mu	0.160	0.883
>sp|P97857|ATS1_MOUSE A disintegrin and metalloproteinase with thrombospondin motifs	0.209	0.895
>sp|Q60847|COCA1_MOUSE Collagen alpha-1(XII) chain OS=Mus musculus GN=Col12a1	0.294	0.907
>sp|P18242|CATD_MOUSE Cathepsin D OS=Mus musculus GN=Ctsd PE=1 SV=1	0.378	0.920
>sp|P14211|CALR_MOUSE Calreticulin OS=Mus musculus GN=Calr PE=1 SV=1	0.603	0.932
>sp|P10493|NID1_MOUSE Nidogen-1 OS=Mus musculus GN=Nid1 PE=1 SV=2	0.631	0.944
>sp|Q99MQ4|ASPN_MOUSE Asporin OS=Mus musculus GN=Aspn PE=1 SV=1	0.657	0.957
>sp|P07901|HS90A_MOUSE Heat shock protein HSP 90-alpha OS=Mus musculus GN=Hsp	1.222	0.969
>sp|P07214|SPRC_MOUSE SPARC OS=Mus musculus GN=Sparc PE=1 SV=1	1.547	0.981
>sp|Q5FW85|ECM2_MOUSE Extracellular matrix protein 2 OS=Mus musculus GN=Ecm2 P	1.723	0.994

Focal adhesion GO:0005925

Protein identification	Zq	rank/N
>sp|Q6ZWQ0|SYNE2_MOUSE Nesprin-2 OS=Mus musculus GN=Syne2 PE=1 SV=2	-3.369	0.010
>sp|Q5SX40|MYH1_MOUSE Myosin-1 OS=Mus musculus GN=Myh1 PE=1 SV=1	-2.997	0.031
>sp|Q62523|ZYX_MOUSE Zyxin OS=Mus musculus GN=Zyx PE=1 SV=2	-2.059	0.052
>sp|Q5SX39|MYH4_MOUSE Myosin-4 OS=Mus musculus GN=Myh4 PE=1 SV=1	-1.783	0.073
>sp|Q03173|ENAH_MOUSE Protein enabled homolog OS=Mus musculus GN=Enah PE=1 S	-1.771	0.094
>sp|Q91XD2|LIMS2_MOUSE LIM and senescent cell antigen-like-containing domain protei	-1.394	0.115
>sp|P11688|ITA5_MOUSE Integrin alpha-5 OS=Mus musculus GN=Itga5 PE=1 SV=3	-1.370	0.135
>sp|Q8CGB6|TENC1_MOUSE Tensin-like C1 domain-containing phosphatase OS=Mus mu	-1.350	0.156
>sp|P26039|TLN1_MOUSE Talin-1 OS=Mus musculus GN=Tln1 PE=1 SV=2	-1.208	0.177
>sp|P09055|ITB1_MOUSE Integrin beta-1 OS=Mus musculus GN=Itgb1 PE=1 SV=1	-1.132	0.198
>sp|Q7TPR4|ACTN1_MOUSE Alpha-actinin-1 OS=Mus musculus GN=Actn1 PE=1 SV=1	-1.092	0.219
>sp|Q99JW4|LIMS1_MOUSE LIM and senescent cell antigen-like-containing domain protei	-1.035	0.240
>sp|Q9R1Z8|VINEX_MOUSE Vinexin OS=Mus musculus GN=Sorbs3 PE=1 SV=1	-0.898	0.260
>sp|P26041|MOES_MOUSE Moesin OS=Mus musculus GN=Msn PE=1 SV=3	-0.880	0.281
>sp|Q8VI36|PAXI_MOUSE Paxillin OS=Mus musculus GN=Pxn PE=1 SV=1	-0.879	0.302
>tr|E9Q0S6|E9Q0S6_MOUSE Protein Tns1 OS=Mus musculus GN=Tns1 PE=4 SV=1	-0.795	0.323

>sp|P14206|RSSA_MOUSE 40S ribosomal protein SA OS=Mus musculus GN=Rpsa PE=1 SV=4	0.076	0.695
>sp|P62311|LSM3_MOUSE U6 snRNA-associated Sm-like protein LSm3 OS=Mus musculus GN=Lsı	0.101	0.701
>sp|Q64012|RALY_MOUSE RNA-binding protein Raly OS=Mus musculus GN=Raly PE=1 SV=3	0.126	0.708
>sp|P61255|RL26_MOUSE 60S ribosomal protein L26 OS=Mus musculus GN=Rpl26 PE=2 SV=1	0.153	0.714
>sp|Q9CXW2|RT22_MOUSE 28S ribosomal protein S22, mitochondrial OS=Mus musculus GN=Mrp	0.174	0.720
>sp|Q9D0T1|NH2L1_MOUSE NHP2-like protein 1 OS=Mus musculus GN=Nhp2l1 PE=2 SV=4	0.186	0.726
>sp|P62908|RS3_MOUSE 40S ribosomal protein S3 OS=Mus musculus GN=Rps3 PE=1 SV=1	0.190	0.733
>sp|O35900|LSM2_MOUSE U6 snRNA-associated Sm-like protein LSm2 OS=Mus musculus GN=Ls	0.193	0.739
>sp|Q9Z2X1|HNRPF_MOUSE Heterogeneous nuclear ribonucleoprotein F OS=Mus musculus GN=H	0.205	0.745
>sp|P35550|FBRL_MOUSE rRNA 2'-O-methyltransferase fibrillarin OS=Mus musculus GN=Fbl PE=	0.207	0.752
>sp|P84099|RL19_MOUSE 60S ribosomal protein L19 OS=Mus musculus GN=Rpl19 PE=1 SV=1	0.211	0.758
>sp|P14869|RLA0_MOUSE 60S acidic ribosomal protein P0 OS=Mus musculus GN=Rplp0 PE=1 SV	0.212	0.764
>sp|P62242|RS8_MOUSE 40S ribosomal protein S8 OS=Mus musculus GN=Rps8 PE=1 SV=2	0.212	0.770
>sp|P47911|RL6_MOUSE 60S ribosomal protein L6 OS=Mus musculus GN=Rpl6 PE=1 SV=3	0.219	0.777
>tr|Q6ZWZ6|Q6ZWZ6_MOUSE 40S ribosomal protein S12 OS=Mus musculus GN=Rps12 PE=2 SV=	0.219	0.783
>sp|P67984|RL22_MOUSE 60S ribosomal protein L22 OS=Mus musculus GN=Rpl22 PE=2 SV=2	0.224	0.789
>sp|Q9Z1X4|ILF3_MOUSE Interleukin enhancer-binding factor 3 OS=Mus musculus GN=Ilf3 PE=1 S	0.261	0.796
>sp|P25444|RS2_MOUSE 40S ribosomal protein S2 OS=Mus musculus GN=Rps2 PE=1 SV=3	0.266	0.802
>sp|Q5SSK3|TEFM_MOUSE Transcription elongation factor, mitochondrial OS=Mus musculus GN=	0.267	0.808
>sp|P47955|RLA1_MOUSE 60S acidic ribosomal protein P1 OS=Mus musculus GN=Rplp1 PE=1 SV	0.303	0.814
>sp|P49962|SRP09_MOUSE Signal recognition particle 9 kDa protein OS=Mus musculus GN=Srp9 P	0.365	0.821
>tr|Q8VHM5|Q8VHM5_MOUSE Heterogeneous nuclear ribonucleoprotein R OS=Mus musculus GN=	0.412	0.827
>sp|P63325|RS10_MOUSE 40S ribosomal protein S10 OS=Mus musculus GN=Rps10 PE=1 SV=1	0.416	0.833
>sp|P35979|RL12_MOUSE 60S ribosomal protein L12 OS=Mus musculus GN=Rpl12 PE=1 SV=2	0.457	0.840
>sp|P49312|ROA1_MOUSE Heterogeneous nuclear ribonucleoprotein A1 OS=Mus musculus GN=Hn	0.474	0.846
>sp|Q9CX86|ROA0_MOUSE Heterogeneous nuclear ribonucleoprotein A0 OS=Mus musculus GN=H	0.550	0.852
>sp|Q9D8E6|RL4_MOUSE 60S ribosomal protein L4 OS=Mus musculus GN=Rpl4 PE=1 SV=3	0.573	0.858
>sp|Q8BG05|ROA3_MOUSE Heterogeneous nuclear ribonucleoprotein A3 OS=Mus musculus GN=H	0.587	0.865
>sp|O88569|ROA2_MOUSE Heterogeneous nuclear ribonucleoproteins A2/B1 OS=Mus musculus GN	0.603	0.871
>sp|P60335|PCBP1_MOUSE Poly(rC)-binding protein 1 OS=Mus musculus GN=Pcbp1 PE=1 SV=1	0.679	0.877
>sp|P62889|RL30_MOUSE 60S ribosomal protein L30 OS=Mus musculus GN=Rpl30 PE=2 SV=2	0.711	0.884
>sp|P70333|HNRH2_MOUSE Heterogeneous nuclear ribonucleoprotein H2 OS=Mus musculus GN=H	0.712	0.890
>sp|Q9JIK9|RT34_MOUSE 28S ribosomal protein S34, mitochondrial OS=Mus musculus GN=Mrps3	0.773	0.896
>sp|P61979|HNRPK_MOUSE Heterogeneous nuclear ribonucleoprotein K OS=Mus musculus GN=Hı	0.783	0.903
>sp|P60710|ACTB_MOUSE Actin, cytoplasmic 1 OS=Mus musculus GN=Actb PE=1 SV=1	0.902	0.909
>sp|P50580|PA2G4_MOUSE Proliferation-associated protein 2G4 OS=Mus musculus GN=Pa2g4 PE=	0.942	0.915
>sp|O55142|RL35A_MOUSE 60S ribosomal protein L35a OS=Mus musculus GN=Rpl35a PE=2 SV=	0.975	0.921
>sp|Q9ESX5|DKC1_MOUSE H/ACA ribonucleoprotein complex subunit 4 OS=Mus musculus GN=D	0.983	0.928
>sp|P47963|RL13_MOUSE 60S ribosomal protein L13 OS=Mus musculus GN=Rpl13 PE=2 SV=3	1.052	0.934
>sp|P83882|RL36A_MOUSE 60S ribosomal protein L36a OS=Mus musculus GN=Rpl36a PE=3 SV=2	1.110	0.940
>sp|Q8CJG0|AGO2_MOUSE Protein argonaute-2 OS=Mus musculus GN=Eif2c2 PE=1 SV=3	1.195	0.947
>sp|Q9CQR2|RS21_MOUSE 40S ribosomal protein S21 OS=Mus musculus GN=Rps21 PE=2 SV=1	1.221	0.953
>sp|P62315|SMD1_MOUSE Small nuclear ribonucleoprotein Sm D1 OS=Mus musculus GN=Snrpd1	1.222	0.959
>sp|P60867|RS20_MOUSE 40S ribosomal protein S20 OS=Mus musculus GN=Rps20 PE=1 SV=1	1.321	0.965
>sp|Q8CJG1|AGO1_MOUSE Protein argonaute-1 OS=Mus musculus GN=Eif2c1 PE=1 SV=2	1.327	0.972
>sp|P62858|RS28_MOUSE 40S ribosomal protein S28 OS=Mus musculus GN=Rps28 PE=2 SV=1	1.365	0.978
>sp|P63323|RS12_MOUSE 40S ribosomal protein S12 OS=Mus musculus GN=Rps12 PE=1 SV=2	1.528	0.984
>sp|P41105|RL28_MOUSE 60S ribosomal protein L28 OS=Mus musculus GN=Rpl28 PE=1 SV=2	2.092	0.991
>sp|Q9CZX8|RS19_MOUSE 40S ribosomal protein S19 OS=Mus musculus GN=Rps19 PE=1 SV=3	3.059	0.997

Mitochondrion GO:0005739

Protein identification	Zq	rank/N
>sp|Q9CZT5|VASN_MOUSE Vasorin OS=Mus musculus GN=Vasn PE=2 SV=2	-3.778	0.001

>sp|P26040|EZRI_MOUSE Ezrin OS=Mus musculus GN=Ezr PE=1 SV=3	-0.782	0.344
>sp|Q9JJ28|FLII_MOUSE Protein flightless-1 homolog OS=Mus musculus GN=Flii PE=1 S	-0.738	0.365
>sp|P70460|VASP_MOUSE Vasodilator-stimulated phosphoprotein OS=Mus musculus GN=	-0.715	0.385
>sp|P26043|RADI_MOUSE Radixin OS=Mus musculus GN=Rdx PE=1 SV=3	-0.706	0.406
>sp|Q9EPC1|PARVA_MOUSE Alpha-parvin OS=Mus musculus GN=Parva PE=1 SV=1	-0.690	0.427
>sp|Q61792|LASP1_MOUSE LIM and SH3 domain protein 1 OS=Mus musculus GN=Lasp1	-0.652	0.448
>sp|Q3UTJ2|SRBS2_MOUSE Sorbin and SH3 domain-containing protein 2 OS=Mus muscu	-0.651	0.469
>sp|Q8BFW7|LPP_MOUSE Lipoma-preferred partner homolog OS=Mus musculus GN=Lpp	-0.638	0.490
>sp|Q62219|TGFI1_MOUSE Transforming growth factor beta-1-induced transcript 1 protein	-0.636	0.510
>sp|Q71FD7|FBLI1_MOUSE Filamin-binding LIM protein 1 OS=Mus musculus GN=Fblim	-0.561	0.531
>sp|Q62417|SRBS1_MOUSE Sorbin and SH3 domain-containing protein 1 OS=Mus muscul	-0.448	0.552
>sp|P63085|MK01_MOUSE Mitogen-activated protein kinase 1 OS=Mus musculus GN=Ma	-0.428	0.573
>sp|Q9JI91|ACTN2_MOUSE Alpha-actinin-2 OS=Mus musculus GN=Actn2 PE=1 SV=2	-0.396	0.594
>sp|O70309|ITB5_MOUSE Integrin beta-5 OS=Mus musculus GN=Itgb5 PE=1 SV=2	-0.368	0.615
>sp|Q64727|VINC_MOUSE Vinculin OS=Mus musculus GN=Vcl PE=1 SV=4	-0.368	0.635
>sp|Q01768|NDKB_MOUSE Nucleoside diphosphate kinase B OS=Mus musculus GN=Nme	-0.363	0.656
>tr|Q3U0Q9|Q3U0Q9_MOUSE Putative uncharacterized protein (Fragment) OS=Mus muscu	-0.211	0.677
>sp|Q3TJD7|PDLI7_MOUSE PDZ and LIM domain protein 7 OS=Mus musculus GN=Pdlim	-0.173	0.698
>sp|Q8BZF8|PGM5_MOUSE Phosphoglucomutase-like protein 5 OS=Mus musculus GN=P	-0.154	0.719
>sp|Q62165|DAG1_MOUSE Dystroglycan OS=Mus musculus GN=Dag1 PE=1 SV=4	0.131	0.740
>sp|Q80X90|FLNB_MOUSE Filamin-B OS=Mus musculus GN=Flnb PE=1 SV=3	0.136	0.760
>sp|O55222|ILK_MOUSE Integrin-linked protein kinase OS=Mus musculus GN=Ilk PE=1 S	0.239	0.781
>sp|P34914|HYES_MOUSE Bifunctional epoxide hydrolase 2 OS=Mus musculus GN=Ephx	0.367	0.802
>sp|Q63844|MK03_MOUSE Mitogen-activated protein kinase 3 OS=Mus musculus GN=Ma	0.484	0.823
>sp|Q8CIB5|FERM2_MOUSE Fermitin family homolog 2 OS=Mus musculus GN=Fermt2 P	0.503	0.844
>sp|Q9CVB6|ARPC2_MOUSE Actin-related protein 2/3 complex subunit 2 OS=Mus muscu	0.521	0.865
>sp|P47226|TES_MOUSE Testin OS=Mus musculus GN=Tes PE=1 SV=1	0.549	0.885
>sp|Q9ET54|PALLD_MOUSE Palladin OS=Mus musculus GN=Palld PE=1 SV=2	0.701	0.906
>sp|P31938|MP2K1_MOUSE Dual specificity mitogen-activated protein kinase kinase 1 OS=	1.227	0.927
>sp|Q71LX4|TLN2_MOUSE Talin-2 OS=Mus musculus GN=Tln2 PE=1 SV=3	1.251	0.948
>tr|Q3TN69|Q3TN69_MOUSE Putative uncharacterized protein (Fragment) OS=Mus muscu	1.263	0.969
>sp|Q02566|MYH6_MOUSE Myosin-6 OS=Mus musculus GN=Myh6 PE=1 SV=2	3.701	0.990

Regulation of cell shape GO:0008360

Protein identification	Zq	rank/N
>tr|Q6ZWQ9|Q6ZWQ9_MOUSE MCG5400 OS=Mus musculus GN=Myl12a PE=2 SV=1	-3.282	0.020
>sp|Q6URW6|MYH14_MOUSE Myosin-14 OS=Mus musculus GN=Myh14 PE=1 SV=1	-2.680	0.060
>sp|P11276|FINC_MOUSE Fibronectin OS=Mus musculus GN=Fn1 PE=1 SV=4	-2.610	0.100
>tr|Q3UFT0|Q3UFT0_MOUSE Putative uncharacterized protein (Fragment) OS=Mus muscu	-2.267	0.140
>sp|Q8VDD5|MYH9_MOUSE Myosin-9 OS=Mus musculus GN=Myh9 PE=1 SV=4	-2.160	0.180
>sp|Q3THE2|ML12B_MOUSE Myosin regulatory light chain 12B OS=Mus musculus GN=M	-1.838	0.220
>sp|P08032|SPTA1_MOUSE Spectrin alpha chain, erythrocytic 1 OS=Mus musculus GN=Sp	-1.687	0.260
>sp|Q61879|MYH10_MOUSE Myosin-10 OS=Mus musculus GN=Myh10 PE=1 SV=2	-1.350	0.300
>sp|Q07076|ANXA7_MOUSE Annexin A7 OS=Mus musculus GN=Anxa7 PE=2 SV=2	-1.013	0.340
>sp|Q8VI36|PAXI_MOUSE Paxillin OS=Mus musculus GN=Pxn PE=1 SV=1	-0.879	0.380
>sp|P26040|EZRI_MOUSE Ezrin OS=Mus musculus GN=Ezr PE=1 SV=3	-0.782	0.420
>sp|P19221|THRB_MOUSE Prothrombin OS=Mus musculus GN=F2 PE=1 SV=1	-0.765	0.460
>sp|Q9EPC1|PARVA_MOUSE Alpha-parvin OS=Mus musculus GN=Parva PE=1 SV=1	-0.690	0.500
>sp|Q71FD7|FBLI1_MOUSE Filamin-binding LIM protein 1 OS=Mus musculus GN=Fblim	-0.561	0.540
>sp|Q9Z0P4|PALM_MOUSE Paralemmin-1 OS=Mus musculus GN=Palm PE=1 SV=1	-0.416	0.580
>sp|O08808|DIAP1_MOUSE Protein diaphanous homolog 1 OS=Mus musculus GN=Diaph1	-0.107	0.620
>sp|Q7TMB8|CYFP1_MOUSE Cytoplasmic FMR1-interacting protein 1 OS=Mus musculus	-0.098	0.660
>sp|P27601|GNA13_MOUSE Guanine nucleotide-binding protein subunit alpha-13 OS=Mus	0.300	0.700

>sp|Q9R257|HEBP1_MOUSE Heme-binding protein 1 OS=Mus musculus GN=Hebp1 PE=1 SV=2	-3.281	0.004	
>sp|Q80U23|SNPH_MOUSE Syntaphilin OS=Mus musculus GN=Snph PE=1 SV=3	-3.068	0.006	
>sp|P00329|ADH1_MOUSE Alcohol dehydrogenase 1 OS=Mus musculus GN=Adh1 PE=2 SV=2	-2.654	0.009	
>sp|Q924X2|CPT1B_MOUSE Carnitine O-palmitoyltransferase 1, muscle isoform OS=Mus musculus	-2.619	0.011	
>sp|Q8R2Y8|PTH2_MOUSE Peptidyl-tRNA hydrolase 2, mitochondrial OS=Mus musculus GN=Ptrh2	-2.188	0.014	
>sp|O35459|ECH1_MOUSE Delta(3,5)-Delta(2,4)-dienoyl-CoA isomerase, mitochondrial OS=Mus m	-2.026	0.016	
>sp|Q791T5|MTCH1_MOUSE Mitochondrial carrier homolog 1 OS=Mus musculus GN=Mtch1 PE=1	-2.016	0.019	
>sp|O35658|C1QBP_MOUSE Complement component 1 Q subcomponent-binding protein, mitochond	-1.916	0.021	
>sp|P98083|SHC1_MOUSE SHC-transforming protein 1 OS=Mus musculus GN=Shc1 PE=1 SV=3	-1.855	0.023	
>sp|Q9CRD2|EMC2_MOUSE ER membrane protein complex subunit 2 OS=Mus musculus GN=Emc2	-1.837	0.026	
>sp|P32020|NLTP_MOUSE Non-specific lipid-transfer protein OS=Mus musculus GN=Scp2 PE=1 SV	-1.807	0.028	
>sp|Q8CG76|ARK72_MOUSE Aflatoxin B1 aldehyde reductase member 2 OS=Mus musculus GN=A	-1.800	0.031	
>sp|Q8QZS1|HIBCH_MOUSE 3-hydroxyisobutyryl-CoA hydrolase, mitochondrial OS=Mus musculus	-1.718	0.033	
>sp|O09164|SODE_MOUSE Extracellular superoxide dismutase [Cu-Zn] OS=Mus musculus GN=Sod	-1.698	0.036	
>sp|Q9ERU9|RBP2_MOUSE E3 SUMO-protein ligase RanBP2 OS=Mus musculus GN=Ranbp2 PE=	-1.674	0.038	
>sp|Q9QX60|DGUOK_MOUSE Deoxyguanosine kinase, mitochondrial OS=Mus musculus GN=Dguo	-1.673	0.041	
>sp|P19157|GSTP1_MOUSE Glutathione S-transferase P 1 OS=Mus musculus GN=Gstp1 PE=1 SV=2	-1.621	0.043	
>sp|P46638|RB11B_MOUSE Ras-related protein Rab-11B OS=Mus musculus GN=Rab11b PE=1 SV=	-1.605	0.046	
>sp|Q8BMP6|GCP60_MOUSE Golgi resident protein GCP60 OS=Mus musculus GN=Acbd3 PE=1 SV	-1.545	0.048	
>sp|O08756|HCD2_MOUSE 3-hydroxyacyl-CoA dehydrogenase type-2 OS=Mus musculus GN=Hsd1	-1.530	0.051	
>sp|O55137|ACOT1_MOUSE Acyl-coenzyme A thioesterase 1 OS=Mus musculus GN=Acot1 PE=1 S	-1.468	0.053	
>sp|Q9Z1Q9|SYVC_MOUSE Valine--tRNA ligase OS=Mus musculus GN=Vars PE=2 SV=1	-1.426	0.056	
>sp|P23927|CRYAB_MOUSE Alpha-crystallin B chain OS=Mus musculus GN=Cryab PE=1 SV=2	-1.419	0.058	
>sp|P59017|B2L13_MOUSE Bcl-2-like protein 13 OS=Mus musculus GN=Bcl2l13 PE=1 SV=2	-1.411	0.060	
>sp|Q8BWM0|PGES2_MOUSE Prostaglandin E synthase 2 OS=Mus musculus GN=Ptges2 PE=1 SV=	-1.377	0.063	
>sp|Q8BMD8|SCMC1_MOUSE Calcium-binding mitochondrial carrier protein SCaMC-1 OS=Mus m	-1.342	0.065	
>sp|P97807|FUMH_MOUSE Fumarate hydratase, mitochondrial OS=Mus musculus GN=Fh PE=1 SV	-1.326	0.068	
>sp|P41216|ACSL1_MOUSE Long-chain-fatty-acid--CoA ligase 1 OS=Mus musculus GN=Acsl1 PE=	-1.322	0.070	
>sp|Q99LB6|MAT2B_MOUSE Methionine adenosyltransferase 2 subunit beta OS=Mus musculus GN	-1.296	0.073	
>sp|P61222|ABCE1_MOUSE ATP-binding cassette sub-family E member 1 OS=Mus musculus GN=A	-1.283	0.075	
>sp|Q8R0Y6|AL1L1_MOUSE Cytosolic 10-formyltetrahydrofolate dehydrogenase OS=Mus musculus	-1.282	0.078	
>sp|Q9D0K2|SCOT1_MOUSE Succinyl-CoA:3-ketoacid coenzyme A transferase 1, mitochondrial OS	-1.268	0.080	
>sp|P05202|AATM_MOUSE Aspartate aminotransferase, mitochondrial OS=Mus musculus GN=Got2	-1.231	0.083	
>sp|P39688|FYN_MOUSE Tyrosine-protein kinase Fyn OS=Mus musculus GN=Fyn PE=1 SV=3	-1.212	0.085	
>sp|P54869|HMCS2_MOUSE Hydroxymethylglutaryl-CoA synthase, mitochondrial OS=Mus musculu	-1.189	0.088	
>sp|Q9DCW4|ETFB_MOUSE Electron transfer flavoprotein subunit beta OS=Mus musculus GN=Etfb	-1.157	0.090	
>sp|Q9DCT2|NDUS3_MOUSE NADH dehydrogenase [ubiquinone] iron-sulfur protein 3, mitochondr	-1.139	0.093	
>sp|Q920E5|FPPS_MOUSE Farnesyl pyrophosphate synthase OS=Mus musculus GN=Fdps PE=2 SV=	-1.132	0.095	
>sp|Q64133|AOFA_MOUSE Amine oxidase [flavin-containing] A OS=Mus musculus GN=Maoa PE=	-1.120	0.098	
>sp|P56375|ACYP2_MOUSE Acylphosphatase-2 OS=Mus musculus GN=Acyp2 PE=2 SV=2	-1.115	0.100	
>sp|P63328|PP2BA_MOUSE Serine/threonine-protein phosphatase 2B catalytic subunit alpha isoform	-1.108	0.102	
>sp|P62897|CYC_MOUSE Cytochrome c, somatic OS=Mus musculus GN=Cycs PE=1 SV=2	-1.106	0.105	
>sp|Q8BWT1|THIM_MOUSE 3-ketoacyl-CoA thiolase, mitochondrial OS=Mus musculus GN=Acaa2	-1.099	0.107	
>sp|Q04447|KCRB_MOUSE Creatine kinase B-type OS=Mus musculus GN=Ckb PE=1 SV=1	-1.094	0.110	
>sp|Q8BH95|ECHM_MOUSE Enoyl-CoA hydratase, mitochondrial OS=Mus musculus GN=Echs1 PE	-1.064	0.112	
>sp|P97478|COQ7_MOUSE Ubiquinone biosynthesis protein COQ7 homolog OS=Mus musculus GN=	-1.055	0.115	
>sp|Q8K009|AL1L2_MOUSE Mitochondrial 10-formyltetrahydrofolate dehydrogenase OS=Mus musc	-1.051	0.117	
>sp|P54071|IDHP_MOUSE Isocitrate dehydrogenase [NADP], mitochondrial OS=Mus musculus GN=	-1.047	0.120	
>sp|Q62465|VAT1_MOUSE Synaptic vesicle membrane protein VAT-1 homolog OS=Mus musculus	-1.014	0.122	
>sp|Q8CGK3|LONM_MOUSE Lon protease homolog, mitochondrial OS=Mus musculus GN=Lonp1	-0.976	0.125	
>sp|Q8BMS1|ECHA_MOUSE Trifunctional enzyme subunit alpha, mitochondrial OS=Mus musculus	-0.975	0.127	
>sp|Q99JB2|STML2_MOUSE Stomatin-like protein 2 OS=Mus musculus GN=Stoml2 PE=1 SV=1	-0.966	0.130	
>sp|Q9JM14|NT5C_MOUSE 5'(3')-deoxyribonucleotidase, cytosolic type OS=Mus musculus GN=Nt5	-0.952	0.132	

>sp|Q8BR92|PALM2_MOUSE Paralemmin-2 OS=Mus musculus GN=Palm2 PE=1 SV=1	0.392	0.740
>sp|P39688|FYN_MOUSE Tyrosine-protein kinase Fyn OS=Mus musculus GN=Fyn PE=1 S	0.499	0.780
>sp|Q8CIB5|FERM2_MOUSE Fermitin family homolog 2 OS=Mus musculus GN=Fermt2 P	0.503	0.820
>sp|O70318|E41L2_MOUSE Band 4.1-like protein 2 OS=Mus musculus GN=Epb41l2 PE=1	0.704	0.860
>sp|O89053|COR1A_MOUSE Coronin-1A OS=Mus musculus GN=Coro1a PE=1 SV=5	1.348	0.900
>sp|Q61738|ITA7_MOUSE Integrin alpha-7 OS=Mus musculus GN=Itga7 PE=1 SV=3	1.587	0.940
>sp|Q9JM96|BORG4_MOUSE Cdc42 effector protein 4 OS=Mus musculus GN=Cdc42ep4	2.568	0.980

Actin binding GO:0003779

Protein identification	Zq	rank/N
>sp|Q6ZWQ0|SYNE2_MOUSE Nesprin-2 OS=Mus musculus GN=Syne2 PE=1 SV=2	-3.369	0.004
>sp|P20065-2|TYB4_MOUSE Isoform Short of Thymosin beta-4 OS=Mus musculus GN=Tm	-3.090	0.012
>sp|Q64331|MYO6_MOUSE Unconventional myosin-VI OS=Mus musculus GN=Myo6 PE=	-3.068	0.020
>tr|Q69ZX3|Q69ZX3_MOUSE MKIAA0866 protein (Fragment) OS=Mus musculus GN=M	-3.047	0.028
>sp|Q5SX40|MYH1_MOUSE Myosin-1 OS=Mus musculus GN=Myh1 PE=1 SV=1	-2.997	0.035
>sp|Q5SYD0|MYO1D_MOUSE Unconventional myosin-Id OS=Mus musculus GN=Myo1d	-2.771	0.043
>sp|Q6URW6|MYH14_MOUSE Myosin-14 OS=Mus musculus GN=Myh14 PE=1 SV=1	-2.680	0.051
>sp|P13020|GELS_MOUSE Gelsolin OS=Mus musculus GN=Gsn PE=1 SV=3	-2.602	0.059
>sp|Q9DAW9|CNN3_MOUSE Calponin-3 OS=Mus musculus GN=Cnn3 PE=2 SV=1	-2.489	0.067
>sp|O70373|XIRP1_MOUSE Xin actin-binding repeat-containing protein 1 OS=Mus muscul	-2.202	0.075
>sp|Q8BVA4|LMOD1_MOUSE Leiomodin-1 OS=Mus musculus GN=Lmod1 PE=2 SV=1	-2.191	0.083
>sp|Q8VDD5|MYH9_MOUSE Myosin-9 OS=Mus musculus GN=Myh9 PE=1 SV=4	-2.160	0.091
>sp|Q08093|CNN2_MOUSE Calponin-2 OS=Mus musculus GN=Cnn2 PE=2 SV=1	-2.036	0.098
>sp|Q6PDN3|MYLK_MOUSE Myosin light chain kinase, smooth muscle OS=Mus musculus	-2.023	0.106
>sp|Q9WUM4|COR1C_MOUSE Coronin-1C OS=Mus musculus GN=Coro1c PE=1 SV=2	-1.975	0.114
>sp|P04919|B3AT_MOUSE Band 3 anion transport protein OS=Mus musculus GN=Slc4a1 P	-1.923	0.122
>sp|Q5SX39|MYH4_MOUSE Myosin-4 OS=Mus musculus GN=Myh4 PE=1 SV=1	-1.783	0.130
>sp|Q03173|ENAH_MOUSE Protein enabled homolog OS=Mus musculus GN=Enah PE=1 S	-1.771	0.138
>tr|Q8VCQ8|Q8VCQ8_MOUSE Caldesmon 1 OS=Mus musculus GN=Cald1 PE=2 SV=1	-1.720	0.146
>sp|Q9R0Q6|ARC1A_MOUSE Actin-related protein 2/3 complex subunit 1A OS=Mus musc	-1.690	0.154
>sp|P08032|SPTA1_MOUSE Spectrin alpha chain, erythrocytic 1 OS=Mus musculus GN=Sp	-1.687	0.161
>sp|P26645|MARCS_MOUSE Myristoylated alanine-rich C-kinase substrate OS=Mus muscu	-1.626	0.169
>sp|Q9JHJ0|TMOD3_MOUSE Tropomodulin-3 OS=Mus musculus GN=Tmod3 PE=1 SV=1	-1.626	0.177
>sp|Q62418|DBNL_MOUSE Drebrin-like protein OS=Mus musculus GN=Dbnl PE=1 SV=2	-1.613	0.185
>tr|D3YVV9|D3YVV9_MOUSE Synaptopodin-2 OS=Mus musculus GN=Synpo2 PE=4 SV=	-1.567	0.193
>sp|P57780|ACTN4_MOUSE Alpha-actinin-4 OS=Mus musculus GN=Actn4 PE=1 SV=1	-1.556	0.201
>sp|Q7TPW1|NEXN_MOUSE Nexilin OS=Mus musculus GN=Nexn PE=1 SV=3	-1.518	0.209
>sp|P24452|CAPG_MOUSE Macrophage-capping protein OS=Mus musculus GN=Capg PE=	-1.478	0.217
>sp|P21614|VTDB_MOUSE Vitamin D-binding protein OS=Mus musculus GN=Gc PE=1 S	-1.428	0.224
>sp|P40124|CAP1_MOUSE Adenylyl cyclase-associated protein 1 OS=Mus musculus GN=C	-1.394	0.232
>sp|Q91YE8|SYNP2_MOUSE Synaptopodin-2 OS=Mus musculus GN=Synpo2 PE=1 SV=2	-1.353	0.240
>sp|Q61879|MYH10_MOUSE Myosin-10 OS=Mus musculus GN=Myh10 PE=1 SV=2	-1.350	0.248
>sp|Q9QXS6|DREB_MOUSE Drebrin OS=Mus musculus GN=Dbn1 PE=1 SV=4	-1.288	0.256
>sp|P11531|DMD_MOUSE Dystrophin OS=Mus musculus GN=Dmd PE=1 SV=3	-1.252	0.264
>sp|Q8VHX6|FLNC_MOUSE Filamin-C OS=Mus musculus GN=Flnc PE=1 SV=3	-1.237	0.272
>sp|Q3V0K9|PLSI_MOUSE Plastin-1 OS=Mus musculus GN=Pls1 PE=2 SV=1	-1.220	0.280
>sp|P47754|CAZA2_MOUSE F-actin-capping protein subunit alpha-2 OS=Mus musculus GI	-1.220	0.287
>sp|P26039|TLN1_MOUSE Talin-1 OS=Mus musculus GN=Tln1 PE=1 SV=2	-1.208	0.295
>sp|P09055|ITB1_MOUSE Integrin beta-1 OS=Mus musculus GN=Itgb1 PE=1 SV=1	-1.132	0.303
>sp|P46735|MYO1B_MOUSE Unconventional myosin-Ib OS=Mus musculus GN=Myo1b P	-1.122	0.311
>tr|E9Q6R7|E9Q6R7_MOUSE Protein Utrn OS=Mus musculus GN=Utrn PE=4 SV=1	-1.104	0.319
>sp|Q8BTM8|FLNA_MOUSE Filamin-A OS=Mus musculus GN=Flna PE=1 SV=5	-1.103	0.327
>sp|Q91YR1|TWF1_MOUSE Twinfilin-1 OS=Mus musculus GN=Twf1 PE=1 SV=2	-1.096	0.335

>sp|Q78PY7|SND1_MOUSE Staphylococcal nuclease domain-containing protein 1 OS=Mus musculus	-0.947	0.135	>sp|Q7TPR4|ACTN1_MOUSE Alpha-actinin-1 OS=Mus musculus GN=Actn1 PE=1 SV=1	-1.092	0.343
>sp|Q9D2G2|ODO2_MOUSE Dihydrolipoyllysine-residue succinyltransferase component of 2-oxoglu	-0.930	0.137	>sp|P45591|COF2_MOUSE Cofilin-2 OS=Mus musculus GN=Cfl2 PE=1 SV=1	-1.087	0.350
>sp|P58281|OPA1_MOUSE Dynamin-like 120 kDa protein, mitochondrial OS=Mus musculus GN=Op	-0.927	0.140	>sp|P47753|CAZA1_MOUSE F-actin-capping protein subunit alpha-1 OS=Mus musculus GI	-1.079	0.358
>sp|Q99L13|3HIDH_MOUSE 3-hydroxyisobutyrate dehydrogenase, mitochondrial OS=Mus musculus	-0.923	0.142	>sp|Q9CYT6|CAP2_MOUSE Adenylyl cyclase-associated protein 2 OS=Mus musculus GN=	-1.048	0.366
>sp|Q8BX02|KANK2_MOUSE KN motif and ankyrin repeat domain-containing protein 2 OS=Mus m	-0.916	0.144	>sp|Q08091|CNN1_MOUSE Calponin-1 OS=Mus musculus GN=Cnn1 PE=2 SV=1	-1.048	0.374
>tr|Q99K87|Q99K87_MOUSE Serine hydroxymethyltransferase OS=Mus musculus GN=Shmt2 PE=2	-0.915	0.147	>tr|Q99LB4|Q99LB4_MOUSE Capping protein (Actin filament), gelsolin-like OS=Mus mus	-1.045	0.382
>tr|Q3U2G2|Q3U2G2_MOUSE Heat shock 70 kDa protein 4 OS=Mus musculus GN=Hspa4 PE=2 SV	-0.915	0.149	>tr|Q3TR59|Q3TR59_MOUSE Putative uncharacterized protein (Fragment) OS=Mus muscu	-0.993	0.390
>sp|Q9D1G1|RAB1B_MOUSE Ras-related protein Rab-1B OS=Mus musculus GN=Rab1b PE=1 SV=	-0.911	0.152	>sp|Q9WTI7|MYO1C_MOUSE Unconventional myosin-Ic OS=Mus musculus GN=Myo1c I	-0.969	0.398
>sp|Q91ZP3-2|LPIN1_MOUSE Isoform 2 of Phosphatidate phosphatase LPIN1 OS=Mus musculus GI	-0.909	0.154	>sp|O08638|MYH11_MOUSE Myosin-11 OS=Mus musculus GN=Myh11 PE=1 SV=1	-0.965	0.406
>sp|P47738|ALDH2_MOUSE Aldehyde dehydrogenase, mitochondrial OS=Mus musculus GN=Aldh2	-0.897	0.157	>sp|P26041|MOES_MOUSE Moesin OS=Mus musculus GN=Msn PE=1 SV=3	-0.880	0.413
>sp|Q6PB66|LPPRC_MOUSE Leucine-rich PPR motif-containing protein, mitochondrial OS=Mus mu	-0.883	0.159	>sp|Q99K51|PLST_MOUSE Plastin-3 OS=Mus musculus GN=Pls3 PE=1 SV=3	-0.849	0.421
>sp|Q99JY0|ECHB_MOUSE Trifunctional enzyme subunit beta, mitochondrial OS=Mus musculus GN	-0.879	0.162	>sp|Q8VD75|HIP1_MOUSE Huntingtin-interacting protein 1 OS=Mus musculus GN=Hip1 I	-0.827	0.429
>sp|P09671|SODM_MOUSE Superoxide dismutase [Mn], mitochondrial OS=Mus musculus GN=Sod2	-0.851	0.164	>tr|E9Q0S6|E9Q0S6_MOUSE Protein Tns1 OS=Mus musculus GN=Tns1 PE=4 SV=1	-0.795	0.437
>sp|Q99MN9|PCCB_MOUSE Propionyl-CoA carboxylase beta chain, mitochondrial OS=Mus muscul	-0.848	0.167	>sp|P58774|TPM2_MOUSE Tropomyosin beta chain OS=Mus musculus GN=Tpm2 PE=1 S	-0.784	0.445
>sp|Q8BU85|MSRB3_MOUSE Methionine-R-sulfoxide reductase B3, mitochondrial OS=Mus muscul	-0.846	0.169	>sp|P26040|EZRI_MOUSE Ezrin OS=Mus musculus GN=Ezr PE=1 SV=3	-0.782	0.453
>sp|Q8QZT1|THIL_MOUSE Acetyl-CoA acetyltransferase, mitochondrial OS=Mus musculus GN=Ac	-0.836	0.172	>sp|P07091|S10A4_MOUSE Protein S100-A4 OS=Mus musculus GN=S100a4 PE=1 SV=1	-0.747	0.461
>sp|Q05920|PYC_MOUSE Pyruvate carboxylase, mitochondrial OS=Mus musculus GN=Pc PE=1 SV	-0.824	0.174	>sp|Q9JJ28|FLII_MOUSE Protein flightless-1 homolog OS=Mus musculus GN=Flii PE=1 S	-0.738	0.469
>sp|Q9CZD3|SYG_MOUSE Glycine--tRNA ligase OS=Mus musculus GN=Gars PE=1 SV=1	-0.824	0.177	>sp|P70460|VASP_MOUSE Vasodilator-stimulated phosphoprotein OS=Mus musculus GN=	-0.715	0.476
>sp|Q61191|HCFC1_MOUSE Host cell factor 1 OS=Mus musculus GN=Hcfc1 PE=1 SV=2	-0.815	0.179	>sp|P26043|RADI_MOUSE Radixin OS=Mus musculus GN=Rdx PE=1 SV=3	-0.706	0.484
>sp|Q07813|BAX_MOUSE Apoptosis regulator BAX OS=Mus musculus GN=Bax PE=1 SV=1	-0.808	0.181	>sp|Q9EPC1|PARVA_MOUSE Alpha-parvin OS=Mus musculus GN=Parva PE=1 SV=1	-0.690	0.492
>sp|Q3ULD5|MCCB_MOUSE Methylcrotonoyl-CoA carboxylase beta chain, mitochondrial OS=Mus	-0.807	0.184	>sp|Q61792|LASP1_MOUSE LIM and SH3 domain protein 1 OS=Mus musculus GN=Lasp1	-0.652	0.500
>sp|Q9JHI5|IVD_MOUSE Isovaleryl-CoA dehydrogenase, mitochondrial OS=Mus musculus GN=Ivd	-0.793	0.186	>sp|Q99JY9|ARP3_MOUSE Actin-related protein 3 OS=Mus musculus GN=Actr3 PE=1 SV	-0.649	0.508
>sp|P10639|THIO_MOUSE Thioredoxin OS=Mus musculus GN=Txn PE=1 SV=3	-0.789	0.189	>sp|P15508|SPTB1_MOUSE Spectrin beta chain, erythrocytic OS=Mus musculus GN=Sptb	-0.628	0.516
>sp|Q63932|MP2K2_MOUSE Dual specificity mitogen-activated protein kinase kinase 2 OS=Mus mu	-0.769	0.191	>sp|P61161|ARP2_MOUSE Actin-related protein 2 OS=Mus musculus GN=Actr2 PE=1 SV=	-0.572	0.524
>sp|Q9JLN9|MTOR_MOUSE Serine/threonine-protein kinase mTOR OS=Mus musculus GN=Mtor P	-0.769	0.194	>sp|Q61235|SNTB2_MOUSE Beta-2-syntrophin OS=Mus musculus GN=Sntb2 PE=1 SV=2	-0.463	0.531
>sp|P50516|VATA_MOUSE V-type proton ATPase catalytic subunit A OS=Mus musculus GN=Atp6v	-0.755	0.196	>sp|P47757-2|CAPZB_MOUSE Isoform 2 of F-actin-capping protein subunit beta OS=Mus r	-0.458	0.539
>sp|Q5U458|DJC11_MOUSE DnaJ homolog subfamily C member 11 OS=Mus musculus GN=Dnajc1	-0.740	0.199	>sp|Q9JI91|ACTN2_MOUSE Alpha-actinin-2 OS=Mus musculus GN=Actn2 PE=1 SV=2	-0.396	0.547
>sp|Q9D880|TIM50_MOUSE Mitochondrial import inner membrane translocase subunit TIM50 OS=M	-0.722	0.201	>sp|Q8K4L3|SVIL_MOUSE Supervillin OS=Mus musculus GN=Svil PE=1 SV=1	-0.384	0.555
>sp|O55126|NIPS2_MOUSE Protein NipSnap homolog 2 OS=Mus musculus GN=Gbas PE=2 SV=1	-0.661	0.204	>sp|O08579|EMD_MOUSE Emerin OS=Mus musculus GN=Emd PE=1 SV=1	-0.381	0.563
>sp|Q99MN1|SYK_MOUSE Lysine--tRNA ligase OS=Mus musculus GN=Kars PE=1 SV=1	-0.659	0.206	>sp|Q64727|VINC_MOUSE Vinculin OS=Mus musculus GN=Vcl PE=1 SV=4	-0.368	0.571
>sp|Q99KI0|ACON_MOUSE Aconitate hydratase, mitochondrial OS=Mus musculus GN=Aco2 PE=1	-0.657	0.209	>sp|Q9D898|ARP5L_MOUSE Actin-related protein 2/3 complex subunit 5-like protein OS=I	-0.363	0.579
>sp|Q8BP47|SYNC_MOUSE Asparagine--tRNA ligase, cytoplasmic OS=Mus musculus GN=Nars PE	-0.656	0.211	>sp|Q61233|PLSL_MOUSE Plastin-2 OS=Mus musculus GN=Lcp1 PE=1 SV=4	-0.313	0.587
>sp|O54724|PTRF_MOUSE Polymerase I and transcript release factor OS=Mus musculus GN=Ptrf PE	-0.648	0.214	>sp|Q9WV32|ARC1B_MOUSE Actin-related protein 2/3 complex subunit 1B OS=Mus musc	-0.285	0.594
>sp|P38060|HMGCL_MOUSE Hydroxymethylglutaryl-CoA lyase, mitochondrial OS=Mus musculus (	-0.646	0.216	>sp|Q8CC35|SYNPO_MOUSE Synaptopodin OS=Mus musculus GN=Synpo PE=1 SV=2	-0.262	0.602
>sp|P11499|HS90B_MOUSE Heat shock protein HSP 90-beta OS=Mus musculus GN=Hsp90ab1 PE=	-0.643	0.219	>sp|P18760|COF1_MOUSE Cofilin-1 OS=Mus musculus GN=Cfl1 PE=1 SV=3	-0.262	0.610
>sp|Q9JMH6|TRXR1_MOUSE Thioredoxin reductase 1, cytoplasmic OS=Mus musculus GN=Txnrd1	-0.637	0.221	>sp|Q9CPW4|ARPC5_MOUSE Actin-related protein 2/3 complex subunit 5 OS=Mus muscu	-0.261	0.618
>sp|Q9JHW2|NIT2_MOUSE Omega-amidase NIT2 OS=Mus musculus GN=Nit2 PE=1 SV=1	-0.631	0.223	>sp|Q0GNC1|INF2_MOUSE Inverted formin-2 OS=Mus musculus GN=Inf2 PE=1 SV=1	-0.251	0.626
>sp|P45952|ACADM_MOUSE Medium-chain specific acyl-CoA dehydrogenase, mitochondrial OS=M	-0.623	0.226	>sp|P49813|TMOD1_MOUSE Tropomodulin-1 OS=Mus musculus GN=Tmod1 PE=2 SV=2	-0.238	0.634
>sp|Q8K1J6|TRNT1_MOUSE CCA tRNA nucleotidyltransferase 1, mitochondrial OS=Mus musculus	-0.617	0.228	>sp|P21107|TPM3_MOUSE Tropomyosin alpha-3 chain OS=Mus musculus GN=Tpm3 PE=	-0.230	0.642
>sp|Q9QXB9|DRG2_MOUSE Developmentally-regulated GTP-binding protein 2 OS=Mus musculus (	-0.615	0.231	>tr|Q3U0Q9|Q3U0Q9_MOUSE Putative uncharacterized protein (Fragment) OS=Mus muscu	-0.211	0.650
>sp|Q8BYC6|TAOK3_MOUSE Serine/threonine-protein kinase TAO3 OS=Mus musculus GN=Taok3	-0.610	0.233	>sp|Q8CI51|PDLI5_MOUSE PDZ and LIM domain protein 5 OS=Mus musculus GN=Pdlim	-0.156	0.657
>sp|P07901|HS90A_MOUSE Heat shock protein HSP 90-alpha OS=Mus musculus GN=Hsp90aa1 PE	-0.586	0.236	>tr|A1BN54|A1BN54_MOUSE Alpha actinin 1a OS=Mus musculus GN=Actn1 PE=2 SV=1	-0.131	0.665
>sp|Q9D0S9|HINT2_MOUSE Histidine triad nucleotide-binding protein 2, mitochondrial OS=Mus mu	-0.562	0.238	>sp|Q9R0P5|DEST_MOUSE Destrin OS=Mus musculus GN=Dstn PE=1 SV=3	-0.107	0.673
>sp|Q6X893|CTL1_MOUSE Choline transporter-like protein 1 OS=Mus musculus GN=Slc44a1 PE=1	-0.554	0.241	>sp|O08808|DIAP1_MOUSE Protein diaphanous homolog 1 OS=Mus musculus GN=Diaph1	-0.107	0.681
>sp|P97742|CPT1A_MOUSE Carnitine O-palmitoyltransferase 1, liver isoform OS=Mus musculus GN	-0.552	0.243	>sp|Q7TMB8|CYFP1_MOUSE Cytoplasmic FMR1-interacting protein 1 OS=Mus musculus	-0.098	0.689
>sp|Q91VR2|ATPG_MOUSE ATP synthase subunit gamma, mitochondrial OS=Mus musculus GN=A	-0.542	0.246	>sp|P97434|MPRIP_MOUSE Myosin phosphatase Rho-interacting protein OS=Mus musculu	-0.059	0.697
>sp|Q8K4Z3|NNRE_MOUSE NAD(P)H-hydrate epimerase OS=Mus musculus GN=Apoa1bp PE=1 S	-0.536	0.248	>sp|P59999|ARPC4_MOUSE Actin-related protein 2/3 complex subunit 4 OS=Mus musculu	-0.047	0.705
>sp|P24270|CATA_MOUSE Catalase OS=Mus musculus GN=Cat PE=1 SV=4	-0.530	0.251	>sp|O70566|DIAP2_MOUSE Protein diaphanous homolog 2 OS=Mus musculus GN=Diaph2	-0.045	0.713
>sp|Q9CWJ9|PUR9_MOUSE Bifunctional purine biosynthesis protein PURH OS=Mus musculus GN=	-0.528	0.253	>sp|Q8VDP3|MICA1_MOUSE Protein-methionine sulfoxide oxidase MICAL1 OS=Mus mu	-0.020	0.720
>sp|Q9Z2I0|LETM1_MOUSE LETM1 and EF-hand domain-containing protein 1, mitochondrial OS=I	-0.527	0.256	>sp|Q9EPK2|XRP2_MOUSE Protein XRP2 OS=Mus musculus GN=Rp2 PE=1 SV=3	-0.016	0.728
>sp|Q922E6|FAKD2_MOUSE FAST kinase domain-containing protein 2 OS=Mus musculus GN=Fas	-0.524	0.258	>sp|Q99KW3|TARA_MOUSE TRIO and F-actin-binding protein OS=Mus musculus GN=Tr	0.082	0.736
>sp|Q922D8|C1TC_MOUSE C-1-tetrahydrofolate synthase, cytoplasmic OS=Mus musculus GN=Mth	-0.523	0.260	>sp|Q7TSE6|ST38L_MOUSE Serine/threonine-protein kinase 38-like OS=Mus musculus GN	0.112	0.744
>sp|P05132|KAPCA_MOUSE cAMP-dependent protein kinase catalytic subunit alpha OS=Mus muscu	-0.513	0.263	>tr|Q3TNK2|Q3TNK2_MOUSE Putative uncharacterized protein OS=Mus musculus GN=W	0.121	0.752

>sp|Q921S7|RM37_MOUSE 39S ribosomal protein L37, mitochondrial OS=Mus musculus GN=Mrpl3	-0.493	0.265	>sp|Q62165|DAG1_MOUSE Dystroglycan OS=Mus musculus GN=Dag1 PE=1 SV=4	0.131	0.760
>sp|P53026|RL10A_MOUSE 60S ribosomal protein L10a OS=Mus musculus GN=Rpl10a PE=1 SV=3	-0.491	0.268	>sp|O88342|WDR1_MOUSE WD repeat-containing protein 1 OS=Mus musculus GN=Wdr1	0.131	0.768
>sp|O08553|DPYL2_MOUSE Dihydropyrimidinase-related protein 2 OS=Mus musculus GN=Dpysl2	-0.477	0.270	>sp|Q80X90|FLNB_MOUSE Filamin-B OS=Mus musculus GN=Flnb PE=1 SV=3	0.136	0.776
>sp|P62264|RS14_MOUSE 40S ribosomal protein S14 OS=Mus musculus GN=Rps14 PE=2 SV=3	-0.465	0.273	>sp|Q9JM76|ARPC3_MOUSE Actin-related protein 2/3 complex subunit 3 OS=Mus muscul	0.152	0.783
>sp|P54320|ELN_MOUSE Elastin OS=Mus musculus GN=Eln PE=2 SV=2	-0.458	0.275	>sp|Q9QYC0|ADDA_MOUSE Alpha-adducin OS=Mus musculus GN=Add1 PE=1 SV=2	0.182	0.791
>sp|P70404|IDHG1_MOUSE Isocitrate dehydrogenase [NAD] subunit gamma 1, mitochondrial OS=M	-0.455	0.278	>sp|Q8BH43|WASF2_MOUSE Wiskott-Aldrich syndrome protein family member 2 OS=Mu	0.209	0.799
>sp|P63038|CH60_MOUSE 60 kDa heat shock protein, mitochondrial OS=Mus musculus GN=Hspd1	-0.452	0.280	>sp|Q61234|SNTA1_MOUSE Alpha-1-syntrophin OS=Mus musculus GN=Snta1 PE=1 SV=	0.352	0.807
>sp|P08249|MDHM_MOUSE Malate dehydrogenase, mitochondrial OS=Mus musculus GN=Mdh2 PE	-0.451	0.283	>sp|P59242|CING_MOUSE Cingulin OS=Mus musculus GN=Cgn PE=1 SV=1	0.379	0.815
>sp|Q9EQ20|MMSA_MOUSE Methylmalonate-semialdehyde dehydrogenase [acylating], mitochondri	-0.450	0.285	>sp|Q9CVB6|ARPC2_MOUSE Actin-related protein 2/3 complex subunit 2 OS=Mus muscu	0.521	0.823
>sp|P70296|PEBP1_MOUSE Phosphatidylethanolamine-binding protein 1 OS=Mus musculus GN=Pel	-0.447	0.288	>sp|P58771|TPM1_MOUSE Tropomyosin alpha-1 chain OS=Mus musculus GN=Tpm1 PE=	0.584	0.831
>sp|Q3UV70|PDP1_MOUSE [Pyruvate dehydrogenase [acetyl-transferring]]-phosphatase 1, mitochon	-0.437	0.290	>sp|Q9CQI3|GMFB_MOUSE Glia maturation factor beta OS=Mus musculus GN=Gmfb PE=	0.679	0.839
>sp|Q5SWU9|ACACA_MOUSE Acetyl-CoA carboxylase 1 OS=Mus musculus GN=Acaca PE=1 SV=	-0.436	0.293	>sp|Q9ET54|PALLD_MOUSE Palladin OS=Mus musculus GN=Palld PE=1 SV=2	0.701	0.846
>sp|Q9Z2I9|SUCB1_MOUSE Succinyl-CoA ligase [ADP-forming] subunit beta, mitochondrial OS=M	-0.422	0.295	>sp|O70318|E41L2_MOUSE Band 4.1-like protein 2 OS=Mus musculus GN=Epb41l2 PE=1	0.704	0.854
>sp|Q91VM9-2|IPYR2_MOUSE Isoform 2 of Inorganic pyrophosphatase 2, mitochondrial OS=Mus m	-0.420	0.298	>sp|Q9QXS1|PLEC_MOUSE Plectin OS=Mus musculus GN=Plec PE=1 SV=2	0.743	0.862
>sp|P17156|HSP72_MOUSE Heat shock-related 70 kDa protein 2 OS=Mus musculus GN=Hspa2 PE=	-0.419	0.300	>sp|Q3UH68|LIMC1_MOUSE LIM and calponin homology domains-containing protein 1 O	0.756	0.870
>sp|O55028|BCKD_MOUSE [3-methyl-2-oxobutanoate dehydrogenase [lipoamide]] kinase, mitochon	-0.414	0.302	>sp|Q62261|SPTB2_MOUSE Spectrin beta chain, non-erythrocytic 1 OS=Mus musculus GN	0.786	0.878
>sp|P35235|PTN11_MOUSE Tyrosine-protein phosphatase non-receptor type 11 OS=Mus musculus G	-0.407	0.305	>tr|F6T2Z7|F6T2Z7_MOUSE Protein Cald1 (Fragment) OS=Mus musculus GN=Cald1 PE=4	0.853	0.886
>sp|Q9QUJ7|ACSL4_MOUSE Long-chain-fatty-acid--CoA ligase 4 OS=Mus musculus GN=Acsl4 PE	-0.399	0.307	>sp|Q9QYB5|ADDG_MOUSE Gamma-adducin OS=Mus musculus GN=Add3 PE=1 SV=2	1.040	0.894
>sp|P51660|DHB4_MOUSE Peroxisomal multifunctional enzyme type 2 OS=Mus musculus GN=Hsd	-0.394	0.310	>sp|P16546|SPTN1_MOUSE Spectrin alpha chain, non-erythrocytic 1 OS=Mus musculus GN	1.067	0.902
>sp|P85094|ISC2A_MOUSE Isochorismatase domain-containing protein 2A, mitochondrial OS=Mus m	-0.390	0.312	>sp|P61982|1433G_MOUSE 14-3-3 protein gamma OS=Mus musculus GN=Ywhag PE=1 SV	1.152	0.909
>sp|P51175|PPOX_MOUSE Protoporphyrinogen oxidase OS=Mus musculus GN=Ppox PE=2 SV=1	-0.380	0.315	>sp|P62962|PROF1_MOUSE Profilin-1 OS=Mus musculus GN=Pfn1 PE=1 SV=2	1.237	0.917
>sp|Q64433|CH10_MOUSE 10 kDa heat shock protein, mitochondrial OS=Mus musculus GN=Hspe1	-0.369	0.317	>sp|Q641P0|ARP3B_MOUSE Actin-related protein 3B OS=Mus musculus GN=Actr3b PE=2	1.243	0.925
>sp|Q61462|CY24A_MOUSE Cytochrome b-245 light chain OS=Mus musculus GN=Cyba PE=1 SV=	-0.366	0.320	>sp|Q71LX4|TLN2_MOUSE Talin-2 OS=Mus musculus GN=Tln2 PE=1 SV=3	1.251	0.933
>sp|Q9D051|ODPB_MOUSE Pyruvate dehydrogenase E1 component subunit beta, mitochondrial OS=	-0.366	0.322	>tr|Q3TN69|Q3TN69_MOUSE Putative uncharacterized protein (Fragment) OS=Mus muscu	1.263	0.941
>sp|P35486|ODPA_MOUSE Pyruvate dehydrogenase E1 component subunit alpha, somatic form, mit	-0.349	0.325	>sp|Q6IRU2|TPM4_MOUSE Tropomyosin alpha-4 chain OS=Mus musculus GN=Tpm4 PE=	1.292	0.949
>sp|P50544|ACADV_MOUSE Very long-chain specific acyl-CoA dehydrogenase, mitochondrial OS=	-0.340	0.327	>sp|O89053|COR1A_MOUSE Coronin-1A OS=Mus musculus GN=Coro1a PE=1 SV=5	1.348	0.957
>sp|P26638|SYSC_MOUSE Serine--tRNA ligase, cytoplasmic OS=Mus musculus GN=Sars PE=2 SV	-0.338	0.330	>sp|P84075|HPCA_MOUSE Neuron-specific calcium-binding protein hippocalcin OS=Mus m	1.554	0.965
>sp|O35855|BCAT2_MOUSE Branched-chain-amino-acid aminotransferase, mitochondrial OS=Mus m	-0.328	0.332	>sp|Q9CQI6|COTL1_MOUSE Coactosin-like protein OS=Mus musculus GN=Cotl1 PE=1 SV	1.566	0.972
>sp|P56382|ATP5E_MOUSE ATP synthase subunit epsilon, mitochondrial OS=Mus musculus GN=At	-0.325	0.335	>sp|P68510|1433F_MOUSE 14-3-3 protein eta OS=Mus musculus GN=Ywhah PE=1 SV=2	1.750	0.980
>sp|Q3U9G9|LBR_MOUSE Lamin-B receptor OS=Mus musculus GN=Lbr PE=1 SV=2	-0.324	0.337	>sp|Q99L88|SNTB1_MOUSE Beta-1-syntrophin OS=Mus musculus GN=Sntb1 PE=1 SV=4	1.751	0.988
>sp|Q2TPA8|HSDL2_MOUSE Hydroxysteroid dehydrogenase-like protein 2 OS=Mus musculus GN=	-0.322	0.340	>sp|Q02566|MYH6_MOUSE Myosin-6 OS=Mus musculus GN=Myh6 PE=1 SV=2	3.701	0.996
>sp|Q9CZW5|TOM70_MOUSE Mitochondrial import receptor subunit TOM70 OS=Mus musculus GI	-0.314	0.342			
>sp|Q8C0V9|FRMD6_MOUSE FERM domain-containing protein 6 OS=Mus musculus GN=Frmd6 P	-0.312	0.344	**Cell adhesion GO:0007155**		
>sp|Q8BHC4|DCAKD_MOUSE Dephospho-CoA kinase domain-containing protein OS=Mus musculu	-0.310	0.347	Protein identification	Zq	rank/N
>sp|Q9DBF1|AL7A1_MOUSE Alpha-aminoadipic semialdehyde dehydrogenase OS=Mus musculus C	-0.310	0.349	>sp|Q61282|PGCA_MOUSE Aggrecan core protein OS=Mus musculus GN=Acan PE=1 SV=	-4.710	0.005
>sp|Q9DAR7|DCPS_MOUSE m7GpppX diphosphatase OS=Mus musculus GN=Dcps PE=1 SV=1	-0.297	0.352	>sp|Q62059|CSPG2_MOUSE Versican core protein OS=Mus musculus GN=Vcan PE=1 SV=	-3.806	0.015
>sp|P84091|AP2M1_MOUSE AP-2 complex subunit mu OS=Mus musculus GN=Ap2m1 PE=1 SV=1	-0.294	0.354	>sp|Q9QZZ6|DERM_MOUSE Dermatopontin OS=Mus musculus GN=Dpt PE=2 SV=1	-3.617	0.026
>sp|Q99LC5|ETFA_MOUSE Electron transfer flavoprotein subunit alpha, mitochondrial OS=Mus mus	-0.293	0.357	>sp|Q61581|IBP7_MOUSE Insulin-like growth factor-binding protein 7 OS=Mus musculus G	-3.596	0.036
>sp|O88587|COMT_MOUSE Catechol O-methyltransferase OS=Mus musculus GN=Comt PE=1 SV=	-0.286	0.359	>sp|P29788|VTNC_MOUSE Vitronectin OS=Mus musculus GN=Vtn PE=1 SV=2	-3.072	0.046
>sp|Q9JK48|SHLB1_MOUSE Endophilin-B1 OS=Mus musculus GN=Sh3glb1 PE=1 SV=1	-0.272	0.362	>sp|Q91V88|NPNT_MOUSE Nephronectin OS=Mus musculus GN=Npnt PE=1 SV=1	-3.021	0.056
>sp|Q8K1M6|DNM1L_MOUSE Dynamin-1-like protein OS=Mus musculus GN=Dnm1l PE=1 SV=2	-0.265	0.364	>sp|P39061|COIA1_MOUSE Collagen alpha-1(XVIII) chain OS=Mus musculus GN=Col18a	-2.832	0.066
>sp|Q99LD8|DDAH2_MOUSE N(G),N(G)-dimethylarginine dimethylaminohydrolase 2 OS=Mus mus	-0.232	0.367	>sp|P11276|FINC_MOUSE Fibronectin OS=Mus musculus GN=Fn1 PE=1 SV=4	-2.610	0.077
>sp|Q9D8B4|NDUAB_MOUSE NADH dehydrogenase [ubiquinone] 1 alpha subcomplex subunit 11 C	-0.215	0.369	>tr|Q3UFT0|Q3UFT0_MOUSE Putative uncharacterized protein (Fragment) OS=Mus muscu	-2.267	0.087
>sp|P28271|ACOC_MOUSE Cytoplasmic aconitate hydratase OS=Mus musculus GN=Aco1 PE=1 SV	-0.207	0.372	>sp|P21956|MFGM_MOUSE Lactadherin OS=Mus musculus GN=Mfge8 PE=1 SV=3	-2.184	0.097
>sp|O35857|TIM44_MOUSE Mitochondrial import inner membrane translocase subunit TIM44 OS=M	-0.195	0.374	>sp|Q8VDD5|MYH9_MOUSE Myosin-9 OS=Mus musculus GN=Myh9 PE=1 SV=4	-2.160	0.107
>sp|Q9Z1J3|NFS1_MOUSE Cysteine desulfurase, mitochondrial OS=Mus musculus GN=Nfs1 PE=2 S	-0.195	0.377	>sp|O88207|CO5A1_MOUSE Collagen alpha-1(V) chain OS=Mus musculus GN=Col5a1 PE	-2.086	0.117
>sp|P16460|ASSY_MOUSE Argininosuccinate synthase OS=Mus musculus GN=Ass1 PE=1 SV=1	-0.191	0.379	>sp|Q62523|ZYX_MOUSE Zyxin OS=Mus musculus GN=Zyx PE=1 SV=2	-2.059	0.128
>sp|O35683|NDUA1_MOUSE NADH dehydrogenase [ubiquinone] 1 alpha subcomplex subunit 1 OS	-0.182	0.381	>sp|Q64314|CD34_MOUSE Hematopoietic progenitor cell antigen CD34 OS=Mus musculus	-1.933	0.138
>sp|Q9JHR7|IDE_MOUSE Insulin-degrading enzyme OS=Mus musculus GN=Ide PE=1 SV=1	-0.165	0.384	>sp|Q61001|LAMA5_MOUSE Laminin subunit alpha-5 OS=Mus musculus GN=Lama5 PE=	-1.923	0.148
>sp|Q99LX0|PARK7_MOUSE Protein DJ-1 OS=Mus musculus GN=Park7 PE=1 SV=1	-0.160	0.386	>sp|Q04857|CO6A1_MOUSE Collagen alpha-1(VI) chain OS=Mus musculus GN=Col6a1 P	-1.838	0.158
>sp|Q8CHT0|AL4A1_MOUSE Delta-1-pyrroline-5-carboxylate dehydrogenase, mitochondrial OS=Mu	-0.158	0.389	>sp|A2ARA8|ITA8_MOUSE Integrin alpha-8 OS=Mus musculus GN=Itga8 PE=1 SV=1	-1.758	0.168
>sp|Q9CZU6|CISY_MOUSE Citrate synthase, mitochondrial OS=Mus musculus GN=Cs PE=1 SV=1	-0.158	0.391	>sp|Q9R069|BCAM_MOUSE Basal cell adhesion molecule OS=Mus musculus GN=Bcam P	-1.640	0.179
>sp|P03930|ATP8_MOUSE ATP synthase protein 8 OS=Mus musculus GN=Mtatp8 PE=1 SV=1	-0.151	0.394	>sp|Q80X19|COEA1_MOUSE Collagen alpha-1(XIV) chain OS=Mus musculus GN=Col14a	-1.625	0.189

>sp|Q9DCC8|TOM20_MOUSE Mitochondrial import receptor subunit TOM20 homolog OS=Mus mu	-0.149	0.396	>sp|Q8C6K9|CO6A6_MOUSE Collagen alpha-6(VI) chain OS=Mus musculus GN=Col6a6 I	-1.617	0.199
>sp|Q60936|ADCK3_MOUSE Chaperone activity of bc1 complex-like, mitochondrial OS=Mus muscu	-0.147	0.399	>sp|Q640N1|AEBP1_MOUSE Adipocyte enhancer-binding protein 1 OS=Mus musculus GN	-1.583	0.209
>sp|Q9Z2Y8|PROSC_MOUSE Proline synthase co-transcribed bacterial homolog protein OS=Mus mu	-0.134	0.401	>sp|P12023|A4_MOUSE Amyloid beta A4 protein OS=Mus musculus GN=App PE=1 SV=3	-1.581	0.219
>sp|A2ARZ3|FSIP2_MOUSE Fibrous sheath-interacting protein 2 OS=Mus musculus GN=Fsip2 PE=	-0.113	0.404	>sp|A6H584|CO6A5_MOUSE Collagen alpha-5(VI) chain OS=Mus musculus GN=Col6a5 P	-1.559	0.230
>sp|Q91XE0|GLYAT_MOUSE Glycine N-acyltransferase OS=Mus musculus GN=Glyat PE=1 SV=1	-0.112	0.406	>sp|O35206|COFA1_MOUSE Collagen alpha-1(XV) chain OS=Mus musculus GN=Col15a1	-1.486	0.240
>sp|Q9QZD8|DIC_MOUSE Mitochondrial dicarboxylate carrier OS=Mus musculus GN=Slc25a10 PE	-0.108	0.409	>sp|Q62009|POSTN_MOUSE Periostin OS=Mus musculus GN=Postn PE=1 SV=2	-1.372	0.250
>sp|P11352|GPX1_MOUSE Glutathione peroxidase 1 OS=Mus musculus GN=Gpx1 PE=1 SV=2	-0.100	0.411	>sp|P11688|ITA5_MOUSE Integrin alpha-5 OS=Mus musculus GN=Itga5 PE=1 SV=3	-1.370	0.260
>sp|P06801|MAOX_MOUSE NADP-dependent malic enzyme OS=Mus musculus GN=Me1 PE=1 SV	-0.091	0.414	>sp|Q61879|MYH10_MOUSE Myosin-10 OS=Mus musculus GN=Myh10 PE=1 SV=2	-1.350	0.270
>sp|P47740|AL3A2_MOUSE Fatty aldehyde dehydrogenase OS=Mus musculus GN=Aldh3a2 PE=2 S	-0.069	0.416	>sp|Q99K41|EMIL1_MOUSE EMILIN-1 OS=Mus musculus GN=Emilin1 PE=1 SV=1	-1.307	0.281
>sp|Q60597|ODO1_MOUSE 2-oxoglutarate dehydrogenase, mitochondrial OS=Mus musculus GN=O	-0.068	0.419	>sp|O88322|NID2_MOUSE Nidogen-2 OS=Mus musculus GN=Nid2 PE=1 SV=2	-1.257	0.291
>sp|Q9CWS0|DDAH1_MOUSE N(G),N(G)-dimethylarginine dimethylaminohydrolase 1 OS=Mus mu	-0.058	0.421	>sp|P26039|TLN1_MOUSE Talin-1 OS=Mus musculus GN=Tln1 PE=1 SV=2	-1.208	0.301
>sp|Q9Z2I8|SUCB2_MOUSE Succinyl-CoA ligase [GDP-forming] subunit beta, mitochondrial OS=M	-0.056	0.423	>tr|Q8BS97|Q8BS97_MOUSE Versican core protein OS=Mus musculus GN=Vcan PE=2 SV	-1.198	0.311
>sp|P42859|HD_MOUSE Huntingtin OS=Mus musculus GN=Htt PE=1 SV=2	-0.055	0.426	>sp|Q62470|ITA3_MOUSE Integrin alpha-3 OS=Mus musculus GN=Itga3 PE=1 SV=1	-1.156	0.321
>sp|Q9CZ42|NNRD_MOUSE ATP-dependent (S)-NAD(P)H-hydrate dehydratase OS=Mus musculus	-0.050	0.428	>sp|Q61490|CD166_MOUSE CD166 antigen OS=Mus musculus GN=Alcam PE=1 SV=3	-1.151	0.332
>sp|Q9Z1Q5|CLIC1_MOUSE Chloride intracellular channel protein 1 OS=Mus musculus GN=Clic1 P	-0.038	0.431	>sp|P43406|ITAV_MOUSE Integrin alpha-V OS=Mus musculus GN=Itgav PE=1 SV=2	-1.139	0.342
>sp|P55096|ABCD3_MOUSE ATP-binding cassette sub-family D member 3 OS=Mus musculus GN=	-0.035	0.433	>sp|P09055|ITB1_MOUSE Integrin beta-1 OS=Mus musculus GN=Itgb1 PE=1 SV=1	-1.132	0.352
>sp|P16125|LDHB_MOUSE L-lactate dehydrogenase B chain OS=Mus musculus GN=Ldhb PE=1 SV	-0.031	0.436	>sp|P97927|LAMA4_MOUSE Laminin subunit alpha-4 OS=Mus musculus GN=Lama4 PE=	-1.085	0.362
>sp|Q9QUI0|RHOA_MOUSE Transforming protein RhoA OS=Mus musculus GN=Rhoa PE=1 SV=1	-0.026	0.438	>sp|Q9R1V7|ADA23_MOUSE Disintegrin and metalloproteinase domain-containing protein	-1.060	0.372
>sp|O70325|GPX41_MOUSE Phospholipid hydroperoxide glutathione peroxidase, mitochondrial OS=	-0.019	0.441	>sp|Q9R1Z8|VINEX_MOUSE Vinexin OS=Mus musculus GN=Sorbs3 PE=1 SV=1	-0.898	0.383
>sp|P63085|MK01_MOUSE Mitogen-activated protein kinase 1 OS=Mus musculus GN=Mapk1 PE=1	-0.018	0.443	>sp|Q8VI36|PAXI_MOUSE Paxillin OS=Mus musculus GN=Pxn PE=1 SV=1	-0.879	0.393
>sp|P50431|GLYC_MOUSE Serine hydroxymethyltransferase, cytosolic OS=Mus musculus GN=Shm	-0.015	0.446	>sp|Q61292|LAMB2_MOUSE Laminin subunit beta-2 OS=Mus musculus GN=Lamb2 PE=2	-0.875	0.403
>sp|Q9QUM9|PSA6_MOUSE Proteasome subunit alpha type-6 OS=Mus musculus GN=Psma6 PE=1	-0.011	0.448	>sp|Q02788|CO6A2_MOUSE Collagen alpha-2(VI) chain OS=Mus musculus GN=Col6a2 P	-0.863	0.413
>sp|P31750|AKT1_MOUSE RAC-alpha serine/threonine-protein kinase OS=Mus musculus GN=Akt1	-0.009	0.451	>tr|Q91XX7|Q91XX7_MOUSE Protocadherin gamma B2 OS=Mus musculus GN=Pcdhgb2	-0.843	0.423
>sp|Q8BVI4|DHPR_MOUSE Dihydropteridine reductase OS=Mus musculus GN=Qdpr PE=1 SV=2	-0.001	0.453	>sp|Q80YX1|TENA_MOUSE Tenascin OS=Mus musculus GN=Tnc PE=1 SV=1	-0.836	0.434
>sp|Q9CQW1|YKT6_MOUSE Synaptobrevin homolog YKT6 OS=Mus musculus GN=Ykt6 PE=2 SV	0.009	0.456	>sp|Q9WVH9|FBLN5_MOUSE Fibulin-5 OS=Mus musculus GN=Fbln5 PE=2 SV=1	-0.800	0.444
>sp|P56380|AP4A_MOUSE Bis(5'-nucleosyl)-tetraphosphatase [asymmetrical] OS=Mus musculus GN	0.010	0.458	>tr|B8JK39|B8JK39_MOUSE Integrin alpha 9 OS=Mus musculus GN=Itga9 PE=3 SV=1	-0.781	0.454
>sp|Q07417|ACADS_MOUSE Short-chain specific acyl-CoA dehydrogenase, mitochondrial OS=Mus	0.012	0.460	>tr|B9EHT6|B9EHT6_MOUSE Fn1 protein OS=Mus musculus GN=Fn1 PE=2 SV=1	-0.756	0.464
>sp|Q61425|HCDH_MOUSE Hydroxyacyl-coenzyme A dehydrogenase, mitochondrial OS=Mus musc	0.013	0.463	>tr|F8VQJ3|F8VQJ3_MOUSE Laminin subunit gamma-1 OS=Mus musculus GN=Lamc1 PE	-0.750	0.474
>sp|Q9D0I9|SYRC_MOUSE Arginine--tRNA ligase, cytoplasmic OS=Mus musculus GN=Rars PE=2	0.015	0.465	>sp|P62746|RHOB_MOUSE Rho-related GTP-binding protein RhoB OS=Mus musculus GN	-0.722	0.485
>sp|Q8BMF4|ODP2_MOUSE Dihydrolipoyllysine-residue acetyltransferase component of pyruvate de	0.016	0.468	>sp|Q9EPC1|PARVA_MOUSE Alpha-parvin OS=Mus musculus GN=Parva PE=1 SV=1	-0.690	0.495
>sp|Q8BGB8|COQ4_MOUSE Ubiquinone biosynthesis protein COQ4 homolog, mitochondrial OS=M	0.024	0.470	>sp|P26231|CTNA1_MOUSE Catenin alpha-1 OS=Mus musculus GN=Ctnna1 PE=1 SV=1	-0.663	0.505
>sp|Q91VD9|NDUS1_MOUSE NADH-ubiquinone oxidoreductase 75 kDa subunit, mitochondrial OS=	0.040	0.473	>sp|Q3UTJ2|SRBS2_MOUSE Sorbin and SH3 domain-containing protein 2 OS=Mus muscu	-0.651	0.515
>sp|Q9CRB9|CHCH3_MOUSE Coiled-coil-helix-coiled-coil-helix domain-containing protein 3, mitoc	0.043	0.475	>sp|Q8BFW7|LPP_MOUSE Lipoma-preferred partner homolog OS=Mus musculus GN=Lpp	-0.638	0.526
>tr|Q3U1C4|Q3U1C4_MOUSE MCG1271 OS=Mus musculus GN=Secisbp2 PE=2 SV=1	0.056	0.478	>sp|Q8CIZ8|VWF_MOUSE von Willebrand factor OS=Mus musculus GN=Vwf PE=1 SV=2	-0.628	0.536
>sp|Q9DCX2|ATP5H_MOUSE ATP synthase subunit d, mitochondrial OS=Mus musculus GN=Atp5h	0.072	0.480	>sp|Q9Z0M6|CD97_MOUSE CD97 antigen OS=Mus musculus GN=Cd97 PE=1 SV=2	-0.620	0.546
>tr|Q99N15|Q99N15_MOUSE 17beta-hydroxysteroid dehydrogenase type 10/short chain L-3-hydroxy	0.073	0.483	>sp|Q71FD7|FBLI1_MOUSE Filamin-binding LIM protein 1 OS=Mus musculus GN=Fblim	-0.561	0.556
>sp|Q9D6J5|NDUB8_MOUSE NADH dehydrogenase [ubiquinone] 1 beta subcomplex subunit 8, mitc	0.078	0.485	>sp|Q9QUP5|HPLN1_MOUSE Hyaluronan and proteoglycan link protein 1 OS=Mus muscul	-0.434	0.566
>sp|Q8BKZ9|ODPX_MOUSE Pyruvate dehydrogenase protein X component, mitochondrial OS=Mus	0.084	0.488	>sp|Q9WTR5|CAD13_MOUSE Cadherin-13 OS=Mus musculus GN=Cdh13 PE=1 SV=2	-0.425	0.577
>sp|Q8BGT8|PHIPL_MOUSE Phytanoyl-CoA hydroxylase-interacting protein-like OS=Mus musculus	0.088	0.490	>sp|O70309|ITB5_MOUSE Integrin beta-5 OS=Mus musculus GN=Itgb5 PE=1 SV=2	-0.368	0.587
>sp|Q91WD5|NDUS2_MOUSE NADH dehydrogenase [ubiquinone] iron-sulfur protein 2, mitochondr	0.095	0.493	>sp|Q64727|VINC_MOUSE Vinculin OS=Mus musculus GN=Vcl PE=1 SV=4	-0.368	0.597
>sp|Q8CAY6|THIC_MOUSE Acetyl-CoA acetyltransferase, cytosolic OS=Mus musculus GN=Acat2	0.096	0.495	>sp|P02468|LAMC1_MOUSE Laminin subunit gamma-1 OS=Mus musculus GN=Lamc1 PE	-0.350	0.607
>sp|Q8BIJ6|SYIM_MOUSE Isoleucine--tRNA ligase, mitochondrial OS=Mus musculus GN=Iars2 PE	0.099	0.498	>sp|Q8R2Y2|MUC18_MOUSE Cell surface glycoprotein MUC18 OS=Mus musculus GN=M	-0.318	0.617
>sp|P51174|ACADL_MOUSE Long-chain specific acyl-CoA dehydrogenase, mitochondrial OS=Mus	0.102	0.500	>tr|A2RS43|A2RS43_MOUSE Protein Pcdh7 OS=Mus musculus GN=Pcdh7 PE=2 SV=1	-0.284	0.628
>sp|P08228|SODC_MOUSE Superoxide dismutase [Cu-Zn] OS=Mus musculus GN=Sod1 PE=1 SV=2	0.115	0.502	>sp|Q61735|CD47_MOUSE Leukocyte surface antigen CD47 OS=Mus musculus GN=Cd47	-0.238	0.638
>sp|Q99LP6|GRPE1_MOUSE GrpE protein homolog 1, mitochondrial OS=Mus musculus GN=Grpel1	0.126	0.505	>sp|Q9D1H9|MFAP4_MOUSE Microfibril-associated glycoprotein 4 OS=Mus musculus GN	-0.237	0.648
>sp|P80313|TCPH_MOUSE T-complex protein 1 subunit eta OS=Mus musculus GN=Cct7 PE=1 SV=	0.127	0.507	>sp|Q8BZF8|PGM5_MOUSE Phosphoglucomutase-like protein 5 OS=Mus musculus GN=P	-0.154	0.658
>sp|P38647|GRP75_MOUSE Stress-70 protein, mitochondrial OS=Mus musculus GN=Hspa9 PE=1 S	0.147	0.510	>sp|P97300|NPTN_MOUSE Neuroplastin OS=Mus musculus GN=Nptn PE=1 SV=3	-0.099	0.668
>sp|P63168|DYL1_MOUSE Dynein light chain 1, cytoplasmic OS=Mus musculus GN=Dynll1 PE=1 S	0.157	0.512	>sp|Q08481|PECA1_MOUSE Platelet endothelial cell adhesion molecule OS=Mus musculus	-0.094	0.679
>sp|Q9DBM2|ECHP_MOUSE Peroxisomal bifunctional enzyme OS=Mus musculus GN=Ehhadh PE=	0.165	0.515	>sp|P14206|RSSA_MOUSE 40S ribosomal protein SA OS=Mus musculus GN=Rpsa PE=1 S	-0.062	0.689
>sp|P43024|CX6A1_MOUSE Cytochrome c oxidase subunit 6A1, mitochondrial OS=Mus musculus G	0.169	0.517	>sp|P29533|VCAM1_MOUSE Vascular cell adhesion protein 1 OS=Mus musculus GN=Vca	-0.025	0.699
>sp|Q9CXW2|RT22_MOUSE 28S ribosomal protein S22, mitochondrial OS=Mus musculus GN=Mrp	0.174	0.520	>tr|E9QB01|E9QB01_MOUSE Neural cell adhesion molecule 1 OS=Mus musculus GN=Nca	0.000	0.709
>sp|Q9DC70|NDUS7_MOUSE NADH dehydrogenase [ubiquinone] iron-sulfur protein 7, mitochondri	0.175	0.522	>sp|P30999|CTND1_MOUSE Catenin delta-1 OS=Mus musculus GN=Ctnnd1 PE=1 SV=2	0.095	0.719
>sp|Q9Z1Z2|STRAP_MOUSE Serine-threonine kinase receptor-associated protein OS=Mus musculus	0.176	0.525	>sp|P35441|TSP1_MOUSE Thrombospondin-1 OS=Mus musculus GN=Thbs1 PE=1 SV=1	0.104	0.730

>sp|P52825|CPT2_MOUSE Carnitine O-palmitoyltransferase 2, mitochondrial OS=Mus musculus GN	0.176	0.527
>sp|P47934|CACP_MOUSE Carnitine O-acetyltransferase OS=Mus musculus GN=Crat PE=1 SV=3	0.179	0.530
>sp|Q9CQH3|NDUB5_MOUSE NADH dehydrogenase [ubiquinone] 1 beta subcomplex subunit 5, mi	0.185	0.532
>sp|P56480|ATPB_MOUSE ATP synthase subunit beta, mitochondrial OS=Mus musculus GN=Atp5b	0.200	0.535
>sp|Q63844|MK03_MOUSE Mitogen-activated protein kinase 3 OS=Mus musculus GN=Mapk3 PE=1	0.207	0.537
>sp|P53395|ODB2_MOUSE Lipoamide acyltransferase component of branched-chain alpha-keto acid	0.210	0.540
>sp|P28352|APEX1_MOUSE DNA-(apurinic or apyrimidinic site) lyase OS=Mus musculus GN=Apex	0.221	0.542
>sp|Q64521|GPDM_MOUSE Glycerol-3-phosphate dehydrogenase, mitochondrial OS=Mus musculus	0.227	0.544
>sp|Q8VCL2|SCO2_MOUSE Protein SCO2 homolog, mitochondrial OS=Mus musculus GN=Sco2 PE	0.228	0.547
>sp|Q8BFR5|EFTU_MOUSE Elongation factor Tu, mitochondrial OS=Mus musculus GN=Tufm PE=1	0.229	0.549
>sp|P62492|RB11A_MOUSE Ras-related protein Rab-11A OS=Mus musculus GN=Rab11a PE=1 SV=	0.232	0.552
>sp|Q9D855|QCR7_MOUSE Cytochrome b-c1 complex subunit 7 OS=Mus musculus GN=Uqcrb PE=	0.234	0.554
>sp|O70378|EMC8_MOUSE ER membrane protein complex subunit 8 OS=Mus musculus GN=Emc8	0.236	0.557
>sp|Q9Z0X1|AIFM1_MOUSE Apoptosis-inducing factor 1, mitochondrial OS=Mus musculus GN=Ai	0.244	0.559
>sp|P54775|PRS6B_MOUSE 26S protease regulatory subunit 6B OS=Mus musculus GN=Psmc4 PE=	0.245	0.562
>sp|Q9CPV4|GLOD4_MOUSE Glyoxalase domain-containing protein 4 OS=Mus musculus GN=Glod	0.249	0.564
>tr|Q8JZU2|Q8JZU2_MOUSE Protein Slc25a1 OS=Mus musculus GN=Slc25a1 PE=2 SV=1	0.257	0.567
>sp|Q9Z1X4|ILF3_MOUSE Interleukin enhancer-binding factor 3 OS=Mus musculus GN=Ilf3 PE=1 S	0.261	0.569
>sp|Q5SSK3|TEFM_MOUSE Transcription elongation factor, mitochondrial OS=Mus musculus GN=	0.267	0.572
>tr|Q924B0|Q924B0_MOUSE Inositol (Myo)-1(Or 4)-monophosphatase 1 OS=Mus musculus GN=Im	0.271	0.574
>sp|Q9QYB1|CLIC4_MOUSE Chloride intracellular channel protein 4 OS=Mus musculus GN=Clic4	0.271	0.577
>sp|Q6ZWQ0|SYNE2_MOUSE Nesprin-2 OS=Mus musculus GN=Syne2 PE=1 SV=2	0.274	0.579
>sp|P25688|URIC_MOUSE Uricase OS=Mus musculus GN=Uox PE=1 SV=2	0.286	0.581
>sp|Q9DCM0|ETHE1_MOUSE Protein ETHE1, mitochondrial OS=Mus musculus GN=Ethe1 PE=1 S	0.302	0.584
>sp|Q91V92|ACLY_MOUSE ATP-citrate synthase OS=Mus musculus GN=Acly PE=1 SV=1	0.325	0.586
>sp|P52480|KPYM_MOUSE Pyruvate kinase isozymes M1/M2 OS=Mus musculus GN=Pkm PE=1 SV	0.327	0.589
>sp|Q99JR1|SFXN1_MOUSE Sideroflexin-1 OS=Mus musculus GN=Sfxn1 PE=1 SV=3	0.329	0.591
>sp|O08749|DLDH_MOUSE Dihydrolipoyl dehydrogenase, mitochondrial OS=Mus musculus GN=Dl	0.330	0.594
>sp|Q8VEM8|MPCP_MOUSE Phosphate carrier protein, mitochondrial OS=Mus musculus GN=Slc25	0.336	0.596
>sp|Q922W5|P5CR1_MOUSE Pyrroline-5-carboxylate reductase 1, mitochondrial OS=Mus musculus	0.342	0.599
>sp|Q8CH40|NUDT6_MOUSE Nucleoside diphosphate-linked moiety X motif 6 OS=Mus musculus G	0.349	0.601
>sp|Q9D3D9|ATPD_MOUSE ATP synthase subunit delta, mitochondrial OS=Mus musculus GN=Atp	0.368	0.604
>sp|P56395|CYB5_MOUSE Cytochrome b5 OS=Mus musculus GN=Cyb5a PE=1 SV=2	0.370	0.606
>sp|Q9WTP6|KAD2_MOUSE Adenylate kinase 2, mitochondrial OS=Mus musculus GN=Ak2 PE=1 S	0.376	0.609
>sp|Q99J99|THTM_MOUSE 3-mercaptopyruvate sulfurtransferase OS=Mus musculus GN=Mpst PE=	0.383	0.611
>sp|Q921H8|THIKA_MOUSE 3-ketoacyl-CoA thiolase A, peroxisomal OS=Mus musculus GN=Acaa	0.390	0.614
>sp|P17665|COX7C_MOUSE Cytochrome c oxidase subunit 7C, mitochondrial OS=Mus musculus GI	0.413	0.616
>sp|Q9D3P8|PLRKT_MOUSE Plasminogen receptor (KT) OS=Mus musculus GN=Plgrkt PE=1 SV=1	0.414	0.619
>sp|Q8BH04|PCKGM_MOUSE Phosphoenolpyruvate carboxykinase [GTP], mitochondrial OS=Mus	0.426	0.621
>sp|P28474|ADHX_MOUSE Alcohol dehydrogenase class-3 OS=Mus musculus GN=Adh5 PE=1 SV=	0.439	0.623
>sp|P62259|1433E_MOUSE 14-3-3 protein epsilon OS=Mus musculus GN=Ywhae PE=1 SV=1	0.441	0.626
>sp|Q9D6K8|FUND2_MOUSE FUN14 domain-containing protein 2 OS=Mus musculus GN=Fundc2	0.455	0.628
>sp|Q9R112|SQRD_MOUSE Sulfide:quinone oxidoreductase, mitochondrial OS=Mus musculus GN=	0.483	0.631
>sp|P19096|FAS_MOUSE Fatty acid synthase OS=Mus musculus GN=Fasn PE=1 SV=2	0.490	0.633
>sp|Q9CQX2|CYB5B_MOUSE Cytochrome b5 type B OS=Mus musculus GN=Cyb5b PE=1 SV=1	0.490	0.636
>sp|Q64105|SPRE_MOUSE Sepiapterin reductase OS=Mus musculus GN=Spr PE=1 SV=1	0.498	0.638
>sp|Q8VHJ7|PRGC2_MOUSE Peroxisome proliferator-activated receptor gamma coactivator 1-beta C	0.512	0.641
>sp|Q9WUM5|SUCA_MOUSE Succinyl-CoA ligase [ADP/GDP-forming] subunit alpha, mitochondri	0.512	0.643
>tr|Q91VA7|Q91VA7_MOUSE Isocitrate dehydrogenase 3 (NAD+) beta OS=Mus musculus GN=Idh3	0.517	0.646
>sp|P26443|DHE3_MOUSE Glutamate dehydrogenase 1, mitochondrial OS=Mus musculus GN=Glud	0.522	0.648
>sp|Q9QZH6|ECSIT_MOUSE Evolutionarily conserved signaling intermediate in Toll pathway, mitoc	0.524	0.651
>sp|P37040|NCPR_MOUSE NADPH--cytochrome P450 reductase OS=Mus musculus GN=Por PE=1	0.537	0.653
>sp|O09005|DEGS1_MOUSE Sphingolipid delta(4)-desaturase DES1 OS=Mus musculus GN=Degs1	0.537	0.656

>sp|Q99JY8|LPP3_MOUSE Lipid phosphate phosphohydrolase 3 OS=Mus musculus GN=P	0.143	0.740
>sp|P82198|BGH3_MOUSE Transforming growth factor-beta-induced protein ig-h3 OS=Mu	0.160	0.750
>sp|Q61330|CNTN2_MOUSE Contactin-2 OS=Mus musculus GN=Cntn2 PE=2 SV=2	0.247	0.760
>sp|O70423|AOC3_MOUSE Membrane primary amine oxidase OS=Mus musculus GN=Aoc	0.258	0.770
>sp|Q9QUI0|RHOA_MOUSE Transforming protein RhoA OS=Mus musculus GN=Rhoa PE	0.275	0.781
>sp|Q60847|COCA1_MOUSE Collagen alpha-1(XII) chain OS=Mus musculus GN=Col12a1	0.294	0.791
>sp|P35330|ICAM2_MOUSE Intercellular adhesion molecule 2 OS=Mus musculus GN=Icar	0.459	0.801
>sp|Q8CIB5|FERM2_MOUSE Fermitin family homolog 2 OS=Mus musculus GN=Fermt2 P	0.503	0.811
>sp|Q8VCC9|SPON1_MOUSE Spondin-1 OS=Mus musculus GN=Spon1 PE=2 SV=1	0.552	0.821
>sp|O54890|ITB3_MOUSE Integrin beta-3 OS=Mus musculus GN=Itgb3 PE=1 SV=2	0.585	0.832
>sp|P10493|NID1_MOUSE Nidogen-1 OS=Mus musculus GN=Nid1 PE=1 SV=2	0.631	0.842
>sp|Q60634|FLOT2_MOUSE Flotillin-2 OS=Mus musculus GN=Flot2 PE=1 SV=2	0.671	0.852
>sp|P13595|NCAM1_MOUSE Neural cell adhesion molecule 1 OS=Mus musculus GN=Nca	0.864	0.862
>sp|P40240|CD9_MOUSE CD9 antigen OS=Mus musculus GN=Cd9 PE=1 SV=2	0.942	0.872
>tr|G3UW60|G3UW60_MOUSE MCG14773 OS=Mus musculus GN=Susd5 PE=4 SV=1	0.992	0.883
>sp|Q60675|LAMA2_MOUSE Laminin subunit alpha-2 OS=Mus musculus GN=Lama2 PE=	1.083	0.893
>sp|Q71LX4|TLN2_MOUSE Talin-2 OS=Mus musculus GN=Tln2 PE=1 SV=3	1.251	0.903
>sp|P63001|RAC1_MOUSE Ras-related C3 botulinum toxin substrate 1 OS=Mus musculus G	1.328	0.913
>sp|Q02248|CTNB1_MOUSE Catenin beta-1 OS=Mus musculus GN=Ctnnb1 PE=1 SV=1	1.411	0.923
>sp|Q61738|ITA7_MOUSE Integrin alpha-7 OS=Mus musculus GN=Itga7 PE=1 SV=3	1.587	0.934
>sp|O35114|SCRB2_MOUSE Lysosome membrane protein 2 OS=Mus musculus GN=Scarb2	1.649	0.944
>sp|Q3V3R4|ITA1_MOUSE Integrin alpha-1 OS=Mus musculus GN=Itga1 PE=2 SV=2	2.446	0.954
>sp|Q08857|CD36_MOUSE Platelet glycoprotein 4 OS=Mus musculus GN=Cd36 PE=1 SV=	2.737	0.964
>sp|P14094|AT1B1_MOUSE Sodium/potassium-transporting ATPase subunit beta-1 OS=Mu	5.091	0.974
>sp|P02469|LAMB1_MOUSE Laminin subunit beta-1 OS=Mus musculus GN=Lamb1 PE=1	5.615	0.985
>sp|Q2UY11|COSA1_MOUSE Collagen alpha-1(XXVIII) chain OS=Mus musculus GN=Co	12.820	0.995

Calcium ion binding GO:0005509

Protein identification	Zq	rank/N
>sp|P70663|SPRL1_MOUSE SPARC-like protein 1 OS=Mus musculus GN=Sparcl1 PE=1 S	-7.129	0.005
>sp|Q62059|CSPG2_MOUSE Versican core protein OS=Mus musculus GN=Vcan PE=1 SV=	-3.806	0.014
>sp|Q8BPB5|FBLN3_MOUSE EGF-containing fibulin-like extracellular matrix protein 1 OS	-3.415	0.023
>tr|Q6ZWQ9|Q6ZWQ9_MOUSE MCG5400 OS=Mus musculus GN=Myl12a PE=2 SV=1	-3.282	0.032
>sp|Q91V88|NPNT_MOUSE Nephronectin OS=Mus musculus GN=Npnt PE=1 SV=1	-3.021	0.041
>sp|Q8K4G1|LTBP4_MOUSE Latent-transforming growth factor beta-binding protein 4 OS=	-2.490	0.050
>tr|F8WIT2|F8WIT2_MOUSE Annexin OS=Mus musculus GN=Anxa6 PE=3 SV=1	-1.915	0.059
>sp|Q3THE2|ML12B_MOUSE Myosin regulatory light chain 12B OS=Mus musculus GN=M	-1.838	0.068
>sp|Q9D2N4|DTNA_MOUSE Dystrobrevin alpha OS=Mus musculus GN=Dtna PE=1 SV=2	-1.804	0.077
>sp|Q60605|MYL6_MOUSE Myosin light polypeptide 6 OS=Mus musculus GN=Myl6 PE=	-1.760	0.086
>sp|P08032|SPTA1_MOUSE Spectrin alpha chain, erythrocytic 1 OS=Mus musculus GN=Sp	-1.687	0.095
>sp|Q9R0K7|AT2B2_MOUSE Plasma membrane calcium-transporting ATPase 2 OS=Mus m	-1.621	0.104
>sp|Q9CQ19|MYL9_MOUSE Myosin regulatory light polypeptide 9 OS=Mus musculus GN	-1.587	0.113
>sp|P57780|ACTN4_MOUSE Alpha-actinin-4 OS=Mus musculus GN=Actn4 PE=1 SV=1	-1.556	0.122
>tr|A2AQ53|A2AQ53_MOUSE Fibrillin 1 OS=Mus musculus GN=Fbn1 PE=4 SV=1	-1.539	0.131
>sp|Q8CI43|MYL6B_MOUSE Myosin light chain 6B OS=Mus musculus GN=Myl6b PE=2	-1.483	0.140
>tr|Q61636|Q61636_MOUSE G-utrophin (Predicted protein) OS=Mus musculus GN=Utrn P	-1.294	0.149
>sp|O88322|NID2_MOUSE Nidogen-2 OS=Mus musculus GN=Nid2 PE=1 SV=2	-1.257	0.158
>tr|Q8C845|Q8C845_MOUSE EF hand domain containing 2 OS=Mus musculus GN=Efhd2	-1.255	0.167
>sp|P11531|DMD_MOUSE Dystrophin OS=Mus musculus GN=Dmd PE=1 SV=3	-1.252	0.176
>sp|Q3V0K9|PLSI_MOUSE Plastin-1 OS=Mus musculus GN=Pls1 PE=2 SV=1	-1.220	0.185
>sp|Q08879|FBLN1_MOUSE Fibulin-1 OS=Mus musculus GN=Fbln1 PE=1 SV=2	-1.197	0.194
>sp|O08795|GLU2B_MOUSE Glucosidase 2 subunit beta OS=Mus musculus GN=Prkcsh PE	-1.195	0.203
>sp|P21981|TGM2_MOUSE Protein-glutamine gamma-glutamyltransferase 2 OS=Mus musc	-1.193	0.212

>sp|P08074|CBR2_MOUSE Carbonyl reductase [NADPH] 2 OS=Mus musculus GN=Cbr2 PE=1 SV=	0.539	0.658	>sp|O08529|CAN2_MOUSE Calpain-2 catalytic subunit OS=Mus musculus GN=Capn2 PE=	-1.151	0.221
>sp|Q9D7B6|ACAD8_MOUSE Isobutyryl-CoA dehydrogenase, mitochondrial OS=Mus musculus GN	0.553	0.660	>sp|P37889|FBLN2_MOUSE Fibulin-2 OS=Mus musculus GN=Fbln2 PE=1 SV=2	-1.150	0.230
>sp|P35700|PRDX1_MOUSE Peroxiredoxin-1 OS=Mus musculus GN=Prdx1 PE=1 SV=1	0.567	0.663	>tr|E9Q6R7|E9Q6R7_MOUSE Protein Utrn OS=Mus musculus GN=Utrn PE=4 SV=1	-1.104	0.239
>sp|Q9QYR9|ACOT2_MOUSE Acyl-coenzyme A thioesterase 2, mitochondrial OS=Mus musculus G	0.567	0.665	>sp|Q7TPR4|ACTN1_MOUSE Alpha-actinin-1 OS=Mus musculus GN=Actn1 PE=1 SV=1	-1.092	0.248
>sp|Q9D6R2|IDH3A_MOUSE Isocitrate dehydrogenase [NAD] subunit alpha, mitochondrial OS=Mus	0.579	0.668	>sp|A2ASQ1|AGRIN_MOUSE Agrin OS=Mus musculus GN=Agrn PE=1 SV=1	-1.088	0.257
>sp|O89023|TPP1_MOUSE Tripeptidyl-peptidase 1 OS=Mus musculus GN=Tpp1 PE=1 SV=2	0.588	0.670	>sp|P10107|ANXA1_MOUSE Annexin A1 OS=Mus musculus GN=Anxa1 PE=1 SV=2	-1.077	0.266
>sp|Q60932|VDAC1_MOUSE Voltage-dependent anion-selective channel protein 1 OS=Mus musculu	0.607	0.673	>sp|Q07076|ANXA7_MOUSE Annexin A7 OS=Mus musculus GN=Anxa7 PE=2 SV=2	-1.013	0.275
>sp|Q9CPY7|AMPL_MOUSE Cytosol aminopeptidase OS=Mus musculus GN=Lap3 PE=1 SV=3	0.610	0.675	>sp|P14069|S10A6_MOUSE Protein S100-A6 OS=Mus musculus GN=S100a6 PE=1 SV=3	-0.894	0.284
>sp|P36552|HEM6_MOUSE Coproporphyrinogen-III oxidase, mitochondrial OS=Mus musculus GN=	0.639	0.678	>sp|Q99K51|PLST_MOUSE Plastin-3 OS=Mus musculus GN=Pls3 PE=1 SV=3	-0.849	0.293
>sp|Q9CQN1|TRAP1_MOUSE Heat shock protein 75 kDa, mitochondrial OS=Mus musculus GN=Tra	0.641	0.680	>tr|Q91XX7|Q91XX7_MOUSE Protocadherin gamma B2 OS=Mus musculus GN=Pcdhgb2	-0.843	0.302
>sp|Q60930|VDAC2_MOUSE Voltage-dependent anion-selective channel protein 2 OS=Mus musculu	0.642	0.683	>sp|Q9D4J1|EFHD1_MOUSE EF-hand domain-containing protein D1 OS=Mus musculus G	-0.817	0.311
>sp|Q8C196|CPSM_MOUSE Carbamoyl-phosphate synthase [ammonia], mitochondrial OS=Mus mus	0.642	0.685	>sp|Q8CG19|LTBP1_MOUSE Latent-transforming growth factor beta-binding protein 1 OS=	-0.808	0.320
>sp|P46471|PRS7_MOUSE 26S protease regulatory subunit 7 OS=Mus musculus GN=Psmc2 PE=1 S	0.645	0.688	>sp|Q9WVH9|FBLN5_MOUSE Fibulin-5 OS=Mus musculus GN=Fbln5 PE=2 SV=1	-0.800	0.329
>sp|P33434|MMP2_MOUSE 72 kDa type IV collagenase OS=Mus musculus GN=Mmp2 PE=2 SV=1	0.653	0.690	>sp|Q05186|RCN1_MOUSE Reticulocalbin-1 OS=Mus musculus GN=Rcn1 PE=1 SV=1	-0.767	0.338
>sp|E9Q557|DESP_MOUSE Desmoplakin OS=Mus musculus GN=Dsp PE=3 SV=1	0.664	0.693	>sp|P19221|THRB_MOUSE Prothrombin OS=Mus musculus GN=F2 PE=1 SV=1	-0.765	0.347
>sp|P06151|LDHA_MOUSE L-lactate dehydrogenase A chain OS=Mus musculus GN=Ldha PE=1 SV	0.665	0.695	>sp|P07091|S10A4_MOUSE Protein S100-A4 OS=Mus musculus GN=S100a4 PE=1 SV=1	-0.747	0.356
>sp|Q9CR61|NDUB7_MOUSE NADH dehydrogenase [ubiquinone] 1 beta subcomplex subunit 7 OS=	0.672	0.698	>sp|Q62356|FSTL1_MOUSE Follistatin-related protein 1 OS=Mus musculus GN=Fstl1 PE=	-0.724	0.365
>sp|P21981|TGM2_MOUSE Protein-glutamine gamma-glutamyltransferase 2 OS=Mus musculus GN=	0.673	0.700	>sp|P62204|CALM_MOUSE Calmodulin OS=Mus musculus GN=Calm1 PE=1 SV=2	-0.716	0.374
>sp|Q641K1|CBPC1_MOUSE Cytosolic carboxypeptidase 1 OS=Mus musculus GN=Agtpbp1 PE=1 S	0.675	0.702	>sp|Q61592|GAS6_MOUSE Growth arrest-specific protein 6 OS=Mus musculus GN=Gas6 P	-0.623	0.383
>sp|Q921G7|ETFD_MOUSE Electron transfer flavoprotein-ubiquinone oxidoreductase, mitochondrial	0.678	0.705	>sp|Q9Z0M6|CD97_MOUSE CD97 antigen OS=Mus musculus GN=Cd97 PE=1 SV=2	-0.620	0.392
>sp|Q8BTZ7|GMPPB_MOUSE Mannose-1-phosphate guanyltransferase beta OS=Mus musculus GN=	0.686	0.707	>sp|P97352|S10AD_MOUSE Protein S100-A13 OS=Mus musculus GN=S100a13 PE=1 SV=	-0.591	0.401
>sp|O08709|PRDX6_MOUSE Peroxiredoxin-6 OS=Mus musculus GN=Prdx6 PE=1 SV=3	0.692	0.710	>sp|P70302|STIM1_MOUSE Stromal interaction molecule 1 OS=Mus musculus GN=Stim1 P	-0.562	0.410
>sp|Q9CQZ5|NDUA6_MOUSE NADH dehydrogenase [ubiquinone] 1 alpha subcomplex subunit 6 OS	0.702	0.712	>sp|Q9EQP2|EHD4_MOUSE EH domain-containing protein 4 OS=Mus musculus GN=Ehd4	-0.554	0.419
>sp|Q9WTP7|KAD3_MOUSE GTP:AMP phosphotransferase, mitochondrial OS=Mus musculus GN=	0.745	0.715	>sp|O35887|CALU_MOUSE Calumenin OS=Mus musculus GN=Calu PE=1 SV=1	-0.543	0.428
>sp|Q9CR21|ACPM_MOUSE Acyl carrier protein, mitochondrial OS=Mus musculus GN=Ndufab1 PE	0.761	0.717	>sp|Q9ESD7|DYSF_MOUSE Dysferlin OS=Mus musculus GN=Dysf PE=1 SV=3	-0.542	0.437
>sp|Q9JLJ2|AL9A1_MOUSE 4-trimethylaminobutyraldehyde dehydrogenase OS=Mus musculus GN=	0.763	0.720	>sp|Q60902|EP15R_MOUSE Epidermal growth factor receptor substrate 15-like 1 OS=Mus	-0.502	0.446
>sp|Q9JIK9|RT34_MOUSE 28S ribosomal protein S34, mitochondrial OS=Mus musculus GN=Mrps3	0.773	0.722	>sp|Q9D8Y0|EFHD2_MOUSE EF-hand domain-containing protein D2 OS=Mus musculus G	-0.500	0.455
>sp|Q8VCM4|LIPT_MOUSE Lipoyltransferase 1, mitochondrial OS=Mus musculus GN=Lipt1 PE=2	0.774	0.725	>sp|P12815|PDCD6_MOUSE Programmed cell death protein 6 OS=Mus musculus GN=Pdcd	-0.469	0.464
>sp|Q9D6U8|F162A_MOUSE Protein FAM162A OS=Mus musculus GN=Fam162a PE=2 SV=1	0.778	0.727	>sp|P97347|RPTN_MOUSE Repetin OS=Mus musculus GN=Rptn PE=1 SV=1	-0.458	0.473
>sp|P99029|PRDX5_MOUSE Peroxiredoxin-5, mitochondrial OS=Mus musculus GN=Prdx5 PE=1 SV	0.783	0.730	>sp|Q9WVJ9|FBLN4_MOUSE EGF-containing fibulin-like extracellular matrix protein 2 OS	-0.449	0.482
>sp|Q791V5|MTCH2_MOUSE Mitochondrial carrier homolog 2 OS=Mus musculus GN=Mtch2 PE=1	0.786	0.732	>sp|Q06138|CAB39_MOUSE Calcium-binding protein 39 OS=Mus musculus GN=Cab39 PE	-0.437	0.491
>sp|Q9CQJ8|NDUB9_MOUSE NADH dehydrogenase [ubiquinone] 1 beta subcomplex subunit 9 OS=	0.795	0.735	>sp|Q9WTR5|CAD13_MOUSE Cadherin-13 OS=Mus musculus GN=Cdh13 PE=1 SV=2	-0.425	0.500
>sp|Q9CQ54|NDUC2_MOUSE NADH dehydrogenase [ubiquinone] 1 subunit C2 OS=Mus musculus	0.797	0.737	>sp|Q9JI91|ACTN2_MOUSE Alpha-actinin-2 OS=Mus musculus GN=Actn2 PE=1 SV=2	-0.396	0.509
>sp|Q68FD5|CLH1_MOUSE Clathrin heavy chain 1 OS=Mus musculus GN=Cltc PE=1 SV=3	0.801	0.740	>sp|Q61233|PLSL_MOUSE Plastin-2 OS=Mus musculus GN=Lcp1 PE=1 SV=4	-0.313	0.518
>sp|Q9CZW4|ACSL3_MOUSE Long-chain-fatty-acid--CoA ligase 3 OS=Mus musculus GN=Acsl3 P	0.806	0.742	>sp|Q8R3B1|PLCD1_MOUSE 1-phosphatidylinositol 4,5-bisphosphate phosphodiesterase de	-0.295	0.527
>sp|Q9CQ62|DECR_MOUSE 2,4-dienoyl-CoA reductase, mitochondrial OS=Mus musculus GN=Decr	0.823	0.744	>tr|A2RS43|A2RS43_MOUSE Protein Pcdh7 OS=Mus musculus GN=Pcdh7 PE=2 SV=1	-0.284	0.536
>sp|P18242|CATD_MOUSE Cathepsin D OS=Mus musculus GN=Ctsd PE=1 SV=1	0.824	0.747	>sp|Q8BLY1|SMOC1_MOUSE SPARC-related modular calcium-binding protein 1 OS=Mus	-0.263	0.545
>sp|Q9CXZ1|NDUS4_MOUSE NADH dehydrogenase [ubiquinone] iron-sulfur protein 4, mitochondr	0.853	0.749	>sp|P43025|TETN_MOUSE Tetranectin OS=Mus musculus GN=Clec3b PE=1 SV=2	-0.257	0.554
>sp|Q62425|NDUA4_MOUSE NADH dehydrogenase [ubiquinone] 1 alpha subcomplex subunit 4 OS=	0.855	0.752	>sp|Q8BP92|RCN2_MOUSE Reticulocalbin-2 OS=Mus musculus GN=Rcn2 PE=2 SV=1	-0.227	0.563
>sp|P47791|GSHR_MOUSE Glutathione reductase, mitochondrial OS=Mus musculus GN=Gsr PE=2 S	0.894	0.754	>sp|O88456|CPNS1_MOUSE Calpain small subunit 1 OS=Mus musculus GN=Capns1 PE=2	-0.194	0.572
>sp|Q9Z2Z6|MCAT_MOUSE Mitochondrial carnitine/acylcarnitine carrier protein OS=Mus musculus	0.902	0.757	>tr|A3KGU7|A3KGU7_MOUSE Protein Spna2 OS=Mus musculus GN=Spna2 PE=4 SV=1	-0.148	0.581
>sp|Q03265|ATPA_MOUSE ATP synthase subunit alpha, mitochondrial OS=Mus musculus GN=Atp5	0.909	0.759	>sp|O35639|ANXA3_MOUSE Annexin A3 OS=Mus musculus GN=Anxa3 PE=1 SV=4	-0.144	0.590
>sp|P63101|1433Z_MOUSE 14-3-3 protein zeta/delta OS=Mus musculus GN=Ywhaz PE=1 SV=1	0.912	0.762	>sp|Q61554|FBN1_MOUSE Fibrillin-1 OS=Mus musculus GN=Fbn1 PE=1 SV=1	-0.142	0.599
>sp|Q06890|CLUS_MOUSE Clusterin OS=Mus musculus GN=Clu PE=1 SV=1	0.943	0.764	>tr|A1BN54|A1BN54_MOUSE Alpha actinin 1a OS=Mus musculus GN=Actn1 PE=2 SV=1	-0.131	0.608
>sp|Q61171|PRDX2_MOUSE Peroxiredoxin-2 OS=Mus musculus GN=Prdx2 PE=1 SV=3	0.952	0.767	>sp|Q8R429|AT2A1_MOUSE Sarcoplasmic/endoplasmic reticulum calcium ATPase 1 OS=M	-0.054	0.617
>sp|P00405|COX2_MOUSE Cytochrome c oxidase subunit 2 OS=Mus musculus GN=Mtco2 PE=1 SV	0.970	0.769	>sp|P52430|PON1_MOUSE Serum paraoxonase/arylesterase 1 OS=Mus musculus GN=Pon1	-0.033	0.626
>sp|O88844|IDHC_MOUSE Isocitrate dehydrogenase [NADP] cytoplasmic OS=Mus musculus GN=Id	0.992	0.772	>sp|P52633|STAT6_MOUSE Signal transducer and transcription activator 6 OS=Mus muscu	0.004	0.635
>sp|Q9WVL0|MAAI_MOUSE Maleylacetoacetate isomerase OS=Mus musculus GN=Gstz1 PE=1 SV	1.000	0.774	>sp|P07356|ANXA2_MOUSE Annexin A2 OS=Mus musculus GN=Anxa2 PE=1 SV=2	0.027	0.644
>sp|Q9CYW4|HDHD3_MOUSE Haloacid dehalogenase-like hydrolase domain-containing protein 3 C	1.026	0.777	>tr|Q91UZ1|Q91UZ1_MOUSE Phospholipase C beta 4 OS=Mus musculus GN=Plcb4 PE=2	0.102	0.653
>sp|P42125|ECI1_MOUSE Enoyl-CoA delta isomerase 1, mitochondrial OS=Mus musculus GN=Eci1	1.030	0.779	>sp|P35441|TSP1_MOUSE Thrombospondin-1 OS=Mus musculus GN=Thbs1 PE=1 SV=1	0.104	0.662
>sp|P10605|CATB_MOUSE Cathepsin B OS=Mus musculus GN=Ctsb PE=1 SV=2	1.037	0.781	>sp|Q62165|DAG1_MOUSE Dystroglycan OS=Mus musculus GN=Dag1 PE=1 SV=4	0.131	0.671
>sp|P15532|NDKA_MOUSE Nucleoside diphosphate kinase A OS=Mus musculus GN=Nme1 PE=1 S	1.037	0.784	>sp|P97384|ANX11_MOUSE Annexin A11 OS=Mus musculus GN=Anxa11 PE=1 SV=2	0.139	0.680
>sp|P29758|OAT_MOUSE Ornithine aminotransferase, mitochondrial OS=Mus musculus GN=Oat PE	1.039	0.786	>sp|P63028|TCTP_MOUSE Translationally-controlled tumor protein OS=Mus musculus GN	0.162	0.689

>sp|Q8CI78|RMND1_MOUSE Required for meiotic nuclear division protein 1 homolog OS=Mus mus	1.047	0.789
>sp|Q9DCN2|NB5R3_MOUSE NADH-cytochrome b5 reductase 3 OS=Mus musculus GN=Cyb5r3 PE	1.047	0.791
>sp|Q8R404|QIL1_MOUSE Protein QIL1 OS=Mus musculus GN=Qil1 PE=2 SV=1	1.060	0.794
>sp|Q9QYA2|TOM40_MOUSE Mitochondrial import receptor subunit TOM40 homolog OS=Mus mu	1.067	0.796
>sp|Q8VCW8|ACSF2_MOUSE Acyl-CoA synthetase family member 2, mitochondrial OS=Mus musc	1.067	0.799
>sp|Q9CQC7|NDUB4_MOUSE NADH dehydrogenase [ubiquinone] 1 beta subcomplex subunit 4 OS=	1.083	0.801
>sp|P56135|ATPK_MOUSE ATP synthase subunit f, mitochondrial OS=Mus musculus GN=Atp5j2 PE	1.089	0.804
>sp|Q06185|ATP5I_MOUSE ATP synthase subunit e, mitochondrial OS=Mus musculus GN=Atp5i PE	1.098	0.806
>sp|P14152|MDHC_MOUSE Malate dehydrogenase, cytoplasmic OS=Mus musculus GN=Mdh1 PE=	1.100	0.809
>sp|Q01768|NDKB_MOUSE Nucleoside diphosphate kinase B OS=Mus musculus GN=Nme2 PE=1 S	1.117	0.811
>sp|Q9CXT8|MPPB_MOUSE Mitochondrial-processing peptidase subunit beta OS=Mus musculus GN	1.118	0.814
>sp|P16675|PPGB_MOUSE Lysosomal protective protein OS=Mus musculus GN=Ctsa PE=1 SV=1	1.125	0.816
>sp|P12787|COX5A_MOUSE Cytochrome c oxidase subunit 5A, mitochondrial OS=Mus musculus G	1.129	0.819
>sp|Q8K2B3|DHSA_MOUSE Succinate dehydrogenase [ubiquinone] flavoprotein subunit, mitochond	1.153	0.821
>sp|Q99LC3|NDUAA_MOUSE NADH dehydrogenase [ubiquinone] 1 alpha subcomplex subunit 10, m	1.161	0.823
>sp|Q9DCS3|MECR_MOUSE Trans-2-enoyl-CoA reductase, mitochondrial OS=Mus musculus GN=M	1.207	0.826
>sp|Q60715|P4HA1_MOUSE Prolyl 4-hydroxylase subunit alpha-1 OS=Mus musculus GN=P4ha1 PE	1.226	0.828
>sp|Q9DC69|NDUA9_MOUSE NADH dehydrogenase [ubiquinone] 1 alpha subcomplex subunit 9, m	1.266	0.831
>sp|Q9CR62|M2OM_MOUSE Mitochondrial 2-oxoglutarate/malate carrier protein OS=Mus musculus	1.298	0.833
>sp|Q9WTQ8|TIM23_MOUSE Mitochondrial import inner membrane translocase subunit Tim23 OS=	1.311	0.836
>sp|Q91YT0|NDUV1_MOUSE NADH dehydrogenase [ubiquinone] flavoprotein 1, mitochondrial OS	1.335	0.838
>sp|P19536|COX5B_MOUSE Cytochrome c oxidase subunit 5B, mitochondrial OS=Mus musculus GN	1.339	0.841
>sp|P54310|LIPS_MOUSE Hormone-sensitive lipase OS=Mus musculus GN=Lipe PE=1 SV=2	1.340	0.843
>sp|Q7TMF3|NDUAC_MOUSE NADH dehydrogenase [ubiquinone] 1 alpha subcomplex subunit 12 O	1.340	0.846
>sp|Q60575-3|KIF1B_MOUSE Isoform 3 of Kinesin-like protein KIF1B OS=Mus musculus GN=Kif1	1.353	0.848
>sp|P56392|CX7A1_MOUSE Cytochrome c oxidase subunit 7A1, mitochondrial OS=Mus musculus C	1.376	0.851
>sp|Q60931|VDAC3_MOUSE Voltage-dependent anion-selective channel protein 3 OS=Mus musculu	1.378	0.853
>sp|P17710|HXK1_MOUSE Hexokinase-1 OS=Mus musculus GN=Hk1 PE=1 SV=3	1.392	0.856
>sp|P18572|BASI_MOUSE Basigin OS=Mus musculus GN=Bsg PE=1 SV=2	1.419	0.858
>sp|Q9DCJ5|NDUA8_MOUSE NADH dehydrogenase [ubiquinone] 1 alpha subcomplex subunit 8 OS	1.436	0.860
>sp|Q925I1|ATAD3_MOUSE ATPase family AAA domain-containing protein 3 OS=Mus musculus G	1.444	0.863
>sp|P00397|COX1_MOUSE Cytochrome c oxidase subunit 1 OS=Mus musculus GN=Mtco1 PE=3 SV	1.446	0.865
>sp|Q99KK9|SYHM_MOUSE Probable histidine--tRNA ligase, mitochondrial OS=Mus musculus GN	1.463	0.868
>sp|Q9CR68|UCRI_MOUSE Cytochrome b-c1 complex subunit Rieske, mitochondrial OS=Mus musc	1.464	0.870
>sp|P99028|QCR6_MOUSE Cytochrome b-c1 complex subunit 6, mitochondrial OS=Mus musculus G	1.523	0.873
>sp|A6H611|MIPEP_MOUSE Mitochondrial intermediate peptidase OS=Mus musculus GN=Mipep P	1.525	0.875
>sp|Q9Z110|P5CS_MOUSE Delta-1-pyrroline-5-carboxylate synthase OS=Mus musculus GN=Aldh18	1.525	0.878
>sp|P31938|MP2K1_MOUSE Dual specificity mitogen-activated protein kinase kinase 1 OS=Mus mus	1.539	0.880
>sp|Q9CPQ3|TOM22_MOUSE Mitochondrial import receptor subunit TOM22 homolog OS=Mus mus	1.539	0.883
>sp|Q8BH59|CMC1_MOUSE Calcium-binding mitochondrial carrier protein Aralar1 OS=Mus muscu	1.565	0.885
>sp|Q62167|DDX3X_MOUSE ATP-dependent RNA helicase DDX3X OS=Mus musculus GN=Ddx3x	1.592	0.888
>sp|Q99L04|DHRS1_MOUSE Dehydrogenase/reductase SDR family member 1 OS=Mus musculus G	1.620	0.890
>sp|P31786|ACBP_MOUSE Acyl-CoA-binding protein OS=Mus musculus GN=Dbi PE=1 SV=2	1.621	0.893
>sp|Q91V61|SFXN3_MOUSE Sideroflexin-3 OS=Mus musculus GN=Sfxn3 PE=1 SV=1	1.633	0.895
>sp|Q9CPP6|NDUA5_MOUSE NADH dehydrogenase [ubiquinone] 1 alpha subcomplex subunit 5 OS	1.637	0.898
>sp|Q64442|DHSO_MOUSE Sorbitol dehydrogenase OS=Mus musculus GN=Sord PE=1 SV=3	1.643	0.900
>sp|Q8BGC4|ZADH2_MOUSE Zinc-binding alcohol dehydrogenase domain-containing protein 2 OS=	1.657	0.902
>sp|Q8BGH2|SAM50_MOUSE Sorting and assembly machinery component 50 homolog OS=Mus mu	1.672	0.905
>sp|Q9CPQ1|COX6C_MOUSE Cytochrome c oxidase subunit 6C OS=Mus musculus GN=Cox6c PE=	1.696	0.907
>tr|Q91WX5|Q91WX5_MOUSE Bak1 protein OS=Mus musculus GN=Bak1 PE=2 SV=1	1.719	0.910
>tr|Q8R5L1|Q8R5L1_MOUSE Complement component 1 Q subcomponent-binding protein, mitochon	1.728	0.912
>sp|P54822|PUR8_MOUSE Adenylosuccinate lyase OS=Mus musculus GN=Adsl PE=2 SV=2	1.752	0.915
>sp|Q9CZ13|QCR1_MOUSE Cytochrome b-c1 complex subunit 1, mitochondrial OS=Mus musculus G	1.774	0.917

>sp|Q8BH59|CMC1_MOUSE Calcium-binding mitochondrial carrier protein Aralar1 OS=M	0.184	0.698
>sp|Q91ZX7|LRP1_MOUSE Prolow-density lipoprotein receptor-related protein 1 OS=Mus	0.228	0.707
>tr|Q6XLQ8|Q6XLQ8_MOUSE Calumenin OS=Mus musculus GN=Calu PE=2 SV=1	0.253	0.716
>sp|O70423|AOC3_MOUSE Membrane primary amine oxidase OS=Mus musculus GN=Aoc	0.258	0.725
>sp|O35350|CAN1_MOUSE Calpain-1 catalytic subunit OS=Mus musculus GN=Capn1 PE=	0.289	0.734
>sp|P08207|S10AA_MOUSE Protein S100-A10 OS=Mus musculus GN=S100a10 PE=2 SV=	0.345	0.743
>sp|Q9WVK4|EHD1_MOUSE EH domain-containing protein 1 OS=Mus musculus GN=Ehd	0.413	0.752
>sp|P61022|CHP1_MOUSE Calcineurin B homologous protein 1 OS=Mus musculus GN=Ch	0.478	0.761
>sp|P14824|ANXA6_MOUSE Annexin A6 OS=Mus musculus GN=Anxa6 PE=1 SV=3	0.481	0.770
>sp|O70258|SGCE_MOUSE Epsilon-sarcoglycan OS=Mus musculus GN=Sgce PE=2 SV=2	0.551	0.779
>sp|P14211|CALR_MOUSE Calreticulin OS=Mus musculus GN=Calr PE=1 SV=1	0.603	0.788
>sp|Q8BH97|RCN3_MOUSE Reticulocalbin-3 OS=Mus musculus GN=Rcn3 PE=2 SV=1	0.607	0.797
>sp|P10493|NID1_MOUSE Nidogen-1 OS=Mus musculus GN=Nid1 PE=1 SV=2	0.631	0.806
>sp|Q99MQ4|ASPN_MOUSE Asporin OS=Mus musculus GN=Aspn PE=1 SV=1	0.657	0.815
>sp|Q61576|FKB10_MOUSE Peptidyl-prolyl cis-trans isomerase FKBP10 OS=Mus musculu	0.701	0.824
>sp|Q9QXY6|EHD3_MOUSE EH domain-containing protein 3 OS=Mus musculus GN=Ehd	0.731	0.833
>sp|P62748|HPCL1_MOUSE Hippocalcin-like protein 1 OS=Mus musculus GN=Hpcal1 PE=	0.833	0.842
>sp|P50543|S10AB_MOUSE Protein S100-A11 OS=Mus musculus GN=S100a11 PE=2 SV=	0.870	0.851
>sp|P47713|PA24A_MOUSE Cytosolic phospholipase A2 OS=Mus musculus GN=Pla2g4a P	0.886	0.860
>sp|Q9Z247|FKBP9_MOUSE Peptidyl-prolyl cis-trans isomerase FKBP9 OS=Mus musculus	0.982	0.869
>sp|P42225|STAT1_MOUSE Signal transducer and activator of transcription 1 OS=Mus mus	0.987	0.878
>sp|Q02819|NUCB1_MOUSE Nucleobindin-1 OS=Mus musculus GN=Nucb1 PE=1 SV=2	1.003	0.887
>sp|P82350|SGCA_MOUSE Alpha-sarcoglycan OS=Mus musculus GN=Sgca PE=1 SV=1	1.013	0.896
>sp|P16546|SPTN1_MOUSE Spectrin alpha chain, non-erythrocytic 1 OS=Mus musculus GN	1.067	0.905
>sp|Q8BH64|EHD2_MOUSE EH domain-containing protein 2 OS=Mus musculus GN=Ehd2	1.143	0.914
>sp|Q3UYK3|TBCD9_MOUSE TBC1 domain family member 9 OS=Mus musculus GN=Tb	1.231	0.923
>sp|Q99M71|EPDR1_MOUSE Mammalian ependymin-related protein 1 OS=Mus musculus	1.259	0.932
>sp|P35564|CALX_MOUSE Calnexin OS=Mus musculus GN=Canx PE=1 SV=1	1.466	0.941
>sp|Q64521|GPDM_MOUSE Glycerol-3-phosphate dehydrogenase, mitochondrial OS=Mus	1.487	0.950
>sp|P07214|SPRC_MOUSE SPARC OS=Mus musculus GN=Sparc PE=1 SV=1	1.547	0.959
>sp|P84075|HPCA_MOUSE Neuron-specific calcium-binding protein hippocalcin OS=Mus m	1.554	0.968
>sp|P97429|ANXA4_MOUSE Annexin A4 OS=Mus musculus GN=Anxa4 PE=2 SV=4	1.588	0.977
>sp|P48036|ANXA5_MOUSE Annexin A5 OS=Mus musculus GN=Anxa5 PE=1 SV=1	1.906	0.986
>sp|Q9Z184|PADI3_MOUSE Protein-arginine deiminase type-3 OS=Mus musculus GN=Pad	3.369	0.995

Lipid metabolic process GO:0006629

Protein identification	Zq	rank/N
>sp|P33622|APOC3_MOUSE Apolipoprotein C-III OS=Mus musculus GN=Apoc3 PE=2 SV	-2.513	0.006
>sp|Q00623|APOA1_MOUSE Apolipoprotein A-I OS=Mus musculus GN=Apoa1 PE=1 SV=	-2.316	0.019
>sp|P01027|CO3_MOUSE Complement C3 OS=Mus musculus GN=C3 PE=1 SV=3	-1.640	0.031
>sp|Q9Z2V4|PCKGC_MOUSE Phosphoenolpyruvate carboxykinase, cytosolic [GTP] OS=M	-1.170	0.044
>tr|O35452|O35452_MOUSE Protein Tnxb OS=Mus musculus GN=Tnxb PE=2 SV=1	-0.794	0.056
>sp|P08226|APOE_MOUSE Apolipoprotein E OS=Mus musculus GN=Apoe PE=1 SV=2	-0.785	0.069
>sp|Q62264|THRSP_MOUSE Thyroid hormone-inducible hepatic protein OS=Mus musculu	-0.749	0.081
>sp|E9Q414|APOB_MOUSE Apolipoprotein B-100 OS=Mus musculus GN=Apob PE=1 SV	-0.651	0.094
>sp|O35074|PTGIS_MOUSE Prostacyclin synthase OS=Mus musculus GN=Ptgis PE=2 SV=	-0.603	0.106
>sp|P19096|FAS_MOUSE Fatty acid synthase OS=Mus musculus GN=Fasn PE=1 SV=2	-0.597	0.119
>sp|Q921H8|THIKA_MOUSE 3-ketoacyl-CoA thiolase A, peroxisomal OS=Mus musculus G	-0.566	0.131
>sp|Q9DCN2|NB5R3_MOUSE NADH-cytochrome b5 reductase 3 OS=Mus musculus GN=C	-0.564	0.144
>sp|O70503|DHB12_MOUSE Estradiol 17-beta-dehydrogenase 12 OS=Mus musculus GN=H	-0.501	0.156
>sp|Q8VCW8|ACSF2_MOUSE Acyl-CoA synthetase family member 2, mitochondrial OS=M	-0.423	0.169
>sp|P22437|PGH1_MOUSE Prostaglandin G/H synthase 1 OS=Mus musculus GN=Ptgs1 PE	-0.418	0.181
>sp|Q9R0Q7|TEBP_MOUSE Prostaglandin E synthase 3 OS=Mus musculus GN=Ptges3 PE=	-0.337	0.194

>sp|Q9ERS2|NDUAD_MOUSE NADH dehydrogenase [ubiquinone] 1 alpha subcomplex subunit 13 O	1.778	0.920
>sp|P67778|PHB_MOUSE Prohibitin OS=Mus musculus GN=Phb PE=1 SV=1	1.791	0.922
>sp|Q9CQ75|NDUA2_MOUSE NADH dehydrogenase [ubiquinone] 1 alpha subcomplex subunit 2 OS	1.951	0.925
>sp|Q922Q1|MOSC2_MOUSE MOSC domain-containing protein 2, mitochondrial OS=Mus musculus	1.978	0.927
>sp|Q9R0X4|ACOT9_MOUSE Acyl-coenzyme A thioesterase 9, mitochondrial OS=Mus musculus GI	1.999	0.930
>sp|P48962|ADT1_MOUSE ADP/ATP translocase 1 OS=Mus musculus GN=Slc25a4 PE=1 SV=4	2.032	0.932
>sp|Q9D6J6|NDUV2_MOUSE NADH dehydrogenase [ubiquinone] flavoprotein 2, mitochondrial OS=	2.033	0.935
>sp|P56391|CX6B1_MOUSE Cytochrome c oxidase subunit 6B1 OS=Mus musculus GN=Cox6b1 PE=	2.037	0.937
>sp|Q9CQA3|DHSB_MOUSE Succinate dehydrogenase [ubiquinone] iron-sulfur subunit, mitochondri	2.051	0.940
>sp|P30416|FKBP4_MOUSE Peptidyl-prolyl cis-trans isomerase FKBP4 OS=Mus musculus GN=Fkb	2.073	0.942
>sp|Q8CAQ8|IMMT_MOUSE Mitochondrial inner membrane protein OS=Mus musculus GN=Immt P	2.103	0.944
>sp|P13707|GPDA_MOUSE Glycerol-3-phosphate dehydrogenase [NAD(+)], cytoplasmic OS=Mus m	2.150	0.947
>sp|Q9DB77|QCR2_MOUSE Cytochrome b-c1 complex subunit 2, mitochondrial OS=Mus musculus	2.186	0.949
>sp|O35129|PHB2_MOUSE Prohibitin-2 OS=Mus musculus GN=Phb2 PE=1 SV=1	2.200	0.952
>sp|P51881|ADT2_MOUSE ADP/ATP translocase 2 OS=Mus musculus GN=Slc25a5 PE=1 SV=3	2.206	0.954
>sp|Q9CQ69|QCR8_MOUSE Cytochrome b-c1 complex subunit 8 OS=Mus musculus GN=Uqcrq PE=	2.250	0.957
>sp|Q8K3J1|NDUS8_MOUSE NADH dehydrogenase [ubiquinone] iron-sulfur protein 8, mitochondria	2.259	0.959
>sp|P03888|NU1M_MOUSE NADH-ubiquinone oxidoreductase chain 1 OS=Mus musculus GN=Mtn	2.400	0.962
>sp|Q9DCS9|NDUBA_MOUSE NADH dehydrogenase [ubiquinone] 1 beta subcomplex subunit 10 O	2.468	0.964
>sp|Q9DB20|ATPO_MOUSE ATP synthase subunit O, mitochondrial OS=Mus musculus GN=Atp5o	2.566	0.967
>sp|Q9R269|PEPL_MOUSE Periplakin OS=Mus musculus GN=Ppl PE=1 SV=1	2.594	0.969
>sp|P20108|PRDX3_MOUSE Thioredoxin-dependent peroxide reductase, mitochondrial OS=Mus mus	2.757	0.972
>sp|O08807|PRDX4_MOUSE Peroxiredoxin-4 OS=Mus musculus GN=Prdx4 PE=1 SV=1	2.789	0.974
>sp|P19783|COX41_MOUSE Cytochrome c oxidase subunit 4 isoform 1, mitochondrial OS=Mus mus	3.163	0.977
>sp|Q8R1I1|QCR9_MOUSE Cytochrome b-c1 complex subunit 9 OS=Mus musculus GN=Uqcr10 PE=	3.227	0.979
>sp|Q9CPQ8|ATP5L_MOUSE ATP synthase subunit g, mitochondrial OS=Mus musculus GN=Atp5l	3.235	0.981
>sp|Q91W97|HKDC1_MOUSE Putative hexokinase HKDC1 OS=Mus musculus GN=Hkdc1 PE=2 SV	3.246	0.984
>sp|Q3UIU2|NDUB6_MOUSE NADH dehydrogenase [ubiquinone] 1 beta subcomplex subunit 6 OS=	3.314	0.986
>sp|Q9D0M3|CY1_MOUSE Cytochrome c1, heme protein, mitochondrial OS=Mus musculus GN=Cy	3.567	0.989
>sp|Q9CQQ7|AT5F1_MOUSE ATP synthase subunit b, mitochondrial OS=Mus musculus GN=Atp5f1	3.947	0.991
>sp|Q99LY9|NDUS5_MOUSE NADH dehydrogenase [ubiquinone] iron-sulfur protein 5 OS=Mus mu	4.182	0.994
>sp|P12242|UCP1_MOUSE Mitochondrial brown fat uncoupling protein 1 OS=Mus musculus GN=Uc	4.312	0.996
>sp|Q8BQU3|ACN9_MOUSE Protein ACN9 homolog, mitochondrial OS=Mus musculus GN=Acn9 P	8.109	0.999

Extracellular matrix GO:0031012

Protein identification	Zq	rank/N
>tr|Q05504|Q05504_MOUSE Collagen alpha 3 chain type VI (Fragment) OS=Mus musculus GN=Col	-4.119	0.006
>sp|Q9Z1T2|TSP4_MOUSE Thrombospondin-4 OS=Mus musculus GN=Thbs4 PE=1 SV=1	-2.244	0.017
>sp|Q60847|COCA1_MOUSE Collagen alpha-1(XII) chain OS=Mus musculus GN=Col12a1 PE=2 SV	-2.195	0.028
>sp|O09164|SODE_MOUSE Extracellular superoxide dismutase [Cu-Zn] OS=Mus musculus GN=Sod	-1.698	0.039
>sp|P58459|ATS10_MOUSE A disintegrin and metalloproteinase with thrombospondin motifs 10 OS=	-1.626	0.051
>sp|P12246|SAMP_MOUSE Serum amyloid P-component OS=Mus musculus GN=Apcs PE=1 SV=2	-1.551	0.062
>sp|Q99MQ4|ASPN_MOUSE Asporin OS=Mus musculus GN=Aspn PE=1 SV=1	-1.312	0.073
>sp|Q61543|GSLG1_MOUSE Golgi apparatus protein 1 OS=Mus musculus GN=Glg1 PE=1 SV=1	-1.257	0.084
>tr|F8VQJ3|F8VQJ3_MOUSE Laminin subunit gamma-1 OS=Mus musculus GN=Lamc1 PE=4 SV=1	-1.144	0.096
>sp|Q9JHI0|MMP19_MOUSE Matrix metalloproteinase-19 OS=Mus musculus GN=Mmp19 PE=2 SV	-1.139	0.107
>tr|Q8BP04|Q8BP04_MOUSE Putative uncharacterized protein OS=Mus musculus GN=Loxl1 PE=2 S	-1.120	0.118
>sp|P28481|CO2A1_MOUSE Collagen alpha-1(II) chain OS=Mus musculus GN=Col2a1 PE=1 SV=2	-0.986	0.129
>sp|P10493|NID1_MOUSE Nidogen-1 OS=Mus musculus GN=Nid1 PE=1 SV=2	-0.927	0.140
>sp|Q9DCT8|CRIP2_MOUSE Cysteine-rich protein 2 OS=Mus musculus GN=Crip2 PE=1 SV=1	-0.801	0.152
>tr|Q3UH17|Q3UH17_MOUSE Putative uncharacterized protein OS=Mus musculus GN=Fn1 PE=2 S	-0.686	0.163
>tr|Q9JLI2|Q9JLI2_MOUSE Collagen type V alpha 3 chain OS=Mus musculus GN=Col5a3 PE=2 SV	-0.676	0.174
>sp|Q07235|GDN_MOUSE Glia-derived nexin OS=Mus musculus GN=Serpine2 PE=2 SV=2	-0.655	0.185

>sp|Q8R3B1|PLCD1_MOUSE 1-phosphatidylinositol 4,5-bisphosphate phosphodiesterase de	-0.295	0.206
>sp|Q9JHU9|INO1_MOUSE Inositol-3-phosphate synthase 1 OS=Mus musculus GN=Isyna1	-0.290	0.219
>sp|P51174|ACADL_MOUSE Long-chain specific acyl-CoA dehydrogenase, mitochondrial	-0.240	0.231
>sp|Q9DBL1|ACDSB_MOUSE Short/branched chain specific acyl-CoA dehydrogenase, mit	-0.225	0.244
>sp|P50427|STS_MOUSE Steryl-sulfatase OS=Mus musculus GN=Sts PE=2 SV=1	-0.197	0.256
>sp|Q9DCS3|MECR_MOUSE Trans-2-enoyl-CoA reductase, mitochondrial OS=Mus muscu	-0.133	0.269
>sp|Q9D0S9|HINT2_MOUSE Histidine triad nucleotide-binding protein 2, mitochondrial OS	-0.104	0.281
>sp|Q9CR21|ACPM_MOUSE Acyl carrier protein, mitochondrial OS=Mus musculus GN=N	-0.096	0.294
>sp|Q99L43|CDS2_MOUSE Phosphatidate cytidylyltransferase 2 OS=Mus musculus GN=C	-0.078	0.306
>sp|P52430|PON1_MOUSE Serum paraoxonase/arylesterase 1 OS=Mus musculus GN=Pon1	-0.033	0.319
>sp|Q91V92|ACLY_MOUSE ATP-citrate synthase OS=Mus musculus GN=Acly PE=1 SV=	0.029	0.331
>sp|Q9R0H0|ACOX1_MOUSE Peroxisomal acyl-coenzyme A oxidase 1 OS=Mus musculus	0.051	0.344
>sp|P11352|GPX1_MOUSE Glutathione peroxidase 1 OS=Mus musculus GN=Gpx1 PE=1 S	0.068	0.356
>sp|Q5SWU9|ACACA_MOUSE Acetyl-CoA carboxylase 1 OS=Mus musculus GN=Acaca I	0.081	0.369
>tr|Q91UZ1|Q91UZ1_MOUSE Phospholipase C beta 4 OS=Mus musculus GN=Plcb4 PE=2	0.102	0.381
>sp|Q5EG47|AAPK1_MOUSE 5'-AMP-activated protein kinase catalytic subunit alpha-1 OS	0.144	0.394
>sp|Q920E5|FPPS_MOUSE Farnesyl pyrophosphate synthase OS=Mus musculus GN=Fdps	0.263	0.406
>sp|Q9WV54|ASAH1_MOUSE Acid ceramidase OS=Mus musculus GN=Asah1 PE=1 SV=	0.310	0.419
>sp|O35459|ECH1_MOUSE Delta(3,5)-Delta(2,4)-dienoyl-CoA isomerase, mitochondrial O	0.326	0.431
>sp|P45952|ACADM_MOUSE Medium-chain specific acyl-CoA dehydrogenase, mitochond	0.357	0.444
>sp|O54950|AAKG1_MOUSE 5'-AMP-activated protein kinase subunit gamma-1 OS=Mus r	0.364	0.456
>sp|P34914|HYES_MOUSE Bifunctional epoxide hydrolase 2 OS=Mus musculus GN=Ephx	0.367	0.469
>sp|P52825|CPT2_MOUSE Carnitine O-palmitoyltransferase 2, mitochondrial OS=Mus mus	0.497	0.481
>sp|P41216|ACSL1_MOUSE Long-chain-fatty-acid--CoA ligase 1 OS=Mus musculus GN=A	0.561	0.494
>sp|Q61425|HCDH_MOUSE Hydroxyacyl-coenzyme A dehydrogenase, mitochondrial OS=I	0.615	0.506
>sp|P50544|ACADV_MOUSE Very long-chain specific acyl-CoA dehydrogenase, mitochon	0.622	0.519
>sp|P51660|DHB4_MOUSE Peroxisomal multifunctional enzyme type 2 OS=Mus musculus	0.644	0.531
>sp|Q9CQ62|DECR_MOUSE 2,4-dienoyl-CoA reductase, mitochondrial OS=Mus musculus	0.664	0.544
>sp|P97742|CPT1A_MOUSE Carnitine O-palmitoyltransferase 1, liver isoform OS=Mus mu	0.683	0.556
>sp|Q8BH95|ECHM_MOUSE Enoyl-CoA hydratase, mitochondrial OS=Mus musculus GN=	0.686	0.569
>sp|Q05920|PYC_MOUSE Pyruvate carboxylase, mitochondrial OS=Mus musculus GN=Pc	0.749	0.581
>sp|P58044|IDI1_MOUSE Isopentenyl-diphosphate Delta-isomerase 1 OS=Mus musculus G	0.776	0.594
>sp|P47934|CACP_MOUSE Carnitine O-acetyltransferase OS=Mus musculus GN=Crat PE=	0.812	0.606
>sp|Q99JY0|ECHB_MOUSE Trifunctional enzyme subunit beta, mitochondrial OS=Mus mu	0.815	0.619
>sp|Q8BWT1|THIM_MOUSE 3-ketoacyl-CoA thiolase, mitochondrial OS=Mus musculus G	0.817	0.631
>sp|P54310|LIPS_MOUSE Hormone-sensitive lipase OS=Mus musculus GN=Lipe PE=1 SV	0.820	0.644
>sp|Q91VE0|S27A4_MOUSE Long-chain fatty acid transport protein 4 OS=Mus musculus C	0.830	0.656
>sp|P56480|ATPB_MOUSE ATP synthase subunit beta, mitochondrial OS=Mus musculus G	0.835	0.669
>sp|P42125|ECI1_MOUSE Enoyl-CoA delta isomerase 1, mitochondrial OS=Mus musculus	0.854	0.681
>sp|P35235|PTN11_MOUSE Tyrosine-protein phosphatase non-receptor type 11 OS=Mus m	0.881	0.694
>sp|P47713|PA24A_MOUSE Cytosolic phospholipase A2 OS=Mus musculus GN=Pla2g4a I	0.886	0.706
>sp|Q8BMP6|GCP60_MOUSE Golgi resident protein GCP60 OS=Mus musculus GN=Acbd3	0.914	0.719
>sp|Q9D2R0|AACS_MOUSE Acetoacetyl-CoA synthetase OS=Mus musculus GN=Aacs PE	0.916	0.731
>sp|Q03265|ATPA_MOUSE ATP synthase subunit alpha, mitochondrial OS=Mus musculus	0.917	0.744
>sp|Q8VDP6|CDIPT_MOUSE CDP-diacylglycerol--inositol 3-phosphatidyltransferase OS=M	0.943	0.756
>sp|O08709|PRDX6_MOUSE Peroxiredoxin-6 OS=Mus musculus GN=Prdx6 PE=1 SV=3	0.953	0.769
>sp|Q05816|FABP5_MOUSE Fatty acid-binding protein, epidermal OS=Mus musculus GN=	1.013	0.781
>sp|O88307|SORL_MOUSE Sortilin-related receptor OS=Mus musculus GN=Sorl1 PE=2 SV	1.024	0.794
>sp|Q61206|PA1B2_MOUSE Platelet-activating factor acetylhydrolase IB subunit beta OS=M	1.031	0.806
>sp|Q3TCN2|PLBL2_MOUSE Putative phospholipase B-like 2 OS=Mus musculus GN=Plbd	1.049	0.819
>sp|Q8VCT4|CES1D_MOUSE Carboxylesterase 1D OS=Mus musculus GN=Ces1d PE=1 SV	1.110	0.831
>sp|P50171|DHB8_MOUSE Estradiol 17-beta-dehydrogenase 8 OS=Mus musculus GN=Hsd	1.118	0.844
>sp|P52840|ST1A1_MOUSE Sulfotransferase 1A1 OS=Mus musculus GN=Sult1a1 PE=2 SV	1.209	0.856

>sp|Q61398|PCOC1_MOUSE Procollagen C-endopeptidase enhancer 1 OS=Mus musculus GN=Pcolc	-0.618	0.197	>sp|Q8VDJ3|VIGLN_MOUSE Vigilin OS=Mus musculus GN=Hdlbp PE=1 SV=1	1.223	0.869
>sp|P07901|HS90A_MOUSE Heat shock protein HSP 90-alpha OS=Mus musculus GN=Hsp90aa1 PE	-0.586	0.208	>sp|O35678|MGLL_MOUSE Monoglyceride lipase OS=Mus musculus GN=Mgll PE=1 SV=	1.317	0.881
>sp|Q9D2L5|CPXM2_MOUSE Inactive carboxypeptidase-like protein X2 OS=Mus musculus GN=Cp	-0.562	0.219	>sp|Q8JZK9|HMCS1_MOUSE Hydroxymethylglutaryl-CoA synthase, cytoplasmic OS=Mus	1.331	0.894
>sp|Q8CIZ8|VWF_MOUSE von Willebrand factor OS=Mus musculus GN=Vwf PE=1 SV=2	-0.545	0.230	>sp|Q9DBL9|ABHD5_MOUSE 1-acylglycerol-3-phosphate O-acyltransferase ABHD5 OS=	1.404	0.906
>tr|Q3TAF9|Q3TAF9_MOUSE Putative uncharacterized protein OS=Mus musculus GN=Bgn PE=2 S	-0.500	0.242	>sp|Q9CY27|TECR_MOUSE Very-long-chain enoyl-CoA reductase OS=Mus musculus GN=	1.541	0.919
>sp|Q99K41|EMIL1_MOUSE EMILIN-1 OS=Mus musculus GN=Emilin1 PE=1 SV=1	-0.439	0.253	>sp|Q9EQ06|DHB11_MOUSE Estradiol 17-beta-dehydrogenase 11 OS=Mus musculus GN=	1.835	0.931
>sp|Q640N1|AEBP1_MOUSE Adipocyte enhancer-binding protein 1 OS=Mus musculus GN=Aebp1 I	-0.423	0.264	>sp|Q8BMS1|ECHA_MOUSE Trifunctional enzyme subunit alpha, mitochondrial OS=Mus	1.908	0.944
>sp|P11087|CO1A1_MOUSE Collagen alpha-1(I) chain OS=Mus musculus GN=Col1a1 PE=1 SV=4	-0.333	0.275	>sp|P51910|APOD_MOUSE Apolipoprotein D OS=Mus musculus GN=Apod PE=2 SV=1	2.042	0.956
>sp|Q00780|CO8A1_MOUSE Collagen alpha-1(VIII) chain OS=Mus musculus GN=Col8a1 PE=1 SV	-0.328	0.287	>sp|P50172|DHI1_MOUSE Corticosteroid 11-beta-dehydrogenase isozyme 1 OS=Mus musc	2.437	0.969
>tr|Q99K31|Q99K31_MOUSE Col6a3 protein (Fragment) OS=Mus musculus GN=Col6a3 PE=2 SV=	-0.324	0.298	>sp|Q07417|ACADS_MOUSE Short-chain specific acyl-CoA dehydrogenase, mitochondrial	2.528	0.981
>sp|P08121|CO3A1_MOUSE Collagen alpha-1(III) chain OS=Mus musculus GN=Col3a1 PE=2 SV=4	-0.263	0.309	>sp|Q8CGN5|PLIN1_MOUSE Perilipin-1 OS=Mus musculus GN=Plin1 PE=1 SV=2	3.179	0.994
>sp|Q80YX1|TENA_MOUSE Tenascin OS=Mus musculus GN=Tnc PE=1 SV=1	-0.156	0.320			
>sp|O88322|NID2_MOUSE Nidogen-2 OS=Mus musculus GN=Nid2 PE=1 SV=2	-0.137	0.331	**Mitochondrion GO:0005739**		
>sp|P28653|PGS1_MOUSE Biglycan OS=Mus musculus GN=Bgn PE=2 SV=1	-0.137	0.343	Protein identification	Zq	rank/N
>sp|Q61554|FBN1_MOUSE Fibrillin-1 OS=Mus musculus GN=Fbn1 PE=1 SV=1	-0.136	0.354	>sp|O55028|BCKD_MOUSE [3-methyl-2-oxobutanoate dehydrogenase [lipoamide]] kinase,	-5.942	0.001
>sp|Q3UQ28|PXDN_MOUSE Peroxidasin homolog OS=Mus musculus GN=Pxdn PE=2 SV=2	-0.134	0.365	>sp|Q8K1Z0|COQ9_MOUSE Ubiquinone biosynthesis protein COQ9, mitochondrial OS=M	-3.581	0.004
>sp|Q8CD91|SMOC2_MOUSE SPARC-related modular calcium-binding protein 2 OS=Mus musculus	-0.074	0.376	>sp|Q6ZWQ0|SYNE2_MOUSE Nesprin-2 OS=Mus musculus GN=Syne2 PE=1 SV=2	-3.369	0.006
>sp|Q8CG19|LTBP1_MOUSE Latent-transforming growth factor beta-binding protein 1 OS=Mus mus	-0.012	0.388	>sp|Q06890|CLUS_MOUSE Clusterin OS=Mus musculus GN=Clu PE=1 SV=1	-3.265	0.009
>sp|Q01149|CO1A2_MOUSE Collagen alpha-2(I) chain OS=Mus musculus GN=Col1a2 PE=2 SV=2	0.035	0.399	>sp|Q8BGC4|ZADH2_MOUSE Zinc-binding alcohol dehydrogenase domain-containing pro	-2.928	0.011
>tr|O88493|O88493_MOUSE Type VI collagen alpha 3 subunit OS=Mus musculus GN=Col6a3 PE=2	0.036	0.410	>sp|O09164|SODE_MOUSE Extracellular superoxide dismutase [Cu-Zn] OS=Mus musculus	-2.564	0.014
>sp|P97873|LOXL1_MOUSE Lysyl oxidase homolog 1 OS=Mus musculus GN=Loxl1 PE=2 SV=3	0.046	0.421	>sp|Q920A7|AFG31_MOUSE AFG3-like protein 1 OS=Mus musculus GN=Afg3l1 PE=2 SV	-2.471	0.016
>tr|Q9Z0I9|Q9Z0I9_MOUSE Collagen alpha3(VI) (Fragment) OS=Mus musculus GN=Col6a3 PE=2 S	0.065	0.433	>sp|Q8BP47|SYNC_MOUSE Asparagine--tRNA ligase, cytoplasmic OS=Mus musculus GN	-2.422	0.019
>sp|P08228|SODC_MOUSE Superoxide dismutase [Cu-Zn] OS=Mus musculus GN=Sod1 PE=1 SV=	0.115	0.444	>sp|Q60931|VDAC3_MOUSE Voltage-dependent anion-selective channel protein 3 OS=Mu	-1.962	0.021
>sp|Q8R2G6|CCD80_MOUSE Coiled-coil domain-containing protein 80 OS=Mus musculus GN=Ccd	0.146	0.455	>tr|Q8R5L1|Q8R5L1_MOUSE Complement component 1 Q subcomponent-binding protein,	-1.881	0.024
>tr|Q3UZF9|Q3UZF9_MOUSE Putative uncharacterized protein (Fragment) OS=Mus musculus GN=I	0.187	0.466	>sp|Q91V61|SFXN3_MOUSE Sideroflexin-3 OS=Mus musculus GN=Sfxn3 PE=1 SV=1	-1.866	0.026
>sp|Q9QZZ6|DERM_MOUSE Dermatopontin OS=Mus musculus GN=Dpt PE=2 SV=1	0.210	0.478	>sp|Q61171|PRDX2_MOUSE Peroxiredoxin-2 OS=Mus musculus GN=Prdx2 PE=1 SV=3	-1.808	0.029
>sp|Q08879-2|FBLN1_MOUSE Isoform C of Fibulin-1 OS=Mus musculus GN=Fbln1	0.229	0.489	>sp|Q9Z2Y8|PROSC_MOUSE Proline synthase co-transcribed bacterial homolog protein OS	-1.636	0.031
>tr|B1B0C7|B1B0C7_MOUSE Basement membrane-specific heparan sulfate proteoglycan core protei	0.293	0.500	>sp|Q9DC29|ABCB6_MOUSE ATP-binding cassette sub-family B member 6, mitochondrial	-1.606	0.034
>sp|Q62005|ZP1_MOUSE Zona pellucida sperm-binding protein 1 OS=Mus musculus GN=Zp1 PE=1	0.294	0.511	>sp|Q9JM14|NT5C_MOUSE 5'(3')-deoxyribonucleotidase, cytosolic type OS=Mus musculus	-1.507	0.036
>sp|Q8C4U3|SFRP1_MOUSE Secreted frizzled-related protein 1 OS=Mus musculus GN=Sfrp1 PE=1	0.328	0.522	>sp|Q8CH40|NUDT6_MOUSE Nucleoside diphosphate-linked moiety X motif 6 OS=Mus m	-1.485	0.039
>tr|B7ZNH7|B7ZNH7_MOUSE Collagen alpha-1(XIV) chain OS=Mus musculus GN=Col14a1 PE=2	0.332	0.534	>sp|Q3THF9|CQ10B_MOUSE Coenzyme Q-binding protein COQ10 homolog B, mitochond	-1.473	0.041
>sp|P97298|PEDF_MOUSE Pigment epithelium-derived factor OS=Mus musculus GN=Serpinf1 PE=	0.339	0.545	>sp|Q8VCF0|MAVS_MOUSE Mitochondrial antiviral-signaling protein OS=Mus musculus	-1.433	0.044
>sp|P27090|TGFB2_MOUSE Transforming growth factor beta-2 OS=Mus musculus GN=Tgfb2 PE=1	0.361	0.556	>sp|O35658|C1QBP_MOUSE Complement component 1 Q subcomponent-binding protein,	-1.377	0.046
>tr|A2AQ53|A2AQ53_MOUSE Fibrillin 1 OS=Mus musculus GN=Fbn1 PE=4 SV=1	0.365	0.567	>tr|Q3U2G2|Q3U2G2_MOUSE Heat shock 70 kDa protein 4 OS=Mus musculus GN=Hspa4	-1.311	0.049
>sp|P28654|PGS2_MOUSE Decorin OS=Mus musculus GN=Dcn PE=2 SV=1	0.392	0.579	>sp|P13707|GPDA_MOUSE Glycerol-3-phosphate dehydrogenase [NAD(+)], cytoplasmic	-1.267	0.052
>sp|Q61001|LAMA5_MOUSE Laminin subunit alpha-5 OS=Mus musculus GN=Lama5 PE=1 SV=4	0.404	0.590	>tr|D3Z7C8|D3Z7C8_MOUSE Branched-chain-amino-acid aminotransferase OS=Mus musc	-1.244	0.054
>tr|Q3UHH3|Q3UHH3_MOUSE Putative uncharacterized protein OS=Mus musculus GN=Hspg2 PE=	0.445	0.601	>sp|P21981|TGM2_MOUSE Protein-glutamine gamma-glutamyltransferase 2 OS=Mus musc	-1.193	0.057
>sp|P82198|BGH3_MOUSE Transforming growth factor-beta-induced protein ig-h3 OS=Mus musculu	0.446	0.612	>sp|Q9DCS9|NDUBA_MOUSE NADH dehydrogenase [ubiquinone] 1 beta subcomplex sub	-1.158	0.059
>sp|P21844|CMA1_MOUSE Chymase OS=Mus musculus GN=Cma1 PE=1 SV=2	0.514	0.624	>sp|Q8BGB8|COQ4_MOUSE Ubiquinone biosynthesis protein COQ4 homolog, mitochondr	-1.137	0.062
>sp|Q62219|TGFI1_MOUSE Transforming growth factor beta-1-induced transcript 1 protein OS=Mus	0.529	0.635	>sp|O08756|HCD2_MOUSE 3-hydroxyacyl-CoA dehydrogenase type-2 OS=Mus musculus	-1.123	0.064
>sp|P50608|FMOD_MOUSE Fibromodulin OS=Mus musculus GN=Fmod PE=2 SV=1	0.643	0.646	>tr|B1AWZ3|B1AWZ3_MOUSE Novel protein (1700054F22Rik) OS=Mus musculus GN=N	-1.082	0.067
>sp|P33434|MMP2_MOUSE 72 kDa type IV collagenase OS=Mus musculus GN=Mmp2 PE=2 SV=1	0.653	0.657	>sp|Q99JR1|SFXN1_MOUSE Sideroflexin-1 OS=Mus musculus GN=Sfxn1 PE=1 SV=3	-1.071	0.069
>sp|Q62009-2|POSTN_MOUSE Isoform 2 of Periostin OS=Mus musculus GN=Postn	0.670	0.669	>sp|P56395|CYB5_MOUSE Cytochrome b5 OS=Mus musculus GN=Cyb5a PE=1 SV=2	-1.040	0.072
>sp|Q61292|LAMB2_MOUSE Laminin subunit beta-2 OS=Mus musculus GN=Lamb2 PE=2 SV=2	0.737	0.680	>sp|P23927|CRYAB_MOUSE Alpha-crystallin B chain OS=Mus musculus GN=Cryab PE=1	-1.032	0.074
>sp|P18242|CATD_MOUSE Cathepsin D OS=Mus musculus GN=Ctsd PE=1 SV=1	0.824	0.691	>sp|O70325|GPX41_MOUSE Phospholipid hydroperoxide glutathione peroxidase, mitochon	-1.030	0.077
>sp|P14211|CALR_MOUSE Calreticulin OS=Mus musculus GN=Calr PE=1 SV=1	0.890	0.702	>sp|Q9CZW5|TOM70_MOUSE Mitochondrial import receptor subunit TOM70 OS=Mus mu	-0.966	0.079
>sp|Q04857|CO6A1_MOUSE Collagen alpha-1(VI) chain OS=Mus musculus GN=Col6a1 PE=2 SV=	0.914	0.713	>sp|Q9WTP7|KAD3_MOUSE GTP:AMP phosphotransferase, mitochondrial OS=Mus musc	-0.947	0.082
>sp|Q06890|CLUS_MOUSE Clusterin OS=Mus musculus GN=Clu PE=1 SV=1	0.943	0.725	>sp|P56391|CX6B1_MOUSE Cytochrome c oxidase subunit 6B1 OS=Mus musculus GN=C	-0.940	0.084
>sp|Q02788|CO6A2_MOUSE Collagen alpha-2(VI) chain OS=Mus musculus GN=Col6a2 PE=2 SV=	1.038	0.736	>sp|O08807|PRDX4_MOUSE Peroxiredoxin-4 OS=Mus musculus GN=Prdx4 PE=1 SV=1	-0.918	0.087
>sp|Q8VEE1|LMCD1_MOUSE LIM and cysteine-rich domains protein 1 OS=Mus musculus GN=Lm	1.104	0.747	>sp|Q9Z1Q5|CLIC1_MOUSE Chloride intracellular channel protein 1 OS=Mus musculus GN	-0.915	0.089
>sp|O70503|DHB12_MOUSE Estradiol 17-beta-dehydrogenase 12 OS=Mus musculus GN=Hsd17b12	1.125	0.758	>sp|P08074|CBR2_MOUSE Carbonyl reductase [NADPH] 2 OS=Mus musculus GN=Cbr2 P	-0.896	0.092
>sp|P51885|LUM_MOUSE Lumican OS=Mus musculus GN=Lum PE=1 SV=2	1.147	0.770	>sp|Q8BVI4|DHPR_MOUSE Dihydropteridine reductase OS=Mus musculus GN=Qdpr PE=	-0.883	0.094
>sp|P07214|SPRC_MOUSE SPARC OS=Mus musculus GN=Sparc PE=1 SV=1	1.160	0.781	>sp|Q791V5|MTCH2_MOUSE Mitochondrial carrier homolog 2 OS=Mus musculus GN=Mt	-0.860	0.097

>sp|Q05793|PGBM_MOUSE Basement membrane-specific heparan sulfate proteoglycan core protein	1.258	0.792
>sp|Q01339|APOH_MOUSE Beta-2-glycoprotein 1 OS=Mus musculus GN=Apoh PE=1 SV=1	1.264	0.803
>sp|P11276|FINC_MOUSE Fibronectin OS=Mus musculus GN=Fn1 PE=1 SV=4	1.283	0.815
>sp|Q8C6K9|CO6A6_MOUSE Collagen alpha-6(VI) chain OS=Mus musculus GN=Col6a6 PE=1 SV=	1.306	0.826
>tr|B9EHT6|B9EHT6_MOUSE Fn1 protein OS=Mus musculus GN=Fn1 PE=2 SV=1	1.391	0.837
>sp|Q9WVH9|FBLN5_MOUSE Fibulin-5 OS=Mus musculus GN=Fbln5 PE=2 SV=1	1.433	0.848
>sp|Q62000|MIME_MOUSE Mimecan OS=Mus musculus GN=Ogn PE=2 SV=1	1.441	0.860
>sp|Q9R118|HTRA1_MOUSE Serine protease HTRA1 OS=Mus musculus GN=Htra1 PE=1 SV=2	1.540	0.871
>sp|P16045|LEG1_MOUSE Galectin-1 OS=Mus musculus GN=Lgals1 PE=1 SV=3	1.550	0.882
>sp|Q8K4G1|LTBP4_MOUSE Latent-transforming growth factor beta-binding protein 4 OS=Mus mus	1.580	0.893
>sp|Q3UTY6|THSD4_MOUSE Thrombospondin type-1 domain-containing protein 4 OS=Mus muscu	1.586	0.904
>sp|Q99JR5|TINAL_MOUSE Tubulointerstitial nephritis antigen-like OS=Mus musculus GN=Tinagl1	1.630	0.916
>sp|P08122|CO4A2_MOUSE Collagen alpha-2(IV) chain OS=Mus musculus GN=Col4a2 PE=2 SV=4	1.646	0.927
>sp|P39061|COIA1_MOUSE Collagen alpha-1(XVIII) chain OS=Mus musculus GN=Col18a1 PE=1 S	1.773	0.938
>sp|Q8BPB5|FBLN3_MOUSE EGF-containing fibulin-like extracellular matrix protein 1 OS=Mus mu	1.960	0.949
>sp|Q61282|PGCA_MOUSE Aggrecan core protein OS=Mus musculus GN=Acan PE=1 SV=2	2.130	0.961
>sp|Q9D1H9|MFAP4_MOUSE Microfibril-associated glycoprotein 4 OS=Mus musculus GN=Mfap4	2.663	0.972
>sp|Q61245|COBA1_MOUSE Collagen alpha-1(XI) chain OS=Mus musculus GN=Col11a1 PE=1 SV	3.066	0.983
>sp|O35206|COFA1_MOUSE Collagen alpha-1(XV) chain OS=Mus musculus GN=Col15a1 PE=1 SV	3.784	0.994

Intermediate filament GO:0005882

Protein identification	Zq	rank/N
>sp|P46660|AINX_MOUSE Alpha-internexin OS=Mus musculus GN=Ina PE=1 SV=2	-0.172	0.036
>sp|O55135|IF6_MOUSE Eukaryotic translation initiation factor 6 OS=Mus musculus GN=Eif6 PE=1	-0.004	0.107
>sp|P08551|NFL_MOUSE Neurofilament light polypeptide OS=Mus musculus GN=Nefl PE=1 SV=5	0.273	0.179
>sp|P14733|LMNB1_MOUSE Lamin-B1 OS=Mus musculus GN=Lmnb1 PE=1 SV=3	0.427	0.250
>sp|P15331|PERI_MOUSE Peripherin OS=Mus musculus GN=Prph PE=1 SV=2	0.563	0.321
>sp|E9Q557|DESP_MOUSE Desmoplakin OS=Mus musculus GN=Dsp PE=3 SV=1	0.664	0.393
>sp|P48678|LMNA_MOUSE Prelamin-A/C OS=Mus musculus GN=Lmna PE=1 SV=2	0.855	0.464
>sp|P21619|LMNB2_MOUSE Lamin-B2 OS=Mus musculus GN=Lmnb2 PE=1 SV=2	0.922	0.536
>tr|Q3TFD9|Q3TFD9_MOUSE Putative uncharacterized protein OS=Mus musculus GN=Vim PE=2 S	0.979	0.607
>sp|P31001|DESM_MOUSE Desmin OS=Mus musculus GN=Des PE=1 SV=3	1.047	0.679
>sp|Q6P5H2|NEST_MOUSE Nestin OS=Mus musculus GN=Nes PE=1 SV=1	1.222	0.750
>sp|P03995|GFAP_MOUSE Glial fibrillary acidic protein OS=Mus musculus GN=Gfap PE=1 SV=4	1.428	0.821
>sp|Q91ZU6|DYST_MOUSE Dystonin OS=Mus musculus GN=Dst PE=1 SV=1	1.995	0.893
>sp|P20152|VIME_MOUSE Vimentin OS=Mus musculus GN=Vim PE=1 SV=3	2.667	0.964

Muscle contraction GO:0006936

Protein identification	Zq	rank/N
>sp|Q60605|MYL6_MOUSE Myosin light polypeptide 6 OS=Mus musculus GN=Myl6 PE=1 SV=3	-0.430	-0.036
>sp|A2ASS6|TITIN_MOUSE Titin OS=Mus musculus GN=Ttn PE=1 SV=1	0.138	0.012
>sp|Q64018|GLRA1_MOUSE Glycine receptor subunit alpha-1 OS=Mus musculus GN=Glra1 PE=1 S	0.673	0.056
>sp|P58774-2|TPM2_MOUSE Isoform 2 of Tropomyosin beta chain OS=Mus musculus GN=Tpm2	0.737	0.061
>tr|Q8VCQ8|Q8VCQ8_MOUSE Caldesmon 1 OS=Mus musculus GN=Cald1 PE=2 SV=1	1.453	0.121
>tr|F6T2Z7|F6T2Z7_MOUSE Protein Cald1 (Fragment) OS=Mus musculus GN=Cald1 PE=4 SV=1	1.640	0.137
>sp|E9PZQ0|RYR1_MOUSE Ryanodine receptor 1 OS=Mus musculus GN=Ryr1 PE=1 SV=1	1.944	0.162
>sp|Q8CI43|MYL6B_MOUSE Myosin light chain 6B OS=Mus musculus GN=Myl6b PE=2 SV=1	1.978	0.165
>sp|P26883|FKB1A_MOUSE Peptidyl-prolyl cis-trans isomerase FKBP1A OS=Mus musculus GN=Fk	2.168	0.181
>sp|Q5SX39|MYH4_MOUSE Myosin-4 OS=Mus musculus GN=Myh4 PE=1 SV=1	4.217	0.351
>sp|Q02566|MYH6_MOUSE Myosin-6 OS=Mus musculus GN=Myh6 PE=1 SV=2	12.556	1.046
>sp|Q5SX40|MYH1_MOUSE Myosin-1 OS=Mus musculus GN=Myh1 PE=1 SV=1	15.231	1.269

>sp|Q8BW75|AOFB_MOUSE Amine oxidase [flavin-containing] B OS=Mus musculus GN=	-0.855	0.099
>sp|P14152|MDHC_MOUSE Malate dehydrogenase, cytoplasmic OS=Mus musculus GN=M	-0.852	0.102
>sp|Q8BU85|MSRB3_MOUSE Methionine-R-sulfoxide reductase B3, mitochondrial OS=Mu	-0.830	0.104
>sp|Q9DBF1|AL7A1_MOUSE Alpha-aminoadipic semialdehyde dehydrogenase OS=Mus m	-0.818	0.107
>sp|Q9D4J1|EFHD1_MOUSE EF-hand domain-containing protein D1 OS=Mus musculus G	-0.817	0.109
>sp|Q9DCM2|GSTK1_MOUSE Glutathione S-transferase kappa 1 OS=Mus musculus GN=G	-0.777	0.112
>sp|P35700|PRDX1_MOUSE Peroxiredoxin-1 OS=Mus musculus GN=Prdx1 PE=1 SV=1	-0.776	0.114
>sp|Q9CYG7|TOM34_MOUSE Mitochondrial import receptor subunit TOM34 OS=Mus mu	-0.770	0.117
>sp|Q7TMF3|NDUAC_MOUSE NADH dehydrogenase [ubiquinone] 1 alpha subcomplex su	-0.766	0.119
>sp|P12242|UCP1_MOUSE Mitochondrial brown fat uncoupling protein 1 OS=Mus musculu	-0.764	0.122
>sp|Q8K2B3|DHSA_MOUSE Succinate dehydrogenase [ubiquinone] flavoprotein subunit, m	-0.762	0.124
>sp|Q99LB2|DHRS4_MOUSE Dehydrogenase/reductase SDR family member 4 OS=Mus m	-0.741	0.127
>tr|Q924B0|Q924B0_MOUSE Inositol (Myo)-1(Or 4)-monophosphatase 1 OS=Mus musculu	-0.717	0.129
>sp|Q9Z2I0|LETM1_MOUSE LETM1 and EF-hand domain-containing protein 1, mitochond	-0.716	0.132
>sp|Q9CWZ7|SNAG_MOUSE Gamma-soluble NSF attachment protein OS=Mus musculus G	-0.716	0.134
>sp|Q9Z0X1|AIFM1_MOUSE Apoptosis-inducing factor 1, mitochondrial OS=Mus musculu	-0.703	0.137
>sp|Q9CQQ7|AT5F1_MOUSE ATP synthase subunit b, mitochondrial OS=Mus musculus G	-0.692	0.139
>sp|Q2TPA8|HSDL2_MOUSE Hydroxysteroid dehydrogenase-like protein 2 OS=Mus musc	-0.685	0.142
>sp|Q7TNF8|RIMB1_MOUSE Peripheral-type benzodiazepine receptor-associated protein 1	-0.677	0.144
>sp|P17156|HSP72_MOUSE Heat shock-related 70 kDa protein 2 OS=Mus musculus GN=H	-0.676	0.147
>sp|Q60932|VDAC1_MOUSE Voltage-dependent anion-selective channel protein 1 OS=Mu	-0.675	0.149
>sp|Q78PY7|SND1_MOUSE Staphylococcal nuclease domain-containing protein 1 OS=Mus	-0.675	0.152
>sp|P51881|ADT2_MOUSE ADP/ATP translocase 2 OS=Mus musculus GN=Slc25a5 PE=1	-0.656	0.155
>sp|Q91ZR1|RAB4B_MOUSE Ras-related protein Rab-4B OS=Mus musculus GN=Rab4b P	-0.638	0.157
>sp|P56375|ACYP2_MOUSE Acylphosphatase-2 OS=Mus musculus GN=Acyp2 PE=2 SV=	-0.607	0.160
>sp|P19096|FAS_MOUSE Fatty acid synthase OS=Mus musculus GN=Fasn PE=1 SV=2	-0.597	0.162
>sp|P46471|PRS7_MOUSE 26S protease regulatory subunit 7 OS=Mus musculus GN=Psmc	-0.581	0.165
>sp|Q9DCM0|ETHE1_MOUSE Protein ETHE1, mitochondrial OS=Mus musculus GN=Ethe	-0.574	0.167
>sp|Q921H8|THIKA_MOUSE 3-ketoacyl-CoA thiolase A, peroxisomal OS=Mus musculus G	-0.566	0.170
>sp|Q9DCN2|NB5R3_MOUSE NADH-cytochrome b5 reductase 3 OS=Mus musculus GN=G	-0.564	0.172
>sp|P15105|GLNA_MOUSE Glutamine synthetase OS=Mus musculus GN=Glul PE=1 SV=6	-0.554	0.175
>sp|P06151|LDHA_MOUSE L-lactate dehydrogenase A chain OS=Mus musculus GN=Ldha	-0.554	0.177
>sp|Q8BX02|KANK2_MOUSE KN motif and ankyrin repeat domain-containing protein 2 O	-0.549	0.180
>sp|Q9D3P8|PLRKT_MOUSE Plasminogen receptor (KT) OS=Mus musculus GN=Plgrkt PI	-0.536	0.182
>sp|P58281|OPA1_MOUSE Dynamin-like 120 kDa protein, mitochondrial OS=Mus musculu	-0.528	0.185
>sp|Q8BTZ7|GMPPB_MOUSE Mannose-1-phosphate guanyltransferase beta OS=Mus musc	-0.497	0.187
>sp|Q3UIU2|NDUB6_MOUSE NADH dehydrogenase [ubiquinone] 1 beta subcomplex subu	-0.477	0.190
>sp|O70591|PFD2_MOUSE Prefoldin subunit 2 OS=Mus musculus GN=Pfdn2 PE=2 SV=2	-0.456	0.192
>sp|Q9DAR7|DCPS_MOUSE m7GpppX diphosphatase OS=Mus musculus GN=Dcps PE=1	-0.451	0.195
>sp|Q9CQW1|YKT6_MOUSE Synaptobrevin homolog YKT6 OS=Mus musculus GN=Ykt6	-0.438	0.197
>sp|P63085|MK01_MOUSE Mitogen-activated protein kinase 1 OS=Mus musculus GN=Ma	-0.428	0.200
>sp|Q8VCW8|ACSF2_MOUSE Acyl-CoA synthetase family member 2, mitochondrial OS=M	-0.423	0.202
>sp|Q9CRB9|CHCH3_MOUSE Coiled-coil-helix-coiled-coil-helix domain-containing protei	-0.422	0.205
>sp|Q60930|VDAC2_MOUSE Voltage-dependent anion-selective channel protein 2 OS=Mu	-0.416	0.207
>sp|Q62167|DDX3X_MOUSE ATP-dependent RNA helicase DDX3X OS=Mus musculus G	-0.396	0.210
>sp|Q99KR3|LACB2_MOUSE Beta-lactamase-like protein 2 OS=Mus musculus GN=Lactb2	-0.394	0.212
>sp|Q922B1|MACD1_MOUSE O-acetyl-ADP-ribose deacetylase MACROD1 OS=Mus mus	-0.377	0.215
>sp|Q8CAQ8|IMMT_MOUSE Mitochondrial inner membrane protein OS=Mus musculus GI	-0.376	0.217
>sp|P52196|THTR_MOUSE Thiosulfate sulfurtransferase OS=Mus musculus GN=Tst PE=1	-0.373	0.220
>sp|P30416|FKBP4_MOUSE Peptidyl-prolyl cis-trans isomerase FKBP4 OS=Mus musculus	-0.372	0.222
>sp|Q01768|NDKB_MOUSE Nucleoside diphosphate kinase B OS=Mus musculus GN=Nme	-0.363	0.225
>sp|P99028|QCR6_MOUSE Cytochrome b-c1 complex subunit 6, mitochondrial OS=Mus m	-0.360	0.227
>sp|Q921G7|ETFD_MOUSE Electron transfer flavoprotein-ubiquinone oxidoreductase, mito	-0.359	0.230

>sp|Q8QZT1|THIL_MOUSE Acetyl-CoA acetyltransferase, mitochondrial OS=Mus musculu	-0.357	0.232
>sp|Q8K4Z3|NNRE_MOUSE NAD(P)H-hydrate epimerase OS=Mus musculus GN=Apoa1b	-0.356	0.235
>sp|Q9JHW2|NIT2_MOUSE Omega-amidase NIT2 OS=Mus musculus GN=Nit2 PE=1 SV=	-0.348	0.237
>sp|P05132|KAPCA_MOUSE cAMP-dependent protein kinase catalytic subunit alpha OS=M	-0.346	0.240
>sp|Q99LX0|PARK7_MOUSE Protein DJ-1 OS=Mus musculus GN=Park7 PE=1 SV=1	-0.338	0.242
>sp|Q6PHN9|RAB35_MOUSE Ras-related protein Rab-35 OS=Mus musculus GN=Rab35 P	-0.322	0.245
>tr|G5E895|G5E895_MOUSE MCG142264, isoform CRA_b OS=Mus musculus GN=Akr1b	-0.320	0.247
>sp|P62264|RS14_MOUSE 40S ribosomal protein S14 OS=Mus musculus GN=Rps14 PE=2	-0.308	0.250
>sp|P46638|RB11B_MOUSE Ras-related protein Rab-11B OS=Mus musculus GN=Rab11b I	-0.303	0.253
>sp|P08228|SODC_MOUSE Superoxide dismutase [Cu-Zn] OS=Mus musculus GN=Sod1 PI	-0.301	0.255
>sp|Q9CQA3|DHSB_MOUSE Succinate dehydrogenase [ubiquinone] iron-sulfur subunit, mi	-0.298	0.258
>sp|P52503|NDUS6_MOUSE NADH dehydrogenase [ubiquinone] iron-sulfur protein 6, mito	-0.292	0.260
>sp|Q8CG76|ARK72_MOUSE Aflatoxin B1 aldehyde reductase member 2 OS=Mus musculu	-0.291	0.263
>sp|Q64105|SPRE_MOUSE Sepiapterin reductase OS=Mus musculus GN=Spr PE=1 SV=1	-0.291	0.265
>sp|Q64516|GLPK_MOUSE Glycerol kinase OS=Mus musculus GN=Gk PE=2 SV=2	-0.276	0.268
>sp|P03930|ATP8_MOUSE ATP synthase protein 8 OS=Mus musculus GN=Mtatp8 PE=1 S	-0.260	0.270
>sp|P28271|ACOC_MOUSE Cytoplasmic aconitate hydratase OS=Mus musculus GN=Aco1	-0.242	0.273
>sp|P51174|ACADL_MOUSE Long-chain specific acyl-CoA dehydrogenase, mitochondrial	-0.240	0.275
>sp|Q9QX60|DGUOK_MOUSE Deoxyguanosine kinase, mitochondrial OS=Mus musculus (	-0.234	0.278
>sp|Q9DBL1|ACDSB_MOUSE Short/branched chain specific acyl-CoA dehydrogenase, mit	-0.225	0.280
>sp|Q8BMF3|MAON_MOUSE NADP-dependent malic enzyme, mitochondrial OS=Mus mu	-0.210	0.283
>sp|Q9DCT2|NDUS3_MOUSE NADH dehydrogenase [ubiquinone] iron-sulfur protein 3, mi	-0.209	0.285
>sp|Q8R2Y8|PTH2_MOUSE Peptidyl-tRNA hydrolase 2, mitochondrial OS=Mus musculus	-0.198	0.288
>sp|Q9Z1Q9|SYVC_MOUSE Valine--tRNA ligase OS=Mus musculus GN=Vars PE=2 SV=	-0.189	0.290
>sp|P28474|ADHX_MOUSE Alcohol dehydrogenase class-3 OS=Mus musculus GN=Adh5 I	-0.187	0.293
>sp|Q9JLJ2|AL9A1_MOUSE 4-trimethylaminobutyraldehyde dehydrogenase OS=Mus musc	-0.174	0.295
>sp|P35385|HSPB7_MOUSE Heat shock protein beta-7 OS=Mus musculus GN=Hspb7 PE=	-0.173	0.298
>sp|Q8BH04|PCKGM_MOUSE Phosphoenolpyruvate carboxykinase [GTP], mitochondrial (	-0.152	0.300
>sp|P37040|NCPR_MOUSE NADPH--cytochrome P450 reductase OS=Mus musculus GN=I	-0.146	0.303
>sp|Q9CZB0|C560_MOUSE Succinate dehydrogenase cytochrome b560 subunit, mitochond	-0.137	0.305
>sp|Q9DCS3|MECR_MOUSE Trans-2-enoyl-CoA reductase, mitochondrial OS=Mus muscu	-0.133	0.308
>sp|Q6P8J7|KCRS_MOUSE Creatine kinase S-type, mitochondrial OS=Mus musculus GN=(	-0.129	0.310
>sp|Q8C3X2|CC90B_MOUSE Coiled-coil domain-containing protein 90B, mitochondrial OS	-0.126	0.313
>sp|O70378|EMC8_MOUSE ER membrane protein complex subunit 8 OS=Mus musculus G	-0.108	0.315
>sp|Q922D8|C1TC_MOUSE C-1-tetrahydrofolate synthase, cytoplasmic OS=Mus musculus	-0.106	0.318
>sp|Q9D0S9|HINT2_MOUSE Histidine triad nucleotide-binding protein 2, mitochondrial OS	-0.104	0.320
>sp|Q9CR21|ACPM_MOUSE Acyl carrier protein, mitochondrial OS=Mus musculus GN=N	-0.096	0.323
>sp|Q3V132|ADT4_MOUSE ADP/ATP translocase 4 OS=Mus musculus GN=Slc25a31 PE=	-0.092	0.325
>sp|Q9QYB1|CLIC4_MOUSE Chloride intracellular channel protein 4 OS=Mus musculus G	-0.083	0.328
>sp|Q8BGH2|SAM50_MOUSE Sorting and assembly machinery component 50 homolog OS	-0.082	0.330
>sp|Q9CQX2|CYB5B_MOUSE Cytochrome b5 type B OS=Mus musculus GN=Cyb5b PE=1	-0.080	0.333
>sp|P56392|CX7A1_MOUSE Cytochrome c oxidase subunit 7A1, mitochondrial OS=Mus m	-0.078	0.335
>sp|Q99L43|CDS2_MOUSE Phosphatidate cytidylyltransferase 2 OS=Mus musculus GN=C	-0.078	0.338
>sp|O35857|TIM44_MOUSE Mitochondrial import inner membrane translocase subunit TIM	-0.077	0.340
>sp|Q8K1M6|DNM1L_MOUSE Dynamin-1-like protein OS=Mus musculus GN=Dnm1l PE=	-0.057	0.343
>sp|Q9CR61|NDUB7_MOUSE NADH dehydrogenase [ubiquinone] 1 beta subcomplex subu	-0.056	0.345
>sp|P00158|CYB_MOUSE Cytochrome b OS=Mus musculus GN=Mt-Cyb PE=2 SV=1	-0.046	0.348
>sp|Q9DCJ5|NDUA8_MOUSE NADH dehydrogenase [ubiquinone] 1 alpha subcomplex sub	-0.023	0.351
>sp|Q9Z2I8|SUCB2_MOUSE Succinyl-CoA ligase [GDP-forming] subunit beta, mitochondr	-0.022	0.353
>sp|Q9WUM5|SUCA_MOUSE Succinyl-CoA ligase [ADP/GDP-forming] subunit alpha, mi	-0.022	0.356
>sp|P62897|CYC_MOUSE Cytochrome c, somatic OS=Mus musculus GN=Cycs PE=1 SV=2	-0.007	0.358
>sp|Q9Z110|P5CS_MOUSE Delta-1-pyrroline-5-carboxylate synthase OS=Mus musculus GI	0.000	0.361
>sp|P15532|NDKA_MOUSE Nucleoside diphosphate kinase A OS=Mus musculus GN=Nme	0.008	0.363

>sp|P19783|COX41_MOUSE Cytochrome c oxidase subunit 4 isoform 1, mitochondrial OS=	0.020	0.366
>sp|Q9DCV4|RMD1_MOUSE Regulator of microtubule dynamics protein 1 OS=Mus muscu	0.025	0.368
>sp|Q91V92|ACLY_MOUSE ATP-citrate synthase OS=Mus musculus GN=Acly PE=1 SV=	0.029	0.371
>sp|Q9QZ23|NFU1_MOUSE NFU1 iron-sulfur cluster scaffold homolog, mitochondrial OS=	0.034	0.373
>sp|Q9R0H0|ACOX1_MOUSE Peroxisomal acyl-coenzyme A oxidase 1 OS=Mus musculus	0.051	0.376
>sp|Q8C0V9|FRMD6_MOUSE FERM domain-containing protein 6 OS=Mus musculus GN=	0.055	0.378
>sp|Q06185|ATP5I_MOUSE ATP synthase subunit e, mitochondrial OS=Mus musculus GN	0.056	0.381
>sp|P11352|GPX1_MOUSE Glutathione peroxidase 1 OS=Mus musculus GN=Gpx1 PE=1 S	0.068	0.383
>sp|Q5SWU9|ACACA_MOUSE Acetyl-CoA carboxylase 1 OS=Mus musculus GN=Acaca I	0.081	0.386
>sp|P19157|GSTP1_MOUSE Glutathione S-transferase P 1 OS=Mus musculus GN=Gstp1 P	0.084	0.388
>sp|P31786|ACBP_MOUSE Acyl-CoA-binding protein OS=Mus musculus GN=Dbi PE=1 S	0.098	0.391
>sp|P47791|GSHR_MOUSE Glutathione reductase, mitochondrial OS=Mus musculus GN=G	0.101	0.393
>sp|P06801|MAOX_MOUSE NADP-dependent malic enzyme OS=Mus musculus GN=Me1	0.128	0.396
>sp|P28867|KPCD_MOUSE Protein kinase C delta type OS=Mus musculus GN=Prkcd PE=1	0.134	0.398
>sp|Q9CQ75|NDUA2_MOUSE NADH dehydrogenase [ubiquinone] 1 alpha subcomplex sub	0.136	0.401
>sp|Q5U458|DJC11_MOUSE DnaJ homolog subfamily C member 11 OS=Mus musculus GN	0.154	0.403
>sp|Q9JK48|SHLB1_MOUSE Endophilin-B1 OS=Mus musculus GN=Sh3glb1 PE=1 SV=1	0.154	0.406
>sp|Q9R112|SQRD_MOUSE Sulfide:quinone oxidoreductase, mitochondrial OS=Mus muscu	0.160	0.408
>sp|Q99MN9|PCCB_MOUSE Propionyl-CoA carboxylase beta chain, mitochondrial OS=Mu	0.163	0.411
>sp|Q8BIJ6|SYIM_MOUSE Isoleucine--tRNA ligase, mitochondrial OS=Mus musculus GN=	0.165	0.413
>sp|Q91WS0|CISD1_MOUSE CDGSH iron-sulfur domain-containing protein 1 OS=Mus mu	0.175	0.416
>sp|Q99LC3|NDUAA_MOUSE NADH dehydrogenase [ubiquinone] 1 alpha subcomplex sul	0.179	0.418
>tr|A2AFQ2|A2AFQ2_MOUSE 3-hydroxyacyl-CoA dehydrogenase type-2 OS=Mus muscul	0.181	0.421
>sp|Q8K1R7|NEK9_MOUSE Serine/threonine-protein kinase Nek9 OS=Mus musculus GN=	0.183	0.423
>sp|Q8BH59|CMC1_MOUSE Calcium-binding mitochondrial carrier protein Aralar1 OS=M	0.184	0.426
>sp|Q99MN1|SYK_MOUSE Lysine--tRNA ligase OS=Mus musculus GN=Kars PE=1 SV=1	0.205	0.428
>sp|Q9Z1Z2|STRAP_MOUSE Serine-threonine kinase receptor-associated protein OS=Mus	0.214	0.431
>tr|Q5XJF6|Q5XJF6_MOUSE Ribosomal protein OS=Mus musculus GN=Rpl10a PE=2 SV=	0.214	0.433
>sp|Q99JB2|STML2_MOUSE Stomatin-like protein 2 OS=Mus musculus GN=Stoml2 PE=1	0.216	0.436
>sp|O35129|PHB2_MOUSE Prohibitin-2 OS=Mus musculus GN=Phb2 PE=1 SV=1	0.219	0.438
>tr|Q91VA7|Q91VA7_MOUSE Isocitrate dehydrogenase 3 (NAD+) beta OS=Mus musculus	0.231	0.441
>sp|Q8R4N0|CLYBL_MOUSE Citrate lyase subunit beta-like protein, mitochondrial OS=Mu	0.237	0.443
>sp|P62259|1433E_MOUSE 14-3-3 protein epsilon OS=Mus musculus GN=Ywhae PE=1 SV	0.253	0.446
>sp|Q920E5|FPPS_MOUSE Farnesyl pyrophosphate synthase OS=Mus musculus GN=Fdps	0.263	0.448
>sp|Q9WV85|NDK3_MOUSE Nucleoside diphosphate kinase 3 OS=Mus musculus GN=Nm	0.265	0.451
>sp|E9Q557|DESP_MOUSE Desmoplakin OS=Mus musculus GN=Dsp PE=3 SV=1	0.266	0.454
>sp|Q91WK5|GCSH_MOUSE Glycine cleavage system H protein, mitochondrial OS=Mus n	0.267	0.456
>sp|P52480|KPYM_MOUSE Pyruvate kinase isozymes M1/M2 OS=Mus musculus GN=Pkn	0.267	0.459
>sp|P05202|AATM_MOUSE Aspartate aminotransferase, mitochondrial OS=Mus musculus	0.273	0.461
>sp|Q9QUI0|RHOA_MOUSE Transforming protein RhoA OS=Mus musculus GN=Rhoa PE	0.275	0.464
>sp|P47738|ALDH2_MOUSE Aldehyde dehydrogenase, mitochondrial OS=Mus musculus G	0.275	0.466
>sp|O55137|ACOT1_MOUSE Acyl-coenzyme A thioesterase 1 OS=Mus musculus GN=Aco	0.279	0.469
>sp|O70571|PDK4_MOUSE [Pyruvate dehydrogenase [lipoamide]] kinase isozyme 4, mitoch	0.289	0.471
>sp|Q60936|ADCK3_MOUSE Chaperone activity of bc1 complex-like, mitochondrial OS=M	0.293	0.474
>sp|Q9CPY7|AMPL_MOUSE Cytosol aminopeptidase OS=Mus musculus GN=Lap3 PE=1 S	0.294	0.476
>sp|Q9D6K8|FUND2_MOUSE FUN14 domain-containing protein 2 OS=Mus musculus GN=	0.301	0.479
>sp|Q9CPV4|GLOD4_MOUSE Glyoxalase domain-containing protein 4 OS=Mus musculus	0.325	0.481
>sp|O35459|ECH1_MOUSE Delta(3,5)-Delta(2,4)-dienoyl-CoA isomerase, mitochondrial O	0.326	0.484
>sp|P61922|GABT_MOUSE 4-aminobutyrate aminotransferase, mitochondrial OS=Mus mus	0.327	0.486
>sp|Q9Z2Z6|MCAT_MOUSE Mitochondrial carnitine/acylcarnitine carrier protein OS=Mus	0.327	0.489
>sp|O35855|BCAT2_MOUSE Branched-chain-amino-acid aminotransferase, mitochondrial C	0.330	0.491
>sp|Q9JIQ3|DBLOH_MOUSE Diablo homolog, mitochondrial OS=Mus musculus GN=Diab	0.331	0.494
>sp|Q8CHT0|AL4A1_MOUSE Delta-1-pyrroline-5-carboxylate dehydrogenase, mitochondri	0.336	0.496

>sp|Q99L13|3HIDH_MOUSE 3-hydroxyisobutyrate dehydrogenase, mitochondrial OS=Mus	0.356	0.499
>sp|P45952|ACADM_MOUSE Medium-chain specific acyl-CoA dehydrogenase, mitochond	0.357	0.501
>sp|P03911|NU4M_MOUSE NADH-ubiquinone oxidoreductase chain 4 OS=Mus musculus	0.367	0.504
>sp|Q3TL44|NLRX1_MOUSE NLR family member X1 OS=Mus musculus GN=Nlrx1 PE=2	0.369	0.506
>sp|P18242|CATD_MOUSE Cathepsin D OS=Mus musculus GN=Ctsd PE=1 SV=1	0.378	0.509
>sp|P84091|AP2M1_MOUSE AP-2 complex subunit mu OS=Mus musculus GN=Ap2m1 PE	0.384	0.511
>sp|Q99J99|THTM_MOUSE 3-mercaptopyruvate sulfurtransferase OS=Mus musculus GN=I	0.390	0.514
>sp|P80313|TCPH_MOUSE T-complex protein 1 subunit eta OS=Mus musculus GN=Cct7 P	0.392	0.516
>sp|Q9CPQ3|TOM22_MOUSE Mitochondrial import receptor subunit TOM22 homolog OS=	0.398	0.519
>sp|Q922W5|P5CR1_MOUSE Pyrroline-5-carboxylate reductase 1, mitochondrial OS=Mus	0.401	0.521
>sp|Q9DCX2|ATP5H_MOUSE ATP synthase subunit d, mitochondrial OS=Mus musculus C	0.405	0.524
>sp|Q68FD5|CLH1_MOUSE Clathrin heavy chain 1 OS=Mus musculus GN=Cltc PE=1 SV=	0.411	0.526
>sp|P10605|CATB_MOUSE Cathepsin B OS=Mus musculus GN=Ctsb PE=1 SV=2	0.411	0.529
>sp|P70404|IDHG1_MOUSE Isocitrate dehydrogenase [NAD] subunit gamma 1, mitochondr	0.412	0.531
>sp|P16332|MUTA_MOUSE Methylmalonyl-CoA mutase, mitochondrial OS=Mus musculus	0.417	0.534
>sp|P50136|ODBA_MOUSE 2-oxoisovalerate dehydrogenase subunit alpha, mitochondrial O	0.419	0.536
>sp|Q8C5H8|NAKD1_MOUSE NAD kinase domain-containing protein 1 OS=Mus musculus	0.426	0.539
>sp|P48962|ADT1_MOUSE ADP/ATP translocase 1 OS=Mus musculus GN=Slc25a4 PE=1	0.439	0.541
>sp|Q9CZD3|SYG_MOUSE Glycine--tRNA ligase OS=Mus musculus GN=Gars PE=1 SV=	0.441	0.544
>sp|Q9CQ69|QCR8_MOUSE Cytochrome b-c1 complex subunit 8 OS=Mus musculus GN=U	0.444	0.546
>sp|O88844|IDHC_MOUSE Isocitrate dehydrogenase [NADP] cytoplasmic OS=Mus muscul	0.447	0.549
>sp|Q9R0X4|ACOT9_MOUSE Acyl-coenzyme A thioesterase 9, mitochondrial OS=Mus mu	0.453	0.552
>sp|Q9CR62|M2OM_MOUSE Mitochondrial 2-oxoglutarate/malate carrier protein OS=Mus	0.459	0.554
>tr|E9QPQ8|E9QPQ8_MOUSE 39S ribosomal protein L48, mitochondrial OS=Mus musculu	0.466	0.557
>sp|O08749|DLDH_MOUSE Dihydrolipoyl dehydrogenase, mitochondrial OS=Mus musculu	0.468	0.559
>sp|Q99LD8|DDAH2_MOUSE N(G),N(G)-dimethylarginine dimethylaminohydrolase 2 OS=	0.475	0.562
>sp|Q9D6Y7|MSRA_MOUSE Mitochondrial peptide methionine sulfoxide reductase OS=M	0.484	0.564
>sp|Q63844|MK03_MOUSE Mitogen-activated protein kinase 3 OS=Mus musculus GN=Ma	0.484	0.567
>sp|Q99LB6|MAT2B_MOUSE Methionine adenosyltransferase 2 subunit beta OS=Mus mus	0.489	0.569
>sp|P52825|CPT2_MOUSE Carnitine O-palmitoyltransferase 2, mitochondrial OS=Mus mus	0.497	0.572
>sp|P39688|FYN_MOUSE Tyrosine-protein kinase Fyn OS=Mus musculus GN=Fyn PE=1 S	0.499	0.574
>sp|Q9CWJ9|PUR9_MOUSE Bifunctional purine biosynthesis protein PURH OS=Mus musc	0.510	0.577
>sp|P10639|THIO_MOUSE Thioredoxin OS=Mus musculus GN=Txn PE=1 SV=3	0.515	0.579
>sp|Q8R0N6|HOT_MOUSE Hydroxyacid-oxoacid transhydrogenase, mitochondrial OS=Mu	0.517	0.582
>sp|Q99KB8|GLO2_MOUSE Hydroxyacylglutathione hydrolase, mitochondrial OS=Mus mu	0.543	0.584
>sp|P12787|COX5A_MOUSE Cytochrome c oxidase subunit 5A, mitochondrial OS=Mus mu	0.555	0.587
>sp|P41216|ACSL1_MOUSE Long-chain-fatty-acid--CoA ligase 1 OS=Mus musculus GN=A	0.561	0.589
>sp|Q9CZ42|NNRD_MOUSE ATP-dependent (S)-NAD(P)H-hydrate dehydratase OS=Mus	0.562	0.592
>sp|Q8R164|BPHL_MOUSE Valacyclovir hydrolase OS=Mus musculus GN=Bphl PE=2 SV	0.564	0.594
>sp|Q9JK42|PDK2_MOUSE [Pyruvate dehydrogenase [lipoamide]] kinase isozyme 2, mitoch	0.565	0.597
>sp|Q3ULD5|MCCB_MOUSE Methylcrotonoyl-CoA carboxylase beta chain, mitochondrial	0.578	0.599
>sp|Q91VS7|MGST1_MOUSE Microsomal glutathione S-transferase 1 OS=Mus musculus C	0.580	0.602
>sp|Q9D0I9|SYRC_MOUSE Arginine--tRNA ligase, cytoplasmic OS=Mus musculus GN=R	0.586	0.604
>sp|Q9QUM9|PSA6_MOUSE Proteasome subunit alpha type-6 OS=Mus musculus GN=Psm	0.592	0.607
>sp|P70296|PEBP1_MOUSE Phosphatidylethanolamine-binding protein 1 OS=Mus musculu	0.594	0.609
>sp|Q8BFR5|EFTU_MOUSE Elongation factor Tu, mitochondrial OS=Mus musculus GN=T	0.597	0.612
>sp|P00329|ADH1_MOUSE Alcohol dehydrogenase 1 OS=Mus musculus GN=Adh1 PE=2 S	0.604	0.614
>sp|Q9D023|MPC2_MOUSE Mitochondrial pyruvate carrier 2 OS=Mus musculus GN=Mpc	0.606	0.617
>sp|P16125|LDHB_MOUSE L-lactate dehydrogenase B chain OS=Mus musculus GN=Ldhb	0.613	0.619
>sp|Q9D0M3|CY1_MOUSE Cytochrome c1, heme protein, mitochondrial OS=Mus musculu	0.614	0.622
>sp|Q61425|HCDH_MOUSE Hydroxyacyl-coenzyme A dehydrogenase, mitochondrial OS=M	0.615	0.624
>sp|Q8K1J6|TRNT1_MOUSE CCA tRNA nucleotidyltransferase 1, mitochondrial OS=Mus	0.619	0.627
>sp|P50544|ACADV_MOUSE Very long-chain specific acyl-CoA dehydrogenase, mitochon	0.622	0.629

>sp|P51660|DHB4_MOUSE Peroxisomal multifunctional enzyme type 2 OS=Mus musculus	0.644	0.632
>sp|Q9CQ62|DECR_MOUSE 2,4-dienoyl-CoA reductase, mitochondrial OS=Mus musculus	0.664	0.634
>sp|Q9QYA2|TOM40_MOUSE Mitochondrial import receptor subunit TOM40 homolog OS	0.667	0.637
>sp|Q32MW3|ACO10_MOUSE Acyl-coenzyme A thioesterase 10, mitochondrial OS=Mus r	0.669	0.639
>sp|P97742|CPT1A_MOUSE Carnitine O-palmitoyltransferase 1, liver isoform OS=Mus mu	0.683	0.642
>sp|Q8BH95|ECHM_MOUSE Enoyl-CoA hydratase, mitochondrial OS=Mus musculus GN=	0.686	0.644
>sp|P08249|MDHM_MOUSE Malate dehydrogenase, mitochondrial OS=Mus musculus GN=	0.687	0.647
>sp|O08528|HXK2_MOUSE Hexokinase-2 OS=Mus musculus GN=Hk2 PE=1 SV=1	0.707	0.649
>sp|Q9JLZ3|AUHM_MOUSE Methylglutaconyl-CoA hydratase, mitochondrial OS=Mus mu	0.712	0.652
>sp|P29758|OAT_MOUSE Ornithine aminotransferase, mitochondrial OS=Mus musculus GI	0.714	0.655
>sp|P20108|PRDX3_MOUSE Thioredoxin-dependent peroxide reductase, mitochondrial OS=	0.714	0.657
>sp|Q9CQN6|TM14C_MOUSE Transmembrane protein 14C OS=Mus musculus GN=Tmem	0.718	0.660
>sp|Q91WD5|NDUS2_MOUSE NADH dehydrogenase [ubiquinone] iron-sulfur protein 2, m	0.720	0.662
>sp|Q07813|BAX_MOUSE Apoptosis regulator BAX OS=Mus musculus GN=Bax PE=1 SV	0.722	0.665
>sp|Q8JZN5|ACAD9_MOUSE Acyl-CoA dehydrogenase family member 9, mitochondrial C	0.746	0.667
>sp|Q9QYR9|ACOT2_MOUSE Acyl-coenzyme A thioesterase 2, mitochondrial OS=Mus mu	0.746	0.670
>sp|P09671|SODM_MOUSE Superoxide dismutase [Mn], mitochondrial OS=Mus musculus	0.747	0.672
>sp|Q05920|PYC_MOUSE Pyruvate carboxylase, mitochondrial OS=Mus musculus GN=Pc	0.749	0.675
>sp|P63101|1433Z_MOUSE 14-3-3 protein zeta/delta OS=Mus musculus GN=Ywhaz PE=1	0.762	0.677
>sp|Q91VR2|ATPG_MOUSE ATP synthase subunit gamma, mitochondrial OS=Mus muscul	0.762	0.680
>sp|P99029|PRDX5_MOUSE Peroxiredoxin-5, mitochondrial OS=Mus musculus GN=Prdx5	0.763	0.682
>sp|P58044|IDI1_MOUSE Isopentenyl-diphosphate Delta-isomerase 1 OS=Mus musculus G	0.776	0.685
>sp|Q6PB66|LPPRC_MOUSE Leucine-rich PPR motif-containing protein, mitochondrial OS	0.776	0.687
>sp|P67778|PHB_MOUSE Prohibitin OS=Mus musculus GN=Phb PE=1 SV=1	0.781	0.690
>sp|Q9D1G1|RAB1B_MOUSE Ras-related protein Rab-1B OS=Mus musculus GN=Rab1b P	0.798	0.692
>sp|Q9CRD0|OCAD1_MOUSE OCIA domain-containing protein 1 OS=Mus musculus GN=	0.807	0.695
>sp|P47934|CACP_MOUSE Carnitine O-acetyltransferase OS=Mus musculus GN=Crat PE=	0.812	0.697
>sp|P18572|BASI_MOUSE Basigin OS=Mus musculus GN=Bsg PE=1 SV=2	0.813	0.700
>sp|Q99JY0|ECHB_MOUSE Trifunctional enzyme subunit beta, mitochondrial OS=Mus mu	0.815	0.702
>sp|Q91W97|HKDC1_MOUSE Putative hexokinase HKDC1 OS=Mus musculus GN=Hkdc1	0.817	0.705
>sp|Q8BWT1|THIM_MOUSE 3-ketoacyl-CoA thiolase, mitochondrial OS=Mus musculus G	0.817	0.707
>sp|P54310|LIPS_MOUSE Hormone-sensitive lipase OS=Mus musculus GN=Lipe PE=1 SV	0.820	0.710
>sp|Q8JZQ2|AFG32_MOUSE AFG3-like protein 2 OS=Mus musculus GN=Afg3l2 PE=1 SV	0.824	0.712
>sp|Q99L04|DHRS1_MOUSE Dehydrogenase/reductase SDR family member 1 OS=Mus mu	0.824	0.715
>sp|Q99LB7|SARDH_MOUSE Sarcosine dehydrogenase, mitochondrial OS=Mus musculus	0.826	0.717
>sp|P54071|IDHP_MOUSE Isocitrate dehydrogenase [NADP], mitochondrial OS=Mus musc	0.832	0.720
>sp|P56480|ATPB_MOUSE ATP synthase subunit beta, mitochondrial OS=Mus musculus G	0.835	0.722
>sp|Q99KI0|ACON_MOUSE Aconitate hydratase, mitochondrial OS=Mus musculus GN=Ac	0.838	0.725
>sp|Q9DC70|NDUS7_MOUSE NADH dehydrogenase [ubiquinone] iron-sulfur protein 7, mi	0.845	0.727
>sp|Q9WUR2|ECI2_MOUSE Enoyl-CoA delta isomerase 2, mitochondrial OS=Mus musculu	0.847	0.730
>sp|Q9DCB8|ISCA2_MOUSE Iron-sulfur cluster assembly 2 homolog, mitochondrial OS=M	0.851	0.732
>sp|P42125|ECI1_MOUSE Enoyl-CoA delta isomerase 1, mitochondrial OS=Mus musculus	0.854	0.735
>sp|P11499|HS90B_MOUSE Heat shock protein HSP 90-beta OS=Mus musculus GN=Hsp9	0.864	0.737
>sp|Q9CQ54|NDUC2_MOUSE NADH dehydrogenase [ubiquinone] 1 subunit C2 OS=Mus r	0.881	0.740
>sp|P35235|PTN11_MOUSE Tyrosine-protein phosphatase non-receptor type 11 OS=Mus m	0.881	0.742
>sp|Q99MR8|MCCA_MOUSE Methylcrotonoyl-CoA carboxylase subunit alpha, mitochondr	0.887	0.745
>sp|P56135|ATPK_MOUSE ATP synthase subunit f, mitochondrial OS=Mus musculus GN=	0.892	0.747
>sp|Q9JHR7|IDE_MOUSE Insulin-degrading enzyme OS=Mus musculus GN=Ide PE=1 SV=	0.896	0.750
>sp|Q9CXZ1|NDUS4_MOUSE NADH dehydrogenase [ubiquinone] iron-sulfur protein 4, mi	0.904	0.753
>sp|Q91ZA3|PCCA_MOUSE Propionyl-CoA carboxylase alpha chain, mitochondrial OS=M	0.904	0.755
>sp|Q04447|KCRB_MOUSE Creatine kinase B-type OS=Mus musculus GN=Ckb PE=1 SV=	0.912	0.758
>sp|Q8BMP6|GCP60_MOUSE Golgi resident protein GCP60 OS=Mus musculus GN=Acbd3	0.914	0.760
>sp|P63328|PP2BA_MOUSE Serine/threonine-protein phosphatase 2B catalytic subunit alph	0.916	0.763

>sp|Q03265|ATPA_MOUSE ATP synthase subunit alpha, mitochondrial OS=Mus musculus	0.917	0.765
>sp|Q9CZU6|CISY_MOUSE Citrate synthase, mitochondrial OS=Mus musculus GN=Cs PE	0.927	0.768
>sp|P24270|CATA_MOUSE Catalase OS=Mus musculus GN=Cat PE=1 SV=4	0.930	0.770
>sp|Q91VD9|NDUS1_MOUSE NADH-ubiquinone oxidoreductase 75 kDa subunit, mitochor	0.931	0.773
>sp|Q8CGK3|LONM_MOUSE Lon protease homolog, mitochondrial OS=Mus musculus GN	0.933	0.775
>sp|P59017|B2L13_MOUSE Bcl-2-like protein 13 OS=Mus musculus GN=Bcl2l13 PE=1 SV	0.934	0.778
>sp|Q9CQZ5|NDUA6_MOUSE NADH dehydrogenase [ubiquinone] 1 alpha subcomplex sul	0.935	0.780
>sp|Q64373|B2CL1_MOUSE Bcl-2-like protein 1 OS=Mus musculus GN=Bcl2l1 PE=1 SV=	0.942	0.783
>sp|Q9JHI5|IVD_MOUSE Isovaleryl-CoA dehydrogenase, mitochondrial OS=Mus musculus	0.953	0.785
>sp|O08709|PRDX6_MOUSE Peroxiredoxin-6 OS=Mus musculus GN=Prdx6 PE=1 SV=3	0.953	0.788
>sp|Q8VEM8|MPCP_MOUSE Phosphate carrier protein, mitochondrial OS=Mus musculus	0.970	0.790
>sp|Q9D3D9|ATPD_MOUSE ATP synthase subunit delta, mitochondrial OS=Mus musculus	0.975	0.793
>sp|P38647|GRP75_MOUSE Stress-70 protein, mitochondrial OS=Mus musculus GN=Hspa	0.977	0.795
>sp|Q9EQ20|MMSA_MOUSE Methylmalonate-semialdehyde dehydrogenase [acylating], m	0.981	0.798
>sp|Q60597|ODO1_MOUSE 2-oxoglutarate dehydrogenase, mitochondrial OS=Mus muscul	0.985	0.800
>sp|P54775|PRS6B_MOUSE 26S protease regulatory subunit 6B OS=Mus musculus GN=Ps	0.989	0.803
>sp|Q9DB77|QCR2_MOUSE Cytochrome b-c1 complex subunit 2, mitochondrial OS=Mus m	0.995	0.805
>sp|P26638|SYSC_MOUSE Serine--tRNA ligase, cytoplasmic OS=Mus musculus GN=Sars	1.013	0.808
>sp|Q9WTP6|KAD2_MOUSE Adenylate kinase 2, mitochondrial OS=Mus musculus GN=A	1.017	0.810
>sp|Q9CZ13|QCR1_MOUSE Cytochrome b-c1 complex subunit 1, mitochondrial OS=Mus m	1.018	0.813
>sp|Q9CPQ8|ATP5L_MOUSE ATP synthase subunit g, mitochondrial OS=Mus musculus G	1.022	0.815
>sp|Q62465|VAT1_MOUSE Synaptic vesicle membrane protein VAT-1 homolog OS=Mus m	1.034	0.818
>sp|Q9DB20|ATPO_MOUSE ATP synthase subunit O, mitochondrial OS=Mus musculus GN	1.046	0.820
>sp|Q9D0K2|SCOT1_MOUSE Succinyl-CoA:3-ketoacid coenzyme A transferase 1, mitocho	1.048	0.823
>sp|Q9D172|ES1_MOUSE ES1 protein homolog, mitochondrial OS=Mus musculus GN=D1	1.066	0.825
>sp|Q8R0Y6|AL1L1_MOUSE Cytosolic 10-formyltetrahydrofolate dehydrogenase OS=Mus	1.067	0.828
>sp|Q9D8S4|ORN_MOUSE Oligoribonuclease, mitochondrial OS=Mus musculus GN=Rexo	1.096	0.830
>sp|Q99LC5|ETFA_MOUSE Electron transfer flavoprotein subunit alpha, mitochondrial OS=	1.114	0.833
>sp|P50171|DHB8_MOUSE Estradiol 17-beta-dehydrogenase 8 OS=Mus musculus GN=Hsd	1.118	0.835
>sp|Q9WVL0|MAAI_MOUSE Maleylacetoacetate isomerase OS=Mus musculus GN=Gstz1	1.127	0.838
>sp|Q8BWF0|SSDH_MOUSE Succinate-semialdehyde dehydrogenase, mitochondrial OS=M	1.155	0.840
>sp|P53395|ODB2_MOUSE Lipoamide acyltransferase component of branched-chain alpha-	1.157	0.843
>sp|P25799|NFKB1_MOUSE Nuclear factor NF-kappa-B p105 subunit OS=Mus musculus	1.158	0.845
>sp|Q9D6R2|IDH3A_MOUSE Isocitrate dehydrogenase [NAD] subunit alpha, mitochondria	1.168	0.848
>sp|Q91VM9|IPYR2_MOUSE Inorganic pyrophosphatase 2, mitochondrial OS=Mus muscul	1.174	0.851
>sp|Q8BKZ9|ODPX_MOUSE Pyruvate dehydrogenase protein X component, mitochondrial	1.177	0.853
>sp|Q3UJU9|RMD3_MOUSE Regulator of microtubule dynamics protein 3 OS=Mus muscul	1.179	0.856
>sp|Q9Z2I9|SUCB1_MOUSE Succinyl-CoA ligase [ADP-forming] subunit beta, mitochondr	1.185	0.858
>sp|P26443|DHE3_MOUSE Glutamate dehydrogenase 1, mitochondrial OS=Mus musculus	1.188	0.861
>sp|Q91YT0|NDUV1_MOUSE NADH dehydrogenase [ubiquinone] flavoprotein 1, mitocho	1.207	0.863
>sp|Q9D855|QCR7_MOUSE Cytochrome b-c1 complex subunit 7 OS=Mus musculus GN=U	1.213	0.866
>sp|P07901|HS90A_MOUSE Heat shock protein HSP 90-alpha OS=Mus musculus GN=Hsp	1.222	0.868
>sp|P31938|MP2K1_MOUSE Dual specificity mitogen-activated protein kinase kinase 1 OS=	1.227	0.871
>sp|O54724|PTRF_MOUSE Polymerase I and transcript release factor OS=Mus musculus GI	1.249	0.873
>sp|P63168|DYL1_MOUSE Dynein light chain 1, cytoplasmic OS=Mus musculus GN=Dynl	1.258	0.876
>sp|Q9CYH2|F213A_MOUSE Redox-regulatory protein FAM213A OS=Mus musculus GN=	1.308	0.878
>sp|O08553|DPYL2_MOUSE Dihydropyrimidinase-related protein 2 OS=Mus musculus GN	1.323	0.881
>sp|Q64442|DHSO_MOUSE Sorbitol dehydrogenase OS=Mus musculus GN=Sord PE=1 SV	1.324	0.883
>sp|P54822|PUR8_MOUSE Adenylosuccinate lyase OS=Mus musculus GN=Adsl PE=2 SV=	1.329	0.886
>sp|Q9D051|ODPB_MOUSE Pyruvate dehydrogenase E1 component subunit beta, mitochon	1.358	0.888
>sp|Q9DCW4|ETFB_MOUSE Electron transfer flavoprotein subunit beta OS=Mus musculus	1.373	0.891
>sp|Q9CR68|UCRI_MOUSE Cytochrome b-c1 complex subunit Rieske, mitochondrial OS=M	1.378	0.893
>sp|P35486|ODPA_MOUSE Pyruvate dehydrogenase E1 component subunit alpha, somatic	1.379	0.896

>sp|Q9ERS2|NDUAD_MOUSE NADH dehydrogenase [ubiquinone] 1 alpha subcomplex sul	1.431	0.898
>sp|O89023|TPP1_MOUSE Tripeptidyl-peptidase 1 OS=Mus musculus GN=Tpp1 PE=1 SV=	1.441	0.901
>sp|P63038|CH60_MOUSE 60 kDa heat shock protein, mitochondrial OS=Mus musculus GN	1.452	0.903
>sp|Q9CQR4|ACO13_MOUSE Acyl-coenzyme A thioesterase 13 OS=Mus musculus GN=A	1.471	0.906
>sp|Q64433|CH10_MOUSE 10 kDa heat shock protein, mitochondrial OS=Mus musculus G	1.472	0.908
>sp|Q64521|GPDM_MOUSE Glycerol-3-phosphate dehydrogenase, mitochondrial OS=Mus	1.487	0.911
>sp|P19536|COX5B_MOUSE Cytochrome c oxidase subunit 5B, mitochondrial OS=Mus mu	1.488	0.913
>sp|Q9CQ92|FIS1_MOUSE Mitochondrial fission 1 protein OS=Mus musculus GN=Fis1 PE	1.497	0.916
>sp|Q9D2G2|ODO2_MOUSE Dihydrolipoyllysine-residue succinyltransferase component of	1.506	0.918
>sp|P62492|RB11A_MOUSE Ras-related protein Rab-11A OS=Mus musculus GN=Rab11a	1.512	0.921
>sp|Q9CQH3|NDUB5_MOUSE NADH dehydrogenase [ubiquinone] 1 beta subcomplex sub	1.581	0.923
>tr|Q3UKH3|Q3UKH3_MOUSE Putative uncharacterized protein OS=Mus musculus GN=A	1.614	0.926
>sp|Q8QZS1|HIBCH_MOUSE 3-hydroxyisobutyryl-CoA hydrolase, mitochondrial OS=Mus	1.643	0.928
>sp|P85094|ISC2A_MOUSE Isochorismatase domain-containing protein 2A, mitochondrial	1.646	0.931
>sp|Q9D6U8|F162A_MOUSE Protein FAM162A OS=Mus musculus GN=Fam162a PE=2 S	1.688	0.933
>sp|Q8BMF4|ODP2_MOUSE Dihydrolipoyllysine-residue acetyltransferase component of p	1.713	0.936
>sp|Q9CWS0|DDAH1_MOUSE N(G),N(G)-dimethylarginine dimethylaminohydrolase 1 OS	1.721	0.938
>sp|P17710|HXK1_MOUSE Hexokinase-1 OS=Mus musculus GN=Hk1 PE=1 SV=3	1.726	0.941
>sp|P97807|FUMH_MOUSE Fumarate hydratase, mitochondrial OS=Mus musculus GN=Fh	1.778	0.943
>sp|P00405|COX2_MOUSE Cytochrome c oxidase subunit 2 OS=Mus musculus GN=Mtco2	1.827	0.946
>sp|P32020|NLTP_MOUSE Non-specific lipid-transfer protein OS=Mus musculus GN=Scp2	1.893	0.948
>sp|Q8BMS1|ECHA_MOUSE Trifunctional enzyme subunit alpha, mitochondrial OS=Mus	1.908	0.951
>sp|P50516|VATA_MOUSE V-type proton ATPase catalytic subunit A OS=Mus musculus	1.934	0.954
>sp|Q922Q1|MOSC2_MOUSE MOSC domain-containing protein 2, mitochondrial OS=Mus	1.964	0.956
>tr|Q8JZU2|Q8JZU2_MOUSE Protein Slc25a1 OS=Mus musculus GN=Slc25a1 PE=2 SV=1	1.983	0.959
>sp|O08599|STXB1_MOUSE Syntaxin-binding protein 1 OS=Mus musculus GN=Stxbp1 PE	2.123	0.961
>sp|Q05421|CP2E1_MOUSE Cytochrome P450 2E1 OS=Mus musculus GN=Cyp2e1 PE=1	2.193	0.964
>sp|P00397|COX1_MOUSE Cytochrome c oxidase subunit 1 OS=Mus musculus GN=Mtco1	2.371	0.966
>sp|Q07417|ACADS_MOUSE Short-chain specific acyl-CoA dehydrogenase, mitochondrial	2.528	0.969
>sp|Q62425|NDUA4_MOUSE NADH dehydrogenase [ubiquinone] 1 alpha subcomplex subu	2.537	0.971
>sp|Q8R1I1|QCR9_MOUSE Cytochrome b-c1 complex subunit 9 OS=Mus musculus GN=U	2.764	0.974
>sp|Q9DC69|NDUA9_MOUSE NADH dehydrogenase [ubiquinone] 1 alpha subcomplex sub	2.928	0.976
>sp|Q9JMH6|TRXR1_MOUSE Thioredoxin reductase 1, cytoplasmic OS=Mus musculus GN	3.500	0.979
>sp|P50518|VATE1_MOUSE V-type proton ATPase subunit E 1 OS=Mus musculus GN=At	4.363	0.981
>sp|Q64133|AOFA_MOUSE Amine oxidase [flavin-containing] A OS=Mus musculus GN=M	4.437	0.984
>sp|Q8VCL2|SCO2_MOUSE Protein SCO2 homolog, mitochondrial OS=Mus musculus GN	4.665	0.986
>tr|D3YZ32|D3YZ32_MOUSE Mitochondrial fission 1 protein OS=Mus musculus GN=Fis1	4.786	0.989
>tr|Q80X68|Q80X68_MOUSE Citrate synthase OS=Mus musculus GN=Csl PE=1 SV=1	4.863	0.991
>sp|A2ARZ3|FSIP2_MOUSE Fibrous sheath-interacting protein 2 OS=Mus musculus GN=F	9.179	0.994
>tr|Q3TCI7|Q3TCI7_MOUSE Putative uncharacterized protein OS=Mus musculus GN=Ldha	9.691	0.996
>sp|P24529|TY3H_MOUSE Tyrosine 3-monooxygenase OS=Mus musculus GN=Th PE=1 S	13.622	0.999